Dissertation zur Erlangung des Doktorgrades
der Fakultät für Chemie und Pharmazie
der Ludwig-Maximilians-Universität München

Mechanistic dissection of adult muscle formation in *Drosophila*

Manuela Weitkunat

aus

Freudenstadt, Deutschland

2014

Erklärung

Diese Dissertation wurde im Sinne von § 7 der Promotionsordnung vom 28. November 2011 von Frau Prof. Dr. Ulrike Gaul betreut.

Eidesstattliche Versicherung

Diese Dissertation wurde eigenständig und ohne unerlaubte Hilfe erarbeitet. München, den .....

.....

Dissertation eingereicht am 13.11.2014

1. Gutachterin: Prof. Dr. Ulrike Gaul

2. Gutachterin: Prof. Dr. Magdalena Götz

Mündliche Prüfung am 18.12.2014

Parts of this work were published:

Weitkunat, M., Kaya-Çopur, A., Grill, S. W., and Schnorrer, F. (2014). Tension and Force-Resistant Attachment Are Essential for Myofibrillogenesis in *Drosophila* Flight Muscle. Current Biology *24*, 705-716

Weitkunat, M., and Schnorrer, F. (2014). A guide to study *Drosophila* muscle biology. Methods *68*, 2-14

Table of contents

1 Summary

Movement of all higher organisms is highly dependent on muscle function. Improper development of the muscle-tendon system can disrupt muscle function causing severe myopathies. Myogenesis is a sequential process; myoblasts are specified and migrate to sites of myofiber formation where they fuse. The developing myotubes migrate to forming tendon cells and attach to them. This process is followed by myofibrillogenesis and sarcomerogenesis forming the contractile, functional apparatus of the muscle. To date these myogenic processes are still not fully understood.

The purpose of this thesis was to extend our knowledge of myogenesis using *Drosophila melanogaster* as model system. To reach this goal, the following three aims were defined:

(1) Identification of novel genes involved in one or more myogenic steps using functional RNAi screening.
(2) Establishment of live imaging and quantitative tension measurements providing the tools for detailed characterisation of myogenic processes.
(3) Application of these tools for in-depth study of myotube-tendon attachment and myofibrillogenesis.

Aim 1: To identify novel genes involved in myogenesis, I performed muscle-specific RNAi screening for 284 selected genes. Morphological analysis of five different adult *Drosophila* muscle types allowed for identification of 142 genes possibly involved myogenesis. The five phenotypic classes defined in the screen are fiber presence, fiber shape, fiber position, fibrillar organisation and sarcomeric organisation. Each of these classes was further divided into different subclasses providing a detailed description of the morphological defect. Using this phenotypic classification in combination with the affected muscle type, candidate genes for general or muscle type specific factors for all myogenic steps were identified.

Aim 2: I established two-colour live imaging of myotubes and tendons during myogenesis, allowing analysis of myotube-tendon dynamics during attachment formation. Moreover, I established laser-cutting of tendon cells during different myogenic steps in an collaborative effort with Prof. Grill at the Max Planck Institute of Molecular Cell Biology and Genetics. This allowed for quantitative tension measurements and manipulation of tension to analyse its role in myogenesis.

Aim 3: Using these newly established methods, I studied myotube-tendon attachment and its coordination with myofibrillogenesis in indirect flight muscles. I found that an initial cell-cell based myotube-tendon contact, possibly mediated by E-Cadherin, is formed during attachment initiation, while an integrin based myotube-extracellular matrix-tendon attachment is established during attachment maturation. Additionally, I showed that the candidate gene *kon-tiki* (*kon*), identified in my RNAi screen, is essential for initiation of myotube-tendon attachment. Moreover, I could show that tension increases significantly after Kon-dependent attachment initiation and that this tension increase is essential for myofibrillogenesis and sarcomerogenesis. Hence, tension could represent the signal that coordinates attachment formation and myofibrillogenesis.

2 Introduction

Body movements of all higher organisms are highly dependent on muscles. Muscle function is the basis for any kind of active movement from the highly coordinated movements of a piano player to the simple swimming movements of a jellyfish.

2.1 Myotendinous system

The myotendinous system is producing and transmitting the force for controlled movement of the skeleton. Muscles themselves connect to tendon cells via extracellular matrix (ECM) and the tendon cells in turn link to the bone and cartilage containing endoskeleton in vertebrates and to the chitin based exoskeleton in insects. Therefore, force transmission enabling body movements is dependent on stable connections of functional muscles to tendons and the skeleton. Thus, a correctly developed and functional muscle tendon system is essential for higher organisms.

2.1.1 Muscle and sarcomere structure

Depending on the organism and muscle type, one muscle can consist of only one or more than thousand muscle fibers. These myofibers exhibit a specialised cell membrane, the sarcolemma that is linked to largely collagen-based connective tissue. Myofibers themselves are composed of numerous myofibrils that are built by hundreds of sarcomeres. These myofibrils are packed into a precise order and decorated with various sarcomeric proteins like titin that spans both the actin and the myosin filaments. Sarcomeres can contract resulting in contraction of the complete muscle. Therefore, sarcomeres are the functional, force-producing units of the muscle (Figure 1) (Davies and Nowak, 2006).

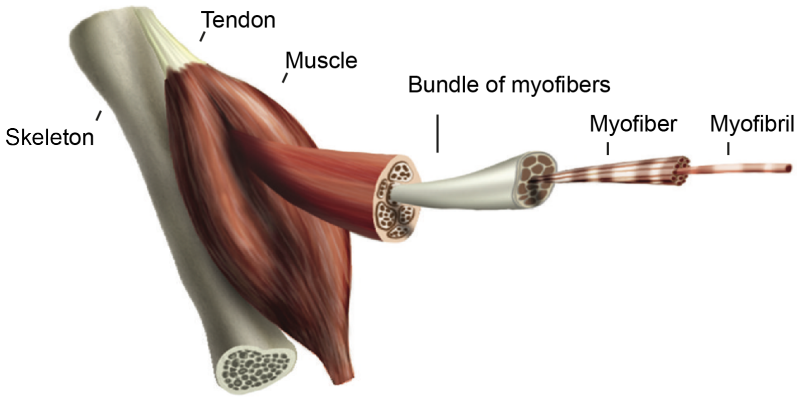

Figure 1 Schematic representation of a skeletal muscle. One muscle consists of myofibers that harbour many hundred myofibrils. Myofibrils are built by alternate stretches of actin and myosin filaments that form sarcomeres. Modified from Myhre and Pilgrim, 2012.

Sarcomeres consist of alternating thin and thick filaments. As they are highly ordered, almost crystalline structures, sarcomeres generate a characteristic pattern in the electron micrograph (Figure 2). The thin filaments are largely formed by actin and intercalate partially with thick filaments formed mainly by myosin. Both actin and myosin filaments are decorated with various other sarcomeric proteins and anchored at defined places in the sarcomere. The thick filaments are anchored by myosin binding proteins at the M-line, while thin filaments are anchored at the Z-disc. Crosslinking of thin filaments at the Z-disc is mainly achieved by the actin crosslinker α-actinin. Interestingly, the giant sarcomeric protein titin spans from the Z-disc throughout actin and myosin filaments to the M-line connecting both elements in vertebrates. Also in insects, titin spans from the Z-disc to the end of thick filament connecting thin and thick filaments with each other (Figure 2) (Tskhovrebova and Trinick, 2003).

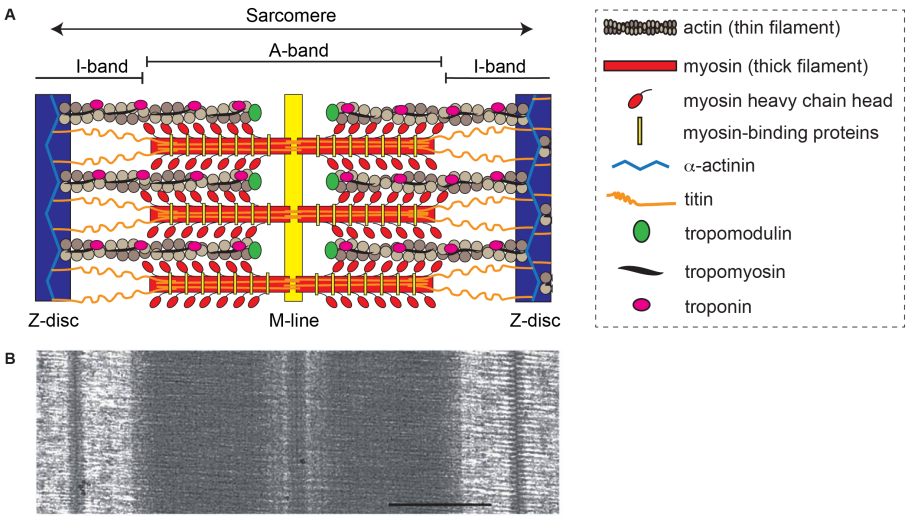

Figure 2 Sarcomere structure. A| Schematic representation of the sarcomere with some of its main components. M-line anchors myosin filaments, Z-disc anchors actin filaments via α-actinin, A-band is the region spanned by myosin filaments, I-band is the region where actin but not myosin is located. Titin spans from the Z-disc to the M-line. Regulatory proteins like Tropomodulin and Tropomyosin are indicated. Image modified from M. Spletter. B| Electron micrograph of longitudinally sectioned white fish muscle. Scale bar: 500 nm, image from Luther, 2009.

In the thick filament multiple myosin hexamers are precisely aligned. These hexamers consist of two heavy chains, two essential light chains and two regulatory light chains. The heavy chains can be divided into a head, a neck or lever arm and a rod domain. The rod domains of two heavy chains coil around each other, while the short neck / lever arm domains bind to myosin light chains. Importantly, the globular head structure of myosin heavy chain harbours an ATPase domain that is essential for muscle function. These head structures are located at the surface of the myosin filament enabling them to bind

neighbouring actin filaments. Therefore, they are also called cross-bridges (Batters et al., 2014).

In contrast, actin filaments consist of polymerised G-actin molecules that are arranged as a helix. They display a barbed (+) and a pointed (-) end (Geeves and Holmes, 1999). In the myofiber, the barbed ends of actin filaments from two neighbouring sarcomeres are anchored via α-actinin at the Z-discs. Importantly, the Z-disc of each sarcomere in the outer fibrils is linked to the sarcolemma via integrin complex based adhesion sites. These adhesion sites, called costameres, are essential to sustain the fibrillar integrity during muscle contraction (LaBeau-DiMenna et al., 2012; Peter et al., 2011).

2.1.2 Muscle contraction

The function of muscles is to create force for movement via muscle contraction. This muscle contraction is initiated by neuronal stimuli and in some specialized muscles like insect flight muscles also via stretch activation. The contractile subunits of muscles are the sarcomeres. They contract via the sliding filament mechanism, in which myosin heads move actin filaments along the myosin filament towards the M-line (Huxley, 2004). The actin movement towards the M-line results in sarcomere shortening that is translated into muscle contraction and mechanical force.

2.1.2.1 The swinging cross-bridge model

A prominent model describing actin filament movement is the swinging cross-bridge theory. According to this theory conformational changes in the myosin lever arm angle displace the cross-bridge and the bound actin filament in a so called power stroke (Batters et al., 2014; Geeves and Holmes, 1999; Spudich, 2001). The swinging cross-bridge model can be described in 6 steps (Figure 3).

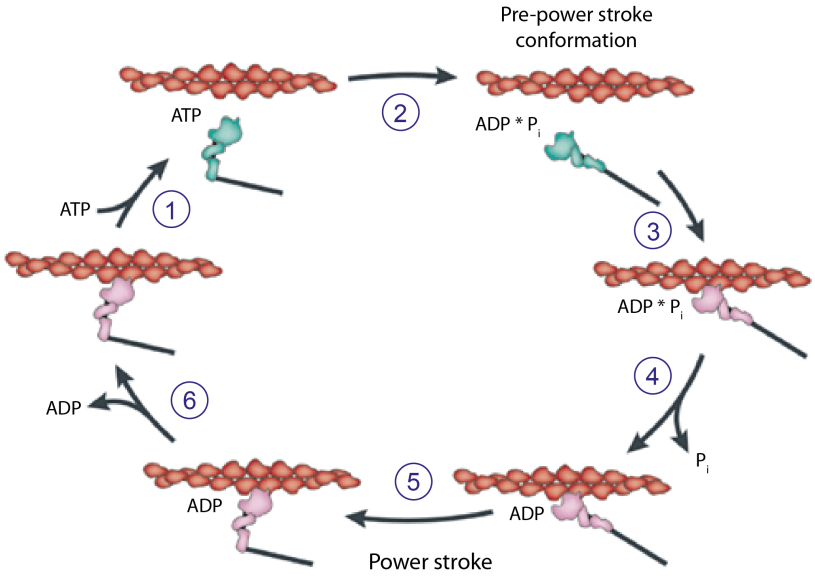

Figure 3 Swinging cross-bridge model of muscle contraction. One cross-bridge cycle can be described by 6 steps (blue numbers). Step 1| ATP binds to the cross-bridge, actin is released. Step 2| ATP hydrolysis triggers a conformational change, the lever arm is moved 70° and consequently bends up into the pre-power stroke conformation. Step 3| Actin binds to the myosin head. Step 4| Phosphate is released. Step 5| Power stroke; a conformational change bends the lever arm down again, actin is moved. Step 6| ADP release. Green myosin cross-bridges have low-actin affinity, rose myosin cross-bridges have high-actin affinity. Modified from Spudich, 2001.

If ATP is bound to the myosin head, the actin affinity of myosin is very low and actin is consequently released (step 1). Actin dissociation induces ATP hydrolyses. Triggered by ATP hydrolysis the myosin cross-bridge undergoes a conformational change, moving the lever arm through a 70° angle and consequently bending it up (step 2). In this pre-power stroke confirmation, myosin has low affinity for actin. Actin binding to the myosin head (step 3) induces phosphate release (step 4), which triggers a conformational change bending the lever arm down again and producing the power stroke. As actin is bound to the myosin head at this stage it is moved 10nm towards the M-line (step 5). Actin affinity is highly increased by phosphate release (during step 4) and increasing actin binding causes ADP release (step 6). The now empty nucleotide-binding pocket of myosin can bind to ATP again re-entering step 1.

2.1.2.2 Regulation of muscle contraction

Muscle contraction is initiated via neuronal stimuli that result in elevated intramuscular Ca^{2+} levels. Translation of Ca^{2+} levels into muscle activity is largely mediated via the Troponin-Tropomyosin (Tn-Tm) complex. The Tn-Tm complex associates closely with the actin filament and is formed by assembly of several different Troponin units with a Tropomyosin (Figure 2).

If Tn-Tm is not bound to Ca^{2+}, Tropomyosin binding to actin blocks myosin-binding domains on actin. Tropomyosin is kept in this blocking position by the Troponin I subunit of Tn-Tm, which is responsible for inhibiting the interaction between actin and myosin, thereby preventing muscle contraction. Binding of Ca^{2+} to the Troponin C subunit of Tn-Tm however induces a conformational change that releases the inhibitory binding of Tn-Tm to actin. Consequently, Ca^{2+} binding to Tn-Tm allows acto-myosin interaction and subsequent muscle contraction (Ohtsuki and Morimoto, 2008; Ostendorp et al., 2011). Therefore, the Tn-Tm complex can translate stimuli from nerve cells, resulting in stark increase of intramuscular Ca^{2+}, to muscle contraction.

Moreover, muscle contraction can be regulated via an additional stretch stimulus. The coupling of stretch and muscle contraction represents an autonomous control that can allow to adapt the frequency of muscle contraction to external conditions like mechanical load. Two muscle types are known to use stretch activation, one is cardiac muscle and the other are asynchronous insect flight muscles. It has been suggested, that stretch activation in cardiac muscle serves as force regulating mechanism, coordinating muscle length and tension. However cardiac muscle contraction pace is mainly induced by oscillating Ca^{2+} levels and the physiological role of stretch activation is still unclear (Campbell and Chandra, 2006).

In contrast, asynchronous flight muscle contraction depends heavily on stretch activation. Asynchronous flight muscle contraction requires permissive Ca^{2+} levels. However, the frequency of the contractions is not induced by changing Ca^{2+} levels, but by stretch. Stretch activated, oscillating movements of asynchronous flight muscles allow for extremely high wing beat frequencies e.g. 200Hz for *Drosophila* asynchronous flight muscles. In *Drosophila*, so called indirect flight muscles produce the power for flight and control wing beat by deformation of the fly's thorax during muscle contraction (Vigoreaux, 2001).

To date the mechanism for stretch activation is not completely understood. One popular model is that Ca^{2+} binds to Tn-Tm and causes a switch from the closed state, where Tropomyosin blocks myosin-binding sites, to a partially open state. The partially open state in turn can be conferred to a completely open state via rapid stretching of the fiber. Contraction will return the sarcomere to the partially open state if priming Ca^{2+} levels are still present and the oscillatory contraction can go on if the muscle is stretched again. As a stop signal rapid shortening of fibrils is supposed to reverse the process and lead to muscle relaxation (Bullard and Pastore, 2011). Additionally, a recent publication using bees proposes that myosin undergoes a stretch induced deformation that could contribute to stretch activation (Iwamoto and Yagi, 2013).

2.2 Muscle development

To ensure optimal performance of skeletal muscles; sarcomeres, myofibrils and myofibers need to be precisely structured, innervated by neurons and stably connected to tendons. Correct muscle-tendon structure is achieved by coordinated development of the myotendinous system. Muscle development can be divided into five main processes. (1) Specification: Muscle cells originate from the mesoderm that is formed in the embryo during gastrulation. The mesoderm is further subdivided into different regions giving rise to specified myoblasts that form distinct muscle types. (2) Migration and (3) fusion: These myoblasts then migrate to the site of muscle formation and fuse to generate multinucleated myotubes. The myotubes migrate to developing tendon cells originating from the ectodermal germ layer. (4) Myotube-tendon attachment: When developing myotubes reach the forming tendon cells, they establish a stable attachment. In the myotendinous junction, both muscle and tendon cells attach to ECM linking them together. (5) Sarcomerogenesis and myofibrillogenesis: Next, the muscular cytoskeleton reorganises into regularly spaced sarcomeres that incorporate structural proteins like titin and form myofibrils (Daczewska et al., 2010; Schnorrer and Dickson, 2004).

2.2.1 *Drosophila* – an established model organism for muscle development

The main processes of muscle development are conserved from flies to humans. Also many of the key molecules involved in specification, migration, fusion, attachment or sarcomerogenesis are closely related in different organisms. The similarity in myogenic proteins and processes allows to study individual steps of muscle development in various model organisms (Daczewska et al., 2010). Therefore, myogenesis is not only intensively

studied in vertebrates like mouse, chicken and zebrafish, but also in invertebrates like *Drosophila* and *C. elegans* (Baylies et al., 1998; Bryson-Richardson and Currie, 2008; Moerman, 2006). This study uses *Drosophila* melanogaster as a model organism.

Drosophila is relatively cheap and easy to grow even in large numbers. It has a short development and life span and is simpler than vertebrate models as it often has fewer gene copies or protein isoforms. Moreover, a rich repertoire of genetic methods allows for fast and efficient manipulation of the *Drosophila* genome. These advantages of *Drosophila* as a model organism can be combined for large-scale screening uncovering novel genes and proteins involved in essential processes. For example the transmembrane protein Kon-tiki was identified to be essential for embryonic muscle tendon targeting by mutagenesis screening (Schnorrer et al., 2007). Furthermore, genome-wide RNAi screens have been successfully applied to identify essential myogenesis genes in *Drosophila* primary cells as well as in intact *Drosophila* embryos, larvae and adults (Bai et al., 2008; Schnorrer et al., 2010).

Drosophila is not only very well suited for large scale screening but also for analysing the function of specific pathways or genes. For example myoblast specification as well as fusion are extensively studied in *Drosophila* embryos (Rochlin et al., 2010; Tixier et al., 2010). Furthermore, expression and function of the conserved transcription factor Mef2 have been analysed in detail in *Drosophila*. Multiple studies could show that *Mef2* expression is restricted to myogenic cells and is essential for muscle differentiation (Bour et al., 1995; Lilly et al., 1995; Nguyen and Xu, 1998; Taylor, 1995).

Additionally, various *Drosophila* disease models have been established. Among these are several models for myopathies such as spinal muscular atrophy, Duchenne muscular dystrophy and inclusion body myopathy (Daczewska et al., 2010; Grice et al., 2011; Mosqueira et al., 2010; Nalbandian et al., 2011).

2.2.2 Overview of *Drosophila* muscle development

Analogous to vertebrates, *Drosophila* possesses different classes of musculature: cardiac musculature pumping hemolymph, visceral musculature essential for digestive movements, and somatic musculature essential for body movement. The somatic musculature is similar to skeletal musculature of vertebrates and is formed twice in *Drosophila*.

The first somatic muscle system develops in the embryo and enables larval locomotion. Each of these embryonic muscles consists of only one myofiber. During metamorphosis the majority of embryonic somatic muscles is degraded and the adult body muscles are

formed. This adult muscle system fulfils different functions like walking and flying and therefore, harbours specialised muscle types consisting of multiple myofibers. Consequently, the adult body muscle system is more complex than the embryonic system and displays a higher similarity to vertebrate skeletal muscles.

2.3 *Drosophila* embryonic muscle development

Drosophila embryos develop a precisely arranged pattern of 30 different somatic muscles, repeated in each abdominal hemisegment (Figure 4) (Bate, 1990). These muscles are formed via fusion of fusion competent myoblasts (FCMs) to specific founder cells (FCs). Each muscle is seeded by one FC determining the individual muscle fate. The resulting muscle exhibits not only a characteristic innervation, attachment position and nuclei number, but also a specific pattern of transcription factors assigning the identity of the muscle. According to their function, these transcription factors are also called identity genes (de Joussineau et al., 2012).

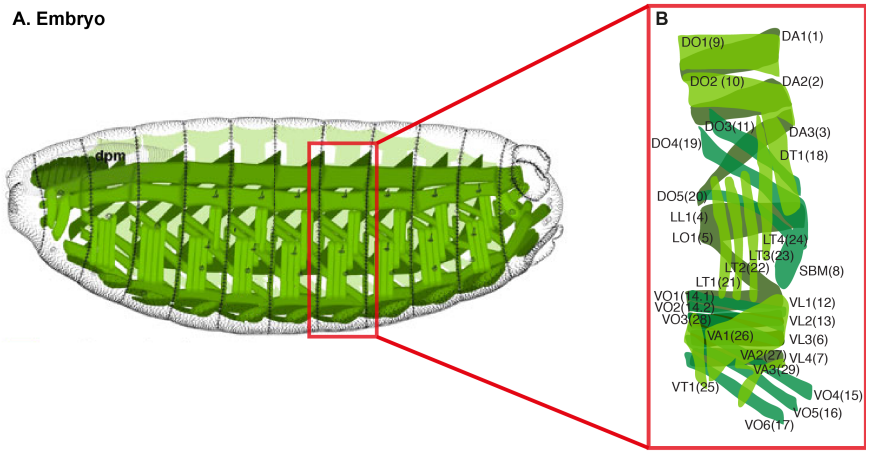

Figure 4 Schematic representation of embryonic musculature. A| Schematic representation of embryonic stage 17 musculature, red box indicates area represented in B. Modified from Hartenstein, 1993. B| Musculature of one hemisegment, external muscles are depicted in brighter green, more internal muscles are depicted in darker green. Modified from Weitkunat and Schnorrer, 2014.

2.3.1 Myoblast specification

All *Drosophila* as well as vertebrate muscles originate from the mesoderm. During *Drosophila* embryogenesis the mesoderm is further divided into different competence domains. Muscle progenitors are singled out from these competence domains and give rise to FCs that will seed embryonic muscles and adult muscle progenitors (AMPs) that will form the adult musculature (Figure 5).

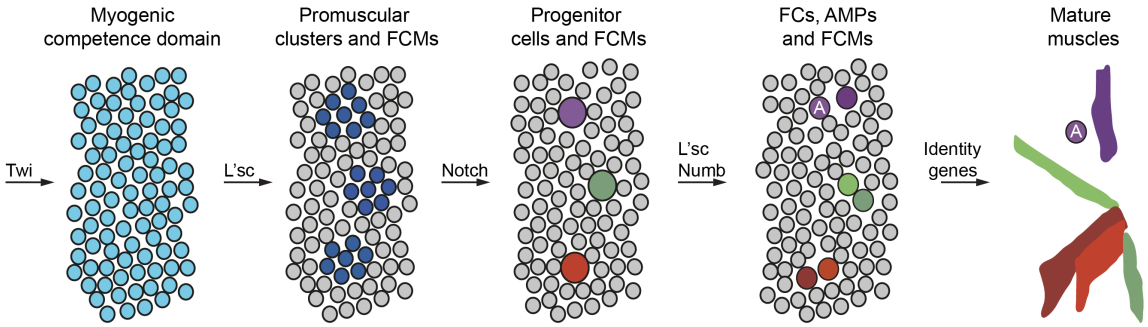

Figure 5 Schematic summary of embryonic muscle specification. Myogenic competence domains are defined by Twist (Twi) expression and subdivided into different promuscular clusters by restricted *l'sc* expression. Progenitor cells are singled out from promuscular clusters (dark blue), via lateral inhibition, the remaining myogenic cells develop into FCMs (grey). Progenitor cells undergo asymmetric cell division giving rise to two founder cells or one founder cell and one AMP (A), only one of the daughter cells inherits the Notch signalling repressor Numb. Each founder develops into one embryonic muscle, AMPs are set aside for adult myogenesis. Based on Schnorrer and Dickson, 2004.

2.3.1.1 Specification of competence domains

Drosophila mesoderm is specified by the function of the Twist and Snail transcription factors (Leptin, 1991). Additionally, Twist is reused after gastrulation to pattern the mesoderm. Mesodermal cells with high levels of Twist develop into cardiac and somatic musculature, while mesodermal cells with low levels of Twist develop into visceral muscles and fat body (Baylies and Bate, 1996; de Joussineau et al., 2012). Further specification of the somatic mesoderm is not only influenced by internal signals but also by external cues from the ectoderm like Wingless (Wg) and Decapentaplegic (Dpp). Wg and Dpp maintain expression of the Twist target *tinman*, which specifies the region of cardiac and somatic dorsal muscle development. The regions of ventral and lateral muscle development are specified by other Twist targets like *Dsix4* and *Pox meso* (Tixier et al., 2010).

2.3.1.2 Specification of muscle progenitor cells

These competence domains are then subdivided into different promuscular clusters via the restricted expression of *lethal of scute* (*l'sc*) mediated via FGF and EGF signals (Buff et al., 1998; Michelson et al., 1998). Next, one muscle progenitor cell is singled out in each promuscular cluster by lateral inhibition mediated via reciprocal interactions of Notch and Ras/MAPK signalling (Carmena et al., 2002) (Figure 5). Cells surrounding a progenitor cell display up regulated Notch signalling that induces expression of *lame duck* (*lmd*), determining FCM fate (Duan et al., 2001). The progenitor cells however display up-regulated MAPK signalling and often express identity genes such as *even skipped*, *Krüppel* or *ladybird* (de Joussineau et al., 2012).

2.3.1.3 Specification of founder cells

The progenitor cells undergo asymmetric cell division that gives rise to either two different founder cells or one founder cell and one AMP. Numb and Inscuteable are asymmetrically distributed in the progenitor cell. Hence only one daughter cell inherits Numb that represses the Notch pathway and therefore continues to express the identity genes. In Numb (-) cells the Notch pathway is active, leading to repression of identity genes and allowing for the adaption of a new fate (Ruiz and Bate, 1997) (Figure 5). Importantly, the special class of Numb (-) cells, that retain *twist* expression develops into AMPs that are set aside for adult myogenesis (Bate et al., 1991; Ruiz-Gómez, 1998).

2.3.2 Myoblast fusion

Myotubes form by fusion of FCMs to FCs. During myoblast fusion, multiple cellular processes take place (Figure 6).

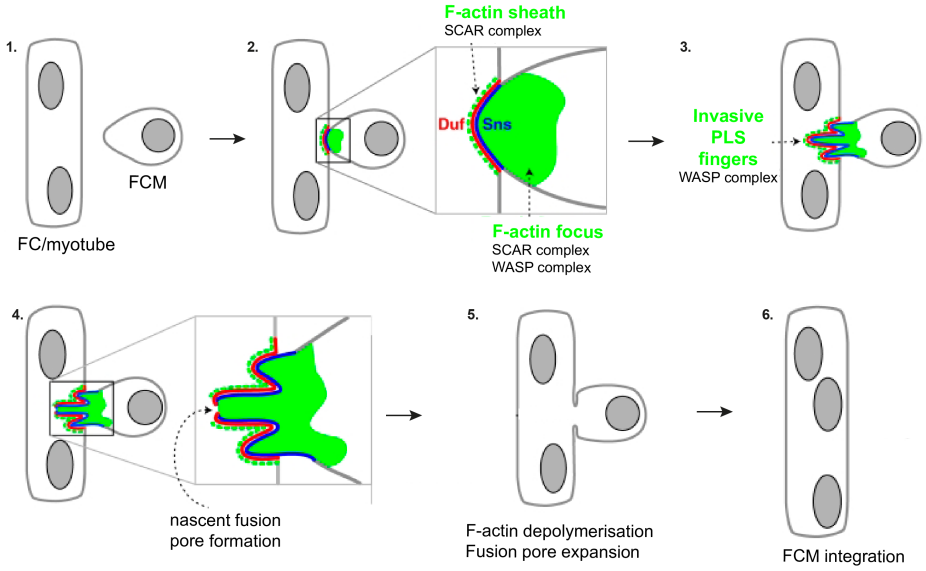

Figure 6 Schematic representation of different fusion steps. 1| Attraction of FCM. 2| Adhesion of FCM to FC/myotube, actin sheath formation in FC/myotube and actin focus formation in FCM. 3| FCM invades FC/myotube with podosome like structure (PLS). 4-5| Fusion pore formation and FCM incorporation. 6| Myotube with an additional nucleus. Modified from Sens et al., 2010.

FCMs migrate to FCs and adhere to them. Both attraction and adhesion of FCMs to FCs is mediated by a group of single-pass transmembrane Immunoglobulin superfamily proteins, namely Dumbfounded (Duf), Roughest (Rst), Sticks and stones (Sns) and Hibris (Hbs). Sns and Hbs are present in high levels in FCMs and are important for migration of FCMs towards FCs. When the FC is reached, Sns and Hbs bind to the FC specific proteins Duf and Rst, mediating cell-cell adhesion (Bour et al., 2000; Dworak et al., 2001; Ruiz-Gómez et al., 2000; Strünkelnberg et al., 2001). Adhesion is followed by cell-type specific actin accumulation at the contact site. Duf action in the FC recruits the actin nucleation promoting factor SCAR/Wave. Moreover, the GTPase Rac is activated. Rac in turn binds and activates SCAR/Wave, which then promotes Actin related protein 2/3 (ARP2/3) mediated formation of branched actin networks resulting in formation of a thin actin sheath at the contact site (Rochlin et al., 2010; Sens et al., 2010). In FCMs, Rac also activates SCAR/Wave. Additionally, Sns promotes recruitment and stabilisation of Wiskott-Aldrich syndrome protein (WASP) by recruiting WASP interacting protein (Wip) to the FCM-FC contact site. Both SCAR/Wave and WASP activate ARP2/3 in FCMs, causing formation

of a dense actin focus (Abmayr and Pavlath, 2012; Sens et al., 2010). This actin focus forms a podosome-like structure invading the FC. Moreover, vesicles accumulate at the contact site. These vesicles are believed to deliver the fusion machinery and give rise to membrane plaques (Doberstein et al., 1997). Next, a fusion pore is formed and expands when the actin focus depolymerises. Expansion of the fusion pore is accompanied by membrane breakdown and removal of the fusion machinery. Finally, the FCM is completely incorporated and a syncytium is formed. The nucleus of the former FCM adopts the fate of the FC. After the first round of fusion the process is repeated by fusion of FCMs to the forming myotube until the final number of nuclei is reached. How the number of fusion events is regulated, however, remains elusive (Abmayr and Pavlath, 2012).

2.3.3 Myotube-tendon attachment

For formation of a stable myotube-tendon attachment, both cell-types need to interact closely. Therefore, myotube and tendon signalling is essential for the three processes that lead to proper muscle attachment. These three processes are (1) myotube guidance and tendon recognition, (2) migration termination and (3) myotube-tendon attachment formation (Figure 7) (Schweitzer et al., 2010).

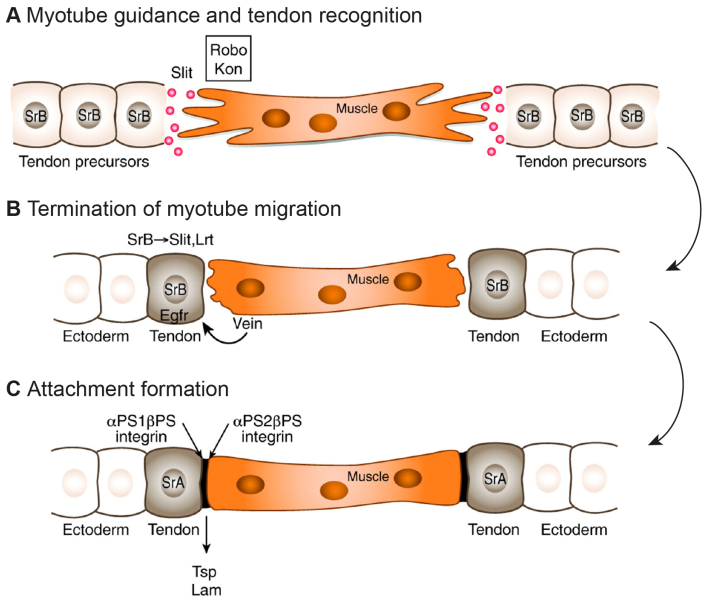

Figure 7 Processes leading to myotube–tendon attachment. Schematic representation of myotube tendon attachment formation. Some of the key players are indicated. A| Myotube guidance and target recognition. *srB* expressing tendon cells secret Slit which binds to Robo on the myotube. Robo, Kon and other molecules guide the myotube to the tendon cell. B| Tendon recognition and migration termination. Upon recognition myotubes secrete Vein inducing EGFR signalling in tendon cells. Tendon cells express LRT mediating myotube arrest. C| Myotube-tendon attachment formation. Tendons localise β-PS1/α-PS1 and myotubes localise β-PS1/α-PS2 integrin complexes to the myotendinous junction. Integrins connect myotubes and tendons by binding to extracellular matrix components like Thrombospondin (Tsp) secreted by tendon cells. Tendons mature and express *srA*. Modified from Schweitzer et al., 2010.

2.3.3.1 Myotube guidance and tendon recognition

After initial fusion, both ends of the myotubes migrate towards epidermal attachment sites at opposing sides of the myotube, resulting in myotube extension (Schnorrer and Dickson, 2004). These epidermal attachment sites, also called tendon cells, are singled out by the early growth response like transcription factor Stripe (Sr). The *sr* gene encodes two isoforms, SrA and SrB. Expression of *srB* in selected ectodermal cells induces the tendon fate. These tendon precursors attract the growing myotubes (Schweitzer et al., 2010; Vorbrüggen and Jäckle, 1997). As each myotube attaches to specific tendon cells, different sets of transmembrane proteins should be involved in the myotube guidance and recognition process of each myotube set.

Proteins known from axon guidance – like Slit, Roundabout (Robo), and Ryk receptor thyrosine kinases – have been shown to mediate guidance of specific myotube subsets. The Ryk tyrosine kinases Derailed (Drl) and doughnut on 2 (Dnt) as well as their potential, secreted ligand Wnt5 have been shown to guide LT 1-3 myotubes to their proper attachment sites (Callahan et al., 1996; Lahaye et al., 2012) (for muscle nomenclature see Figure 4). Moreover, Slit is secreted by a subset of tendon precursors. It is recognised by the transmembrane receptor Robo on embryonic VL1-4, LL1 and LO1 myotubes guiding them to their proper tendon cells (Kramer et al., 2001). Additional proteins found to be essential for guidance and target recognition of VL1-4 myotubes are the orphan receptor Kon and its intracellular binding partner Glutamate receptor binding protein (Grip) (Estrada et al., 2007; Schnorrer et al., 2007; Swan et al., 2004) (Figure 7). Grip also interacts with the cell adhesion molecule Echinoid that is important for VL and LT myotube guidance or attachment (Swan et al., 2006). In addition, the GTPase activating protein dGit has been identified as guidance protein (Bahri et al., 2009). The guidance proteins described here only act on a small set of embryonic muscles and the signalling processes mediating their function are not clear. Therefore, other guidance proteins and their intracellular signalling pathways still remain to be identified.

2.3.3.2 Termination of myotube migration

Upon myotube-tendon contact, myotubes secret the neuregulin-like growth factor Vein, which accumulates at the junction and activates the Epidermal growth factor receptor (EGFR) pathway in tendon cells increasing their *srB* expression (Yarnitzky et al., 1997). Elevated SrB levels induce expression of *Leucine-rich tendon-specific protein* (*Lrt*). Lrt accumulates in the tendons at the site of myotube contact. It binds to Robo on the

myotubes and is essential for myotube migration arrest (Gilsohn and Volk, 2010a; Wayburn and Volk, 2009). Following migration arrest, tendons mature. Maturation of tendon cells is marked by the expression of *srA* inducing not only expression of terminal differentiation markers like *β1-Tubulin* but also expression of *Thrombospondin* (*Tsp*) (Figure 7). Tsp is an ECM protein that is essential for attachment formation (Subramanian et al., 2007).

2.3.3.3 Myotube-tendon attachment formation

The myotube-tendon contact is first established during target recognition. Next, this myotube-tendon contact is extended to a stable hemiadherence-type attachment that withstands large forces during muscle contraction (Prokop et al., 1998; Tepass and Hartenstein, 1994). Formation of this stable attachment requires transmembrane integrin heterodimers and their ECM ligands localised to the myotendinous junction. Integrin heterodimers consist of a β-PS integrin and a α-PS integrin chain. The α-PS1 integrin chain is present in tendon cells, while the α-PS2 integrin chain is present in myotubes. Integrins bind directly to ECM molecules like Laminin A (LanA) in the case of β-PS1/α-PS1 integrin, and Tiggrin as well as Tsp in the case of β-PS1/α-PS2 integrin (Schejter and Baylies, 2010) (Figure 7). Intracellularly, integrins link to the cytoskeleton via a complex of adaptor proteins. One essential adaptor protein is Talin, which binds to the β-PS1 integrin tail and to actin (Brown et al., 2002; Delon and Brown, 2007). Therefore, integrins are not only connecting tendons and myotubes but are also able to transmit force via anchorage to the actin cytoskeleton.

2.4 *Drosophila* adult muscle development

Adult muscles are formed by AMPs that are specified and set aside in the embryo (Fernandes et al., 1991). AMPs migrate to defined regions in the embryo, where they remain quiescent and proliferate during the majority of larval life. In the pupa these AMPs further migrate to places of muscle formation, where they fuse to form the adult muscle system (Roy and Vijayraghavan, 1999) (Figure 8). Most *Drosophila* adult muscles consist of tubular myofibers, whose inside is devoid of myofibrils. Only the highly specialised IFMs that create the power for flight consist of fibrillar myofibers, where myofibrils also fill the inside of the myofiber.

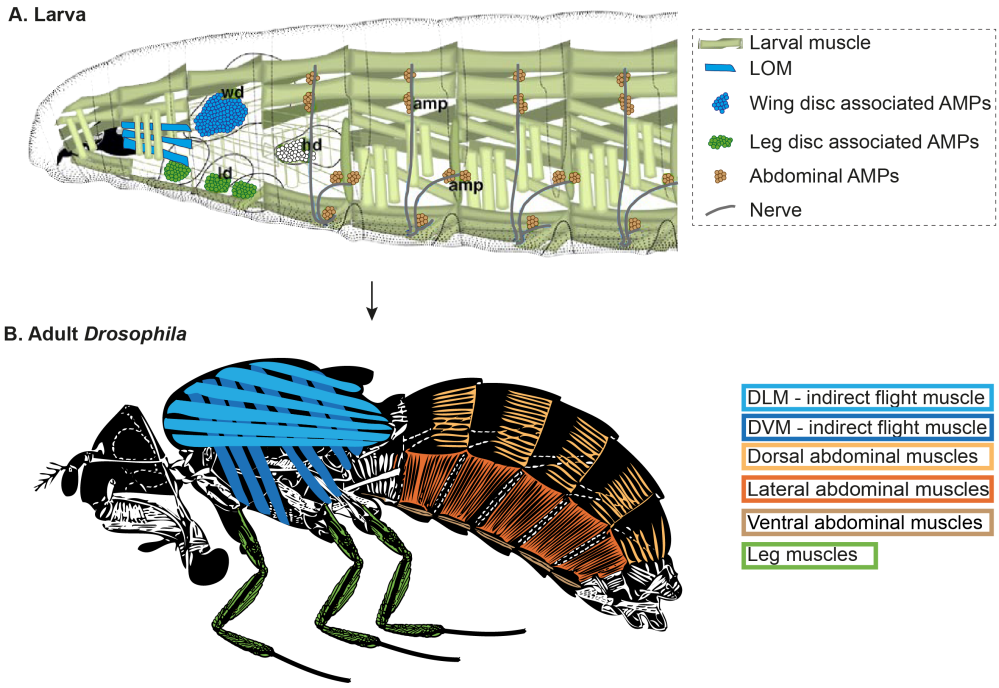

Figure 8 Fate map for adult myogenesis. Schematic representation of AMPs in the larva (A) and corresponding adult muscles. Modified from Hartenstein, 1993 (B). DLM: Dorsal longitudinal indirect flight muscle, DVM – Dorsal ventral indirect flight muscle. For simplicity direct flight muscles and the jump muscle are not shown. Modified from Miller, 1950.

2.4.1 Myoblast specification

As discussed above, the adult musculature is derived from AMPs (section 2.2.2). AMPs are characterised by sustained *twi* expression. After AMPs are born by asymmetric cell division of embryonic progenitor cells, they segregate to precisely defined locations. During larval development AMPs forming the abdominal muscles migrate along nerves and associate with epidermal histoblast nests (Currie and Bate, 1991). In contrast, AMPs forming indirect flight muscles or leg muscles migrate to developing wing and leg discs respectively. These AMPs adhere to the imaginal discs and are in close proximity to their future attachments sites that are characterised by expression of the tendon specific transcription factor *sr* (Roy and Vijayraghavan, 1999). Restriction of AMP adherence to stereotyped regions of the discs and association with nerves indicates a role of extrinsic signals for the segregation of AMPs. But also intrinsic signals are essential for correct AMP segregation. For example ectopic expression of the abdomen specific homeotic gene *abdominal-A* in all myoblasts causes loss of thoracic AMPs and increase of abdominal AMPs (Greig and Akam, 1993). AMPs show a segmental identity specified by expression of different homeotic genes; only for wing disc associated AMPs homeotic gene

expression could not be detected (Roy et al., 1997). Additionally, AMPs express different identity genes, dependent on their location in the embryo (Figeac et al., 2010).

Depending on their precise localisation on the disc, leg and wing disc associated AMPs are further subdivided into different populations. Wing disc associated AMPs with high levels of Vestigial give rise to indirect flight muscles, while AMPs with low levels of Vestigial form direct flight muscles (Sudarsan et al., 2001). Similarly, leg disc associated AMPs display subpopulations that give rise to specific leg muscles (Maqbool et al., 2006). However, AMPs that are transplanted to a different region can fuse to myoblasts of this region and are reprogrammed. For example, AMPs derived from wing discs can fuse to abdominal AMPs and form abdominal muscles (Lawrence and Brower, 1982; Roy and Vijayraghavan, 1997).

Interestingly, segregation of adult FCs and adult FCMs differs from the embryo. For instance, selection of FCs and FCMs from the abdominal pools of AMPs is not mediated by Notch, but by Fibroblast growth factor (FGF) receptor signalling (Dutta et al., 2004; 2005). How the differentiation of myotubes into fibrillar or tubular muscles is controlled is poorly understood. However, the conserved transcription factor Spalt major (Salm) has recently been shown to mediate the fate switch between tubular and fibrillar muscles (Schönbauer et al., 2011).

2.4.2 Myoblast fusion and myotube-tendon attachment

Drosophila myotubes are either formed de novo by fusion of FCs and FCMs (Figure 9) or as in the special case of the dorsal longitudinal muscles (DLMs) by the regeneration type of fusion, where AMPs fuse to remodelled larval templates (Figure 10). The study of myoblast fusion has largely focused on the *Drosophila* embryo. However, many key players identified in the embryo have been shown to play similar roles in adult fusion suggesting that the main mechanisms and molecular players are reused (Dutta et al., 2004; Mukherjee et al., 2011).

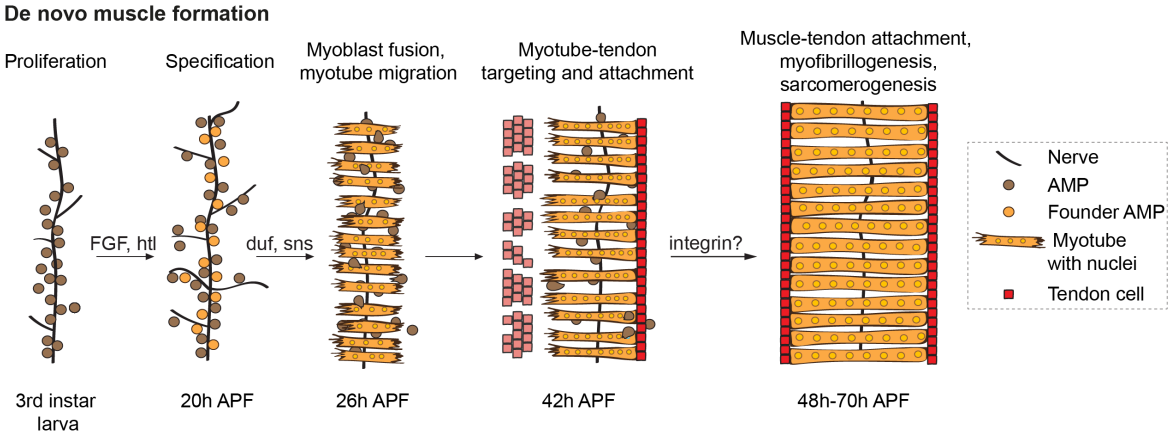

Figure 9 De novo muscle formation of adult dorsal abdominal muscles. Schematic representation of different myogenic steps. Founder myoblasts are singled out from a pool of AMPs while remaining cells become fusion competent cells and fuse to founders. Developing myotubes migrate to tendon cells and form a stable attachment followed by myofibrillogenesis and muscle differentiation. Modified from Weitkunat and Schnorrer, 2014.

The regeneration type of fusion is exclusively used for DLM development. Instead of FCs, three remodelled larval oblique muscles (LOM) serve as templates for FCM fusion (Figure 10). These templates also express the FC marker *duf* (Dutta et al., 2004). Similar to de novo fusion, adhesion of FCMs to templates is also mediated via binding of Duf/Rst to Sns/Hbs on the FCMs indicating that the general molecular players for fusion are reused (Gildor et al., 2012). Fusion of FCMs to the three templates induces their splitting into six developing DLMs, by an unknown mechanism (Fernandes et al., 1991). Interestingly, DLMs can still form if templates are ablated, however myofiber number is often increased (Atreya and Fernandes, 2008; Fernandes and Keshishian, 1996).

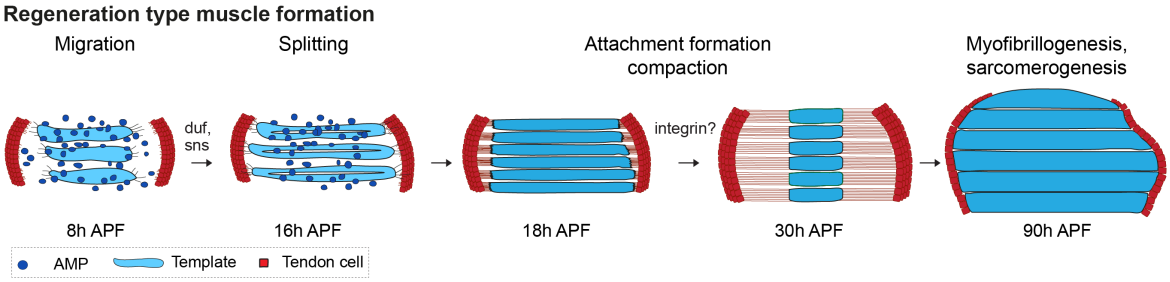

Figure 10 Regeneration type of muscle formation. Schematic representation of the different myogenic steps. AMPs fuse to LOM templates inducing their splitting into six myotubes that target and attach to their tendon cells. After attachment the myotubes compact and myofibrils and sarcomeres are formed. Modified from Weitkunat et al., 2014.

Only little is known about myotube-tendon attachment during adult myogenesis. It has been shown that integrins localise to myotendinous junction during adult myogenesis (Fernandes et al., 1996). Their role during attachment formation has, however, not been studied. Moreover, proteins involved in myotube guidance, tendon recognition, and myotube migration termination have not been identified so far.

2.5 Myofibrillogenesis and sarcomerogenesis

The structure and molecular composition of mature myofibrils and their sarcomeres are well studied as described in 2.1. However, the formation of these myofibrils and sarcomeres is poorly understood. Recent models combine knowledge gained by in silico as well as in vitro, ex vivo and in vivo experiments, performed in different model organisms (Ehler and Gautel, 2008; Myhre and Pilgrim, 2012; Sparrow and Schöck, 2009).

2.5.1 Actin and myosin filament assembly

2.5.1.1 Assembly of actin filaments

The assembly of actin filaments that mature into thin filament pre-cursors, is believed to be the first step during sarcomerogenesis. Actin filaments are formed by ATP dependent polymerisation of monomeric globular actin (G-actin) to fibrous actin (F-actin). The polymerisation of G-actin is usually mediated by actin nucleators such as the Arp2/3 complex and formins (Pollard, 2007). Arp2/3 nucleates formation of branched actin filaments and is essential for fusion (Richardson et al., 2008; Rochlin et al., 2010). In contrast, formins nucleate formation of unbranched actin filaments, reminiscent of those present in sarcomeres (Chesarone et al., 2010; Ono, 2010).

Actin filament growth occurs via the addition of G-Actin to the filament, which can take place at the barbed (+) end or the pointed (-) end of the filament. However, addition of new actin monomers to the actin filament is considerably more efficient at the barbed (+) end. This results in actin treadmilling characterised by higher actin polymerisation at barbed (+) ends and higher actin depolymerisation on pointed (-) ends (Le Clainche and Carlier, 2008). Enhancers of actin treadmilling such as ADF/cofillin or actin-filament stabilisers such as Tropomyosin can modulate actin turnover. This regulation of actin turnover plays a critical role for sarcomere development and stability (Ono, 2010).

2.5.1.2 Integrins as actin nucleation sites

Actin polymerisation has been shown to correlate with the strength of integrin adhesion sites and vice versa (Vicente-Manzanares et al., 2009a). Integrin adhesion complexes are directly connected to actin by interaction with actin-binding proteins like Talin and α-actinin (Wiesner et al., 2005). Talin binds to the adaptor proteins Focal adhesion kinase (FAK) and Vinculin, which can bind to ARP2/3 (DeMali et al., 2002; Serrels et al., 2007). Through this connection to ARP2/3, integrin mediated adhesion could be coupled to actin assembly.

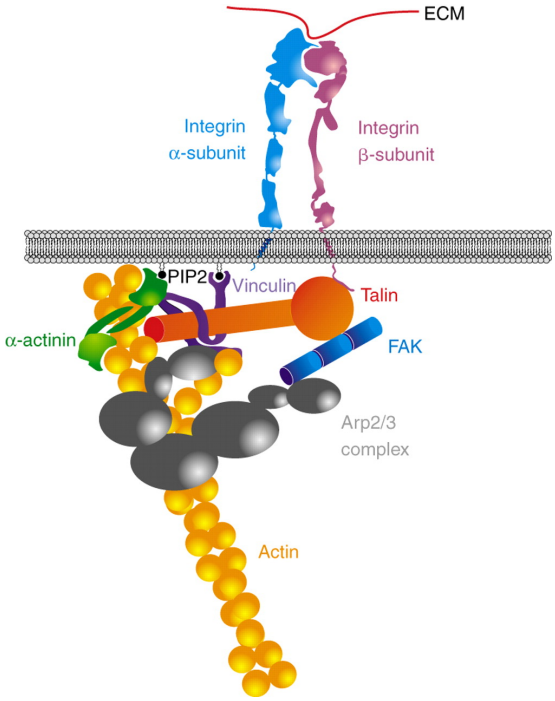

Figure 11 Intracellular adapter molecules link integrins to actin. Talin and Vinculin connect β-Integrin tails directly to actin. Talin further interacts with α-actinin that links actin, and with FAK that interacts with Arp2/3. Image from Vicente-Manzanares et al., 2009a.

Moreover, α-actinin can crosslink different actin filaments at their barbed (+) ends. Crosslinking of actin filaments by α-actinin directly influences actin filament assembly and stiffness, providing an additional link between integrins and actin filament formation (Otey and Carpen, 2004). Importantly, α-actinin is among the first proteins detected in myofibrils, where it forms so called I-Z-I bodies that consist of at least two actin filaments connected via one or more α-actinin molecules (Gregorio and Antin, 2000; Sanger et al., 2005). Thus, integrins could also influence actin polymerisation in the context of myofibrillogenesis.

2.5.1.3 Assembly of myosin filaments

Myosin filaments can be formed of non-muscle or muscle myosin respectively. Myosin filaments form via interactions of essential domains in their C-terminal rod region, resulting in parallel and anti-parallel stacks of myosin (Thompson et al., 2012). Importantly, these filaments can only assemble if myosin hexamers are activated by phosphorylation. If myosin is in the non-phosphorylated off-state it forms a so called inactive-head structure, in which the C-terminal rod domain is not accessible (Vicente-Manzanares et al., 2009b).

For the coordinated formation of thick filaments, core proteins that incorporate into the thick filament like titin, Paramyosin or Flightin as well as chaperones that aid folding and assembly of myosin molecules are essential (Craig and Woodhead, 2006) (Myhre and Pilgrim, 2012). In sarcomeres, myosin bundles are connected tail-to-tail via Obscurin, Myomesin and other M-line proteins forming bi-directional thick filaments (Agarkova and Perriard, 2005).

2.5.1.4 Connecting thick and thin filaments

The organisation of thick filaments depends heavily on thin filaments and vice versa. Actin filaments have been proposed to act as templates for myosin thick filament assembly, while myosin filaments can organise actin filaments into acto-myosin fibrils (Applegate and Pardee, 1992). Especially the activity of myosin ATPase is essential for sarcomerogenesis, as has been shown in ex vivo models (Ramachandran et al., 2003; Soeno et al., 1999). But also in vivo myosin is essential for sarcomere formation. For example, a null-mutation in *myosin heavy chain* (*Mhc*) encoding the only *Drosophila* muscle Mhc leads to severe sarcomerogenesis defects with no thick filaments forming. Z-bodies can assemble in the absence of myosin but do not organise into Z-discs (O'Donnell and Bernstein, 1988). Complementary to these results, a null-mutation of the mainly flight muscle specific actin, *Act88F*, in *Drosophila* leads to severe sarcomerogenesis defects with no thin filaments forming. M-lines and thick filaments can assemble but are not well aligned (Beall et al., 1989; Nongthomba et al., 2001).

Moreover, the giant protein titin has been implied in connecting thick and thin filaments. In vertebrates, titin spans entire half sarcomeres and interacts at its N-terminus with α-actinin and at its C-terminus with myosin and myomesin. Because of titins localisation and its interactions with M-line and Z-disc and because of its early detection with nascent sarcomeres, it has been proposed to act as molecular blueprint for sarcomere assembly. Titin has been suggested to first bind α-actinin and to recruit myosin and myomesin with its N-terminal end. Then titin is believed to recruit M-line proteins via interaction with its C-terminal end (Ehler et al., 1999; Rudy et al., 2001; Tokuyasu, 1987; Tskhovrebova and Trinick, 2003). However, *Drosophila* titin isoforms do not connect all the way from the M-line to the Z-disc, challenging this model (Bullard et al., 2006).

2.5.2 Myofibrillogenesis models

As discussed in section 2.5.1 the precursors of thick and thin filaments can assemble independent of each other. However, it is still debated how they are organised into a periodic sarcomeric pattern. Several models suggest the ordered formation of pre-myofibrils that sequentially develop into mature myofibrils. The most prominent model is the pre-myofibril model of Sanger that was extended by Schöck and colleagues (Sanger et al., 2005, Sparrow and Schöck, 2009). In contrast, the model of Holtzer, which was extended by Rui et al., suggests that multiple protein complexes form separately and assemble in a non-sequential manner (Holtzer et al., 1997; Rui et al., 2010). It is important to note that even though these models are different, they are not mutually exclusive.

2.5.2.1 The pre-myofibril model

The pre-myofibril model from Sanger and colleagues suggests the stepwise maturation of pre-myofibrils via nascent myofibrils to mature myofibrils (Figure 12). The pre-myofibril model assigns a central role to non-muscle myosin, which can be detected in a periodic pattern, before appearance of muscle myosin filaments in early fibrils (Du et al., 2003). According to the model, actin is associated with α-actinin containing Z-bodies (also called I-Z-I complex) and is linked via non–muscle myosin filaments. Non-muscle myosin, actin and Z-bodies form pre-myofibrils consisting of mini-sarcomeres. Successive alignment of Z-bodies as well as integration of titin and muscle myosin filaments matures pre-myofibrils into nascent myofibrils. As muscle myosin filaments in nascent myofibrils are not regularly organised and overlap with each other, nascent myofibrils appear non-striated. Addition of further Z-disc and M-line proteins like Telethonin and Myomesin as well as complete replacement of non-muscle myosin filaments by muscle myosin filaments completes the process and mature myofibrils are formed (Sanger et al., 2010).

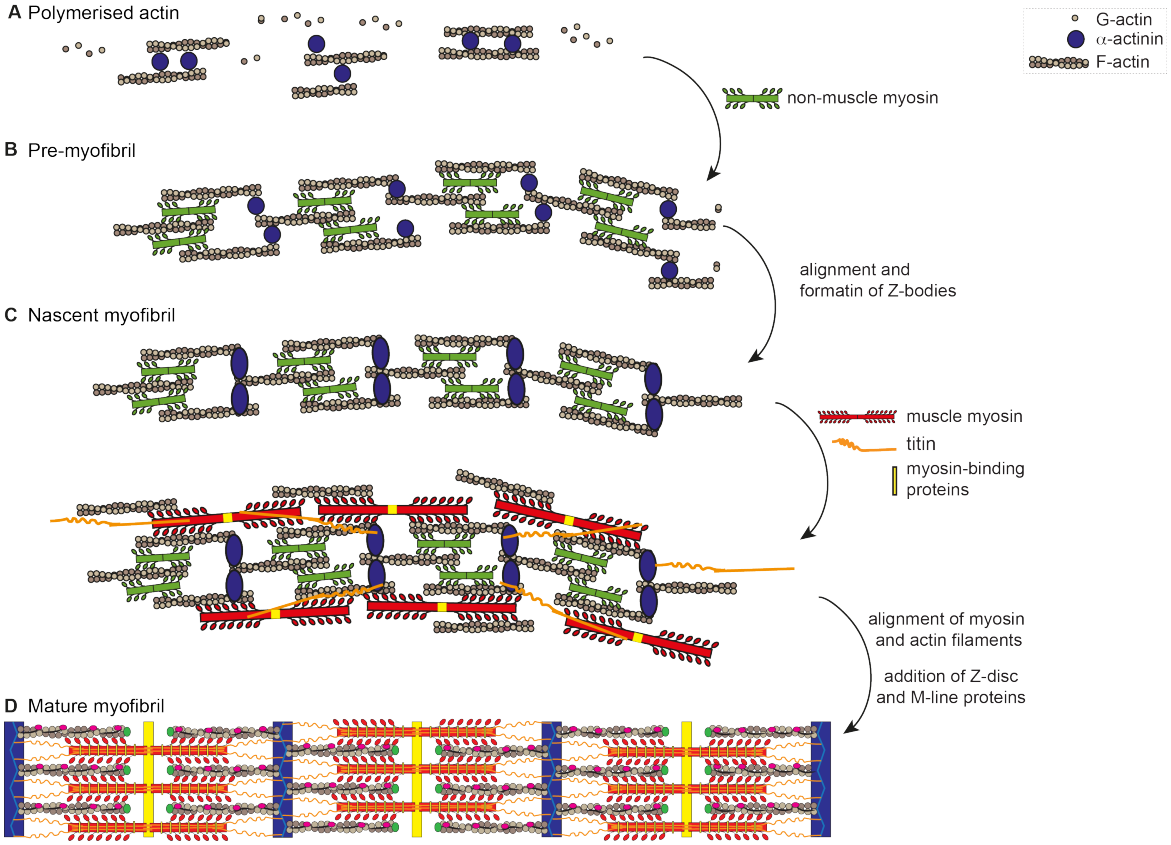

Figure 12 Schematic representation of the pre-myofibril model. A-B| Formation of pre-myofibrils by actin crosslinking via α-actinin and subsequent incorporation of non-muscle myosin C-D| Sequential maturation of non-muscle myosin based pre-myofibrils to nascent myofibrils and finally to mature myofibrils. For simplicity integrins are not depicted. Based on Sanger et al., 2005.

The pre-myofibril model from Sanger was extended by addition of integrins as nucleation and anchoring points by Sparrow and Schöck. According to their model, pre-myofibrils are formed at the cell cortex by integrin triggered actin nucleation and subsequent α-actinin and non-muscle myosin incorporation. Pre-myofibrils are anchored at pre-costameres via the interaction of α-actinin and integrins. The elastic molecule titin localises at α-actinin sites in its coiled form at this step. Next, the essential step for the pre-myofibril model follows. Non-muscle myosin is exchanged for muscle myosin, displacing α-actinin to the costameres, where more α-actinin is recruited and Z-bodies are formed. During this process titin is stretched and regulates spacing of the sarcomere. Finally, Z-bodies are aligned into Z-discs. The mature sarcomere displays regularly spaced Z-discs, M-lines, A-Bands and I-Bands (Sparrow and Schöck, 2009).

2.5.2.2 The two-state model

The two-state model of Rui and colleagues suggests that different small complexes are formed individually (state 1) and then assemble simultaneously into a sarcomeric structure (state 2) (Rui et al., 2010) (Figure 13). The two-state model is an extension of a first model formulated by Holtzer and colleagues. The basis for this model has been provided by the observation that bipolar Mhc filaments and I-Z-I bodies can assemble independently (Ehler et al., 1999; Schultheiss et al., 1990). According to Holtzer et al., first early I-Z-I bodies are formed by actin, α-actinin, titin and nebulin. These I-Z-I bodies differ in length and are irregularly spaced. Independently of I-Z-I bodies, myosin filaments self-assemble via lateral alignment of myosin. These nascent myosin filaments are stabilised by addition of titin and myomesin. Next, non-striated myofibrils form via the incorporation of myosin filaments into stress fiber like structures consisting of I-Z-I bodies. As both complexes are not periodically organised yet and appear in different stages of maturation, no striations are visible. Only irregularly spaced α-actinin dots can be distinguished in non-striated myofibrils. Finally, striations form via the organisation of Mhc-filaments and I-Z-I bodies and the reconfiguration of Z-Band proteins. Following the formation of A- and Z-Bands, I-Z-I bodies mature into I-Z-I-brushes by addition of Troponin and Tropomyosin, regulating the thin filament length (Holtzer et al., 1997).

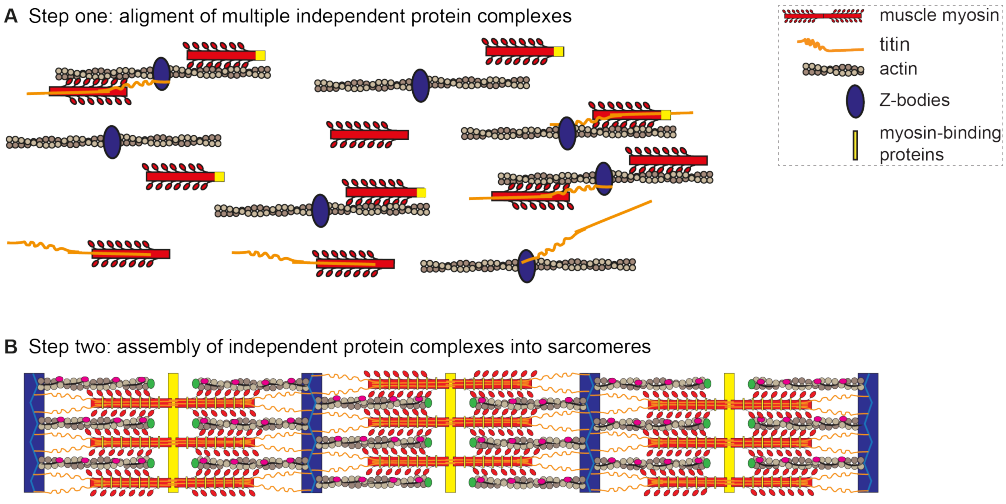

Figure 13 Schematic representation of the two-state model. Multiple protein complexes assemble independent of each other and align then to form a mature sarcomere. For simplicity integrins are not depicted. Based on Rui et al., 2010.

In contrast to the model of Holtzer et al., Rui and colleagues propose not only the separate formation of I-Z-I and myosin complexes, but also of Tn-Tm and integrin complexes as well as a putative tension sensor complex, consisting of Zipper-ZASP-α-actinin, as step

one. In step two, these complexes assemble into sarcomeres. Assembly is aided by integrin complexes at the cell surface that anchor I-Z-I complexes and by subsequent formation of tension (Rui et al., 2010).

2.5.3 Role of tension in myofibrillogenesis

Tension has been suggested to be essential for formation as well as maintenance of myofibrils and sarcomeres. Evidence for a role of tension in these processes is provided from studies on different systems and from modelling data.

Studies analysing the role of tension in sarcomere formation or maturation often prevent force generation by blocking of muscle contraction. This can be achieved by applying myosin inhibitors to myoblast cultures or by using paralysed mutants. For example, Rui and colleagues analysed sarcomere morphology in paralysed *Drosophila* embryos and observed the disruption of sarcomere structure; indicating that force is needed for sarcomere maturation (Rui et al., 2010). Additionally, Skwarek-Maruszewska et al. detected the exchange of complete actin filaments in maturating sarcomeres in cultured rat cardiac myotubes. By addition of myosin inhibitors, they could show that turnover of these actin filaments is dependent on contractility. They propose that new actin filaments are polymerised during myofibril maturation and that non-functional actin filaments undergo contractility-dependent depolymerisation (Skwarek-Maruszewska et al., 2009). Their results indicate that tension created by myotube contraction could serve as quality control for newly assembled actin filaments.

Indications for a role of tension during development are derived from cell culture experiments on chicken skeletal myocytes. Pharmacological inhibition of Mhc motor activity resulted in disorganised arrangement of myofibrils and lack of sarcomeres. Interestingly, these effects can be reversed when the Mhc motor inhibition is removed (Kagawa et al., 2006; Soeno et al., 1999). Similar pharmacological studies have been carried out in cultured *Xenopus* myotubes, where myofibril bundling was affected and sarcomere number was reduced. Sarcomeric defects however were much weaker compared to the experiments using chicken myoblasts (Ramachandran et al., 2003).

Moreover, theoretical predictions propose that bipolar actin and myosin filaments can self-assemble into a periodic pattern, if a defined threshold of directed tension is reached (Yoshinaga et al., 2010). Further modelling approaches predict that the forces generated by actin treadmilling can be sufficient to organise actin filaments and localise myosin filaments to the pointed minus ends. Prerequisites for this self-organisation are

crosslinking of actin filaments and presence of bipolar myosin filaments (Friedrich et al., 2012). Both in silico approaches support a possible self-assembly of bipolar myosin and actin filaments into a striated pattern in the presence of tension.

Taken together, these studies indicate that myofibrillogenesis depends on presence of tension in the forming myofibril. However, comparably few studies investigate the role of tension for myofibrillogenesis and the majority of these studies are based on in vitro and ex vivo systems or in silico approaches that require further testing in model organisms. A fundamental question that has not been tested so far is, if tension is built-up during myogenesis in vivo. Therefore, it would be essential to establish a method to measure tension in vivo and – if tension is formed – to manipulate it, in order to analyse its impact on myofibrillogenesis and sarcomerogenesis.

3 Results

3.1 Identification of novel genes controlling adult myogenesis

3.1.1 Selection of genes for the adult myogenesis screen

In order to identify molecules controlling different steps of *Drosophila* adult myogenesis a muscle specific RNAi screen was performed. Gene selection for this adult myogenesis screen was based on a systematic genome-wide RNAi screen using the muscle-specific driver *Mef2-Gal4* to eliminate gene function exclusively in the muscles. 18.8% of the 10461 genes tested in this genome-wide screen displayed lethality at different developmental stages (Schnorrer et al., 2010). As adults cannot eclose from the pupal case without a functional muscle network, knock-down of genes specifically required for adult myogenesis should lead to late pupal or pharate lethality. Therefore, the 1077 genes scored as late pupal and pharate lethal in the genome-wide screen were chosen as basis for candidate selection for the adult myogenesis screen. From this set of 1077 genes, bioinformatically predicted transcription factors and transmembrane proteins were selected. Transcription factors were selected because they have the potential to regulate myoblast diversification and myotube differentiation by directly influencing gene expression. Transmembrane proteins were selected because they have the potential to regulate migration and myotube attachment by directly influencing cell adhesion and cell-cell signalling. Available *UAS-RNAi-line*s for the selected genes were ordered from the Vienna Drosophila RNAi Center (VDRC) (Dietzl et al., 2007) (Table 13 and Figure 14).

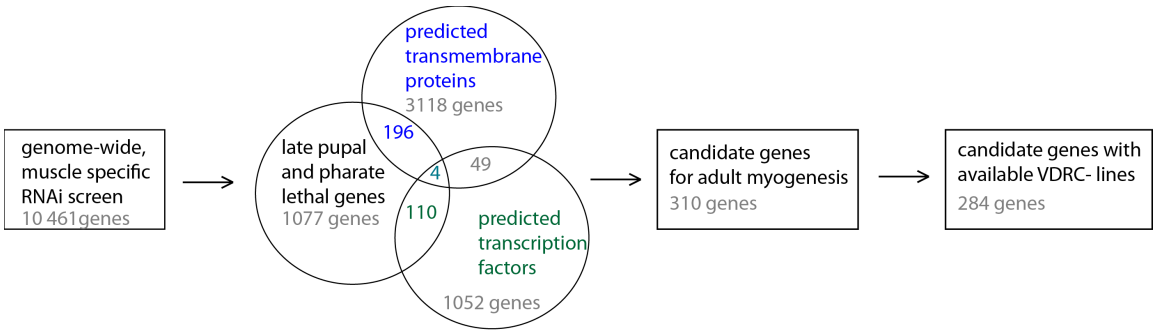

Figure 14 Schematic representation of gene selection for the adult myogenesis screen. 196 predicted transmembrane proteins and 110 predicted transcription factors as well as 4 genes predicted as both were selected from the late pupal and pharate lethal set of the genome-wide screen. RNAi-lines for 284 of those genes were analysed.

3.1.2 Characterisation of phenotypic classes

All analysed genes had been classified as late pupal or pharate lethal and, therefore, are likely to play a role in adult myogenesis (Schnorrer et al., 2010). To determine the specific step of adult myogenesis and the muscle type in which these genes could function, muscle morphology was analysed after gene knock-down. Similar to the genome-wide RNAi screen *Mef2*-Gal4 was used to drive muscle-specific hairpin expression. In addition, actin was genetically labelled by UAS-controlled expression of globular moesin actin-binding domain fused to GFP (GFP-Gma) for visualisation of the muscles (Figure 15).

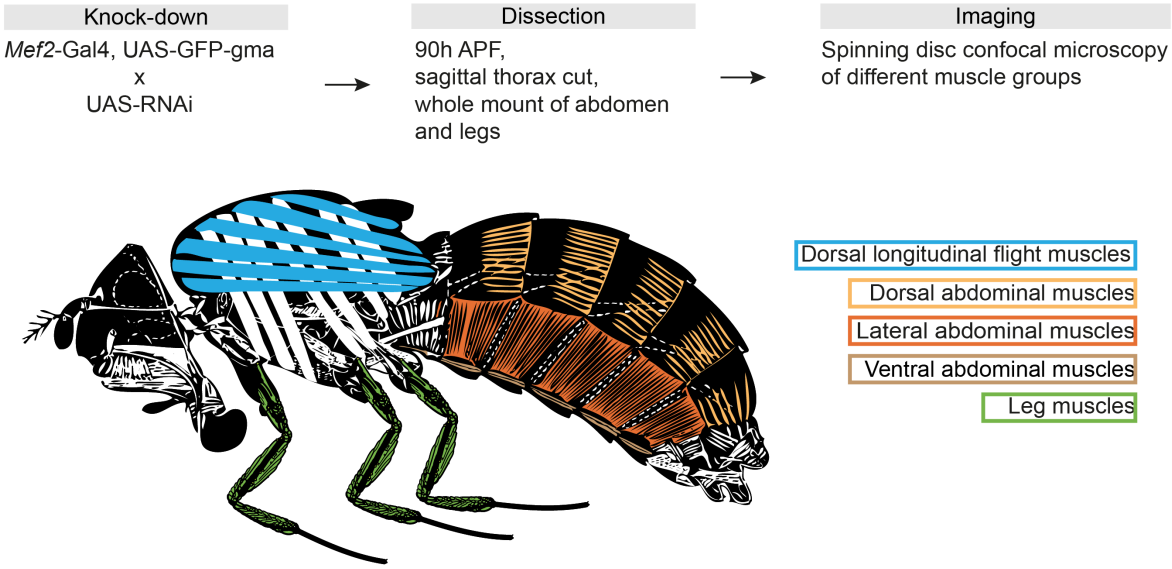

Figure 15 Screening strategy and schematic representation of *Drosophila* adult musculature. *Mef*2-Gal4, UAS-GFP-Gma flies were crossed to UAS-RNAi, dissected at 90h AFP and imaged using a spinning disc confocal microscope. Morphology of dorsal longitudinal indirect flight muscles (blue), dorsal, lateral and ventral abdominal muscles (brown) and leg muscles (green) was analysed. Muscles represented in white were not analysed, scheme modified from Miller, 1950.

At 90h APF pupae were freed from the pupal case, thoraxes were fixed and cut sagittally, while abdomen and legs were prepared as whole mounts. Muscles were imaged with a spinning disc confocal microscope (Weitkunat and Schnorrer, 2014). Control images of *Mef2*-Gal4 crossed to w^- (w^{1118}) are shown in Figure 16.

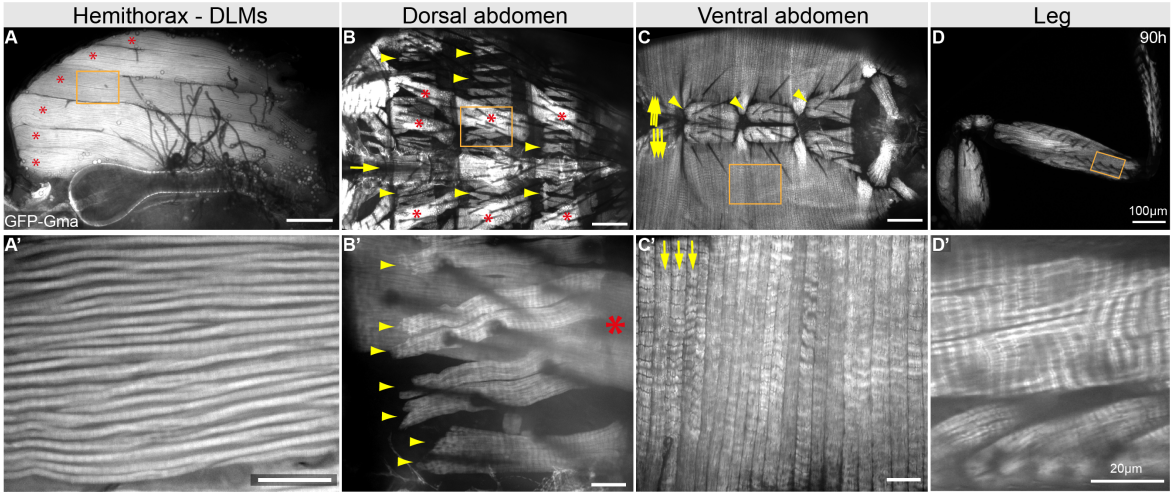

Figure 16 *Drosophila* adult musculature. 90h APF confocal images of whole mount samples and sagittal thorax cuts of *Mef2*-Gal4, UAS-GFP-Gma crossed to w^{-}. A| Hemithorax showing 6 DLMs (asterisks). Box magnified in A'. A'| Higher resolution image of A, showing parallel myofibrils spanning the DLM. B| Dorsal image of an abdomen; showing dorsal abdominal myotubes (arrowheads), persistent larval dorsal muscles (asterisks) and the heart tube (arrow) spanning the abdomen. Box is magnified in B'. B'| Higher resolution image of B showing dorsal abdominal myotubes (arrowheads) and one persistent larval dorsal muscle (asterisk). C| Ventral image of the abdomen, showing lateral myotubes running dorsal to ventral (arrows) and ventral abdominal myotubes spanning the hemisegments anterior to posterior (arrowheads). Box is magnified in C'. C'| Higher resolution image of C showing lateral abdominal myotubes (arrows). D| Image of a leg, showing leg muscles. The box is magnified in D'. D'| Higher resolution image of D showing leg muscles.

Muscle morphology of DLMs, abdominal dorsal, abdominal ventral, abdominal lateral and leg muscles was analysed after RNAi mediated knock-down for each of the 284 genes respectively. Observed phenotypes were categorized into five different classes with up to four subclasses (Figure 17):

(1) Fiber presence – subclasses: missing myofibers, additional myofibers

(2) Fiber shape – subclasses: short myofibers, thin myofibers, other

(3) Fiber position

(4) Fibrillar organisation – subclasses: irregular, frayed, thin, other

(5) Sarcomeric organisation – subclasses: missing sarcomere, other

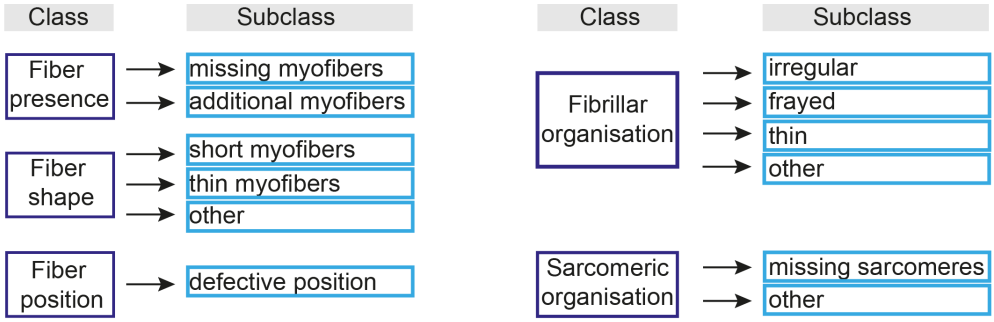

Figure 17 Overview for the five phenotypic classes with their respective subclasses.

Example images for each of the classes and subclasses are presented in Figure 18 and Figure 19.

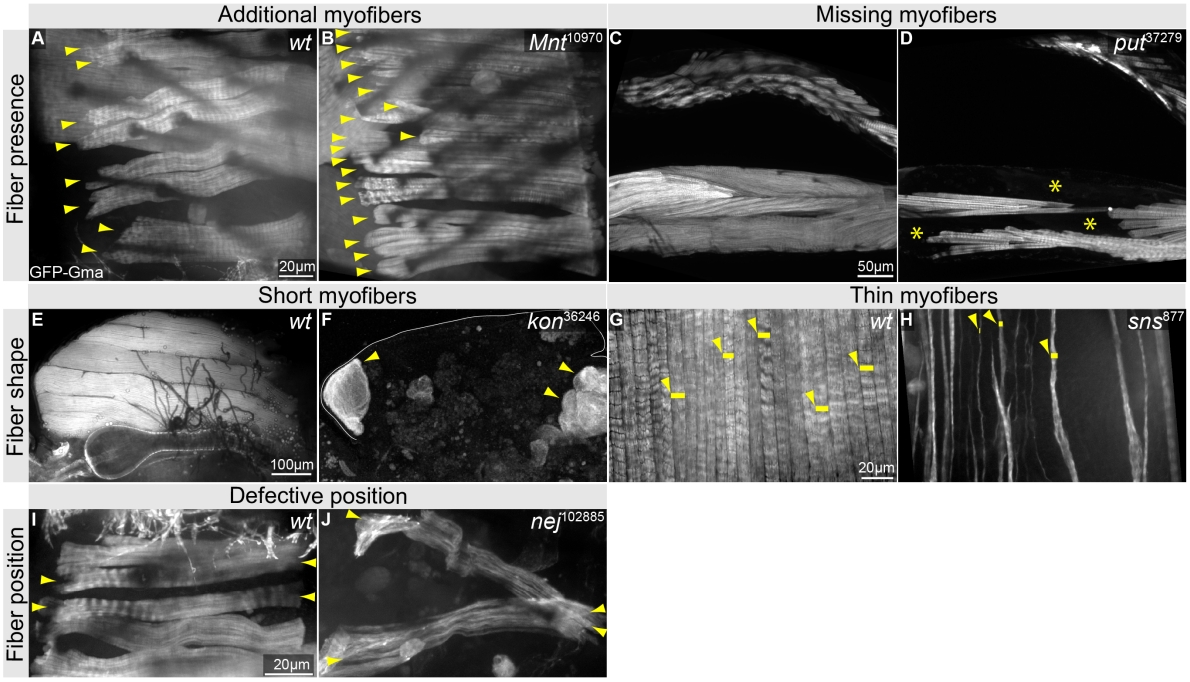

Figure 18 Phenotypic examples for fiber presence, shape and position. 90h APF confocal images of whole mount samples and sagittal thorax cuts of *Mef2*-Gal4, UAS-GFP-Gma crossed to w^- or the indicated RNAi-line (superscript). Classes are depicted in grey boxes on the left and subclasses are indicated in grey boxes on the top. A, B| Dorsal abdominal muscles; w^- (A), 8 myotubes (arrowheads) span the imaged region; Mnt^{10970} (B), 18 myotubes span the imaged region. C, D| Leg muscles; w^- (C), the leg is filled with myotubes; put^{37279} (D), many myofibers are missing (asterisks). E, F| DLMs; w^- (E), 6 DLMs span the complete hemithorax; kon^{36246} (F), DLMs are round (arrowheads) or missing. G, H| Lateral abdominal muscles; w^- (G), equally thick myofibers fill the imaged region; sns^{877} (H), myofibers are thin, and do not fill the imaged region. Arrowheads point to single myotubes, width is indicated with horizontal bars. I, J| Dorsal abdominal muscles; w^- (I), myofibers span a large portion of the segment from anterior to posterior and are horizontally aligned; nej^{102885} (J) , myofibers span a large portion of the segment but are not horizontally aligned, posterior sides of the myofibers seem to attach to the same place. Arrowheads mark both ends of two myofibers.

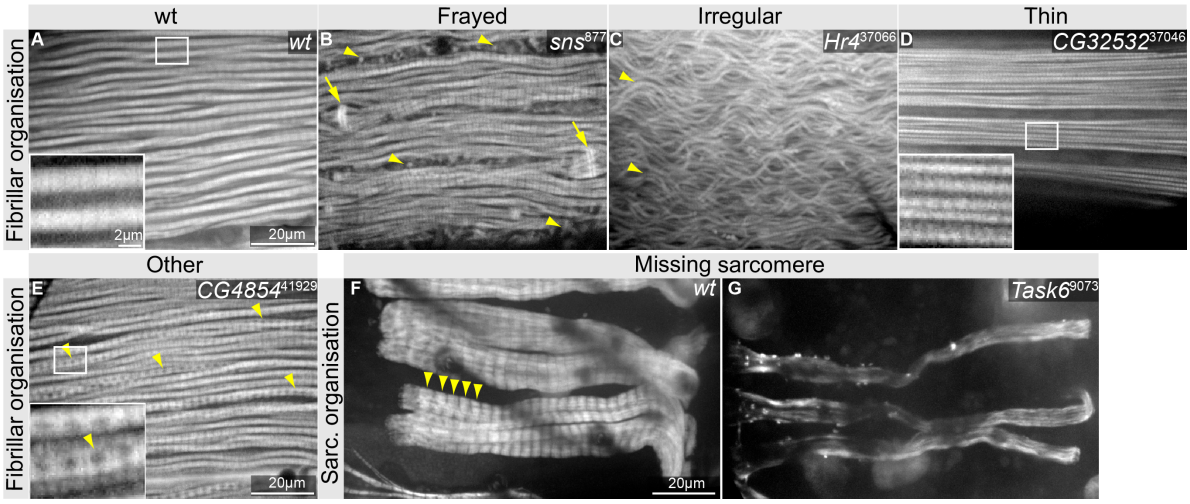

Figure 19 Examples for fibrillar and sarcomeric organisation classes. 90h APF confocal images of whole mount samples and sagittal thorax cuts of *Mef2*-Gal4, UAS-GFP-Gma crossed to w^- or the indicated RNAi-line (superscript). Classes are depicted in grey boxes on the left and subclasses are indicated in grey boxes on the top. A-E| DLM fibrils; w^- (A), myofibrils span the complete fiber and are aligned horizontally; sns^{877} (B), fibrils are frayed (arrowheads), dotted GFP-Gma between fibrils visible, some fibrils fuse together at several Z-discs and form zebra bodies (arrows); $Hr4^{37066}$ (C), myofibrils are organised in irregular waves instead of straight lines (arrowheads); $CG3235^{37046}$ (D), fibrils are very thin; $CG4854^{41929}$ (E), GFP-Gma is excluded from round areas in-between M-lines (arrowheads). Box area is magnified in the inlay. F, G| dorsal abdominal muscles; w^- (F) GFP-Gma localises in sarcomeric pattern. Arrowheads indicate GFP-Gma accumulations at Z-discs. $Task6^{9073}$ (G); GFP-Gma is equally distributed, within the myotube, occasional GFP-Gma blobs are visible on myotube surface.

The different classes were assessed for each muscle type individually. Therefore, one gene can be sorted into multiple classes for various muscle types. Since the DLMs are the only analysed fibrillar muscles, "fibrillar organisation" was exclusively determined for DLMs. Out of the 284 genes screened; 116 genes showed a strong knock-down phenotype in at least one class. Of the genes without strong knock-down phenotype in any class, 26 genes showed a weak knock-down phenotype (Figure 20).

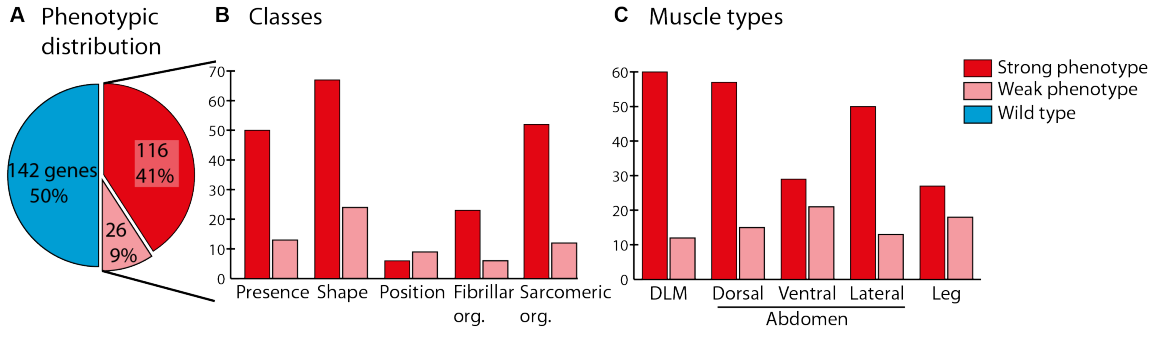

Figure 20 Phenotypic classification of the adult myogenesis screen. A| Phenotypic distribution in total. B| Phenotypic distribution of the five main classes. C| Phenotypic distribution of the five analysed muscle types. Y-axes display gene numbers.

"fiber shape" is the largest class (91 genes) followed by "sarcomeric organisation" (64 genes) and "fiber presence" (63 genes). Fewer genes show a fibrillar organisation defect (29 genes). As "fibrillar organisation" was only scored in the thorax, these 29 genes still represent a fairly large group. The smallest class is "fiber position" (15 genes).
The most affected muscle types are the abdominal dorsal muscles (72 genes) and DLMs (72 genes). They are followed by dorsal lateral muscles (63 genes), dorsal ventral muscles (50 genes) and leg muscles (45 genes).
In conclusion, 143 potential myogenesis genes were identified for one or more of the five different muscle types.

3.1.3 Identification of groups of genes from the adult myogenesis screen

Combination of phenotypic information with the muscle type can lead to the discovery of interesting sets of genes. (1) General regulators of a common myogenic step: genes that are sorted into the same class for various different muscle types could play a general role in myogenesis. (2) Muscle type specific regulators of a common myogenic step: genes that show knock-down phenotypes only for one muscle type could be muscle type specific myogenesis genes. (3) Genes that are involved in the same pathway or are part of the same complex: genes displaying the same pattern of phenotypes in the same muscle types could share a signalling pathway or function in the same complex.

3.1.3.1 General regulators of a common myogenic step – example fusion

Many of the 143 potential myogenesis genes score in more than one phenotypic class and muscle type. Genes that are found within similar classes for more than one muscle type could be general factors for a specific process. For example, thin myotubes can indicate a defect in fusion, as adult muscle precursors in the abdomen target and attach to their correct tendon cell even in the absence of fusion but stay very thin due to the lack of mass addition by fusion (Dutta et al., 2004). Some examples for genes that are classified as "thin myofibers" in several muscle types are *sns*, *VAP-33B* and Adenosine receptor (*AdoR*). The knock-down of all three genes is causing thin fibers in the three different abdominal muscle types indicating a general role in myoblast fusion (Figure 21).

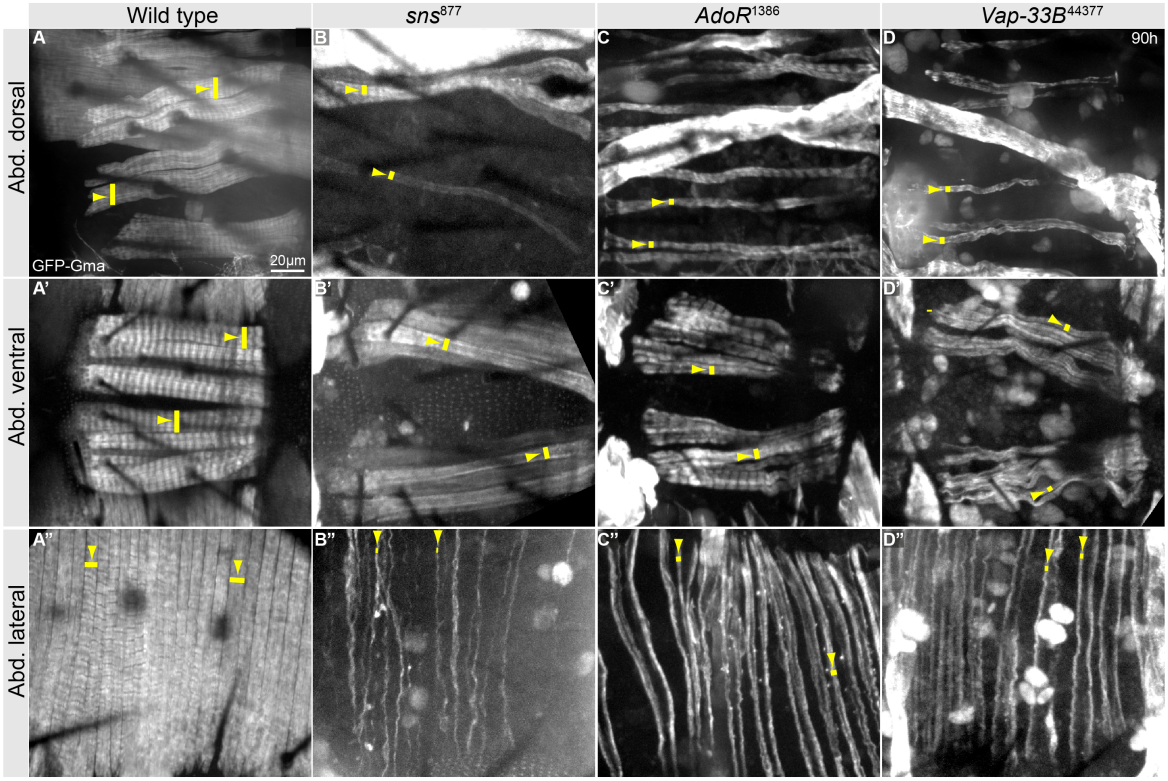

Figure 21 Examples of potential general fusion factors. 90h APF confocal images of whole mount samples of *Mef2*-Gal4, UAS-GFP-Gma crossed to w^- or the indicated RNAi-line. A| w^-, dorsal abdominal muscles. A'| w^-, ventral abdominal muscles. A''| w^-, lateral abdominal muscles B-B''| sns^{877}, all abdominal myofibers are thin. C-C''| $AdoR^{1386}$, all abdominal myofibers are thin. D-D''| $VAP\text{-}33B^{44377}$, all abdominal myofibers are thin. Lines mark myofibril thickness.

As nuclei are added by fusion of adult FCMs, fusion defects should lead to reduced nuclei number in the myofibers. Therefore, nuclei were counted in *sns* knock-down pupae as a readout for the number of fusion events. To label both myofibers and nuclei, *mhc*-GFP, *Mef2*-Gal4>UAS-histone-RFP was crossed to w^- or sns^{877}, pupal offspring were imaged at 90h APF (Figure 22). While control myofibers are syncytial and harbour many nuclei, sns^{877} myofibers harbour only one nucleus indicating a complete fusion block.

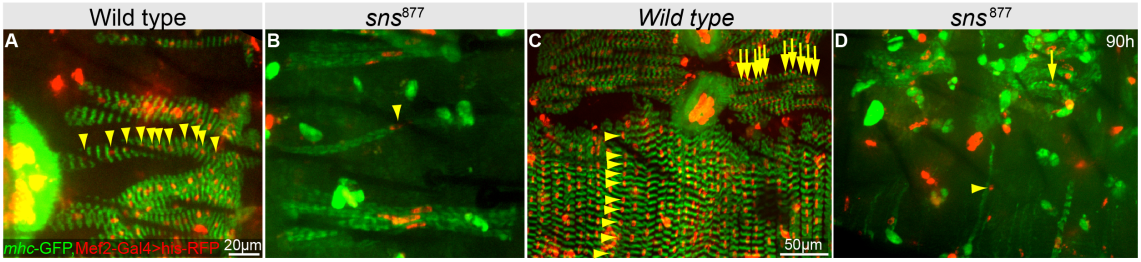

Figure 22 *sns* knock-down myofibers have only one nucleus. 90h APF confocal images of whole mount samples of *mhc*-GFP; *Mef2*-Gal4>UAS-histone-RFP crossed to w^- or sns^{877}. A| w^-, dorsal abdominal muscles, arrowheads point to nuclei within a single myofiber. B| sns^{877}, dorsal abdominal myofibers are thin and have only one nucleus. C| w^-, lateral and ventral abdominal muscles, arrows point to nuclei within a single ventral myofiber, arrowheads point to nuclei within a single lateral myofiber. D| sns^{877} lateral and ventral abdominal myofibers are thin and have only one nucleus.

A complete list of potential fusion genes, displaying a phenotype in the class: “fiber shape” and subclass: “thin myofibers”, is shown in Table 1. Interestingly, not only the known fusion gene *sns*, but also *lame duck* (*lmd*) that initiates *sns* expression in embryonic FCMs (Duan et al., 2001) is identified as potential fusion regulator in the adult myogenesis screen. This indicates the reuse of embryonic fusion genes for adult myogenesis. Moreover, identification of known fusion genes shows that fusion regulators can be detected using the adult myogenesis screen.

Table 1 Potential fusion regulators. Genes that show a “thin myofiber” knock-down phenotype.

Gene	Phenotype strength	Process or characteristic (predicted)
Dl	strong	Fusion
lmd	strong	Fusion
N	strong	Fusion
sing	strong	Fusion
sns	strong	Fusion
kon	strong	Myogenesis
nej	strong	Myogenesis
slmo	strong	Myogenesis
H15	weak	Myogenesis
Kul	strong	Metalloproteinase
CG34420	weak	Metalloproteinase
AdoR	strong	Receptor
Ddr	strong	Receptor
Hr78	strong	Receptor
put	strong	Receptor
babo	weak	Receptor
CG30340	weak	Receptor
Task6	strong	Transporter/ channel
CG3409	weak	Transporter/ channel
Trn	weak	Transporter/ channel

Gene	Phenotype strength	Process or characteristic (predicted)
kto	strong	Mediator complex subunit
MED7	weak	Mediator complex subunit
MED17	weak	Mediator complex subunit
Rpb10	strong	General processes
RpII15	strong	General processes
RpL28	strong	General processes
CG2990	weak	General processes
Ccp84Ag	strong	Chitin binding
dup	strong	Replication
Vap-33B	strong	Vesicle binding
kek1	weak	EGFR signaling
Gnf1	weak	AAA ATPase
Dref	weak	Spindle formation
CG1161	strong	Transmembrane domain
CG4552	strong	Rab GTPase activator act.
CG5969	strong	Transmembrane domain
CG6470	strong	Transcription factor
CG8974	strong	E3 ring finger domain
CG13047	strong	
CG30377	strong	Transmembrane domain
CG32532	strong	Hox domain
CG13287	weak	Transcription factor

3.1.3.2 Muscle type specific regulators – example TFIID

In addition to general factors for different myogenic steps, muscle type specific factors can be isolated from the screen data. This muscle specificity however, has to be taken with care since inefficient knock-down could mask a general phenotype. A group of genes that show exclusively thoracic knock-down phenotypes are *TBP-associated factor 1* (*Taf1*), *Taf4* and *Taf6*. (Figure 23). The phenotype of all three Tafs looks strikingly similar. All are sorted into the class “fiber shape” for DLMs. The subclass is “other”, since DLM myofibers are in most cases not completely round but often display muscle fiber regions that still span the

thorax. As *Taf4* and *Taf6* are both part of the core complex of TFIID, which is decorated with Taf1 (Wright et al., 2006), the similar phenotype of all three knock-downs indicates an important role for TFIID during DLM development.

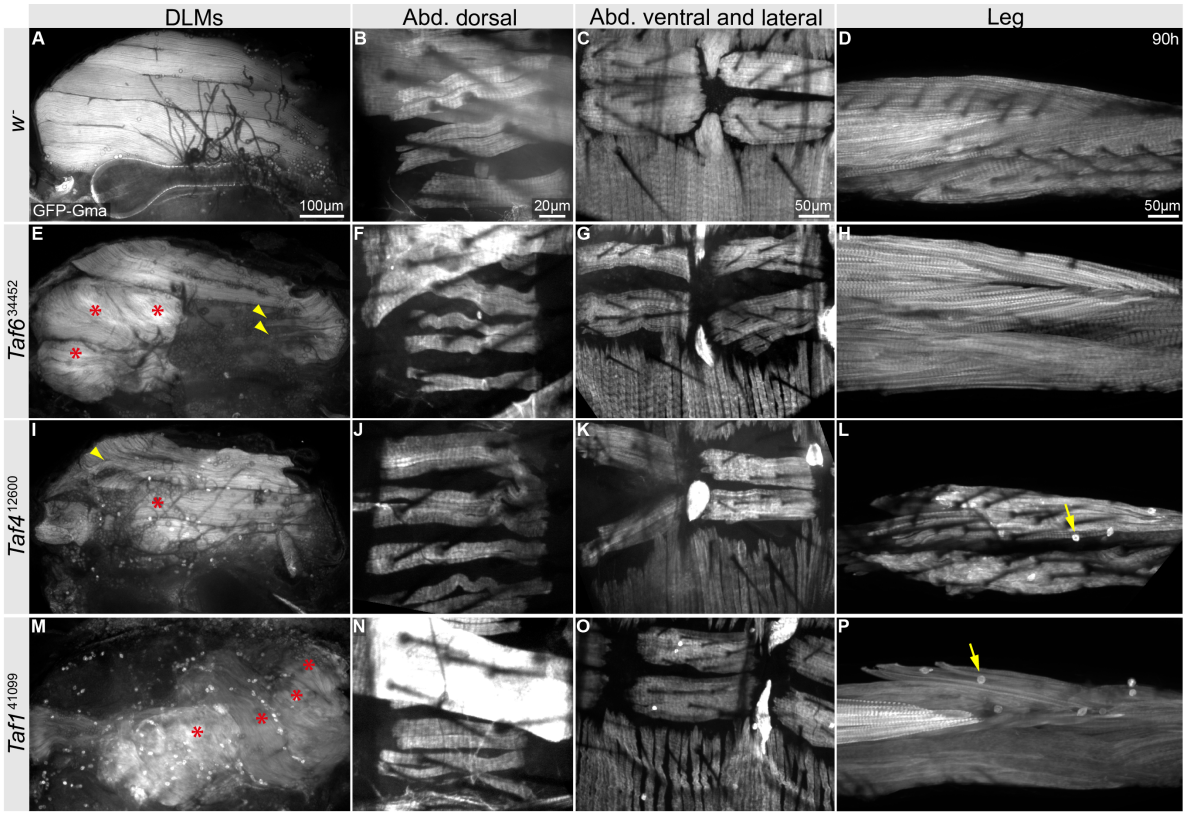

Figure 23 Taf1, Taf4 and Taf6 show a strong shape defect specific for DLMs. 90h APF confocal images of sagittal thorax cuts and whole mount samples of *Mef2*-Gal4, UAS-GFP-Gma crossed to w^- or the indicated RNAi-line. A| w^-, DLMs, myofibers span the width of the thorax. B| w^-, abdominal dorsal muscles. C| w^-, abdominal ventral and lateral muscles. D| w^-, leg muscles. E| $Taf6^{34452}$, DLMs show defective shape (asterisk) and display thin myofiber parts (arrowhead). F-H| $Taf6^{34452}$, abdominal dorsal, ventral and lateral muscles as well as leg muscles do not show a phenotype. I| $Taf4^{12600}$, DLMs show defective shape (asterisk) and display thin myofiber parts (arrowhead). J,K| $Taf4^{12600}$, abdominal dorsal, ventral and lateral muscles don't show a phenotype. L| $Taf4^{12600}$, leg muscles, additional round cells (arrow) most likely unfused AMPs. M| $Taf1^{41099}$, DLMs, show short myofibers (asterisk). N,O| $Taf1^{41099}$, abdominal dorsal, ventral and lateral muscles don't show a phenotype. P| $Taf1^{41099}$, leg muscles, additional round cells (arrow) most likely unfused AMPs.

3.1.3.3 Genes involved in the same pathway – examples Notch and TGF-β pathways

The identification of Taf1, Taf4 and Taf6 as potentially essential DLM developmental regulators could also serve as example for the identification of genes that might work together in a complex or pathway to ensure normal muscle development. By isolating genes with similar knock-down phenotypes from the adult myogenesis screen, more groups of genes, working together in a complex or pathway, can be identified. Two examples are genes involved in TGFβ and Notch pathways.

Notch is known to influence the expression of *sns* and thereby playing an essential role for fusion in both, embryonic and adult myogenesis (Bour et al., 2000; Gildor et al., 2012). Depletion of Notch prevents splitting of the three LOM templates. Consequently, three instead of six DLMs form (Anant et al., 1998). This phenotype can be explained by stark reduction of fusion, due to fusion arrest or a defect in earlier steps that are required for fusion. Both Notch and its ligand Delta could be identified in the adult myogenesis screen. Notch and Delta knock-downs result in extremely similar phenotypes. Both genes are classified as "missing myofibers" for DLMs, as they display only three fibers. Moreover, Notch and Delta are classified as "thin myofibers" for abdominal lateral muscles. Both phenotypes, missing DLMs and thin abdominal fibers are indicating fusion defects.

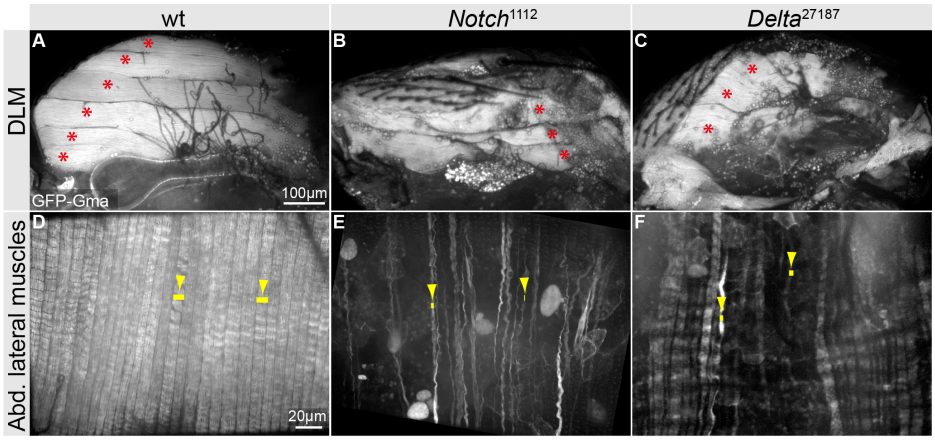

Figure 24 Delta and Notch show similar phenotypes. 90h APF confocal images of sagittal thorax cuts and whole mount samples of *Mef2*-Gal4, UAS-GFP-Gma crossed to w^- or the indicated RNAi-line. A| w^-, hemithorax with six DLMs (asterisks). B, C| *Notch*^{1112} (B), *Delta*^{27187} (C), hemithorax with three DLMs. D| w^-, abdominal lateral myofibers, lines span the width of single lateral myofibers. E, F| *Notch*^{1112} (E), *Delta*^{27187} (F) lateral myofibers are thin.

Three components of the TGF-β pathway were analysed in the adult myogenesis screen. These are the TGF-β family receptors *punt* (*put*) and *baboon* (*babo*), as well as *Smad on X* (*Smox, dSMAD2*), a transcription factor acting downstream of Babo (Brummel et al., 1999; Das et al., 1999). Interestingly, all three are classified as "missing leg myofibers" and "thin abdominal dorsal myofibers". Moreover, S*mox* and *babo* knock-downs cause thin DLMs. These data strongly indicate an essential role for TGF-β signalling during adult myogenesis.

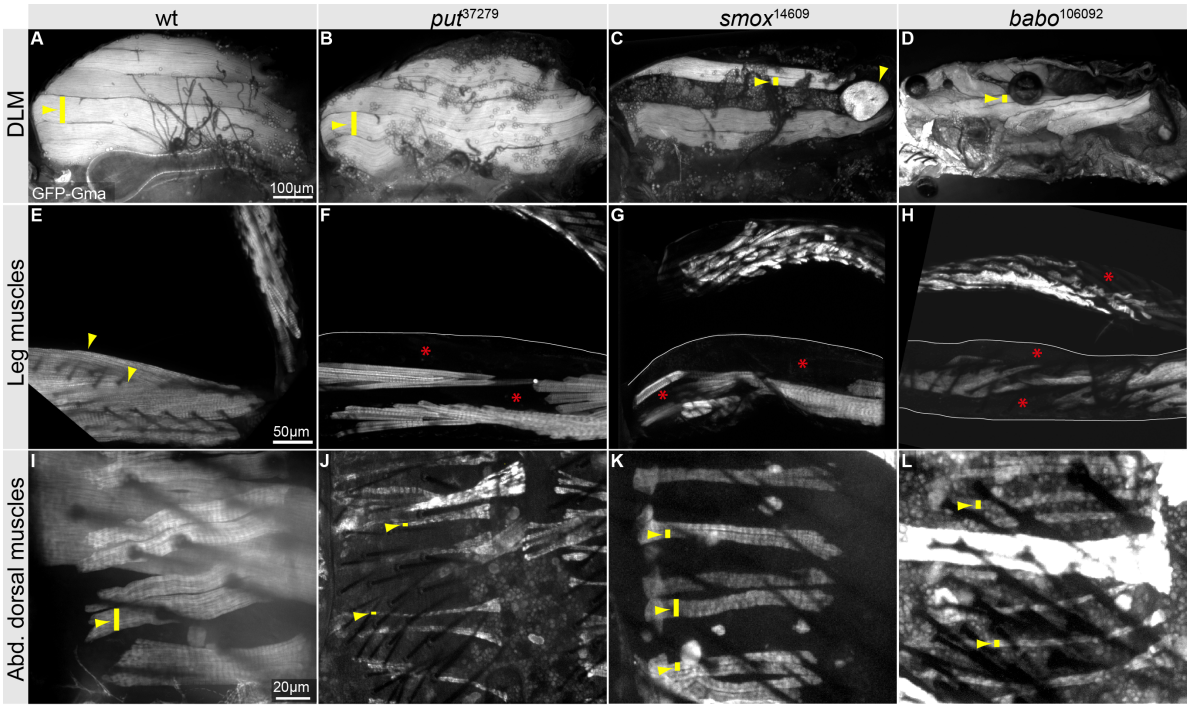

Figure 25 The TGF-β pathway components Put, Smox and Babo show similar phenotypes. 90h APF confocal images of sagittal thorax cuts and whole mount samples of *Mef2*-Gal4, UAS-GFP-Gma crossed to w^- or the indicated RNAi-line. A| w^-, hemithorax with 6 DLMs. B| *put*^{37279}, hemithorax with 6 DLMs. C| S*mox*^{14609}, hemithorax with 4 stretched, thin and 1 to 2 round DLMs. D| babo^{106092}, hemithorax with thin DLMs. E| w^-, leg muscles. F-H| *put*^{37279} (F), *Smox*^{14609} (G) and *babo*^{106092} (H), leg myofibers are missing (asterisk). I| w^-, abdominal dorsal muscles. J-L| *put*^{37279} (J), *Smox*^{14609} (K) and *babo*^{106092} (L), abdominal dorsal myofibers are thin. Lines span the width of a single myofiber, leg outlines are partially indicated with white lines.

3.1.4 Detailed phenotypic classification of DLMs and abdominal dorsal muscles

A detailed analysis for each class including subclasses is provided in this section. The analysis focuses on DLMs and abdominal dorsal muscles since they are well suited for both live imaging and immunohistochemistry analysis enabling detailed characterisation of selected candidates. Further, only genes with strong knock-down phenotypes in DLMs (60 genes) or abdominal muscles (57 genes) were selected from the adult myogenesis screen to restrict the analysis to the strongest candidates (Figure 26).

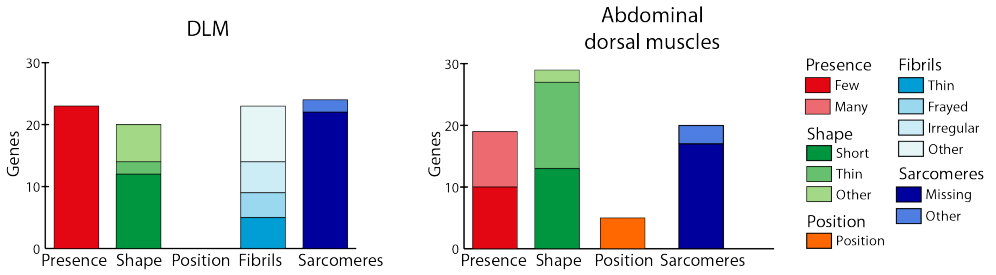

Figure 26 Phenotypic distribution of DLMs and abdominal dorsal muscles. Stack charts representing sorting of the 60 genes with strong DLM phenotypes and the 57 genes with strong abdominal dorsal muscle phenotypes into classes and subclasses. Note that genes can be sorted into more than one class.

3.1.4.1 DLM classes

The phenotypic distribution of the 60 genes with a strong DLM knock-down phenotype is illustrated in Figure 26. Interestingly, additional DLMs were not observed in the adult myogenesis screen. Similarly, no strong position defects indicating muscle guidance failure could be observed in DLMs. As DLMs form via fusion of adult myoblasts to remodelled larval templates, which are specified as founders of DLMs and are positioned during head eversion, DLMs might be more resistant to specification and guidance defects. As no additional DLM fibers could be discovered in the adult myogenesis screen all of the 23 genes in the class “fiber presence” are found in the subclass “missing myofibers”. DLMs are the only muscle type, for which few myofibers do not indicate a specification defect for founder myoblasts since their number is specified by splitting of the larval templates. Therefore, missing DLMs indicate splitting defects as in Delta and Notch (Figure 24), but could also be caused by myotube degradation.

For DLM “ fiber shape” the largest subgroup is “short myofibers”. The 12 genes in DLM “short myofibers” are potential candidates for attachment initiation, maturation or maintenance, since unattached muscles are rounding up as shown for example in the case of integrin mutant embryonic muscles (Newman and Wright, 1981). Genes with a very strong attachment phenotype could in addition be classified as “missing myofibers”, since short fibers can be degraded until 90h APF. Interestingly, all genes categorised as strong for “DLM fiber shape” in the subclass “other” show a similar phenotype of DLMs that display very different thickness and shape throughout a single myofiber, which was introduced in Figure 23. Apart from *TAF1* and *TAF6* this group includes *CG3634, enhancer of yellow 3* (*e(y)3*), *kohtalo* (*kto)* , and *Transportin* (*Trn)*.

The two classes scoring for cytoskeletal organisation or myotube differentiation are “sarcomeric organisation” and “fibrillar organisation”. The class “sarcomeric organisation” harbours 24 genes. 22 of these genes are scored as “missing sarcomeres” representing an

extremely severe phenotype. Weaker phenotypes are most likely not visible due to the limited resolution used in the adult myogenesis screen. Defects at the next higher level – the DLM-fibrils – are much easier to detect with the screening strategy. The class "fibrillar organisation", which was exclusively scored for DLMs, since they are the only fibrillar muscles analysed, harbours 23 genes (Table 2). Examples for the subclasses "frayed", "irregular" and "other" are displayed in Figure 19. Importantly, only 7 out of the 23 genes showing a "fibrillar organisation" knock-down phenotype are also scored as DLM "fiber presence" or "fiber shape", suggesting that the fibrillar defect is not a secondary effect due to myofiber defects. Both fibrillar and sarcomeric organisation phenotypes indicate defective cytoskeletal remodelling or muscle differentiation.

Table 2 List of genes showing a strong fibrillar organisation phenotype.

Gene	Process or characteristic (predicted)
dnt	Myogenesis
ebi	Myogenesis
H15	Myogenesis
sns	Myogenesis
AdoR	Receptor
Ddr	Receptor
Hr4	Receptor
Hr78	Receptor
Task6	Transporter / channel
Trn	Transporter / channel
VhaPPA1-1	Transporter / channel
Chd1	Helicase
dom	Helicase

Gene	Process or characteristic (predicted)
CG32532	Hox domain
CG4854	Transcription factor
Taf1	Transcription factor
Trf4-2	Nuclear localisation signal
CG1161	Transmembrane protein
CG3625	Signaling sequence
CG5096	Leucine rich repeats
not	Deubiquitination
RpL28	Spindle organisaton
Vap33B	Vesicle binding

3.1.4.2 Abdominal dorsal muscle classes

The phenotypic distribution of the 57 genes with a strong knock-down phenotype in abdominal dorsal muscles is illustrated in Figure 26.

The class "fiber presence" harbours 19 genes (Table 3). "fiber presence" is a very interesting class since missing or additional fibers can indicate an early specification defect. Especially exciting is the subclass of "additional myofibers" since they, in contrast to "missing myofibers", cannot result from other defects that lead to myofiber degradation. Therefore, genes classified as additional abdominal dorsal fibers should represent genes that are essential for myoblast specification or proliferation.

Table 3 Candidates for specification. Genes that show a strong knock-down phenotype in abdominal dorsal "fiber presence". "missing myofibers" are marked with "-" and "additional myofibers" are marked with "+". Note groups of histone deacetylases and transcription factors as well as metalloproteinases.

Gene	Subclass	Process or characteristic (predicted)
Etl1	+	Helicase
Rpd3	+	Histone deacetylase
Sirt6	+	Histone deacetylase
CG6470	+	Transcription factor
Mnt	+	Transcription factor
amos	-	Transcription factor
ebi	-	Transcription factor
Cad86c	+	Adhesion protein
kon	-	Adhesion protein, myogenesis

Gene	Subclass	Process or characteristic (predicted)
mmd	+	Metalloproteinases
CG34420	-	Metalloproteinases
Kul	-	Metalloproteinases
Nep1	-	Metalloproteinases
CG18418	+	Mitochondrial process
Marf	-	Mitochondrial process
slmo	-	Mitochondrial process
CG13029	+	Transferase
CG14020	-	Transferase
cnc	-	Microtubule polarisation

For "fiber shape" 13 genes are classified as "short myofibers" (appendix, Table 15) and 12 genes are classified as "thin myofibers", representing potential attachment or fusion genes respectively.

The class for potential guidance genes consists of only five genes with strong position defects upon knock-down. These potential guidance genes are *Cadherine86c* (*Cad86c*), *CG14020*, *kon*, *nej* and *Hr78* (Figure 27). C*ad86c* is also classified as strong in "additional dorsal myofibers" and, therefore, the positional defect is likely secondary. *CG14020*, *kon*, *nej* and *Hr78* however are promising guidance candidates. Interestingly, *kon* has been shown to be essential for guidance of a specific subset of embryonic muscles (Schnorrer et al., 2007). Thus, the data from the adult myogenesis screen indicate that *kon* could be reused for guidance of adult muscles.

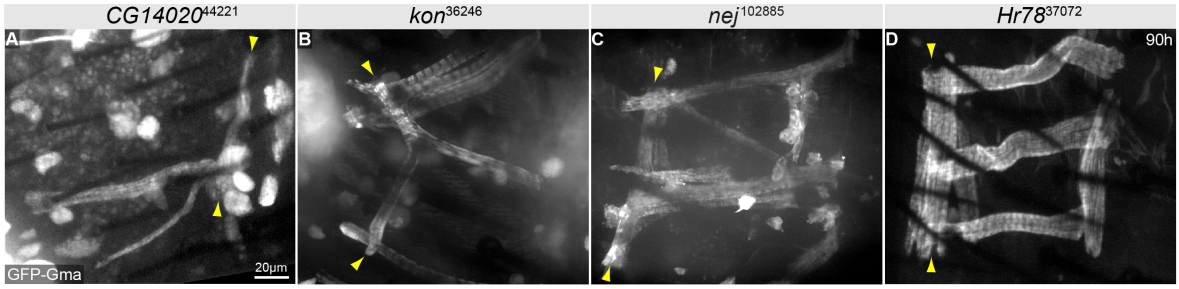

Figure 27 Candidates for muscle guidance of abdominal dorsal muscles. 90h APF confocal images of whole mount samples of *Mef2*-Gal4, UAS-GFP-Gma crossed to the indicated RNAi-line. A-D| *CG14020*^{44221}, *kon*^{36246}, *nej*^{102885} and *Hr78*^{37072}, myofibers show a strong position defect; and seem to share attachment sites. Arrowheads indicate myofibers that are rotated around 90° compared to normally positioned myofibers.

3.1.4.3 Developmental analysis of genes with a strong phenotype

As presented in the last sections (3.1.4.1, 3.1.4.2) "Missing myofibers" indicate specification or splitting defects, while "short myofibers" indicate attachment defects and

"thin myofibers" indicate fusion defects. Any of these three phenotypes, however, might also evolve from partial or complete fiber degradation caused by a different myogenesis defect. Therefore, a group of 36 genes sorted into "fiber presence" or "fiber shape" classes was additionally analysed at an earlier developmental stage, to estimate the contribution of degradation due to other myogenic defects (appendix, Table 20). Furthermore, three genes with a strong position phenotype after knock-down were analysed as guidance candidates. The end of myoblast fusion was selected as early developmental stage. At this stage specification/splitting, migration and guidance are largely completed, while attachment formation and stabilisation is still taking place. Conclusively, genes that show a strong specification/splitting, migration or guidance knock-down phenotype at 90h APF should show this phenotype also at this early stage. In contrast, genes showing an attachment knock-down phenotype should not display a phenotype at the end of fusion since the process is just starting. Therefore, combination of 90h APF and early pupal phenotypes allows for closer characterisation of the process that is defective in the respective knock-down.

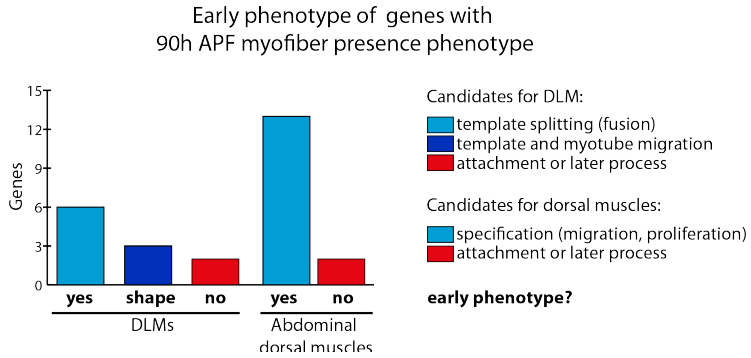

Figure 28 Distribution of early developmental phenotypes for genes that are classified as strong "fiber presence" at 90h. Graph depicts if genes that have a strong presence knock-down phenotype at 90h APF also display a phenotype (weak or strong) at 18h-20h APF (DLMs) or 45-48h APF (abdominal dorsal muscles). X-axes labelling: "yes", fiber presence phenotype is also observed after fusion; "no", no phenotype can be observed after fusion; "shape", myofibers show a shape phenotype.

As timing of DLM and abdominal dorsal development is different, DLMs and abdominal dorsal muscles were analysed at 18h-20h and 45-48h APF, respectively (Figure 28, Figure 30A). More than 80% of the genes classified as "fiber presence" at 90h APF also show a myofiber phenotype at the end of fusion indicating a major role in specification/splitting, proliferation of AMPs or migration (Figure 28).

For DLMs, candidate genes for splitting or template migration can be discriminated. If a gene displays a "missing myofiber" knock-down phenotype at 18h-20h APF it is a strong candidate for splitting since defective splitting prevents the increase of fiber number from

three to six DLM fibers per hemithorax (Figure 29A,B). In contrast, the three genes that display a "myofiber shape" knock-down phenotype are strong candidates for defective template remodelling or migration.

In total 55% of the DLM presence and 87% of the tested abdominal dorsal fiber presence phenotypes could be confirmed at an early stage indicating that they are indeed essential for splitting/specification. These data show that the "fiber presence" class of abdominal dorsal muscles are promising candidates for specification, proliferation and migration of myoblasts.

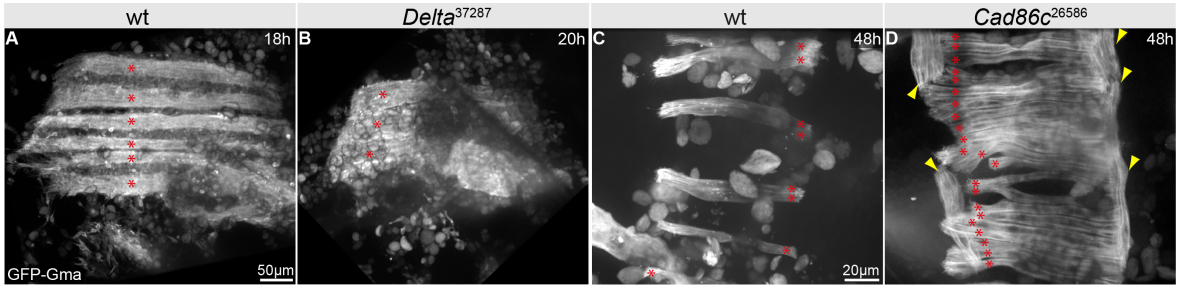

Figure 29 Examples for early presence phenotypes. Confocal images of whole mount samples of *Mef2*-Gal4, UAS-GFP-Gma crossed to w^- or the indicated RNAi-line. DLMs at 18h (A) and 20h APF (B); abdominal dorsal muscles at 48h APF (C,D). A| w^-, templates are completely split, six DLM myofibers are present. B| *Delta*^{37287}, templates are not split, only three DLM myofibers are present. C| w^-, eight abdominal dorsal myofibers span the depicted region. D| Cad86c^{26586}, 22 abdominal dorsal myofibers span the depicted region and are oriented d-v (asterisks), more myofibers are 90° rotated and oriented P-D (arrowheads). Asterisks mark individual myotubes.

Genes classified as strong "fiber shape" at 90h APF are potential fusion or attachment genes. Only 20% of the genes analysed for early DLM knock-down phenotypes show myofiber shape defects and none of the genes analysed for dorsal abdominal myofiber shape knock-down defects do result in an early developmental shape defect (Figure 30A). Attachment defects are not detectable at the end of fusion since attachment is only manifested after that stage. Thus, myotubes that have an attachment defect should appear normal at the early stage. As most myotubes do not show an early defect, the genes classified as "myofiber shape" for DLMs and abdominal dorsal muscles are promising candidates for attachment.

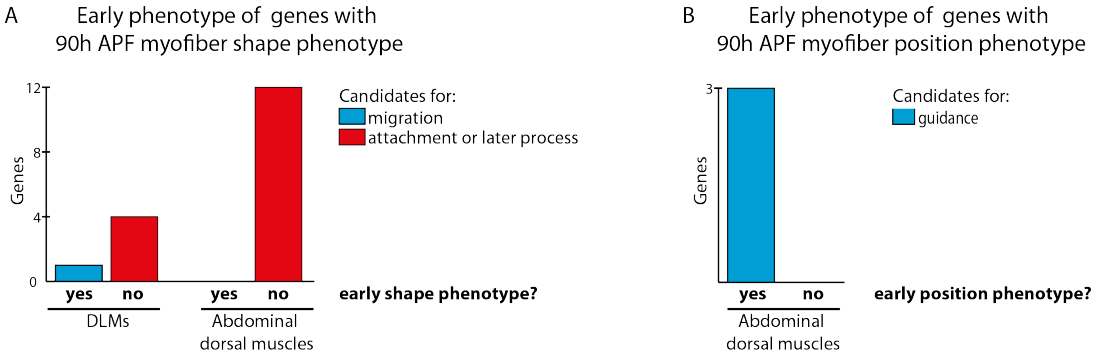

Figure 30 Distribution of early developmental phenotypes. A| Graph depicts if genes that have a strong "myofiber shape" knock-down phenotype at 90h APF also display a "myofiber shape" phenotype (weak or strong) at 18h-20h APF (DLMs) or 45-48h APF (abdominal dorsal muscles). X-axes labelling: "yes", fiber shape phenotype is also observed at an early stage; "no", no phenotype can be observed at an early stage B| Graph depicts if genes that have a strong "fiber position" knock-down phenotype at 90h APF display also a "fiber position" phenotype (weak or strong) at 48h APF. X-axes labelling: "yes", fiber position phenotype is also observed at an early stage; "no", no phenotype can be observed at an early stage.

Moreover, three guidance candidate genes (*Cad86c*, *CG14020* and *kon*) that showed a strong dorsal longitudinal position knock-down phenotype were analysed at 45h-48h APF (Figure 30, Figure 31B,C). Additionally, Kuzbanian-like (Kul) that was classified as weak for "fiber position" was screened early because of an additional strong shape defect at 90h APF. All four genes also show an early position defect after knock-down. *Cad86c* also results in many abdominal dorsal fibers, as in this case the abdomen is filled with myotubes and most space is occupied, defective positioning can be a secondary effect (Figure 29D). In conclusion, genes that were scored as "fiber position" weak or strong and do not display a strong additional myofibers knock-down phenotype are highly likely to be essential for myofiber guidance of abdominal dorsal muscles.

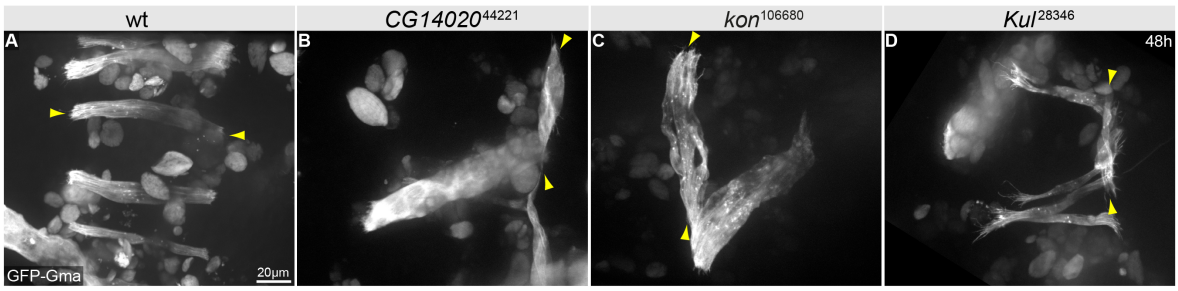

Figure 31 Examples for early position phenotypes. Confocal images of 48h APF whole mount pupae of *Mef2*-Gal4, UAS-GFP-Gma crossed to w^- or the indicated RNAi-line. A| w^-, abdominal dorsal myofibers are oriented d-v. B| *CG14020*^{44221}, abdominal dorsal myofibers are largely oriented P-D. C-D| *kon*^{106680} and *Kul*^{28346} abdominal dorsal myofibers are rotated up to 90°. Arrowheads indicate ends of abdominal myofibers.

3.1.5 Quality control

As the use of RNAi might cause off-target effects, it is important to control for specificity of the hairpin. In order to estimate the possibility of off-target effects the VDRC database provides the s19-score, which is obtained by dividing on-target matches by the sum of on- and off-target matches. But even if the s19-score is close to 1 off-target effects cannot be excluded. In addition, the VDRC GD-hairpins have been randomly inserted into the genome using P-elements, which might cause positional effects and misexpression of neighbouring genes. To confirm the RNAi screening results, additional RNAi-lines from VDRC-KK, TRiP or NIG libraries were analysed for a set of genes that showed strong DLM or abdominal phenotypes. Phenotypes were compared for all 56 genes that were tested with a 2nd RNAi-line, two genes that showed only sarcomeric phenotypes were excluded, since sarcomeric defects are very hard to detect with this screening method (Figure 32).

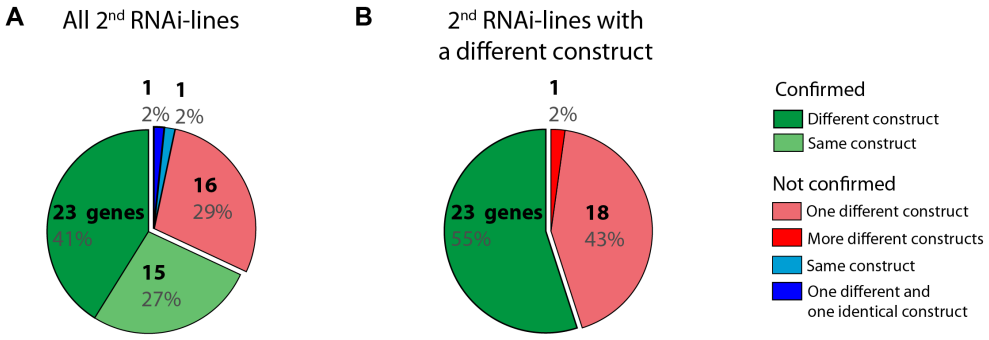

Figure 32 Pie chart showing if knock-down with 2nd RNAi-lines leads to verification of the observed phenotype. Genes that display a strong phenotype in one class and a strong or weak phenotype in the same class for one or more classes are counted as confirmed. A| Showing results for all 2nd RNAi-lines that were screened. B| Showing only the 2nd RNAi-lines that harbour a different hairpin construct. Note: two constructs were confirmed with a 2nd RNAi-line harbouring the same hairpin but could not be confirmed with an other RNAi-line harbouring a different hairpin; these genes are depicted as "confirmed with the same construct" in A and as "not confirmed with a different construct" in B. Numbers of genes and percentage are depicted in the respective pie (2nd RNAi-lines screened together with S. Berchtold).

For 38 genes (68%) of the tested 2nd RNAi-lines, the observed phenotype could verified for one or more classes (Table 4). 2nd RNAi-lines for 23 of these genes contain a different hairpin construct, indicating that the phenotype is not caused by off-target effects or random insertion of the hairpin constructs (appendix, Table 21, Table 22). The remaining 2nd RNAi-lines (15 genes) harbour identical hairpin constructs, excluding positional effects due to random insertion of the constructs (appendix, Table 23) (Figure 32A).

Table 4 Genes that are confirmed with a different hairpin. Genes that display a strong phenotype in one class and a strong or weak phenotype in the same class for at least one out of the 5 main classes are counted as confirmed.

Gene	Different construct	Process or characteristic (predicted)
kon	yes	Myogenesis
lmd	yes	Myogenesis
nej	yes	Myogenesis
slmo	yes	Myogenesis
H15	no	Myogenesis
sing	no	Myogenesis
Delta	yes	Notch pathway
N	yes	Notch pathway
babo	yes	TGF-β pathway
put	yes	TGF-β pathway
Smox	yes	TGF-β pathway
Atac3	yes	Histone modifier
Rpd3	yes	Histone modifier
ato	yes	Transcription factor
Mnt	yes	Transcription factor
CG13287	yes	Transcription factor
CG32532	yes	Transcription factor
CG7372	yes	Transcription factor
Dref	no	Transcription factor
CG10979	no	Transcription factor

Gene	Different construct	Process or characteristic (predicted)
CG34353	yes	Immunoglobulin domains
CG34420	yes	Metalloproteinases
cnc	yes	Microtubule polarisation
Hr4	yes	Receptor
PNUTS	yes	Phagocytosis
rdgA	yes	Kinase
Trn	yes	Transporter/ channel
AdoR	no	Receptor
CG13047	no	Signaling sequence
CG33169	no	Transmembrane domain
CG8974	no	E3 ubiquitin ligase domain
CR13130	no	Signaling sequence
CycG	no	Cycline
Der-1	no	Protein degradation
ox	no	Mitochondrial process
RpL28	no	Spindle organisation
Syx5	no	Vesicle tafficking
Vap-33B	no	Vesicle binding

For a total of 18 genes (32%) the phenotype could not be confirmed (appendix, Table 24). However, only one different hairpin construct was tested for 16 of these genes. It is possible, that the knock-down using this one different construct was inefficient and testing of additional hairpins is recommended.

For two genes (*kto* and *Doa*), the initial phenotype could not be confirmed using 2nd RNAi-lines that carry the same hairpin construct (Figure 32A), indicating that the hairpin did not express well or that the phenotype was caused by a positional effect due to the random insertion of the hairpin construct.

Additionally, second analysis – considering only the 2nd RNAi-lines containing a different hairpin construct – was performed to get a better estimation of the knock-down specificity (Figure 32B). The analysis revealed that 55% of the genes that were re-screened with a 2nd RNAi-line harbouring a different construct could be confirmed.

These data indicate a high knock-down specificity for more than 50% of the analysed genes.

3.1.6 *Kon-tiki* a potential guidance and attachment gene

One especially interesting gene identified in the adult myogenesis screen is *kon*. Kon is conserved up to humans, its mouse homolog is NG2 and its human homolog is CSPG4. Kon is an orphan transmembrane receptor that is essential for targeting of *Drosophila* embryonic VL1 muscles (Estrada et al., 2007; Schnorrer et al., 2007). In the adult myogenesis screen *kon* was classified as "missing myofibers", "thin myofibers", "short myofibers", "myofiber position" defective and "missing sarcomeres" (Figure 34). It displays a strong phenotype in all muscle types, indicating that *kon* is a general myogenesis factor. As attachment defects lead to rounding up and degradation of myofibers, *kon'*s classification as "missing myofibers" and "short myofibers" indicates a role in attachment formation or maintenance. And as guidance defects result in incorrect positioning of myofibers *kon*'s classification as "myofiber position" indicates that *kon* is also involved in myofiber guidance in the adult muscle-tendon system. In conclusion, *kon* is a strong candidate for a general myofiber guidance and attachment factor. As myofiber guidance and attachment are both poorly studied in *Drosophila* adult myogenesis, analysis of the wild type and *kon* knock-down situation should lead to a better insight into guidance and attachment processes.

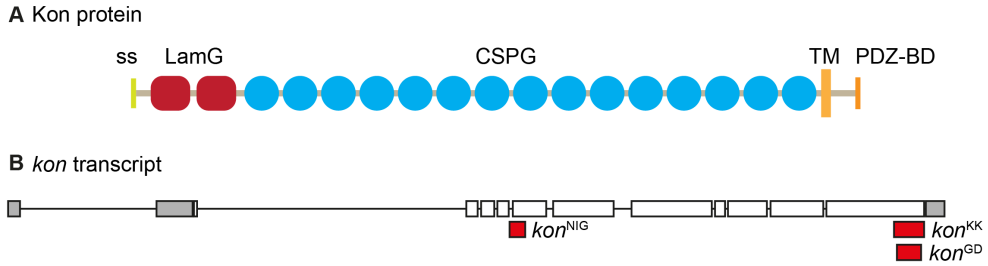

Figure 33 Schematic representation of Kon protein and *kon* transcript. A| Schematic of Kon protein domains: signal sequence (ss), laminin G domains (LamG), chondroitin sulfate proteoglycan (CSPG) repeats, transmembrane domain (TM) and PDZ binding domain (PDZ-B) are depicted. Modified from Schnorrer et al., 2007. B| Schematic of *kon* transcript including regions targeted by the different hairpins. Gray boxes, 5' and 3' UTRs; white boxes, exons; red boxes, regions targeted by the indicated hairpin. Modified from flybase.org.

The *kon* phenotype could be confirmed using several independent hairpins, targeting different regions of the gene, suggesting that the knock-down phenotype is specific to *kon*. All *kon* knock-down phenotypes indicate a strong attachment and guidance defect at 90h APF (Figure 34, Figure 33).

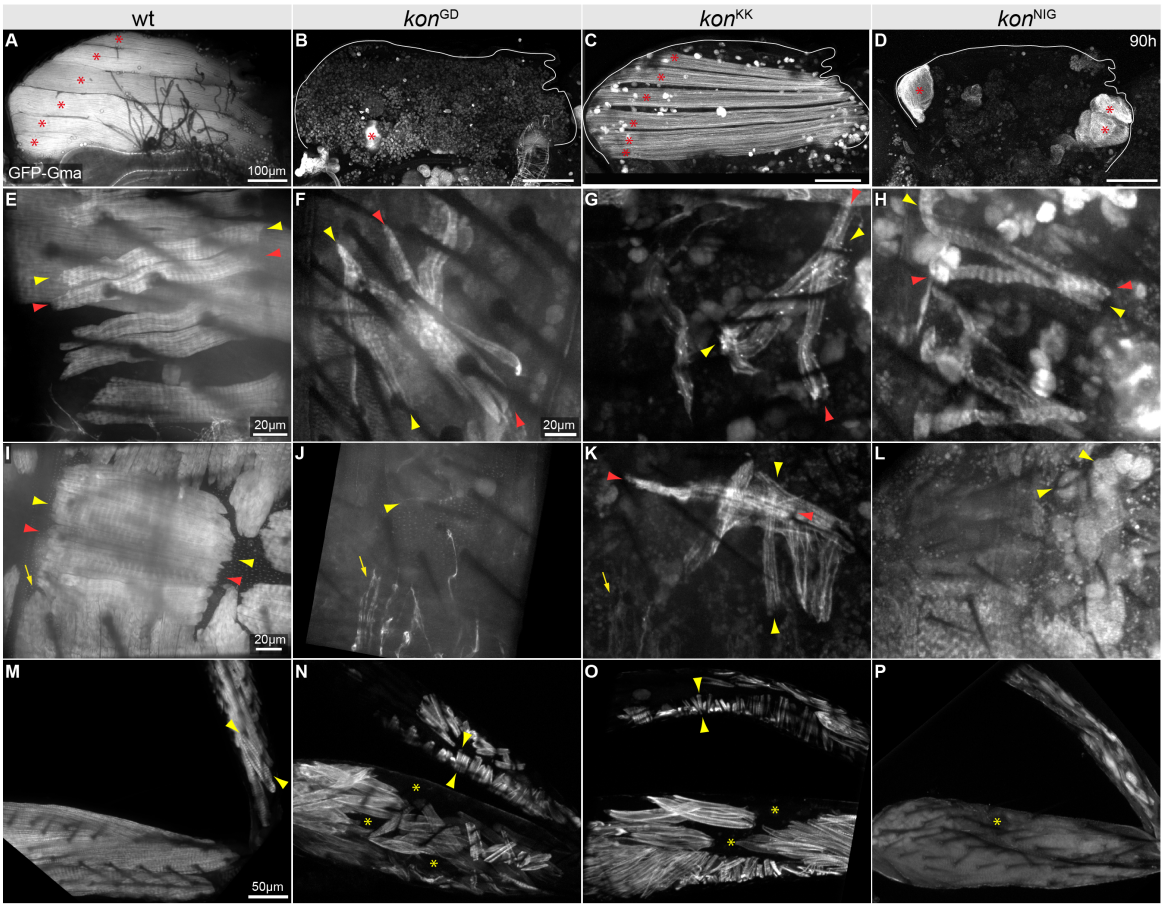

Figure 34 *kon* knock-down phenotype is confirmed with 3 RNAi-lines. Confocal images of 90h APF whole mount of pupal offspring of *Mef2*-Gal4, UAS-GFP-Gma crossed to w^- or the indicated RNAi-line. A| w^-; 6 DLM fibers stretch the thorax, fibers are marked with asterisks. B| kon^{GD}, DLMs are round or missing. C| kon^{KK}, DLMs are thin but stretch through the thorax. D| kon^{NIG}, DLMs are round or missing. E| w^-, abdominal dorsal myofibers run in parallel in A-P position . F| kon^{GD}, abdominal dorsal myofibers are randomly positioned. G| kon^{KK}, many abdominal dorsal myofibers run P-D. H| kon^{NIG}, abdominal dorsal myofibers are not oriented in parallel but meet at the posterior end. I| w^-, abdominal ventral (arrowheads) and lateral (arrow) myofibers. Abdominal ventral fibers run in parallel in A-P position . J| kon^{GD}, abdominal ventral and lateral myofibers are thin. Abdominal ventral myofibers are rotated. J| kon^{KK}, abdominal ventral and lateral myofibers are thin. Many ventral myofibers run P-D. L| kon^{NIG}, some ventral myofibers are thin. M| w^-, leg muscles. N-O| kon^{GD} and kon^{KK} leg muscles; many myofibers are rotated (arrowheads) some regions in the leg do not show myofibers (asterisk). P| kon^{NIG}, leg muscles; some regions in the leg do not show myofibers (asterisk).

To further analyse if short myofibers in *kon* knock-down result from attachment defects, DLM development of pupal offspring of *Mef2*-Gal4>UAS-GFP-Gma crossed to w^-, kon^{NIG} or kon^{KK} was followed by 2-photon imaging (Figure 35). Wild type myotubes migrate to tendon cells, fuse and split (Figure 35A-C). After splitting myotubes compact until the movie stops around 25h APF (Figure 35C-D). In kon^{NIG}, myotubes migrate, fuse and split normally, but form very long protrusions (Figure 35E-H). Moreover, kon^{NIG} myotubes round up when wild type myotubes compact (Figure 35G-H). In kon^{KK}, myotubes migrate, fuse and split normally, but form very long protrusions (Figure 35I-K). Moreover, kon^{KK}

are delayed in compaction and display rounded myotube tips (Figure 35K-L). These results are in accordance with the 90h dissections, where *kon*^{NIG} resulted in round myotubes while *kon*^{KK} caused thin myotubes. The early onset of the round phenotype in *kon*^{NIG} further supports an essential role for Kon during myotube attachment.

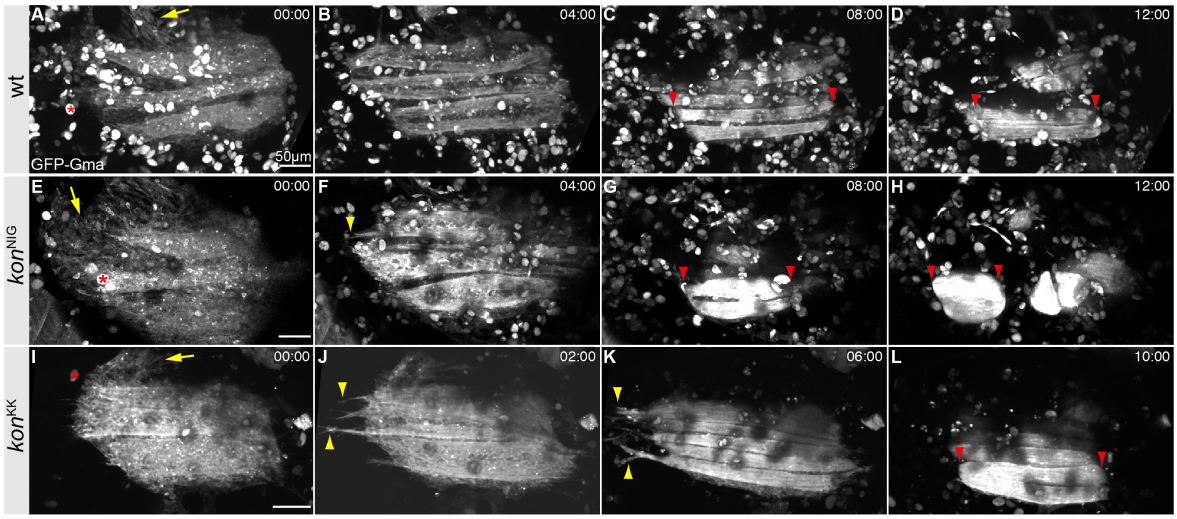

Figure 35 *kon*^{IR} knock-down during DLM-development. Stills from 2-photon microscope movies of pupal offspring of *Mef2*-Gal4>UAS-GFP-Gma crossed to *w*$^{-}$ (A-D), *kon*^{NIG} (E-H) or *kon*^{KK} (I-L). Movies starting around 13h APF (A-H) or 15h APF (I-L). A,E,F| Three templates and surrounding myoblasts (yellow arrows), asterisk marks an exemplary hemocyte. B, F, J| Fusing myoblasts and splitting templates, note long protrusions (yellow arrowheads) in *kon*^{NIG} (F) and *kon*^{KK} (J). C,G,K| DLM myotubes after splitting are starting to compact (w^{-}, C) note rounding myotubes in *kon*^{NIG} (G) and long protrusions in *kon*^{KK} (K). Myotube ends are marked by red arrowheads. D,H,L| Strongly compacted DLMs (w^{-}, D), note round DLMs in *kon*^{NIG} (H) and roundish myotube ends in *kon*^{KK} (L). Red arrows point to myotube ends. Time is indicated in hr:min.

Additionally early phases of abdominal dorsal myogenesis were analysed in pupal offspring of *Mef2*-Gal4>UAS-GFP-Gma crossed to *w*$^{-}$, or *kon*^{6G8} using live imaging (Figure 36). *kon*^{6G8} is a homemade hairpin, that was a gift from G. Dietzl. It shows the same phenotype as the hairpins displayed in Figure 34. Wild type abdominal dorsal myoblasts align A-P and fuse. During fusion they migrate towards their tendon cell and form long filopodia (Figure 36A-C). Filopodia formation ceases after fusion, indicating attachment formation, myotubes run in parallel in A-P direction (Figure 36D). *kon*^{6G8} abdominal dorsal myoblasts align A-P, but also D-P and fuse (Figure 36E). They migrate towards their tendon cell and form very long protrusions (Figure 36F-G). Protrusion formation ceases after fusion, indicating attachment formation. In contrast to wild type, many myotubes run in D-P direction, additionally some myotubes are not aligned in parallel, but target the same tendon field (Figure 36H). Interestingly, *kon*^{6G8} myoblasts already align in the wrong orientation and myotubes that share tendon fields also target

those tendon fields from the beginning of migration. These data strongly indicate an essential role for Kon during myotube guidance.

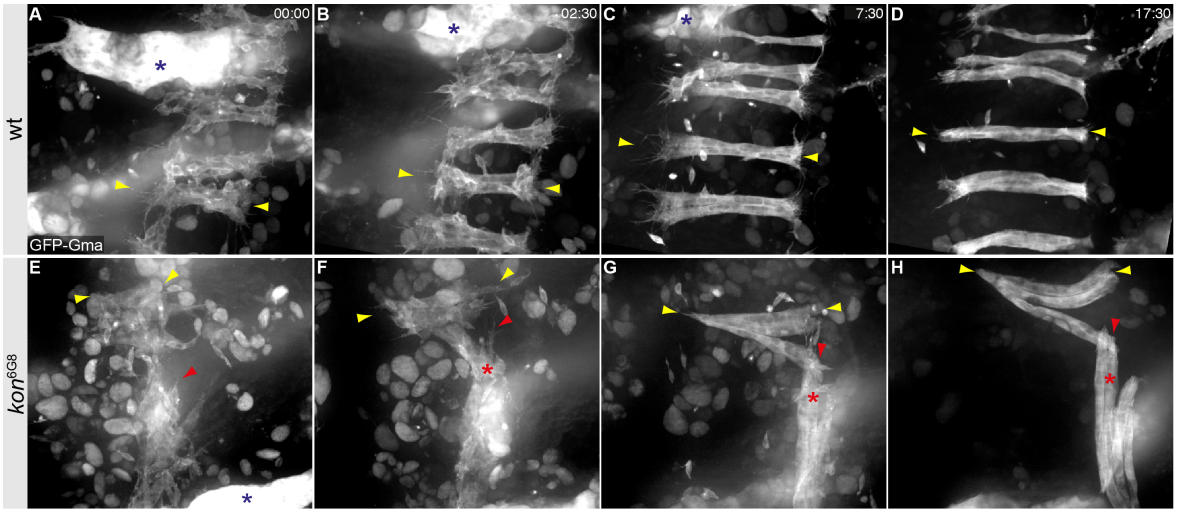

Figure 36 *kon* knock-down during abdominal dorsal myogenesis Stills from spinning disc microscope movies of *Mef2*-Gal4>UAS-GFP-Gma (A-D) or *Mef2*-Gal4>UAS-GFP-Gma, kon^{6G8} (E-H); starting around 30h APF. A| w^-; Adult myoblasts align and fuse, a group of forming myotubes is marked with arrowheads, blue asterisk marks remodelling larval muscle. B,C| w^-; Adult myoblasts continue aligning and fuse. Myotubes form long filopodia. D| w^-; fusion is largely completed. E| kon^{6G8}; Adult myoblasts align and fuse. Lower groups of myoblasts orient in wrong position, red arrowhead. F| kon^{6G8}; Myotubes are formed and continue fusing, long protrusions are formed. Red arrowhead marks the protrusion, asterisk marks the respective myotube. G-H| kon^{6G8}; fusion is largely completed, myotubes are oriented P-D or do not run in parallel but meet at a common tendon field (yellow arrowhead). Time is indicated in hr:min.

If Kon serves as a transmembrane receptor, guiding myotubes to their correct tendon cells, Kon is expected to localise to myotube tips. To analyse Kon's localisation, abdominal dorsal myotubes of *Mef2*-Gal4>UAS-GFP-Gma or w^- pupae and flies were stained at 28h APF, 48h APF and in adult flies. Interestingly, Kon localises to myotube tips during all analysed stages and possibly to nuclei in adult myofibers (Figure 37). These data further support a key role for Kon during myotube guidance.

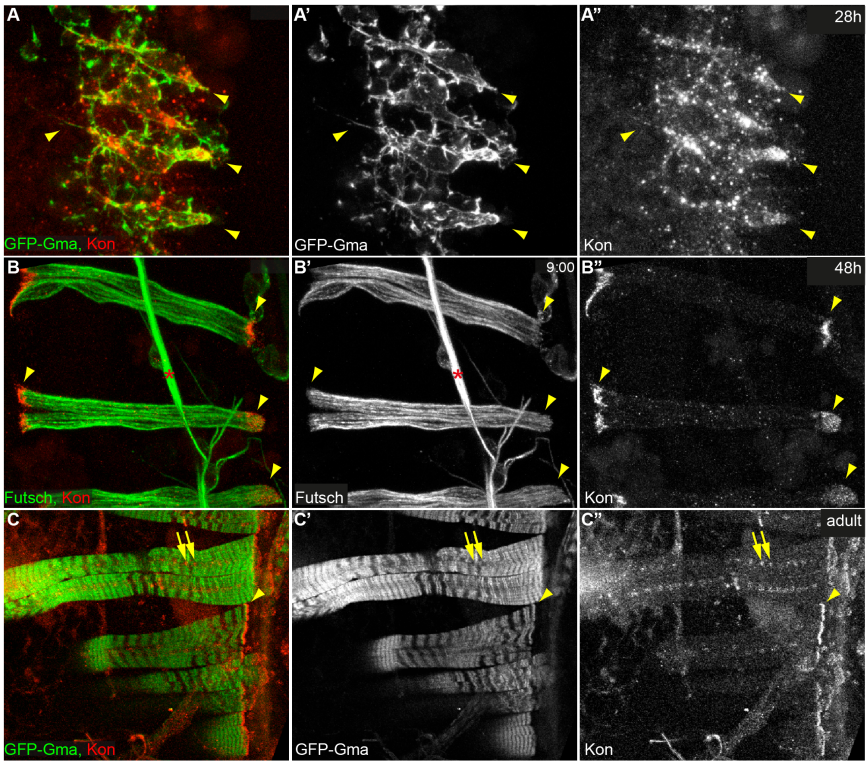

Figure 37 Kon localisation during abdominal dorsal myogenesis. Confocal images of *Mef2*-Gal4>UAS-GFP-Gma at 28h APF (A-A''), and in adult flies (C-C'') stained with Kon. Confocal images of w^- at 48h APF (B-B'') stained with Kon and Futsch. A,A'| 28h APF; Adult myoblasts align and fuse, myotube tips form filopodia. A,A''| 28h APF; Kon localises to myotube tips and is present in filopodia (arrowheads). B| 48h APF; fusion is largely completed. B-B'| 48h APF; myotubes and neurons (asterisk) are marked by Futsch. Myotube is formed and tips straighten, indicating attachment. B''| 48h APF; Kon localises at myotube tips. C-C'| Adult myofibers; fibers are fully formed and display sarcomeres. C''| Adult myofibers; Kon localises to myotube tips and in round structures in the middle of the myotube, possibly nuclei (arrows).

To analyse attachment and guidance in closer detail it is essential to visualise the tendon cells in order to study both components of the myotube-tendon network. To this end the tendon specific driver *sr*-Gal4 could be used to introduce a fluorescent tendon label. Unfortunately *sr*-Gal4 does not drive any detectable fluorescent expression in the dorsal abdomen at early pupal stages and no alternative live tendon marker could be found so far. Tendon labelling however is possible in DLMs, which show rounding of myotubes during development upon *kon* knock-down. Therefore, the focus of further analysis was set on DLM development, and especially DLM attachment in wild type and kon^{IR}.

3.2 Detailed dissection of indirect flight muscle development

Muscle function relies on correct formation of the force-resistant connection between muscles and tendons as well as on precise myofibrillogenesis and sarcomerogenesis. Both processes are still not well understood. Therefore, a strong focus was set on the interactions between myotubes and tendons during development. Moreover, the connection between attachment formation and myofibrillogenesis was analysed. The candidate gene *kon* was included in the analysis. This allowed not only to investigate the role of *kon* during attachment formation but also to provide a better understanding of the process itself and its importance to myofibrillogenesis.

3.2.1 In vivo analysis of DLM development

In order to analyse timing and dynamics of key processes during DLM development, 2-photon live imaging of intact pupae was established. Forming DLMs were labelled with the membrane marker CD8-GFP under control of the adult muscle specific driver *1151*-Gal4 and imaged for 14h during early pupal stages (Figure 38). After head eversion, between 8-10h APF, adult muscle precursors surround the migrating templates and fuse to them (Figure 38A). Fusion of adult muscle precursors to the three templates induces their splitting into six myotubes (Figure 38B) until around 18h APF, which is accompanied by vast formation of dynamic filopodial extensions at myotube tips (Figure 38F-I). Filopodia reach more than 20µm in length and their formation declines when myotubes start to compact along the A-P axis around 18h APF (Figure 38C, J, K). Compaction progresses until the myotubes reach half their original length around 30h APF and then elongate again (Figure 38D, E). These data suggest, that myotube-tendon recognition and attachment initiation of myotubes to tendon cells takes place when highly dynamic filopodia are detectable. Consequently, attachment initiates around 18h APF, when filopodia decline and myotubes compact.

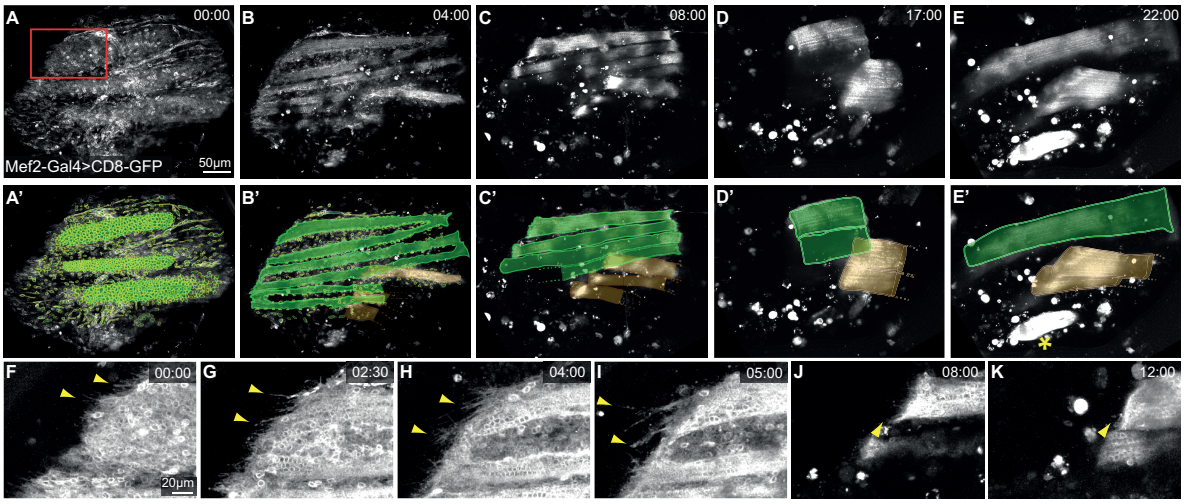

Figure 38 DLM development. Stills from a 2-photon microscope movie of a *1151*-Gal4>UAS-CD8-GFP pupa starting around 10h APF. A, A'| Three remodelled LOM templates (green) and surrounding myoblasts (yellow outlines). B, B'| Fusing myoblasts and splitting templates, note also forming DVMs (brown). C, C'| DLM myotubes after splitting, myotubes start to compact; due to the orientation of the pupae only the topmost DLMs are visible. D, D'| Strongly compacted DLMs and DVMs. E, E'| Elongating DLMs and DVMs, note the forming jump muscle (yellow asterisk). F-K| Magnified red box, focusing on DLM tips. F-I| Increasing filopodia formation (yellow arrowheads). J-K| Filopodia formation is declining when myotubes start to compact. Arrowheads mark filopodia and myotube end, time is indicated in hr:min. (Images from F. Schnorrer)

3.2.2 In vivo analysis of myotube-tendon interactions

The dynamics of myotube-tendon interactions were analysed using in vivo imaging of the myotendinous system in wild type and *kon* knock-down.

3.2.2.1 In vivo analysis of myotube-tendon interactions in wild type

To analyse development of the muscle-tendon system, tendons were co-labelled with CD8-GFP using both, the muscle specific *Mef2*-Gal4 and the tendon specific *sr*-Gal4 (Frommer et al., 1996) driver and imaged up to 36h APF (Figure 39). After myotubes and tendons contact at 16h APF (Figure 39A), long tendon extensions form and myotubes compact. These tendon extensions increase up to a size of 200µm during myotube compaction (Figure 39B-F) and shorten when myotubes elongate again, allowing to maintain the connection to the compacting myotubes (Figure 39G-H).

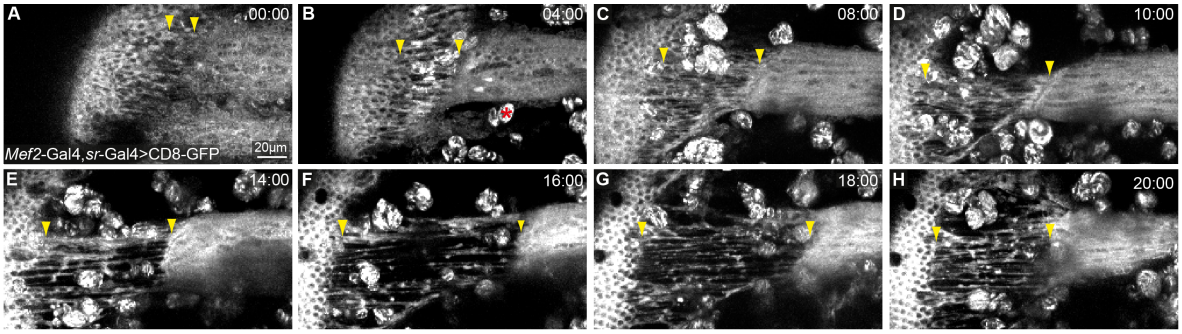

Figure 39 DLM-tendon development. Stills from a 2-photon microscope movie of a *Mef2*-Gal4,*sr*-Gal4>UAS-CD8-GFP pupa starting around 16h APF. A| Myotubes migrate towards tendon precursors. B| Splitting myotubes and tendons contact each other. C-F| tendons form long extensions during myotube compaction. G-H| Tendon extensions shorten during myotube elongation. Arrowheads mark beginning and end of tendon extensions. Red asterisk marks hemocytes, which are engulfing degrading larval muscle tissue and, thus, are labelled with GFP, time is indicated in hr:min.

To assess myotube-tendon dynamics during migration, attachment initiation and attachment maturation in closer detail two-colour live imaging was performed (Figure 40). Tendon membranes were labelled with palmitylated Cherry (UAS-palm-Cherry) under the control of *sr*-Gal4. Myotubes were labelled with *mhc*-TauGFP, a microtubule marker expressed exclusively in muscle. During myotube migration both myotubes and tendons form long filopodia directed towards each other. These filopodia cover the myotube tips entirely. Interestingly, the myotube is ignoring a closely located DVM-tendon field and is specifically targeting its respective tendon cells (Figure 40A). Dynamic myotube and tendon tips interdigitate extensively while the template splits into two myotubes (Figure 40B). At about 18h APF surfaces become smoother, indicating successful attachment initiation (Figure 40C). Attachment initiation is followed by muscle compaction and formation of long tendon extensions (Figure 40D).

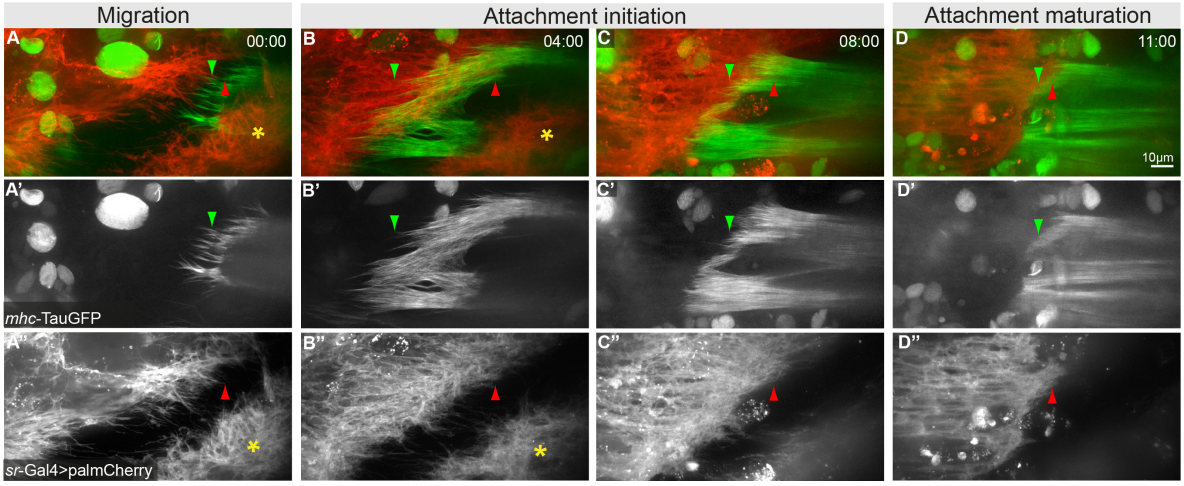

Figure 40 Myotube-tendon dynamics during migration, attachment initiation and attachment maturation. Stills from a spinning disc confocal microscope movie of a *mhc*-TauGFP; *sr*-Gal4>UAS-palm-Cherry pupa starting around 10h APF. A| Template migrates towards tendon precursors; both template and tendons form filopodial extensions. B| Splitting myotube is interdigitating with tendon cells. C| Myotube and tendon tips contact over the complete myotube surface and filopodia decrease. D| Myotube compacts; tendons form extensions. Red arrowheads mark tips of tendon cells, green arrowheads mark myotube tip and filopodial extensions, asterisk marks DVM tendon field, time is indicated in hr:min.

Combining these in vivo imaging results three phases of myotube-tendon morphogenesis can be defined:

1 – **Migration**: Both myotubes and tendons form filopodial extensions, directed at each other, while myotubes migrate straight towards their specific tendon targets.

2 – **Attachment initiation**: Myotubes and tendon cells are in close contact while their tips interdigitate extensively, both recognize each other, and initiate attachment.

3 – **Attachment maturation**: Myotubes and tendon surfaces smoothen, myotubes compact in length and tendons form long cellular extensions.

3.2.2.2 In vivo analysis of myotube-tendon interactions in *kon* knock-down

In vivo imaging data of *kon* knock-down myotubes indicates that myotube migration is normal but myotube-tendon attachment fails (Figure 35). To further confirm Kon's role in attachment formation, in vivo 2-photon imaging was applied during myotube-tendon development of *kon* knock-down pupae. Currently, the only possibility to label tendons for live imaging is the use of *sr*-Gal4 driving expression of a fluorescent marker. As Gal4 is also used to drive hairpin expression, simultaneous live imaging of myotube and tendon development in *kon* knock-down pupae required to perform the knock-down in muscle and tendon cells. The muscle specific driver *Mef2*-Gal4 and the tendon specific driver *sr*-Gal4 were used to express the kon^{NIG} hairpin and the membrane label CD8-GFP. Intact pupae were imaged from 16h APF up to about 26h APF (Figure 41). At 16h APF the major part

of the myotube is not in contact with tendon cells (Figure 41A). Around 18h, however myotubes and tendons are in close proximity and show some contact sites (Figure 41B). Myotube contact sites increase within the first 4h of imaging. Then, however contact areas decrease dramatically until the myotube loses contact and rounds up around 22h APF (Figure 41C-F). The early rounding up of the myotube combined with the loss of tendon contact strongly indicates that attachment initiation is defective in *kon* knock-down pupae.

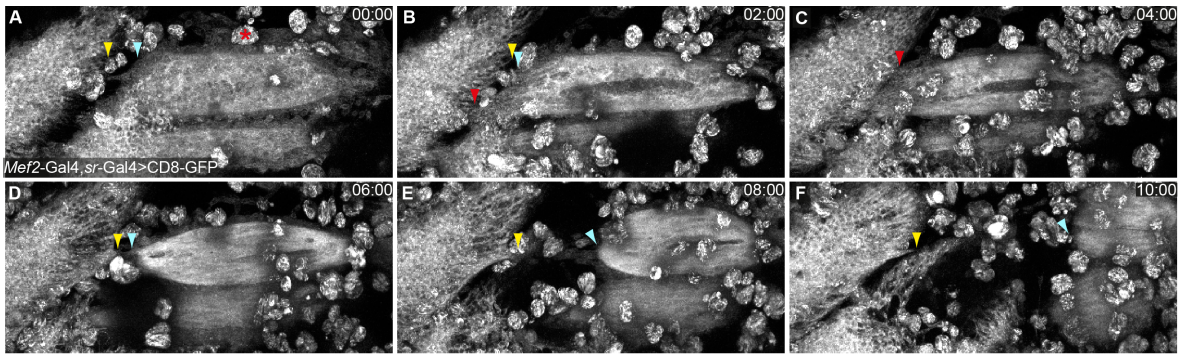

Figure 41 DLM-tendon development of *kon* knock-down myotubes and tendons. Stills from a 2-photon microscope movie of a *Mef2*-Gal4, *sr*-Gal4>UAS-*kon*^{NIG}, UAS-CD8-GFP pupa starting around 16h APF. A| Templates migrate towards tendon precursors. B,C| Splitting myotubes and tendons contact each other. D-F| Myotubes round up and move away from tendon cells. Yellow arrowheads mark tendon cells, blue arrowheads mark end of the myotube, red arrowheads mark myotube-tendon contact sites. Asterisk marks hemocytes; time is indicated in hr:min.

To assess myotube-tendon dynamics in closer detail in *kon* knock-down pupae during migration, attachment initiation and attachment maturation two-colour live imaging was performed (Figure 42). *kon*^{NIG} and UAS-palm-Cherry were expressed in myotubes and tendon cells using *Mef2*-Gal4 and *sr*-Gal4. Moreover, the myotube specific marker *mhc*-TauGFP was introduced to distinguish myotubes from tendon cells and AMPs. During myotube migration tendon cells form short filopodia directed towards the myotube, while the myotube forms extremely long filopodia which are restricted to few areas at the muscle tip (Figure 42A). This is in contrast to wild type myotubes, where the complete tip area is covered with filopodia (Figure 40A). The myotube continues to form extremely long filopodia directed to the tendon cells, these filopodia are also restricted to limited areas on the myotube tip (Figure 42B). Consequently only few areas of the myotube tips contact the tendon cells and the myotube surface does not smoothen (Figure 42C). At around 22h APF myotubes start rounding up and loose all tendon contacts (Figure 42D), indicating that myotube and tendon contacts are not translated into an attachment. This leads to the conclusion that Kon is essential for attachment initiation between myotubes and tendon cells.

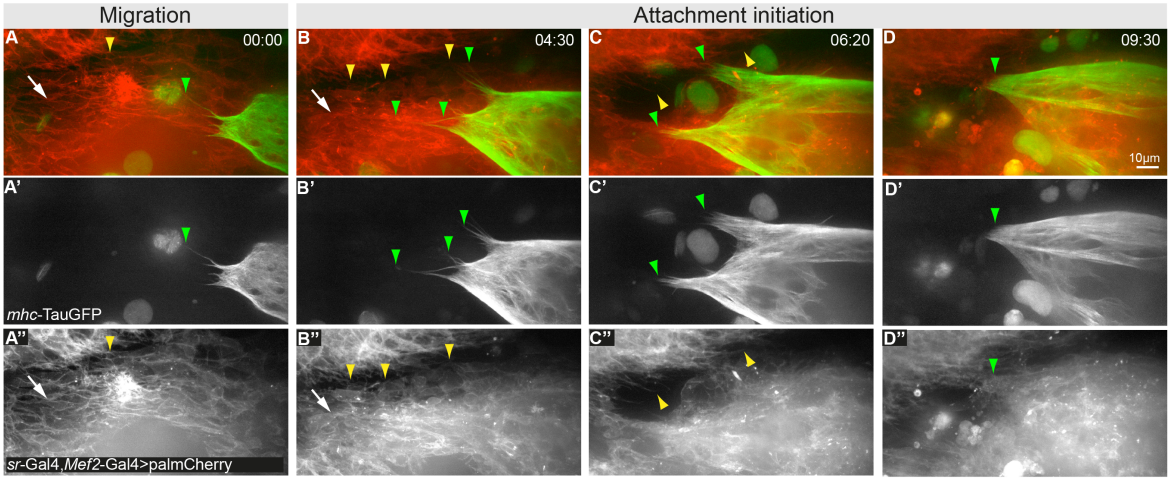

Figure 42 Myotube-tendon dynamics in *kon* knock-down pupa. Stills from a spinning disc confocal microscope movie of a *mhc*-TauGFP; *Mef2*-Gal4, *sr*-Gal4>UAS-palm-Cherry, UAS-*kon*^{NIG} pupa starting after head eversion, around 10h APF. A| Template migrates towards tendon precursors, template forms very long filopodial extensions, tendons form small extensions. B| Splitting myotube is migrating towards tendon cells, long filopodial extensions form mainly in the middle and at the sides of the myotube tip. C| Myotube extends exclusively at the boarders of the myotube tips, only extended tips contact tendons cells. D| Myotube is only contacting the tendons at one region and is rounding up. Yellow arrowheads mark tendon cells, green arrowheads mark myotube tip and filopodial extensions, white arrows point towards groups of adult myoblasts, surrounding the myotube, time is indicated in hr:min.

3.2.3 Morphological analysis of myotube-tendon interactions in *kon* knock-down

Complementary to the in vivo imaging of living *Drosophila* pupae (section 3.2.2.2), attachment initiation and maturation was analysed in immunostained flight muscle preparations. This approach enables for a better morphological analysis and molecular understanding of the myotube-tendon network in muscle specific *kon* knock-down pupae.

Pupal offspring of *Mef2*Gal4>UAS-GFP-Gma crossed to the *kon* hairpins *kon*^{NIG} or *kon*^{KK}, or to *w*$^{-}$ were dissected at 18h and 30h APF. The spectraplakin homologue Shot was used as a tendon marker. Although Shot expression has been reported to be tendon specific in embryonic body muscles (Alves-Silva et al., 2008; Subramanian et al., 2003) and adult abdominal muscles (Uchino et al., 2013) Shot protein is clearly present in DLMs as well as in their respective tendon cells (Figure 43B'' and Figure 44B'').

During attachment initiation at 18h APF, wild type myotubes and tendons are in close contact (Figure 43A, B). Myotube tips show regularly distributed short filopodia (Figure 43B'') while tendons are extended and show Shot accumulation at myotube-tendon contact site (Figure 43B''). In contrast, *kon*^{NIG} knock-down myotubes form only few myotube-tendon contacts preferably at the extremely long myotube protrusions (Figure 43C, D). Tendons show only short extensions, the Shot accumulation at the *kon*^{NIG} myotube-tendon

contact site is lost and Shot levels in the myotubes are strongly reduced (Figure 43D''). Consistent with the live imaging data (Figure 35), *kon*^{KK} hypomorphic knock-down myotubes form the longest myotube protrusions (Figure 43F''). These myotube protrusions frequently overshoot close-by tendon extensions, which meet the myotube mainly at the cell body (Figure 43C,D). Shot accumulation at *kon*^{KK} myotube-tendon contact sites is lost and Shot levels in the myotubes are strongly reduced (Figure 43D''). Taken together these data demonstrate that Kon is essential for correct initiation of myotube-tendon attachment.

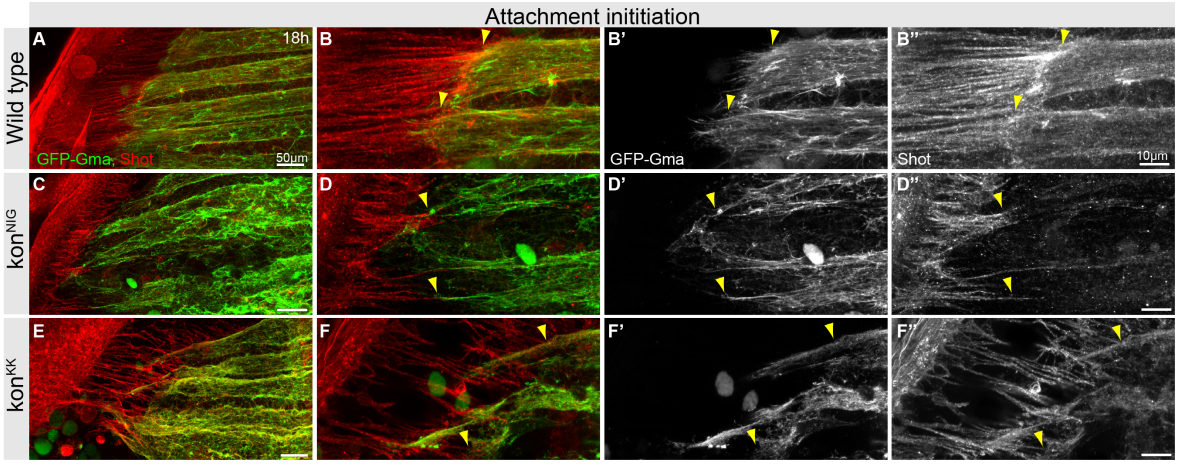

Figure 43 Myotube-tendon connections in wild type and *kon* knock-down pupae at attachment initiation. Confocal images of 18h APF dissections of *Mef2*-Gal4>UAS-GFP-Gma (A-B''), *Mef2*-Gal4>UAS-GFP-Gma, *kon*^{NIG} (C-D'') and *Mef2*-Gal4>UAS-GFP-Gma, *kon*^{KK} (E-F''), myotubes are labelled with GFP in green, myotube and tendons are stained with Shot in red. A-B'| Wild type myotubes are completely split, smoother myotube tips display short filopodia. A, B, B''| Tendons form short tendon extensions and contact myotubes all over myotube tip surface. Shot labels tendons and myotubes; it accumulates at myotube-tendon contact sites. C-D'| *kon*^{NIG} myotubes are delayed in splitting and myotubes tips form very long projections. C, D, D''| Tendon extensions are very short and contact myotube tips only at projections. Shot is predominantly expressed in tendon cells and does not accumulate at myotube-tendon contact sites. E-F'| *kon*^{KK} myotubes are delayed in splitting and myotubes tips form extremely long projections. E, F, F''| Tendons form long extension that overshoot muscle projections. Shot labels muscle and tendons, it does not accumulate at myotube-tendon contact sites. Yellow arrowheads mark myotube-tendon contact sites.

During myotube compaction at 30h APF, wild type myotubes and tendons are in close contact (Figure 44A, B). Myotube tips are smooth (Figure 44B''), while tendons are strongly extended and show Shot accumulation at the myotendinous junction. Interestingly, Shot displays a periodic pattern in the compacted myotube (Figure 44B''), indicating that it is a component of early sarcomeres. As observed by live imaging (Figure 35) *kon*^{NIG} knock-down myotubes round up and only some round myotubes stay in proximity of tendon cells, others move away and are often lost during dissection. *kon*^{NIG} knock-down myotubes are round at 30h APF and form only few myotube-tendon contacts (Figure 44C, D). Tendons show only short extensions and the Shot accumulation at the

myotube-tendon contact site is strongly reduced (Figure 44D''). *kon*^{KK} hypermorphic knock-down myotubes occasionally also round up at 30h APF. The majority of *kon*^{KK} knock-down myotubes however are elongated and display rounded tips. Moreover, *kon*^{KK} knock-down myotubes are significantly less compacted and thinner than wild type myotubes (Figure 44E, F, Figure 75). Tendons are less extended; most likely due to the increased *kon*^{KK} myotube length and display strongly reduced Shot accumulation at the myotube-tendon contact site (Figure 44F''). Interestingly, Shot is restricted to thin actin fibrils, which are only detected at the myotube surface and at myotube-tendon contact sites (Figure 44F). Taken together, these data suggest that Kon is essential for initiation of stable force-resistant attachment of DLMs to their respective tendons.

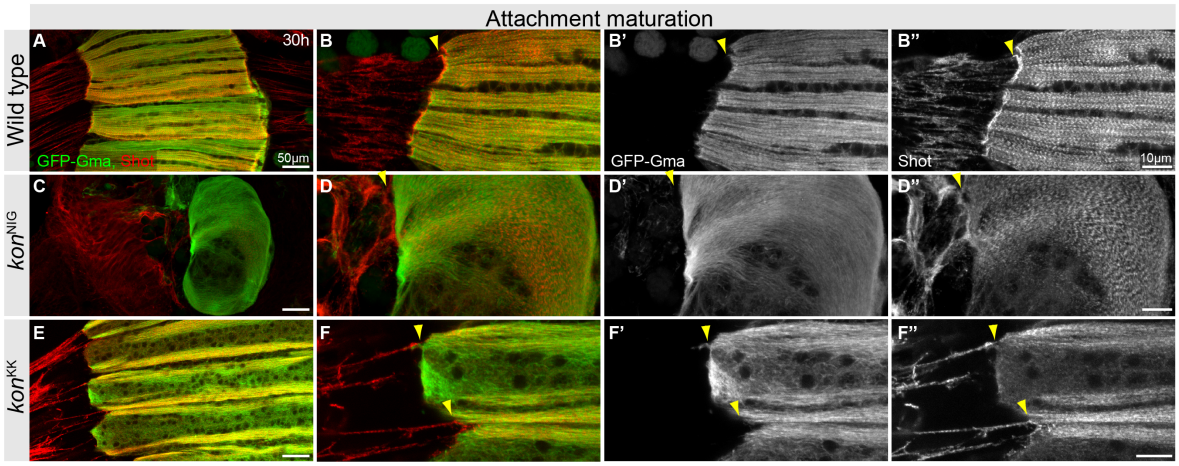

Figure 44 Myotube-tendon network in wild type and *kon* knock-down at attachment maturation. Confocal images of 30h APF dissections of *Mef2*-Gal4>UAS-GFP-Gma (A-B''), *Mef2*-Gal4>UAS-GFP-Gma, *kon*^{NIG} (C-D'') and *Mef2*-Gal4>UAS-GFP-Gma, *kon*^{KK} (E-F''), myotubes are labelled with GFP in green, myotube and tendons are stained with Shot in red. A-B'| *w*$^{-}$; myotubes are compacted and show straight tips. A, B, B''| *w*$^{-}$; long tendon extensions contact myotube all over the myotube tip. Shot labels tendons and myotubes, it accumulates at myotube-tendon contact site. C-D'| *kon*^{NIG}; myotubes are round. C, D, D''| *kon*^{NIG}; only few tendons contact the myotube, Shot does not accumulate at myotube-tendon contact site. E-F'| *kon*^{KK}; myotubes don't compact completely and show rounded tips. E, F, F''| Only few tendons contact the myotube, Shot does not accumulate at myotube-tendon contact site. Arrowheads mark myotube-tendon contact sites

3.2.4 Molecular analysis of myotube-tendon connections in wild type

To get a better insight in the formation and molecular composition of myotube-tendon connections, the localisation of adhesion and ECM proteins was analysed during attachment initiation and maturation.

3.2.4.1 Localisation of basement membrane and cell-cell adhesion proteins

To gain a better understanding of the external environment of myotubes and tendons during attachment initiation and maturation two basement membrane molecules, Perlecan

and Laminin, were analysed. Moreover, the localisation of different cell-cell adhesion proteins was analysed to elucidate if the initial contact between myotubes and tendons could be based on a direct cell-cell contact.

Dissected *Mef2*-Gal4>UAS-GFP-Gma pupae display a sheet-like Perlecan network below tendon cells (Figure 45A, B) and a cable-like Perlecan network surrounding myotubes (Figure 45B). Similarly, Laminin forms sheet like structures below tendon cells and cables below myotubes during attachment initiation (Figure 45C). Additionally, Laminin staining was analysed in dissected *Mef2*-Gal4>UAS-GFP-Gma pupae at 30h APF. During attachment maturation Laminin forms a sheet, embedding myotubes and tendons, it is enriched at myotube surfaces (Figure 45D). These data show that myotubes and tendons are embedded in an ECM of Perlecan and Laminin, possibly resembling the forming basement membrane.

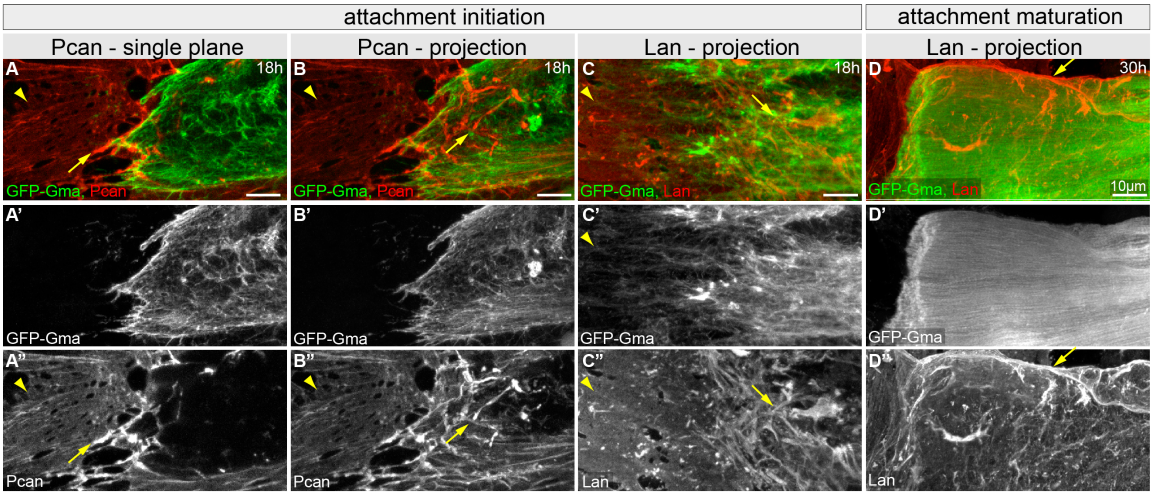

Figure 45 Basement membrane protein localisation during attachment initiation and maturation. Confocal images of 18h (A-C) and 30h (D) APF dissections of *Mef2*-Gal4>UAS-GFP-Gma, myotubes are labelled with GFP in green, Perlecan (Pcan) (A,B) or Laminin (Lan) (C,D) are shown in red. A-A''| 18h APF; Perlecan forms a sheet-like network embedding tendon cells, it seems slightly enriched at myotube-tendon contact site. B-B''| Maximum projection, 18h APF; Perlecan forms cable-like structures surrounding myotubes. C-C''| Maximum projection, 18h APF; Laminin forms sheet-like structures under tendon cells and cable-like structures surrounding myotubes. D-D''| Maximum projection, 30h APF; Laminin embeds myotubes and tendons in sheet-like structures. Arrowheads mark sheet like structures, arrows mark cable-like structures.

To analyse the possibility of a cell-cell based adhesion during attachment initiation, the localisation of adherence and septate junction components was analysed in *Mef2*-Gal4>UAS-GFP-Gma pupae at 18h APF (Figure 46). The septate junction and polarity protein Discs large1 (Dlg1) as well as the septate junction protein Fasciclin3 (Fas3) were stained (Woods and Bryant, 1991; Woods et al., 1997). Both proteins show a strong enrichment at the cell-cell junctions on the apical tendon side indicating a successful and

specific staining (Figure 46A''-B''). Dlg1 is present in myotubes and tendon cells and is enriched at the myotube-tendon interface (Figure 46A''). In contrast, Fas3 is not detected in myotubes and does not localise to the myotube-tendon interface (Figure 46B''). Low levels of Fas3 at the myotube–tendon interface indicate that Dlg1 enrichment at the interface might not characterise a septate junction in this case, but might reflect one of it's many other roles, for example in polarity.

As a read-out of adherence junctions, localisation of the adhesion molecule E-Cadherin was analysed. E-Cadherin is not detectable in myotubes (Figure 46C'), but strongly enriched at the cell-cell junctions on the apical tendon side indicating a successful and specific staining. Moreover, E-Cadherin localises to dot-like structures at the myotube-tendon interface (Figure 46C''), indicating a possible involvement in attachment initiation. These data hint towards a possible formation of an adherence junction-like contact during attachment initiation, which is remodelled to a hemiadherence-type myotendinous junction during attachment maturation.

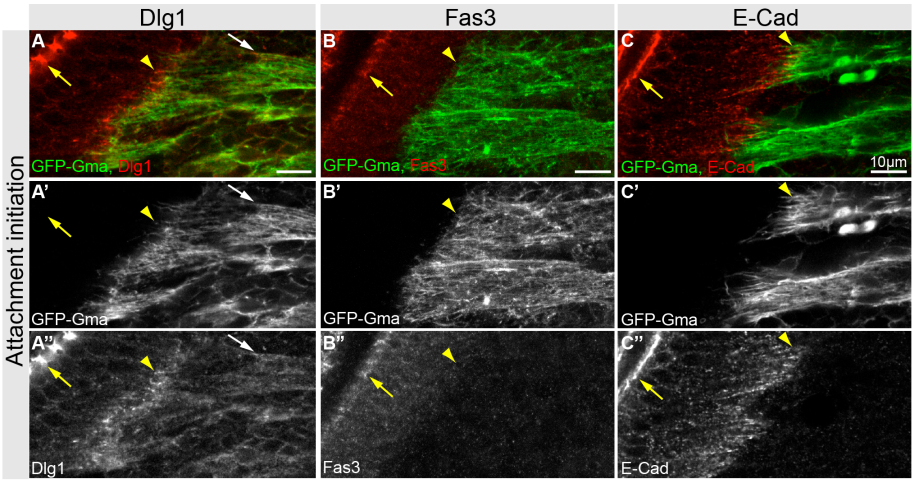

Figure 46 Cell-cell adhesion protein localisation during attachment initiation. Confocal images of 18h APF dissections of *Mef*2-Gal4>UAS-GFP-Gma pupae. Myotubes are labelled with GFP in green, Dlg1 (A), Fas3 (B) or E-Cad (C) are shown in red. A-A''| Dlg1 is present in epithelium, tendon cells and myotubes, Dlg1 is enriched at the myotube-tendon interface. B-B''| Fas3 is present in epithelium and tendon cells, it is not enriched at the myotube-tendon interface. C-C''| E-Cad is present in epithelium and tendon cells, it is enriched at the myotube-tendon interface. Arrowheads mark the myotube-tendon interface, yellow arrows mark the epithelium, white arrow marks myotube expression of Dlg1.

3.2.4.2 Localisation of Kon and integrin complex and signalling components

The main components of the hemiadherence-type myotendinous junction in mammals as well as in *Drosophila* are integrins. Integrins link the muscle via ECM to the tendon. Integrins have also been reported to localise at myotendinous junctions of DLMs starting around 22h APF (Fernandes et al., 1996). Additionally, the *kon* knock-down phenotype indicates a role for the transmembrane receptor during attachment, suggesting that it could be localised at the myotube-tendon contact sites.

To study the molecular composition of the myotendinous junction, dissected *Mef*2-Gal4>UAS-GFP-Gma pupae were stained and analysed for Kon and β-PS integrin localisation during attachment initiation at 18h and attachment maturation at 30h APF (Figure 47). Kon localises strongly to myotube tips during attachment initiation and attachment maturation (Figure 47A, A', B, B'). In contrast, β-PS integrin localises only partially to myotube tips at 18h APF, but localises strongly to myotube tips at 30h APF (Figure 47A, A'', B, B''). To quantify myotube tip localisation the ratio of the mean intensity at the myotube tip versus the mean intensity at the myotube surface was calculated. The quantification shows that Kon localises two-fold stronger to myotube tips than β-PS integrin during attachment initiation. During attachment maturation, however, integrin localisation to the myotube tip increases almost 10-fold resulting in a two-fold stronger tip localisation of β-PS integrin than of Kon at this time point (Figure 47C). These data demonstrate that integrin is strongly recruited to myotube tips after attachment initiation, while Kon is already strongly localised to myotube tips at 18h APF. This early Kon localisation to myotube tips further supports an important role of Kon during attachment initiation.

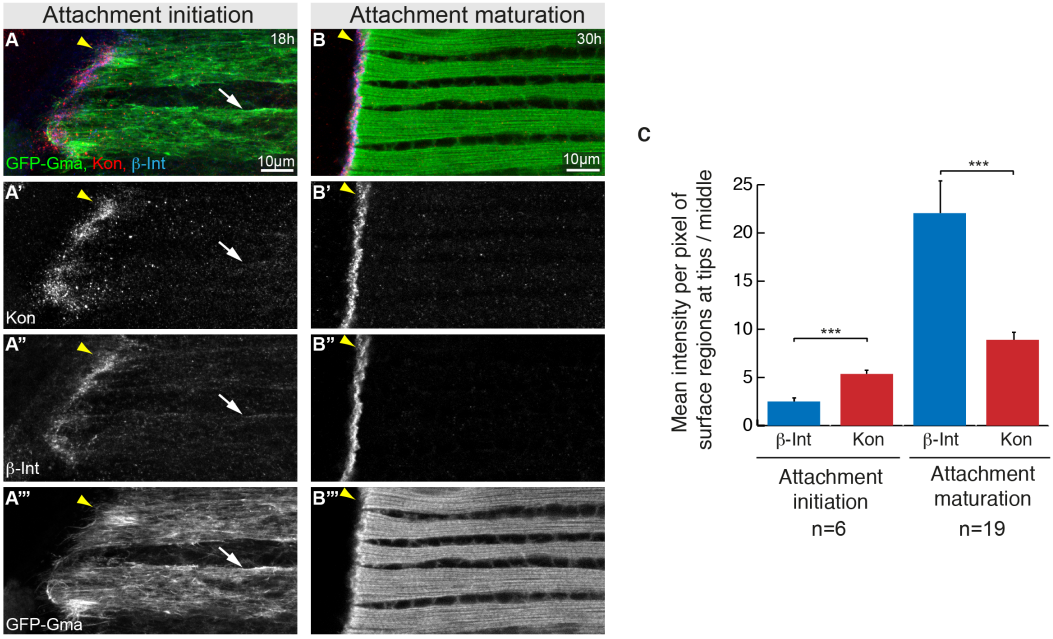

Figure 47 Kon and integrin localisation during attachment initiation and maturation. Confocal images of 18h and 30h APF dissections of *Mef2*-Gal4 >UAS-GFP-Gma pupae (A-B'''), myotubes are labelled with GFP in green, Kon is shown in red and β-PS integrin is shown in blue. A-A'''| 18h myotubes, Kon localises to myotube tips, β-PS integrin is present on the myotube surface but is enriched at the myotube tips. B-B'''| 30h myotubes, both Kon and β-PS integrin localise to myotube tips. Arrowheads mark myotube tips, arrows mark other myotube surface regions. C| Ratios of mean intensity per pixel of myotube tips to myotube surface regions. Error bars represent SEM, $p \leq 0.0005$ (two tailed unpaired t-test).

As a 10-fold increase of β-PS integrin at myotube tips was observed after attachment initiation, localisation of other integrin complex components was also analysed during attachment initiation and maturation. β-PS integrins form heterodimers with α-PS integrins. In *Drosophila* embryos the typical tendon integrin is β-PS/α-PS1 and the typical muscle integrin is β-PS/α-PS2. Therefore, dissected *Mef2*-Gal4, *sr*-Gal4>UAS-GFP-Gma pupae were stained with α-PS1 and α-PS2 integrin during attachment initiation and maturation (Figure 48). During attachment initiation α-PS1 integrin localises prominently to the myotube-tendon contact site. Additionally, α-PS1 integrin might be present in myotube and tendon cells, this signal is however not clearly distinguishable from background (Figure 48A, A''). α-PS2 integrin is present at the myotube surface and is partially enriched at myotube-tendon-contact sites. (Figure 48B, B''). During attachment maturation both α-PS1 and α-PS2 integrins localise strongly to the myotendinous junction (Figure 48C, D''). Taken together, both α-PS1 and α-PS2 integrins localise to myotube-tendon contact sites. Similar to β-PS integrin, the myotube tip localisation of α-PS2 integrin increases after attachment initiation.

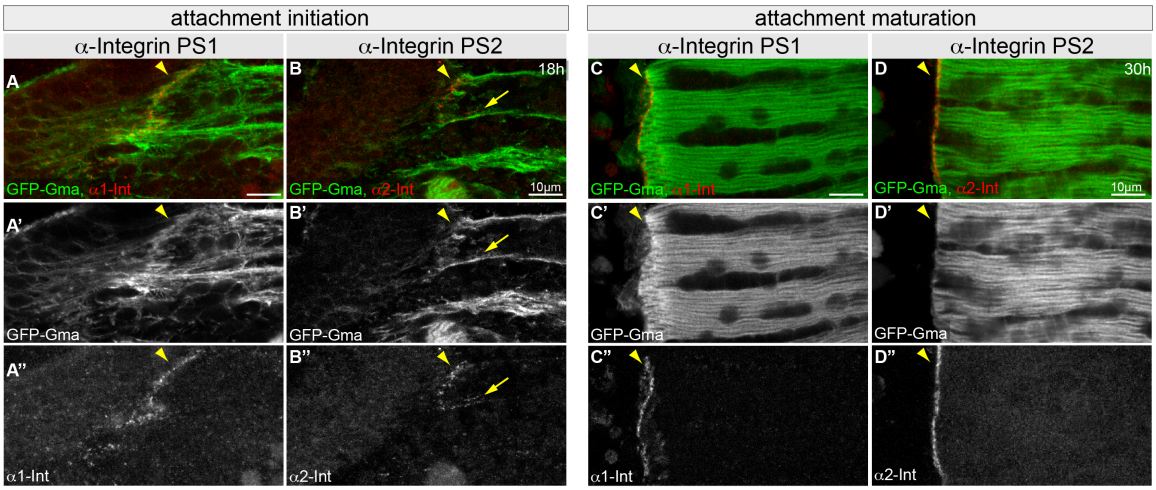

Figure 48 α-PS1 integrin and α- PS2 integrin localisation during attachment initiation and maturation. Confocal images of 18h (A-B'') and 30h (C-D'') APF dissections of *Mef2*-Gal4, *sr*-Gal4>UAS-GFP-Gma pupae, myotubes and tendons are labelled with GFP in green, α-PS1 integrin (α1-Int, A, C) or α-PS2 integrin (α2-Int B, D) are shown in red. A-A''| 18h APF; α-PS1 integrin localises to myotube tips. B-B''| 18h APF; α-PS2 integrin localises to myotube tips and other myotube surfaces. C-C''| 30h APF; α-PS1 integrin localises to myotube tips. D-D''| 30h APF; α-PS2 integrin localises to myotube tips. Arrowheads mark myotube tips, arrows mark other myotube surface regions.

Next, other integrin pathway components – namely Talin, phosphorylated FAK (pFAK) and Tsp – were compared at 18h (Figure 49) and 30h APF (Figure 50) in order to assess if they are also recruited to the myotube tips after attachment initiation. During attachment initiation at 18h APF Talin, the intracellular binding partner of β-PS integrin, is present in myotubes and tendons, but is only weakly localised to the myotube-tendon interface (Figure 49A, B). Interestingly, Talin is highly enriched at the splitting sites of myotubes (Figure 49B, B''). pFAK, a readout for integrin signalling is also present in tendons and myotubes, it localises to the myotube surface and is only weakly enriched at myotube tips during attachment initiation (Figure 49C,C''). Tsp, the extracellular matrix ligand of β-PS integrin, is hardly detectable at 18h APF (Figure 49D,D''). The absence of Tsp in combination with low integrin complex and pathway component localisation to the myotube-tendon interface indicates that the first adhesion formed during attachment initiation is not a typical hemiadherence junction.

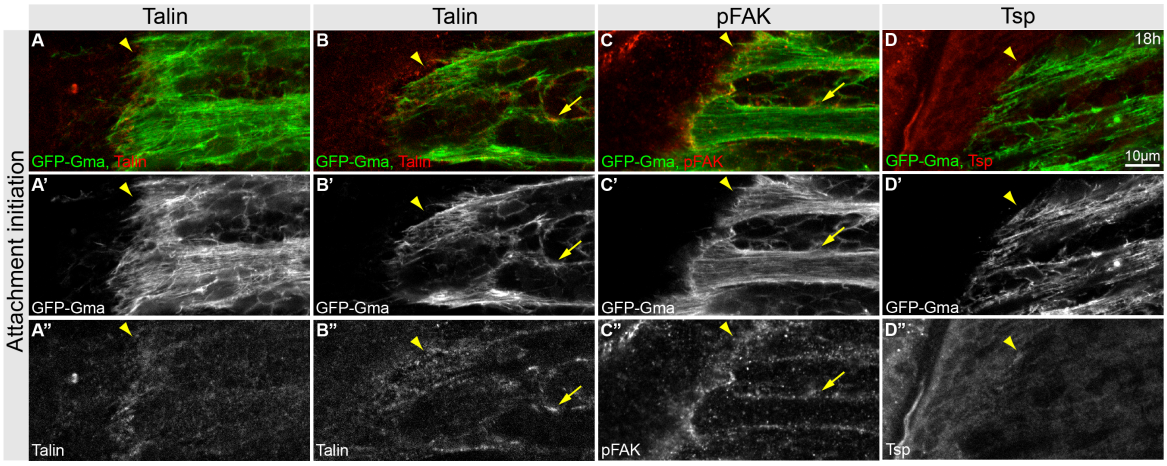

Figure 49 Integrin pathway component localisation during attachment initiation. Confocal images of 18h APF dissections of *Mef2*-Gal4>UAS-GFP-Gma pupae. Myotubes are labelled with GFP in green, Talin (A, B), pFAK (C) or Tsp (D) are shown in red. A-A''| Talin is present in myotubes and tendons, it is enriched at myotube-tendon contact sites. B-B''| Talin localises strongly to the splitting sites of myotubes. C-C''| pFAK is present in myotubes and tendons, it is enriched at myotube-tendon contact sites. D-D''| Tsp is hardly detectable in tendons cells and not present in myotubes. Arrowheads mark myotube tips, arrows mark the splitting site (B) or other myotube surface regions (C).

Similar to the integrin complex, Talin, pFAK and Tsp strongly localise to the myotube-tendon interface during attachment maturation (Figure 50A-C). These data show that all tested integrin complex and pathway components are strongly recruited to the myotube-tendon interface after attachment initiation. The presence of Tsp combined with strong recruitment of integrin complex and pathway components after attachment initiation strongly indicates the formation of a hemiadherence-type myotendinous junction during attachment maturation.

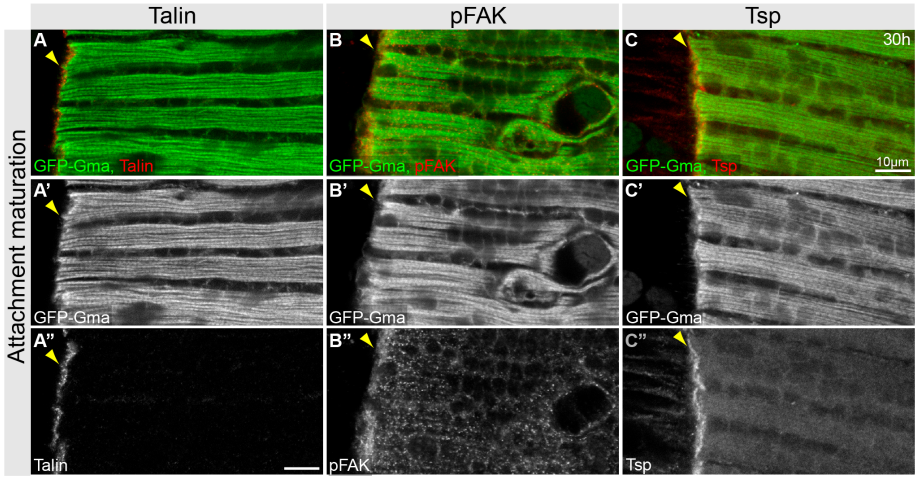

Figure 50 Integrin pathway component localisation during attachment maturation. Confocal images of 30h APF dissections of *Mef2*-Gal4>UAS-GFP-Gma pupae, myotubes are labelled with GFP in green, Talin (A), pFAK (B) or Tsp (C) are shown in red, all localise to the myotendinous junction. Arrowheads point to the myotendinous junction.

3.2.5 Molecular analysis of myotube-tendon connections in *kon* knock-down

To get a closer insight into Kon's role during attachment initiation, basement membrane as well as cell-cell and cell-matrix adhesion molecules were studied during attachment initiation or maturation in *kon* knock-down pupae.

3.2.5.1 Localisation of basement membrane and cell-cell adhesion proteins

The integrity of Perlecan and Laminin networks was analysed in *kon* knock-down pupae at 18h APF (Figure 51). Dissected *Mef2*-Gal4>UAS-GFP-Gma, *kon*^{NIG} pupae display a sheet-like Perlecan network below tendon cells (Figure 51A,B) and a cable-like Perlecan network surrounding myotubes (Figure 51B). Similarly, Laminin forms sheet like structures below tendon cells and cables around myotubes during attachment initiation (Figure 51C). Therefore, no obvious ECM composition defect could be detected in *kon*^{NIG} pupae during attachment initiation, indicating that Kon does not play an essential role in organising this potential basement membrane.

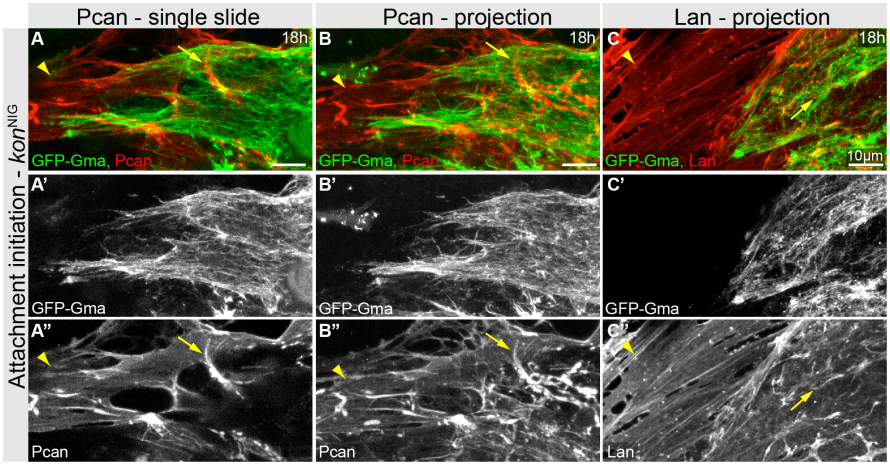

Figure 51 Basement membrane proteins in *kon* knock-down pupae during attachment initiation. Confocal images of 18h APF dissections of *Mef2*-Gal4>UAS-GFP-Gma, *kon*^{NIG} (A-C). Myotubes are labelled with GFP in green, Perlecan (A, B) or Laminin (C, D) are shown in red. A-A''| Perlecan forms a sheet-like network embedding tendon cells. B-B''| Perlecan forms cable-like structures under myotubes. C-C''| Laminin forms sheet-like structures under tendon cells and cable-like structures under myotubes. Arrowheads mark sheet like structures, arrows mark cable-like structures.

Next, adherence junction and septate junction components were stained *Mef2*-Gal4>UAS-GFP-Gma, *kon*^{NIG} pupae at 18h APF and their localisation was compared to the wild type control (Figure 52). In muscle specific *kon*^{NIG} Dlg1 is present in myotubes and tendons. Compared to wild type however, Dlg1 levels seem elevated. Additionally, Dlg1 localises less prominently to the basal tendon surface, facing the myotube (Figure 52B''). Similarly E-Cadherin localises less prominently to the basal tendon surface (Figure 52D''). The less prominent localisation of Dlg1 and E-Cadherin towards the approaching myotube might

indicate a delay or failure in establishing an initial cell-cell adhesion. These data further strengthen a function for Kon in mediating attachment initiation.

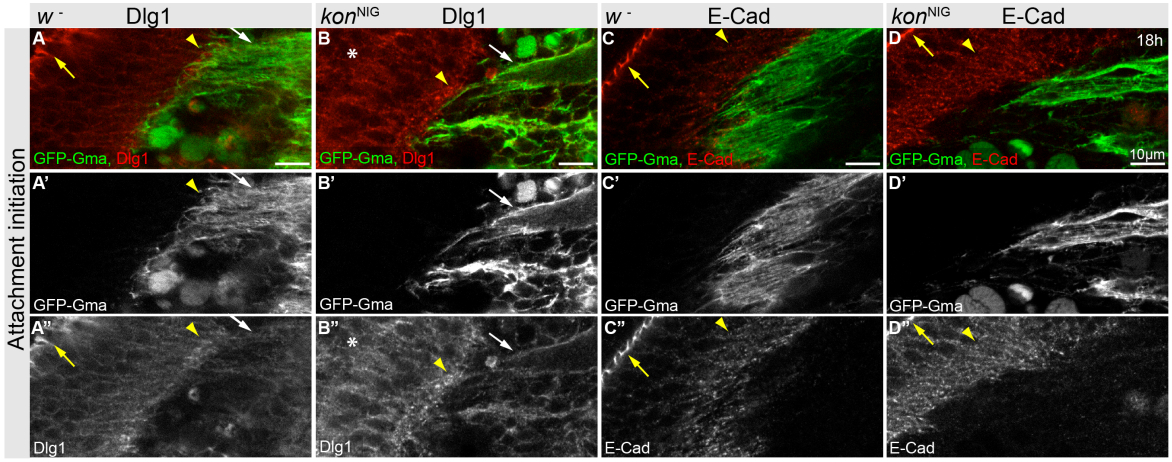

Figure 52 Cell-cell adhesion proteins in *kon* knock-down pupae during attachment initiation. Confocal images of 18h APF dissections of *Mef2*-Gal4>UAS-GFP-Gma (w^-, A,C) or *Mef2*-Gal4>UAS-GFP-Gma, kon^{NIG} (B,D) pupae. Myotubes are labelled with GFP in green, Dlg1 (A,B), or E-Cad (C,D) are shown in red. A-A''| Dlg1 is present in epithelium, tendon cells and myotubes. Dlg1 is enriched at the myotube-tendon interface. B-B''| kon^{NIG}, Dlg1 is present in epithelium, tendon cells and myotubes, it is slightly enriched at the tendon surface facing myotubes. C-C''| E-Cad is present in epithelium and tendon cells, it is enriched at the myotube-tendon interface. D-D''| kon^{NIG}, E-Cad is present in epithelium and tendon cells, it is slightly enriched at the tendon surface facing myotubes. Arrowheads mark the Dlg1 or E-Cad enrichment in the tendon cells, yellow arrows mark the epithelium, white arrows mark myotube expression of Dlg1, asterisks mark enhanced tendon Dlg1 staining.

3.2.5.2 Localisation of the guidance protein Robo in wild type and *kon* knock-down

Live imaging and immunohistochemical analysis of *kon* knock-down myotubes revealed that Kon is essential for attachment initiation. Interestingly, myotube-tendon contacts are highly reduced in *kon* knock-down myotubes. In *kon* hypomorphic kon^{KK} line myotubes overshoot the tendon cells possibly indicating a defect in tendon recognition. In studies in *Drosophila* embryos the transmembrane receptor Robo has been identified as potential myotube guidance protein localising to attachment sites (Kramer et al., 2001; Wayburn and Volk, 2009). To get a better molecular insight on DLM migration and attachment Robo localisation was analysed in wild type and *kon* deficient myotubes.

Dissected *Mef2*Gal4>UAS-GFP-Gma pupae were stained with Robo antibody at 18h APF, when myotube-tendon attachment is initiated. Additionally, *Mef2*Gal4, *sr*-Gal4>UAS-GFP-Gma pupae were stained for Robo at 30h APF, when myotubes are compacted (Figure 53A,C). Like in the embryo, Robo is highly enriched at the myotube-tendon contact site during attachment initiation and maturation. In contrast to the embryonic system however, Robo is hardly detectable in myotubes but clearly present in tendon cell

bodies and extensions (Figure 53A'', C, C''), indicating a possible role for Robo in tendon cells.

In *Mef2*Gal4>UAS-GFP-Gma, *kon*^{NIG} pupae Robo is still present in the tendon cells and also enriched at the basal tendon membrane. However, Robo is also enriched in basal tendon membranes that are not in proximity to a myotube. Therefore, it localises less prominently to the myotube-tendon contact site (Figure 53B,B''). As the localisation of Robo in adult myogenesis is different to the embryonic localisation, it is not clear if Robo is involved in DLM-myotube guidance.

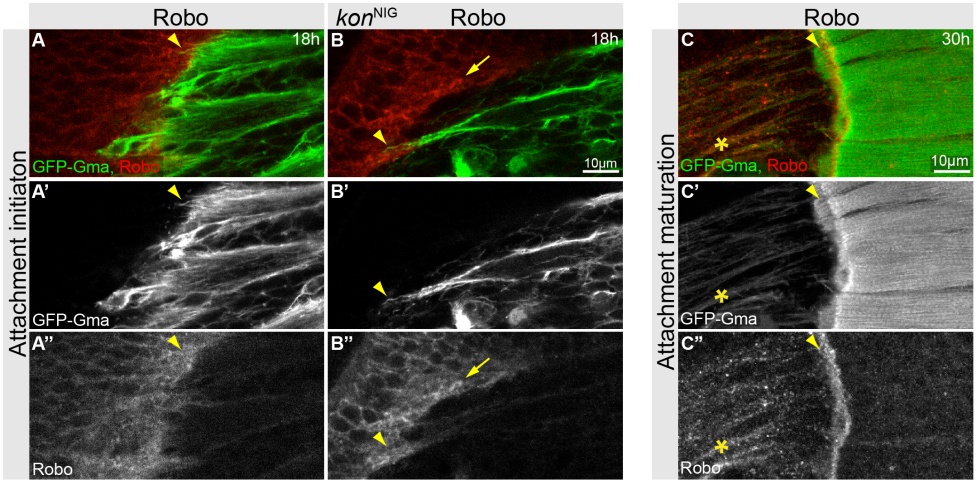

Figure 53 Robo localisation during attachment initiation and maturation. Confocal images of 18h APF dissections of *Mef2*-Gal4>UAS-GFP-Gma (w^-, A-A'') or *Mef2*-Gal4>UAS-GFP-Gma, *kon*^{NIG} (B-B'') pupae and 30h APF dissections of *Mef2*-Gal4, *sr*-Gal4 >UAS-GFP-Gma pupae (C-C''). Myotubes (A-B'') or myotubes and tendons (C-C'') are labelled with GFP in green, Robo staining is shown in red. A-A'| w^-, 18h APF; myotubes are split and tips are smoothening. A''| Robo is only weakly detectable along the muscle membrane and strongly present in tendon cells. Robo is highly enriched at the myotube-tendon contact site. B-B''| *kon*^{NIG}, 18h APF; Robo is hardly detectable in myotubes and strongly present in tendon cells, it is enriched at the basal tendon membrane also outside of myotube-tendon contacts (arrow). C-C''| w^-, 30h APF; Robo is localised to the myotube-tendon contact site. Robo is highly present in tendon extensions marked by *sr*-Gal4 >UAS-GFP-Gma. Arrowheads mark myotube-tendon contact sites, arrows mark Robo enrichment outside of myotube-tendon contacts in *kon*^{NIG}, asterisk marks tendon extensions.

3.2.5.3 Localisation of integrin complex and signalling components

To analyse the development of the myotendinous junction in *kon* knock-down, localisation of integrin complex and signalling pathway components was analysed during attachment initiation and maturation. To this end pupal offspring of *Mef*2-Gal4>UAS-GFP-Gma crossed to w^-, *kon*^{KK} or *kon*^{NIG} were dissected and stained at 18h and 30h APF.

First β-PS integrin localisation was analysed during attachment initiation at 18h APF. In the hypomorphic *kon*^{KK} knock-down line β-PS integrin localises only to parts of myotube tips, especially myotube areas that overshoot tendon cells do not show β-PS integrin accumulation at the tips (Figure 54B). In the strong *kon*^{NIG} knock-down line, β-PS integrin

enrichment at myotube tips is largely abolished (Figure 54C). Defective β-PS integrin localisation in both *kon* knock-down lines demonstrates that Kon or Kon mediated processes are essential for recruitment of β-PS integrin to myotube tips.

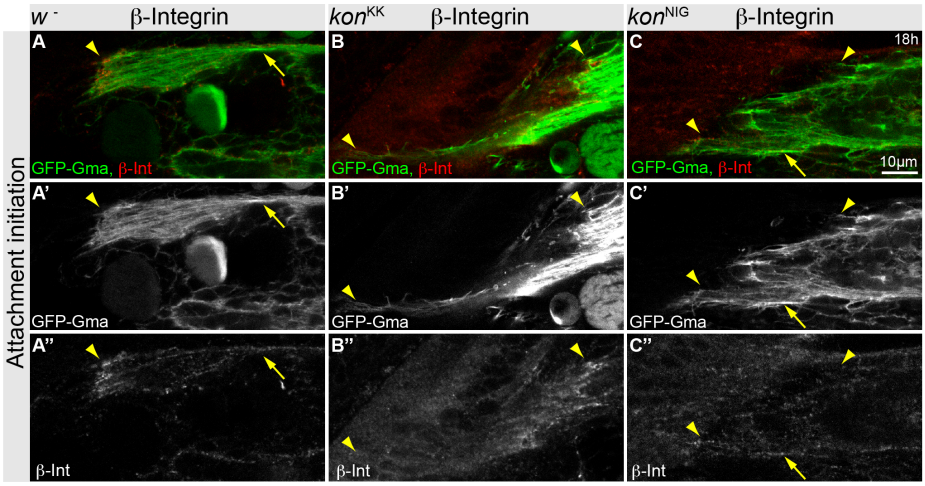

Figure 54 β-PS integrin localisation in wild type and *kon*^{IR} pupae during attachment initiation. Confocal images of 18h APF dissections of *Mef2*-Gal4>UAS-GFP-Gma (w^-, A), *Mef2*-Gal4>UAS-GFP-Gma, *kon*^{KK} (B) or *Mef2*-Gal4>UAS-GFP-Gma, *kon*^{NIG} pupae (C). Myotubes are labelled with GFP in green and β-PS integrin in red. A-A''| w^-; β-PS integrin is present at the myotube surface; it is enriched at myotube tips. B-B''| *kon*^{KK}; β-PS integrin is present at the myotube surface, it is enriched at some myotube tip areas but not in areas where myotubes overshoot tendon cells. C-C''| *kon*^{NIG}; β-PS integrin is present at the myotube surface, it is not enriched at myotube tips. Arrowheads mark myotube tips, arrows mark other myotube surface regions.

Next, localisation of Talin and pFAK was analysed during attachment initiation. The faint localisation of Talin, which can be observed in wild type is abolished in *kon*^{NIG}. Additionally, Talin levels seem extremely low (Figure 55A, B, B''). Similarly, low pFAK enrichment at myotube tips is detected in *kon*^{NIG} (Figure 55C, D, D''), further supporting a role for Kon or Kon mediated processes in recruiting integrin complex and signalling components to myotube tips.

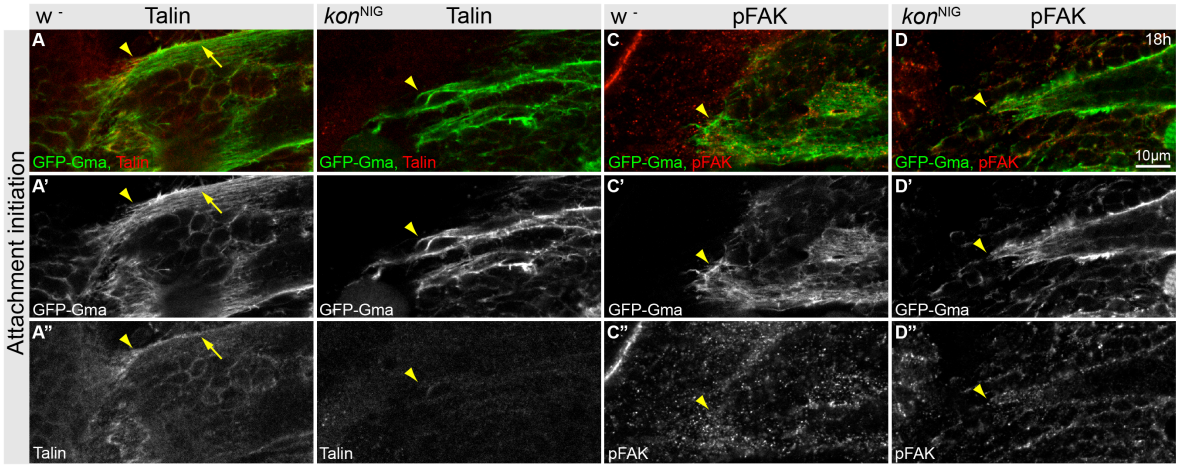

Figure 55 Talin and pFAK localisation in wild type and *kon*^{NIG} pupae during attachment initiation. Confocal images of 18h APF dissections of *Mef2*-Gal4>UAS-GFP-Gma (w^-, A, C) or *Mef2*-Gal4>UAS-GFP-Gma *kon*^{NIG} (B, D) pupae. Myotubes are labelled with GFP in green, Talin or pFAK are shown in red. A-A''| w^-, Talin is present at the myotube surface; it is slightly enriched at myotube tips. B-B''| *kon*^{NIG}; Talin surface levels are reduced, it is not enriched myotube tips C-C''| w^-, pFAK is present at the myotube surface; it is slightly enriched at myotube tips. D-D''| *kon*^{NIG}, pFAK is present at the myotube surface, it is not enriched at myotube tips. Arrowheads mark myotube tips, arrows mark other myotube surface regions.

As integrin complex and signalling components are strongly recruited after attachment initiation (section 3.2.4.2), their localisation was also analysed during attachment maturation at 30h APF (Figure 56,Figure 57). β-PS integrin is present in low levels at the surface of the rounded *kon*^{NIG} myotubes, however no distinct localisation is detectable (Figure 56B''). Interestingly, Talin, which could hardly be detected in *kon*^{NIG} myotubes at 18h APF is still barely detectable at 30h APF (Figure 56D''), indicating that Talin is never enriched at *kon*^{NIG} myotube tips.

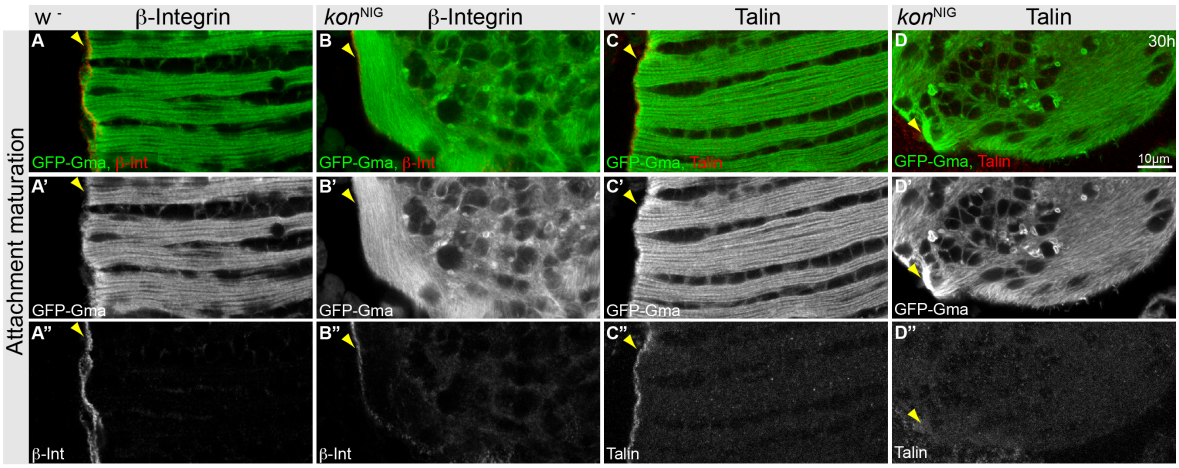

Figure 56 β-PS integrin and Talin localisation in wild type and *kon*^{NIG} pupae during attachment maturation. Confocal images of 30h APF dissections of *Mef2*-Gal4>UAS-GFP-Gma pupae crossed to w^- (A,C) or *kon*^{NIG} (B,D). Myotubes are labelled with GFP in green, β-PS integrin or Talin are shown in red. A-A''| w^-, β-PS integrin localises strongly to myotube tips. B-B''| *kon*^{NIG}; β-PS integrin surface levels are very low; no clear localisation is visible. C-C''| w^-; Talin localises strongly to myotube tips. D-D''| *kon*^{NIG}; Talin is hardly detectable; no clear localisation is visible. Arrowheads mark myotube tips or edges of round myotubes.

Similar to β-PS integrin pFAK; is present at low levels at the surface of rounded *kon*^{NIG} myotubes, however no distinct localisation is detectable (Figure 57B''). Tsp is not detectable in *kon*^{NIG} myotubes, even if they are in close proximity to tendon cells, as visualised by co-staining with Shot (Figure 57D'', Figure 58B), demonstrating the failure of myotendinous junction formation. Taken together, these data show that Kon is essential for recruitment of integrin complex and signalling components to myotube tips. Consequently, no cell-matrix attachment can be formed in the absence of Kon mediated attachment initiation.

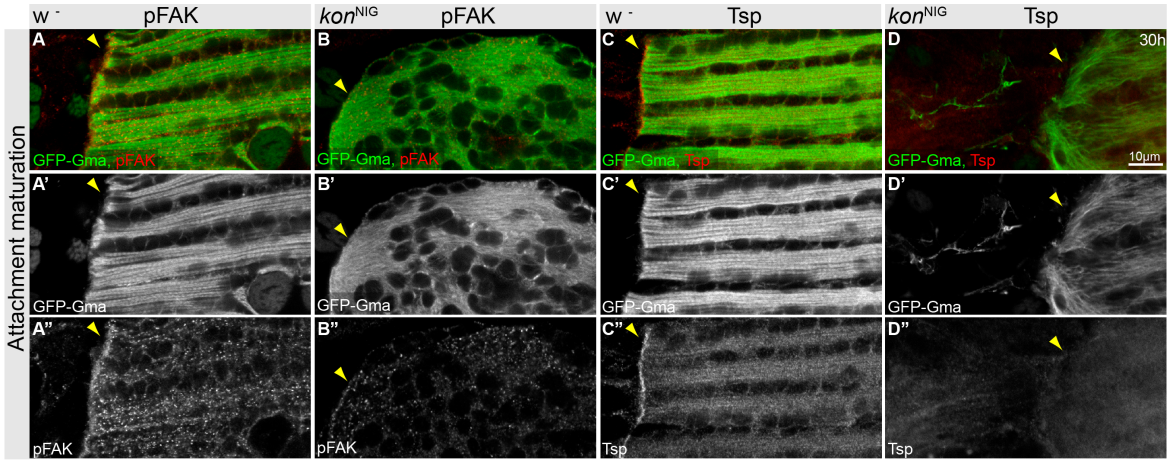

Figure 57 pFAK and Tsp localisation in *w*$^{-}$ and *kon*^{NIG} pupae during attachment maturation. Confocal images of 30h APF dissections of *Mef2*-Gal4>UAS-GFP-Gma pupae (*w*$^{-}$, A, C) or *Mef2*-Gal4>UAS-GFP-Gma, *kon*^{NIG} (B, D). Myotubes are labelled with GFP in green, pFAK or Tsp are shown in red. A-A''| *w*$^{-}$; pFAK localises strongly to myotube tips. B-B''| *kon*^{NIG}; no clear pFAK localisation is visible. C-C''| *w*$^{-}$; Tsp localises strongly to myotendinous junction. D-D''| *kon*^{NIG}; Tsp is hardly detectable, no clear localisation is visible. Arrowheads mark myotube tips or edges of round myotubes.

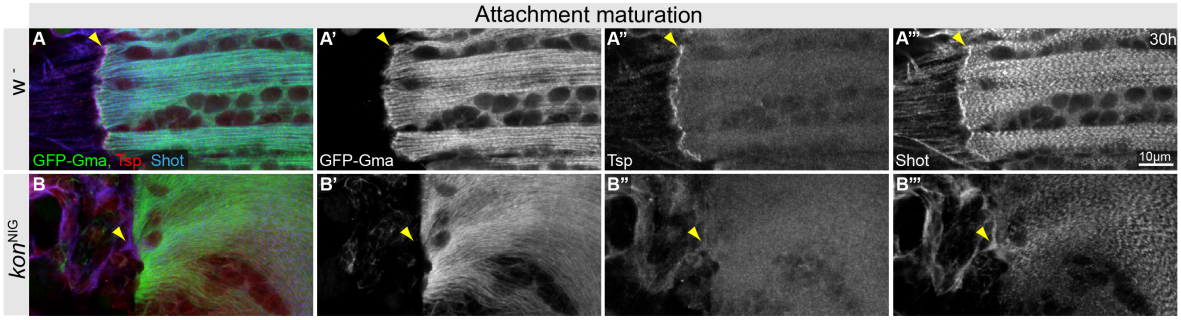

Figure 58 Shot and Tsp localisation in wild type and *kon*^{NIG} pupae during attachment maturation. Confocal images of 30h APF dissections of *Mef2*-Gal4>UAS-GFP-Gma (*w*$^{-}$, A) or *Mef2*-Gal4>UAS-GFP-Gma, *kon*^{NIG} (B) pupae. Myotubes are labelled with GFP in green, Tsp is shown in red and myotubes and tendons are labelled with Shot in blue. A-A'''| *w*$^{-}$, Tsp localises strongly to myotendinous junction, many tendons connect the myotube and Shot is localised to the contact site. B-B''| *kon*^{NIG}; Tsp is hardly detectable; no clear localisation is visible; only few tendons are in proximity to the rounded myotube. Arrowheads mark tendons in proximity to the myotube.

3.2.6 Molecular analysis of myotube-tendon connections in *Grip* knock-down

To date, Grip is the only known interaction partner of Kon. In *Drosophila* embryos Grip mutants show a comparable phenotype to a hypomorphic *kon*^{A04} allele lacking the intracellular domain of Kon. Grip binds to the intracellular PDZ-binding motive of Kon where it is thought to initiate signalling by recruitment of other factors (Schnorrer et al., 2007). To study the relationship of Kon and Grip during DLM development, the *Grip*

knock-down phenotype was analysed for muscle morphology as well as Kon and integrin localisation.

Pupal offspring of *Mef*2-Gal4>UAS-GFP-Gma crossed to w^- or *Grip*^{IR} were dissected at 90h APF and imaged for GFP signal (Figure 59). *Grip* knock-down caused variable myotube phenotypes, most likely resulting form variations in knock-down efficiency. The weaker phenotype results in 2-3 normal looking DLMs and 3-4 round or torn DLMs (Figure 59B), while the stronger phenotype resulting in loss and rounding up of DLMs (Figure 59C). Both *Grip*^{IR} phenotypes are very similar to *kon*^{IR} phenotypes (Figure 34) and indicate an attachment defect.

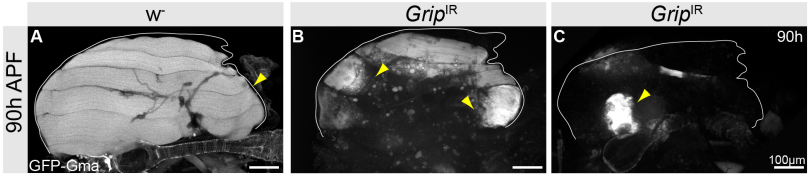

Figure 59 *Grip* knock-down phenotype at 90h APF. Confocal images of 90h APF dissections of *Mef2*-Gal4>UAS-GFP-Gma (w^- ,A) or *Mef2*-Gal4>UAS-GFP-Gma, *Grip*^{IR} (B, C) pupae. Muscles are labelled with GFP depicted in grey. A| w^-; muscles are elongated and fill the complete thorax. B| *Grip*^{IR}; weaker phenotype; some muscles are elongated and appear normal, other muscles are torn and round C| *Grip*^{IR}; strong phenotype; most muscles are missing, remaining are round or extremely thin. Arrowheads mark elongated, normal muscles in A or round and torn muscles in B and C.

To elucidate the influence of *Grip* knock-down on attachment initiation, pupal offspring of *Mef*2-Gal4>UAS-GFP-Gma crossed to w^- or *Grip*^{IR} were stained for Shot and Robo, which localise to the myotube-tendon contact site at 18h APF (Figure 60). Robo staining in *Grip*^{IR}, similarly to wild type, is enriched at the myotube-tendon contact site. Interestingly, however, Robo is hardly detectable in wild type myotubes but is clearly present in *Grip*^{IR} myotubes (Figure 60A'''- C'''). If Robo is almost completely localised to the myotendinous junction it is difficult to distinguish if the antibody signal originates from the tendon or the myotube. Therefore, enhanced myotube staining in *Grip*^{IR} could reflect reduced localisation of Robo to the myotendinous junction, possibly indicating a role for Grip in localising Robo to the myotendinous junction in myotubes.

During attachment initiation *Grip*^{IR} myotubes form long protrusions that overshoot tendon cells extensions, resembling the hypomorphic *kon*^{KK} knock-down (Figure 60A-C, Figure 43). Accordingly, Shot accumulation at the myotube-tendon contact site is not detectable in *Grip*^{IR} (Figure 60A''-C''). Taken together, these data demonstrate that Grip, similar to Kon, is essential for correct initiation of myotube-tendon attachment.

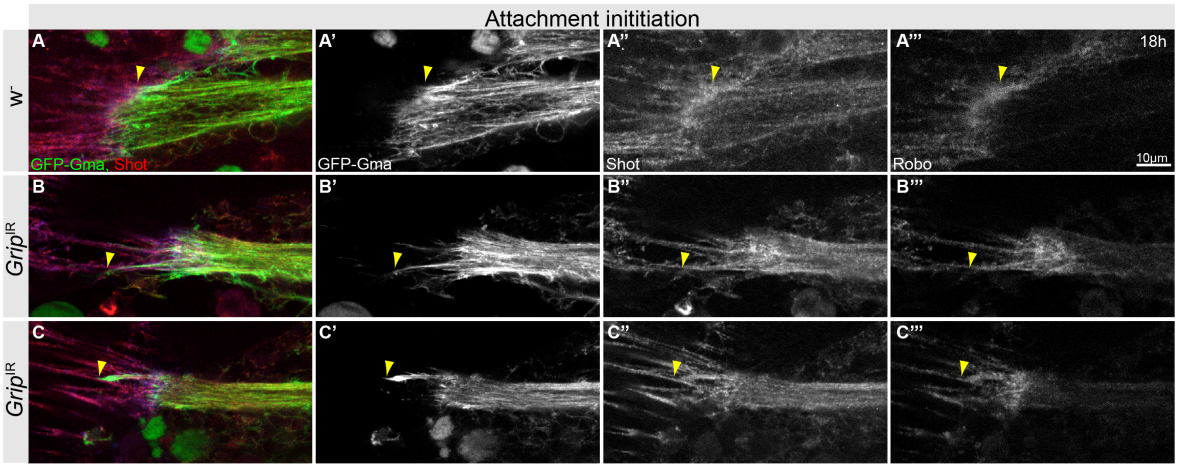

Figure 60 Myotube and tendon network in *Grip* knock-down pupae during attachment initiation. Confocal images of 18h APF dissections of *Mef2*-Gal4 >UAS-GFP-Gma (w^- , A) or *Mef2*-Gal4 >UAS-GFP-Gma, $grip^{IR}$ (B, C) pupae, myotubes are labelled with GFP in green, myotube and tendons are stained with Shot in red, Robo is shown in blue. A-A'''| w^-, smooth myotube tips display small filopodia, myotubes and tendons are in close contact, Shot and Robo accumulate at myotube-tendon contact site. B-B'''| $grip^{IR}$, myotubes tips form very long projections, which overshoot tendon cells. Yellow arrowheads mark myotube-tendon contact sites.

To explore the effect of *Grip* knock-down on Kon and β-PS integrin localisation during attachment initiation and maturation, pupal offspring of *Mef*2-Gal4>UAS-GFP-Gma crossed to w^- or $Grip^{IR}$ were stained for Kon and β-PS integrin at 18h APF (Figure 61) and 30h APF respectively (Figure 62). *Grip* knock-down causes variable morphological phenotypes accompanied by different localisation patterns of Kon and β-PS integrin. At 18h APF $Grip^{IR}$ myotubes display rarely a weak phenotype where filopodia are comparable to wild type and Kon as well as β-PS integrin localise to myotube tips (Figure 61A,B). Often, $Grip^{IR}$ myotubes show a stronger morphological defect, they form long protrusions and fail to localise Kon and β-PS integrin to myotube tips (Figure 61C,D). In these $Grip^{IR}$ myotubes, Kon can be found at myoblast and myotube surfaces, where it seems enriched at the surface facing the split side of the myotube (Figure 61C), or Kon is only detected as small dots without any obvious localisation (Figure 61D). The strength β-PS integrin localisation defects corresponds to that of Kon. These data suggest that Grip is localising Kon to myotube tips. Taken together, these data indicate that Grip mediated localisation of Kon to myotube tips is essential for attachment initiation and successive β-PS integrin recruitment to myotube tips.

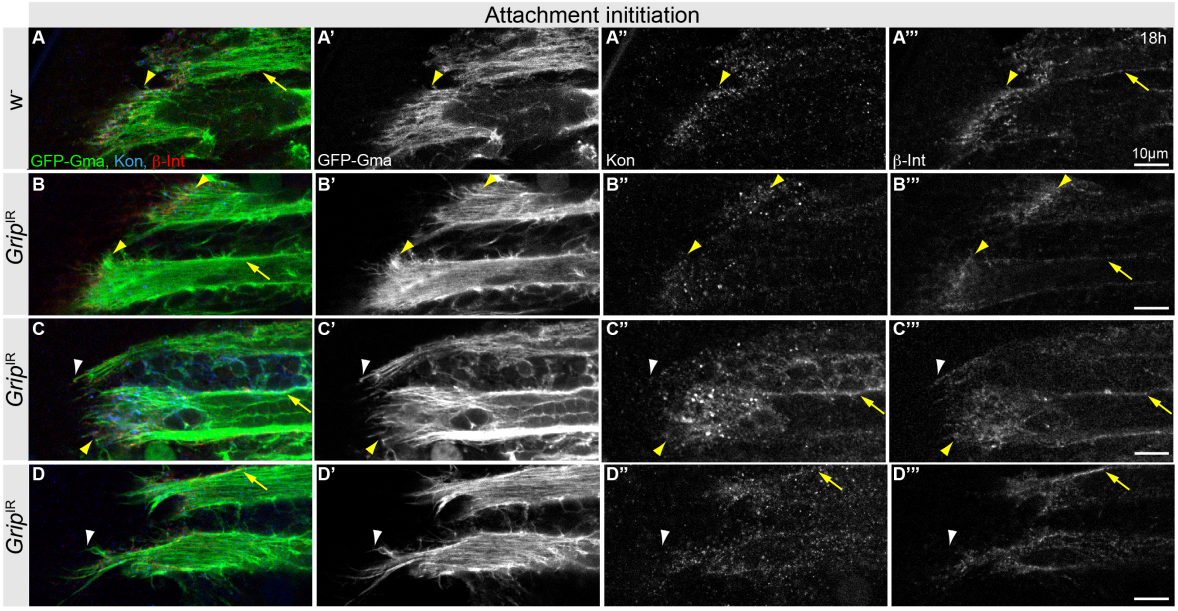

Figure 61 Kon and β-PS integrin localisation in wild type and *Grip* knock-down pupae during attachment initiation. Confocal images of 18h APF dissections of *Mef2*-Gal4>UAS-GFP-Gma (w^-, A) or $Grip^{IR}$ (B-D) pupae. Myotubes are labelled with GFP in green, Kon in blue and β-PS integrin in red. A-A'''| w^-; myotube tips show only short filopodia, Kon localises to myotube tips. β-PS integrin is present at the myotube surface, it is enriched at myotube tips. B-B'''| $Grip^{IR}$; myotube tips show only short filopodia, Kon localises mainly to myotube tips. β-PS integrin is present at the myotube surface, it is enriched at myotube tips. C-C'''| $Grip^{IR}$, myotubes show long protrusions (white arrowhead) or filopodia (yellow arrowhead), Kon and β-PS integrin do not localise to myotube tips of long protrusions but are slightly enriched at myotube tips with filopodia. Kon localises to split myotube surfaces and myoblast surfaces. D-D'''| $Grip^{IR}$, myotubes show long protrusions, Kon does not show a clear localisation, β-PS integrin localises to myotube surfaces but is not enriched at myotube tips. Yellow arrowheads mark myotube tips, white arrowheads mark myotube protrusions, yellow arrows mark other myotube surface regions.

At 30h APF w^- myotubes show strong Kon and β-PS integrin localisation to myotube tips. The weaker phenotype that was rarely found at 18h APF, results most likely in the weaker phenotype detected in rare cases at 30h APF. Myotubes that display this weaker phenotype are compacted and have straight tips. However, they show strong β-PS integrin localisation, but only very faint Kon localisation at the myotube tips (Figure 62A-B), demonstrating that Kon localisation to myotube tips cannot be maintained even in morphologically normal $Grip^{IR}$ escaper myotubes. Moreover, strongly reduced Kon levels at the myotendinous junction of these morphologically normal $Grip^{IR}$ myotubes indicate that Kon is not essential for attachment maturation.

Strongly affected $Grip^{IR}$ myotubes are round and do not display detectable levels of Kon (Figure 62C,D). β-PS integrin is mainly restricted to the surface of round $Grip^{IR}$ myotubes (Figure 62C,D). β-PS integrin staining at round myotube surfaces often shows lines, which are frequently at the ends of myofibrils possibly indicating β-PS integrin mediated fibril

anchoring at the myotube surface (Figure 62C). Taken together, these data indicate that Grip dependent Kon localisation to myotube tips is essential for attachment initiation but not for attachment maturation.

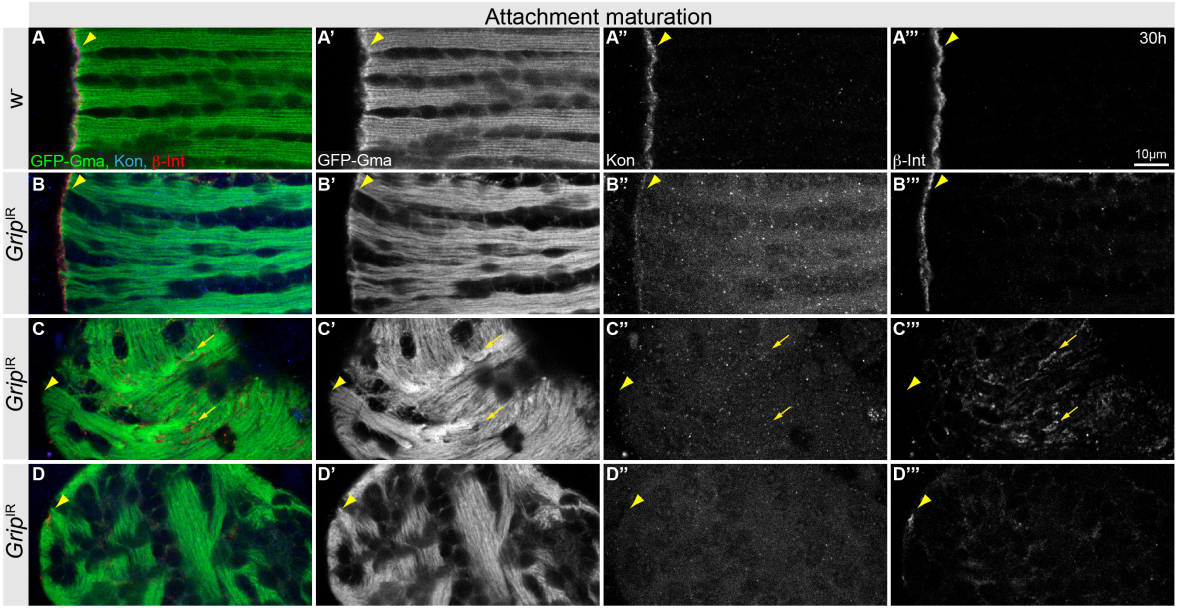

Figure 62 Kon and β-PS integrin localisation in wild type and *Grip* knock-down pupae during attachment maturation. Confocal images of 30h APF dissections of *Mef2*-Gal4>UAS-GFP-Gma (w^-, A) or *Mef2*-Gal4>UAS-GFP-Gma, $Grip^{IR}$ (B-D) pupae. Myotubes are labelled with GFP in green, Kon in blue and β-PS integrin in red. A-A'''| w^-, myotube tips show only short filopodia, Kon localises to myotube tips, β-PS integrin is present at the myotube surface, it is enriched at myotube tips. B-B'''| $Grip^{IR}$, myotube tips show only short filopodia, Kon localises mainly to myotube tips. β-PS integrin is present at the myotube surface; it is enriched at myotube tips. C-C'''| $Grip^{IR}$, myotubes show long protrusions (white arrowhead) or filopodia (yellow arrowhead), Kon and β-PS integrin do not localise to myotube tips of long protrusions but are slightly enriched at myotube tips with filopodia. Kon localises to split myotube surfaces and myoblast surfaces. D-D'''| $Grip^{IR}$, myotubes show long protrusions, Kon does not show a clear localisation, β-PS integrin localises to myotube surfaces but is not enriched at myotube tips. Arrowheads mark myotube tips, arrows mark other myotube surface regions.

3.2.7 Functional investigation of integrin complex components

The previous experiments showed that *kon* is essential for attachment initiation and integrin complex localisation and indicated that integrins could be the key players for attachment maturation. To elucidate at which step during DLM development integrins act, *if*, *rhea* and *mys* encoding for α-PS2 integrin, Talin and β-PS integrin, respectively, were knocked-down. As muscle specific knock-down of either *if*, *rhea* or *mys* causes larval or early pupal lethality the Gal80*ts* system was used for temporal control of hairpin expression. *mhc*GFP; *tub*-$Gal80^{ts}$, *Mef2*-Gal4>UAS-Cherry-Gma was crossed to if^{IR}, $rhea^{IR}$, mys^{IR} or w^-. Different shifting conditions were compared and the condition, which led to the strongest phenotype at 90h APF without causing early pupal lethality, was

determined. Crosses were kept at 18°C, shifted to a permissive temperature of 31°C two days before staging and kept at 31°C until dissections at 90h APF. Under these conditions *if*^{IR} shows a relatively mild phenotype with 0-2 DLMs missing, while the remaining DLMs always fill the thorax (Figure 63B). *rhea*^{IR} causes reduced DLM fiber number and usually displays only three DLMs filling the thorax, indicating a myotube splitting defect (Figure 63C). *mys*^{IR} leads to severe loss and rounding up of DLMs.

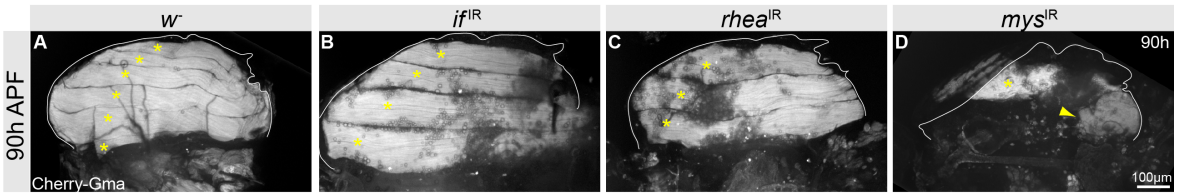

Figure 63 Integrin and Talin knock-down phenotype at 90h APF. Confocal images of hemithoraxes at 90h APF. *mhc*GFP; *tub*-Gal80^{ts}, *Mef2*-Gal4>UAS-Cherry-Gma crossed to w^- (A), *if*^{IR} (B), *rhea*^{IR} (C) or *mys*^{IR} (D). A| w^-; hemithorax is filled with six DLMs . B| *if*^{IR}; hemithorax is filled with four DLMs. C|. *rhea*^{IR}; hemithorax is filled with three DLMs. D| *mys*^{IR}; hemithorax is largely empty, DLMs are missing, 1 DLM spans the thorax from anterior to posterior, 1-2 DLMs are round. Asterisks mark attached DLMs; arrow marks round DLMs, white lines trace the outline of the hemithoraces.

Muscle-specific knock-down of *mys* showed the strongest phenotype (Figure 63). To investigate when the *mys*^{IR} phenotype arises, 2-photon live imaging was applied. Living *tub*Gal80^{ts} ,*Mef2*-Gal4 >UAS-GFP-Gma, *mys*^{IR} pupae were imaged starting around 13.5h APF (Figure 64). Interestingly, only the dorsal most myotube successfully migrates towards the tendon precursors, the lower myotubes span only half of the area and show long protrusions (Figure 64A). At about 14.5h APF the tips of the dorsalmost myotube smoothen while the two lower myotubes continue to migrate towards the anterior and posterior tendon precursors (Figure 64B). Around 17.5h APF the dorsalmost myotube completes splitting and shows smooth myotube tips, the two lower myotubes seem to reach the posterior tendons. Importantly, the lower myotubes continue to form long anterior protrusions, but fail to migrate towards the anterior tendons (Figure 64D). Consequently, the lower myotubes round up, while the dorsalmost myotubes compact (Figure 64E-H). Interestingly, adult myoblast precursors form a swarm like structure at the ventral thorax end, demonstrating that reduction of β-PS levels leads to migration defects of myotubes and myoblasts.

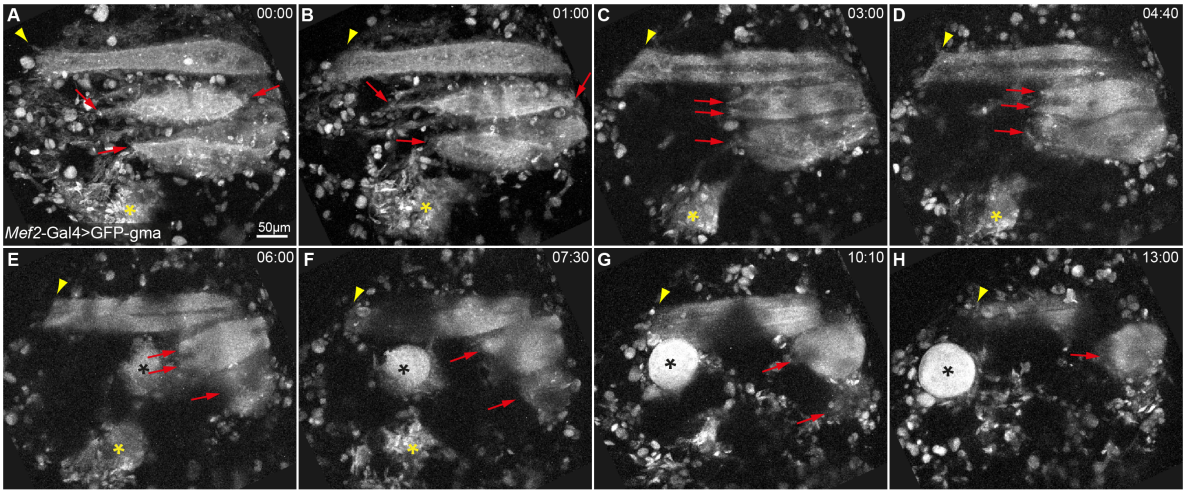

Figure 64 DLM-development of *mys* knock-down myotubes. Stills from a 2-photon movie of *tub*-Gal80^{ts}, *Mef2*-Gal4>UAS-GFP-Gma, *mys*^{IR} starting around 13.5h APF. A| Dorsalmost myotube migrates towards tendon precursors; two lower myotubes are shorter and form long protrusions. B| Dorsalmost, myotube is splitting and tips smoothen; two lower myotubes migrate anteriorly and posteriorly and form long protrusions. C,D| Dorsalmost myotube completed splitting and tips are smooth, two lower myotubes form long protrusions but do not migrate further. E-H| Dorsalmost myotubes compact, lower myotubes round up, DVMs also round up. Arrowheads mark anterior end of dorsalmost template/myotube, arrows mark ends of the two lower templates/myotubes, black asterisk marks round DVM, Yellow asterisk marks large group of myoblasts next to DLMs, time is indicated in hr:min.

Both experiments the 90h stills and the live imaging data show that only the dorsalmost myotubes are elongated while the lower DLMs are missing or round (Figure 63, Figure 64). Moreover, the posterior side seems attached in all remaining myotubes, this variation could indicate an incomplete knock-down. To assess knock-down efficiency pupal offspring of *mhc*GFP; *tub*-Gal80^{ts}, *Mef2*-Gal4>UAS-Cherry-Gma crossed to *if*^{IR} or *mys*^{IR} were dissected at 18h as well as 30h APF. As in the live imaging experiment (Figure 64), dorsalmost *mys*^{IR} myotubes are elongated and split at 18h APF, whereas the lower myotubes are much shorter at the anterior end and seem attached at the posterior end (Figure 65). Importantly, elongated as well as posterior ends of rounding *mys*^{IR} myotubes still display β-PS integrin localised to the tips (Figure 65A,B). At the anterior myotube ends of the rounding *mys*^{IR} myotubes, however, β-PS integrin is not detectable (Figure 65C), indicating that reduction of β-PS integrin levels at myotube tips lead to a strong migration defect.

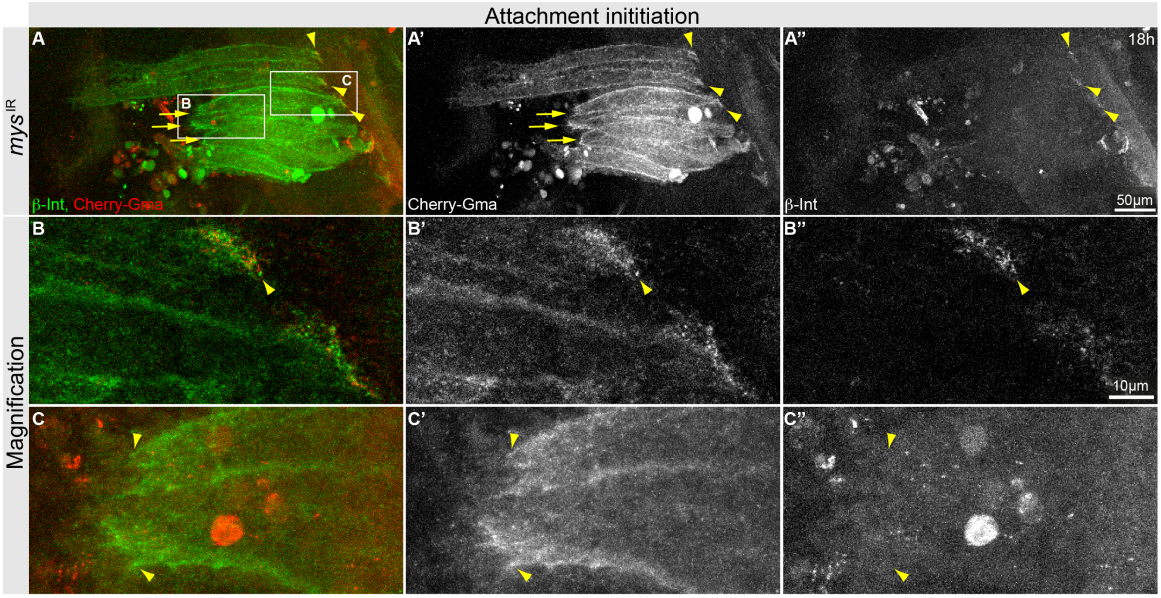

Figure 65 β-PS integrin localisation in *mys* knock-down pupae during attachment initiation. Confocal images of 18h APF dissections of *tub*-Gal80^{ts}; *mhc*GFP; *Mef2*-Gal4>UAS-Cherry-Gma crossed *mys*^{IR}. A| Overview image, topmost myotubes are elongated and split, anterior ends of lower myotubes reach only to half the distance. Topmost myotubes and posterior ends of lower myotubes display β-PS integrin localisation to tips. B| High magnification of attached myotube ends, β-PS integrin localises to myotube tips. C| High magnification of unattached myotube ends; β-PS integrin is not detectable at the myotube. White boxes in A mark positions of magnification in B and C, arrow marks anterior end of shorter DLMs, arrowheads mark posterior myotube ends expressing β-PS integrins.

At 30h APF the dorsalmost myotubes compact, while other myotubes are round (Figure 66A). The compacted, topmost myotube shows β-PS integrin localisation to both ends, while the round myotubes at the posterior side only display posterior β-PS integrin localisation (Figure 66). Taken together, these data show that *mys* knock-down is incomplete, leading only to partial loss of β-PS integrin. If the knock-down is strong enough to diminish β-PS integrin staining from myotube tips, myotubes show a strong migration defect, demonstrating that integrins are not only essential for myotube attachment but also for migration.

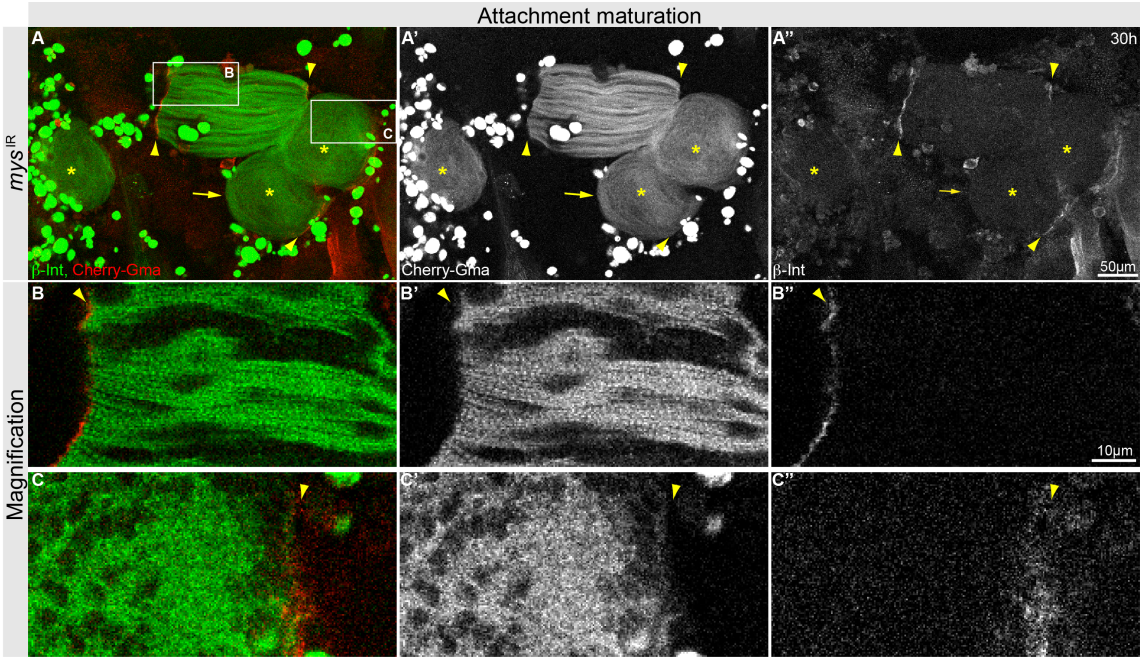

Figure 66 β-PS integrin localisation in *mys* knock-down pupae during attachment maturation. Confocal images of 30h APF dissections of *mhc*GFP; *tub*-Gal80^{ts}, *Mef2*-Gal4>UAS-Cherry-Gma crossed *mys*^{IR}. A| Overview image, topmost myotubes are compacted; lower myotubes are round. Topmost myotubes and posterior ends of lower myotubes display β-PS integrin localisation to tips. B| High magnification of a round myotube, β-PS integrin localises to posterior side of the myotube. C| High magnification dorsalmost, compacted myotube; β-PS integrin localises to myotube tip. White boxes in A mark positions of magnification in B and C, asterisks mark round myotubes, arrow marks anterior end of round DLM, arrowheads mark myotube ends expressing β-PS integrins.

3.2.8 Myofibrillogenesis and sarcomerogenesis

During attachment initiation and maturation the myotube changes its morphology dramatically from a thin myotube with filopodial extensions at the tip to a smooth thickening and compacting myofiber (section 3.2.2). Moreover, the actin cytoskeleton is remodelled after attachment initiation to eventually form myofibrils, with regularly spaced sarcomeres. How myofibrils and sarcomeres are formed is still not clear (section 2.5.2). To get a closer insight into myofibrillogenesis and sarcomerogenesis, changes in DLM morphology, molecular composition and physical properties between attachment initiation and maturation were analysed.

To assess the differences in cytoskeletal morphology between attachment initiation and attachment maturation in closer detail actin distribution was analysed in *Mef2*-Gal4>UAS-GFP-Gma pupae at 18h and 30h APF (Figure 67). Digital cross-sectioning at different positions along the 18h APF myotube reveals that the attaching front shows almost equal actin distribution and is more flat (Figure 67A, 1-2), while the myotube displays a tube-like, hollow structure towards the middle (Figure 67A, 3-5). At 30h APF actin is present throughout the fiber. Cross-sections at different positions along the myofiber show similar actin distribution within the fiber. Along the A-P axes actin is organised in bundled fibrils, which are distributed throughout the myofiber. (Figure 67B) representing a stark change of myotube morphology and actin distribution after attachment initiation.

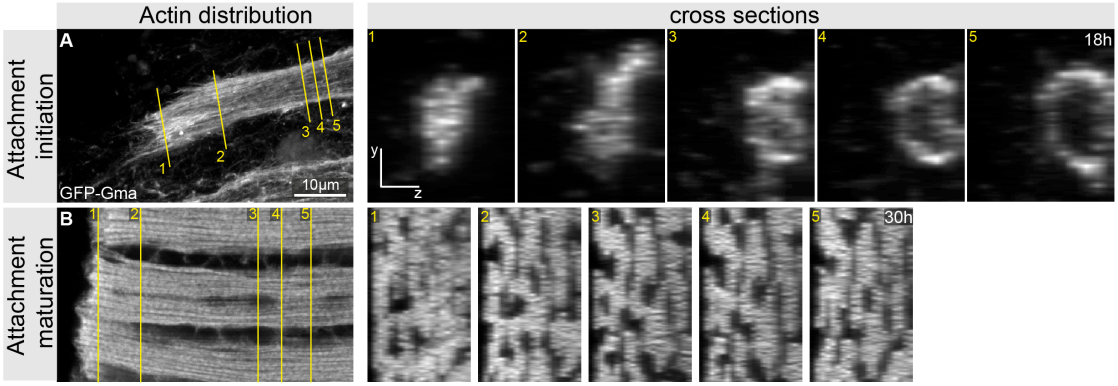

Figure 67 Actin distribution in myotubes during attachment initiation and maturation. Confocal images of dissected *Mef2*-Gal4>UAS-GFP-Gma pupae at 18h (A) and 30h (B) APF and digital cross-sections at different positions of the myotubes (1-5). A| Attachment initiation; myotube displays some filopodia at myotube tip. 1-2; Cross-sections at the tip show flat morphology and equal actin distribution. 3-5; Cross-sections at the middle show round morphology with actin restricted to the surface. B| Attachment maturation; myotube shows smooth ends, fibril bundles are formed throughout the fiber. Lines in A and B mark positions of the cross-sections, separate sections are labelled with yellow numbers.

In order to obtain a more detailed knowledge of the actin cytoskeleton *Mef2*-Gal4>UAS-GFP-Gma pupae were co-stained with the spectraplakin homologue Shot that displayed a periodic pattern at 30h APF (Figure 44). High magnification confocal images of *Mef2*-Gal4>UAS-GFP-Gma pupae stained with Shot were acquired at attachment initiation and maturation. At attachment initiation, 18h APF actin assembly to thin filaments is detected at the myotube surface (Figure 68A,A'). The actin-microtubule crosslinker Shot seems to display a dotted pattern on these actin filaments (Figure 68A''). During attachment maturation actin fibrils spanning the myofiber are formed (Figure 68B). Actin, which is anchored at the Z-line in adult sarcomeres, is already distributed in a sarcomeric pattern along these fibers. Moreover, Shot pattern is also refined and stains mainly in-between actin stripes at 30h APF (Figure 68B), indicating that sarcomerogenesis starts after attachment initiation.

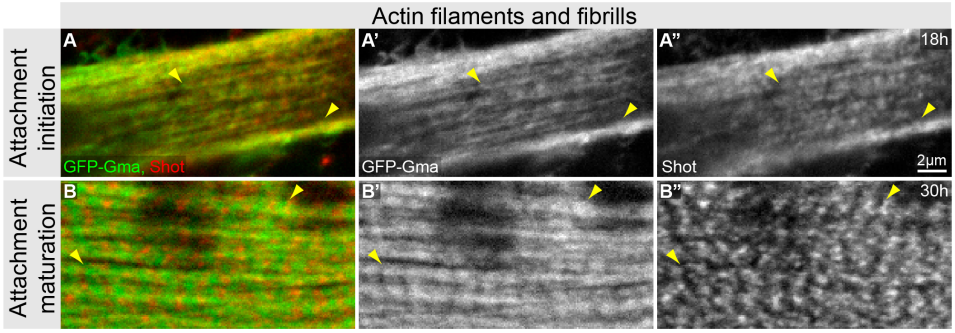

Figure 68 Actin filaments and fibrils during attachment initiation and maturation. Confocal images of dissected *Mef2*-Gal4>UAS-GFP-Gma pupae at 18h (A) and 30h (B) APF. A| Attachment initiation; actin assembles into thin filaments, distributed on myotube surface, Shot localises along actin filaments. B| Attachment maturation, actin assembles into fibrils. displaying a sarcomeric pattern, Shot localises in-between actin stripes. Arrowheads point to single actin filaments and fibers.

To get a closer insight into sarcomere formation, localisation of the M-line marker myosin heavy chain (Mhc) was analysed using the protein trap Mhc$^{Wee\text{-}P26}$-GFP (Mhc-GFP). 2-photon live imaging was applied to image Mhc-GFP pupae starting at 26h APF. Additionally, high-resolution single time-points were imaged between 26h and 34h APF (Figure 69). Mhc-GFP signal is hardly detectable at 26h APF when myotubes are compacting (Figure 69A). With advancing compaction myofiber tips straighten completely and Mhc signal increases strongly (Figure 69B-C). Around 30h APF myotubes are strongly compacted and show high Mhc-GFP signal (Figure 69C, H). Interestingly, Mhc-GFP simultaneously organises into a regularly dotted pattern throughout the imaged area (Figure 69H, H'). The periodic Mhc pattern is maintained during myotube extension and growth (Figure 69I-J'). Taken together, these data show a synchronised incorporation of

Mhc into myofibrills between 28h and 30h APF, which could indicate simultaneous myofibrillogenesis.

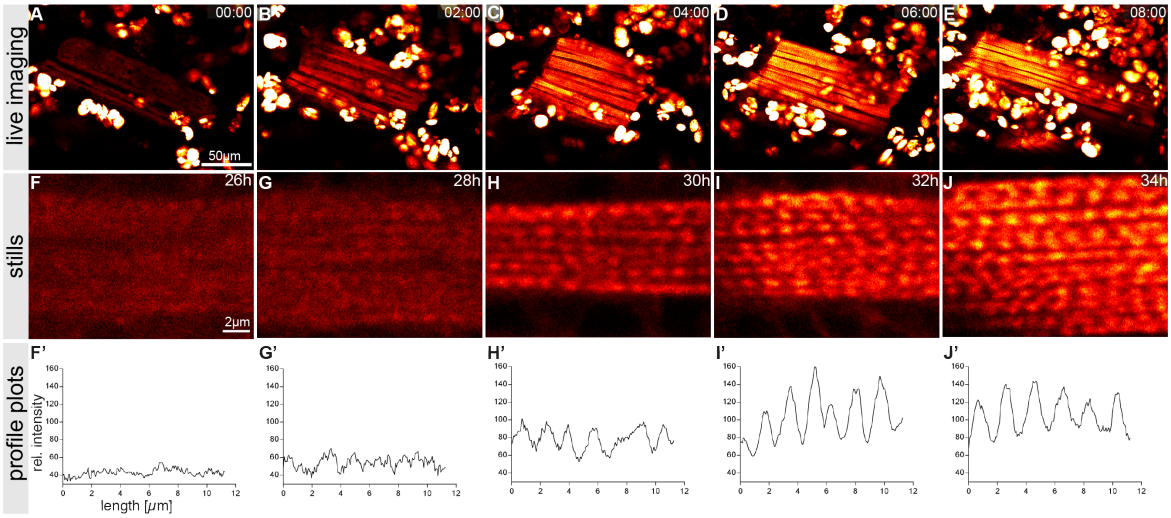

Figure 69 Mhc patterning during attachment maturation. Stills from a 2-photon movie of Mhc-GFP pupa starting at 26h APF (A-E), high-resolution single time-points of Mhc-GFP DLMs (F-J), relative intensity plots of single fibers in F-J (F',G',H',I',J'). A| 26h APF, 00:00; myotube is in the process of compacting but still very long, tips are roundish. Mhc-GFP is hardly detectable B| 02:00; myofiber compacts further, ends are straight, Mhc-GFP signal increases. C| 04:00; myofiber is strongly compacted, Mhc-GFP signal increases further. D| 06:00; myofiber is elongating, Mhc-GFP signal increases further. E| 08:00; myofiber is further elongated, Mhc-GFP signal is very strong. F, F'| 26h APF; Mhc-GFP is hardly detectable G, G'| 28h APF; weak, dot-like Mhc-GFP signal visible. H-J'| 30h-34h APF; a strong Mhc-GFP pattern is visible. Time is indicated in hr:min (A-E) (Images from F. Schnorrer).

3.2.8.1 Tension formation during myogenesis

Mhc-GFP imaging indicates that myofibrils and sarcomeres are formed simultaneously throughout the fiber. This raises the question how such a simultaneous myofibrillogenesis could be achieved. Both, in vitro and in silico studies hypothesised that tension might influence myofibrillogenesis (De Deyne, 2000; Engler, 2004; Kagawa et al., 2006; Yoshinaga et al., 2010). Equal distribution of tension along the developing myofiber could trigger simultaneous myofibrillogenesis throughout the complete fiber. However, so far tension has not been measured in vivo. Therefore, it is still unknown if tension is built-up during myogenesis. Consequently, it is not clear if myotubes are under tension and if this influences myofibrillogenesis and sarcomerogenesis. To analyse if tension is formed or altered in the developing myotube morphological changes and physical properties within the myotendinous system were analysed at various developmental stages.

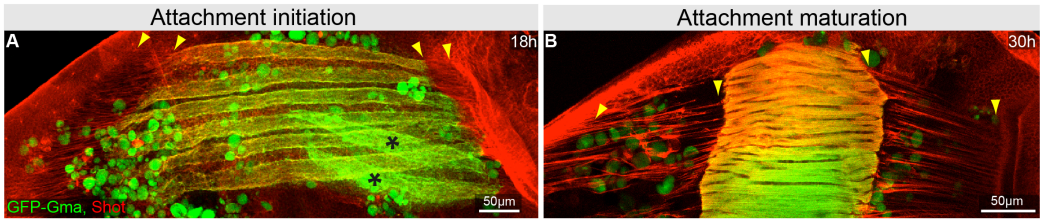

Figure 70 Overview of the myotendinous system at attachment initiation and maturation. Confocal images of 18h and 30h APF dissections of *Mef2*-Gal4>UAS-GFP-Gma pupae crossed to w^-. Myotubes are labelled with GFP in green, myotube and tendons are stained with Shot in red. A| 18h APF, split myotubes are connected to short tendon extensions on both ends. B| 30h APF, strongly compacted myofibers are connected to long tendon extensions at both ends. Arrowheads mark beginning and ends of tendon extensions.

As discussed in section 3.2 long tendon extensions are formed after attachment initiation and increase in length during attachment maturation, when myofibers compact. The morphological changes of the myotendinous network, especially the formation of the long tendon extensions during myotube compaction, suggest development of tension in the myotendinous system (Figure 70).

To investigate if tension is built-up during myogenesis laser-cutting of tendon extensions was performed. The speed of tendon tissue movement after cutting (recoil velocity) was measured and the initial recoil velocity was calculated. The initial recoil velocity of the extensions is proportional to the tension in the analysed system (Mayer et al., 2010). Therefore, the initial recoil velocity is used as readout for tension in the myotendinous system. To compare tension during different myogenic states, tendons were cut at 13h APF, reflecting myotube migration, 18h APF for attachment initiation and 22h APF for attachment maturation. Tendons and myotubes were labelled using UAS-CD8-GFP expressed under control of the muscle specific *Mef2*-Gal4 and the tendon specific *sr*-Gal4 drivers. To perform the laser-cutting experiment, living pupae were prepared for live imaging, then a 2µm long cut was applied to the anterior tendon extensions using a pulsed UV-laser and the myotendinous system was imaged at a high time resolution of 150ms with a spinning disc confocal system. Pupae that were kept after application of the laser-cut were still able to eclose, showing that laser-cutting and live imaging did not impair pupal development. Figure 71 shows stills of live imaging before and after laser-cutting during migration, attachment initiation and attachment maturation. After laser-cutting, tendon tissue adjacent to the cut moves in an orthogonal direction away from the cutting line (Figure 71). If the cut is applied during migration states at 13h a small hole forms in the tendon tissue but largely keeps its size during imaging after the cut (Figure 71A-D). Tendon extensions that were cut during attachment initiation form a larger hole that is

slightly expanding with time (Figure 71E-H). During attachment maturation however, cutting of the long tendon extensions leads to massive recoil of both ends of the severed extension, resulting in the formation of a large hole in the tendon network, which is also expanding during the time of imaging (Figure 71I-L). Taken together, these increasing responses to the tendon-severing at attachment initiation and maturation indicate a higher tension during attachment maturation than at migration states.

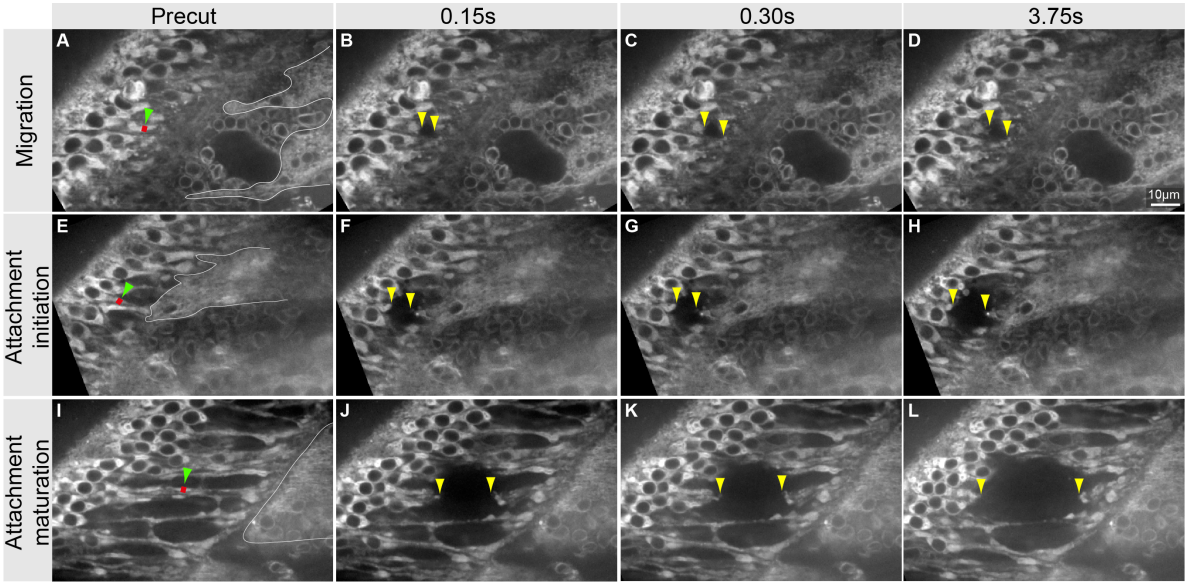

Figure 71 Laser-cutting of tendon extensions during migration, attachment initiation and attachment maturation. Stills from spinning disc confocal movies of *sr*-Gal4, *Mef2*-Gal4>UAS-GFP-Gma pupae at 13h (A-D), 18h (E-H) and 22h (I-L) APF. Pre-cut (A,E,I) and post cut frames (B-D, F-H, I-L) are shown. A| 13h APF, pre-cut; some parts of the myotube are contacting the tendon cells, small tendon elongations are visible. B-C| 0.15s, 0.30s and 3.75s post cut; tendons move orthogonally away from the cut-line. A hole forms in the tendon tissue. E| 18h APF, pre-cut; Myotube tips are in close contact with tendon cells, small tendon extensions are formed. F-H| 0.15s, 0.30s and 3.75s post cut; tendons move orthogonally away from the cut-line, the hole in the tendon tissue increases slightly over time. I| 22h APF, pre-cut; Myotube tips are smooth and completely in contact with tendon cells, long tendon extensions are formed. F-H| 0.15s, 0.30s and 3.75s post cut; tendons move orthogonally away from the cut-line, the hole in the tendon tissue increases over time. Red line in A, E and I indicates the cut-line, green arrowheads point towards the cut-line. Yellow arrowheads indicate ends of the cut tendon extensions. Time indicates post-cut time and is counted from the first frame after the cut.

To assess tension changes in the myotendinous system, tendon movements after laser-cutting were traced using particle image velocimetry (PIV) and initial recoil velocities were calculated for all time points. To generate these PIV flow fields, the movement of points on a defined raster was calculated between two frames. Using the measured distance and the defined time between frames (150ms) the velocity was calculated. For visualisation of the analysis, the velocity vectors for an exemplary cutting movie, during attachment maturation, are shown as overlay in Figure 72E-H.

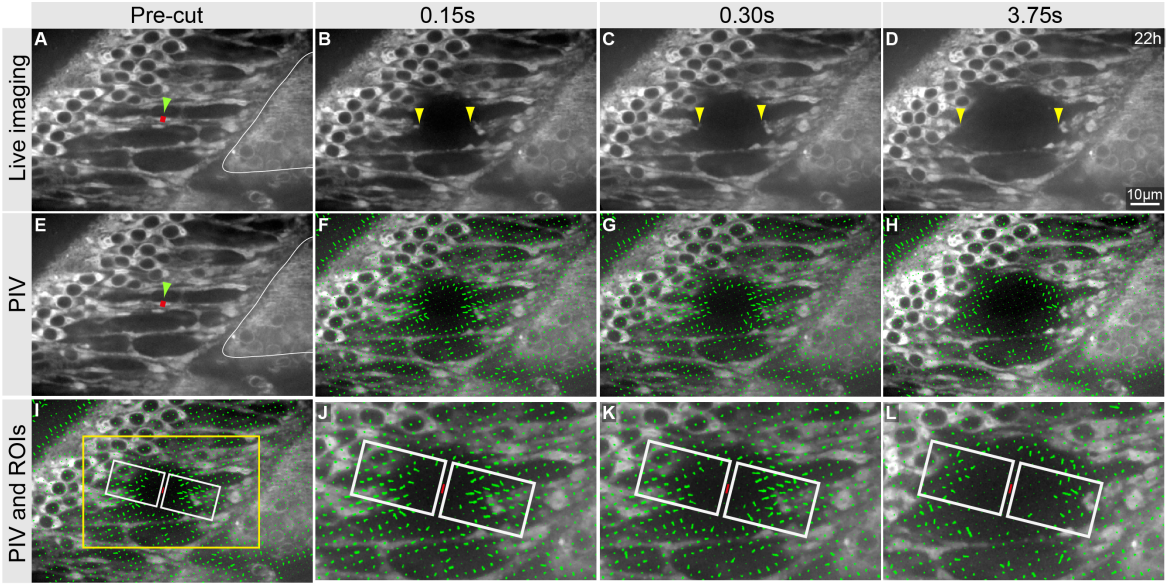

Figure 72 Particle image velocimetry (PIV) on post-cut movies. Stills from a spinning disc confocal movie of a *sr*-Gal4, *Mef2*-Gal4>UAS-GFP-Gma pupa starting at 22h APF and overlays with PIV flow fields (F-L). A-F| Pre- and post-cut stills at 22h APF; tendon tissue moves orthogonally away from the cutline. E-H| Pre- and post-cut stills at 22h APF with PIV flow field. I| Pre- and post-cut stills at 22h APF, with PIV flow field and ROIs for analysis. J-L| Zoom-ins for 0.15s, 0.30s and 3.75s post-cut of the region indicated in I (yellow box). Velocity vectors within ROIs are averaged for calculation of recoil velocities. Red line indicates the cut-line, green arrowheads point towards the cut-line. Yellow arrowheads indicate ends of the cut tendon extensions. White boxes highlight ROIs for analysis. Time indicates post-cut time and is counted from the first frame after the cut.

Further calculations were restricted to regions of interest focusing on the tissue next to the cut site. To this end two 17µm x 26µm boxes were placed in 0.4µm distances on both sides of the cut line (Figure 72J-L). PIV flow fields within these ROIs were averaged to retrieve velocity data for the regions of interest and plot them as a function of time-post-cut. The plot shows an exponential decay of the recoil velocity over time, which is typical for a viscoelastic response (Figure 73A). As a measure for tension, initial recoil velocity was obtained. The initial recoil velocity depends on the tension present in the myotendinous system as well as the friction-like resistance, which the tendon elongations experience with the surrounding material during recoil. The friction is reflected in the relaxation time, which can be measured using the time constant of the recoil τ. Initial recoil velocity and relaxation time constants were obtained by application of a least-square-fitting algorithm to the exponential function (Figure 73A-C). Additionally, initial recoil velocity was calculated directly form the movement of the 1st to the 2nd frame (Figure 73D). Both methods for determination of the initial recoil velocity show almost identical results. Therefore, future text will refer to the initial recoil velocity calculated using 1st and 2nd frames after cutting (Figure 73B,D). Towards the end of myotube migration initial recoil

velocity is 18.7 ± 10.7µm/min. Interestingly, initial recoil velocity increases dramatically to 57.6 ± 7.3µm/min during attachment initiation and doubles again during attachment maturation to 124.5 ± 10.7µm/min (Figure 73D). The prominent increase in initial recoil velocity during attachment initiation and maturation could be either due to an increase in tension or a decrease in friction between the tendon elongations and the extracellular material, measured by the relaxation time constant τ. The time constant τ however is also increasing during attachment initiation and maturation (Figure 73C), indicating a change in the material properties of the tendon extensions and their surrounding material during attachment initiation and maturation that is consistent with either an increase in friction between elongations and extracellular material or a softening of the extensions; for example by decrease of extension elasticity. The decrease of the relaxation time constant τ together with the strong increase of the initial recoil velocity show that tension is generated in the myotendinous system during attachment initiation and maturation.

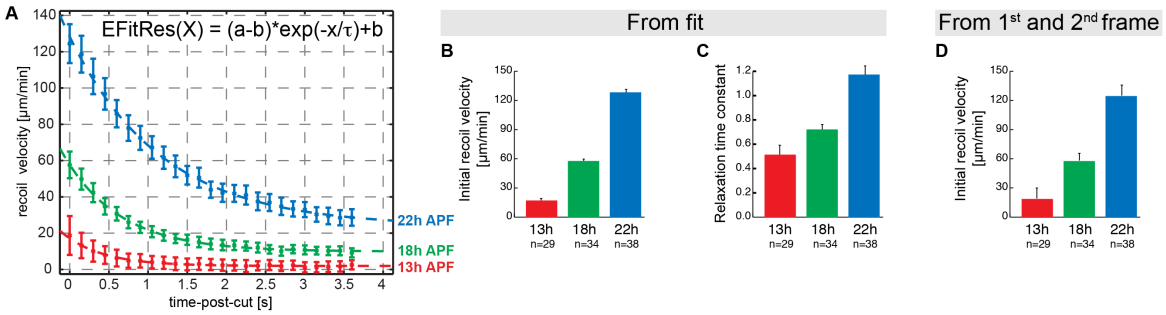

Figure 73 Recoil velocities, initial recoil velocities and relaxation time constants at 13h, 18h and 22h APF. A| Recoil velocities as time-post-cut function and least-square-fitting. 13h APF (red line), 18h APF (green line) and 22h APF (blue line); recoil velocities follow an exponential decay over time. B| Column graph of initial recoil velocity obtained from the fit (a value in the formula in A) at 13h APF, 17.14µm/min (15.2, 19.08); 18h APF, 57.72µm/min (55.81, 59.62) and 22h APF, 128.3µm/min (125.2, 131.5). C| Column graph of relaxation time constant obtained from the fit (τ value in the formula in A) at 13h APF, 0.514µm/min (0.4368, 0.5912); 18h APF, 0.7216µm/min (0.6817, 0.7614) and 22h APF, 1.173µm/min (1.099, 1.247). D| Column graph of initial recoil velocity obtained from 1st and 2nd post-cut frame at 13h APF, 18.7 ± 10.7µm/min; 18h APF, 57.6 ± 7.3 µm/min and 22h APF, 124.5 ± 10.7µm/min. Error bars represent SEM. (Data analysis by S. Grill)

3.2.8.2 Influence of tension on myofibrillogenesis and sarcomerogenesis

The previous results showed that myofibrillogenesis and build-up of tension coincide during attachment maturation (section 3.2.8), indicating that tension could trigger simultaneous myofibrillogenesis and sarcomerogenesis throughout the myofiber.

To test if tension increase after attachment initiation plays a biological role in myofibrillogenesis and sarcomerogenesis two independent assays were established. For the first approach attachment initiation as a prerequisite of tension build-up was prevented

using RNAi against *kon*, and myofibrillogenesis in *kon*^{IR} myotubes was analysed. For the second approach tendons and myotubes were completely separated after attachment initiation using a UV-laser, and myofibrillogenesis was analysed.

3.2.8.2.1 Myofibrillogenesis in *kon* knock-down pupae

As demonstrated in section 3.2.2 Kon is essential for attachment initiation. As tension between myotubes and tendons can only be formed and maintained if both tissues are connected, corruption of myotube-tendon attachment should prevent tension formation and maintenance. Therefore, myofibrillogenesis in *kon* knock-down pupae can serve as model for myofibrillogenesis in the absence of tension in the myotendinous system. To analyse myofibrils in close detail, pupal offspring of *Mef2*-Gal4 flies crossed to w^-, *kon*^{NIG} or *kon*^{KK} were dissected at 30h APF and stained for the early sarcomeric M-line marker Obscurin, additionally actin was labelled using phalloidin (Figure 74). The wild type control shows elongated fibers and is filled with parallel bundles of actin stretching horizontally through the fiber (Figure 74 A-D'). Myofibrils on the surface are not distinguishable from fibrils in the interior of the myofiber. Moreover, fibrils display a fairly regular Obscurin pattern (Figure 74B-D'). As also demonstrated in Figure 35 muscle specific knock-down of *kon* using the hairpin *kon*^{NIG} results in rounding up of most myotubes at 30h APF, while knock-down with the hypomorphic *kon*^{KK} line results in elongated myotubes displaying roundish myotube tips at 30h APF. Importantly, myofibrils are formed exclusively on the myotube surface while the interior displays only short actin filaments in *kon*^{NIG} and *kon*^{KK} myotubes. Consequently, Obscurin is not organised in a periodic pattern on internal actin filaments (Figure 74E-L'). To quantify fibril length at the surface, fibrils were traced in a volume of 34 x 34 x 2.5µm. Fibril length in the interior was measured directly below the surface measurement-area, also in a volume of for 34 x 34 x 2.5µm (Figure 74 C, C', G, G', K, K', M). Fibrils span the complete area in the w^- control both on the surface and in the interior. In *kon*^{NIG} myotubes, however fibrils are thinner and harder to follow than in wild type, this could contribute to *kon*^{NIG} myofibrils scoring as significantly shorter. In the interior of the myofiber, starting 2.5µm below the surface, length of the traced actin filaments is significantly shorter than the length of the actin fibrils in wild type. Both *kon*^{NIG} and *kon*^{KK} actin filament lengths are reduced more than 3 fold compared to control actin fibers (Figure 74 M). Taken together, these data show that myofibrillogenesis is strongly defective in *kon*^{NIG} myotubes that are not able to attach and thus should not experience tension.

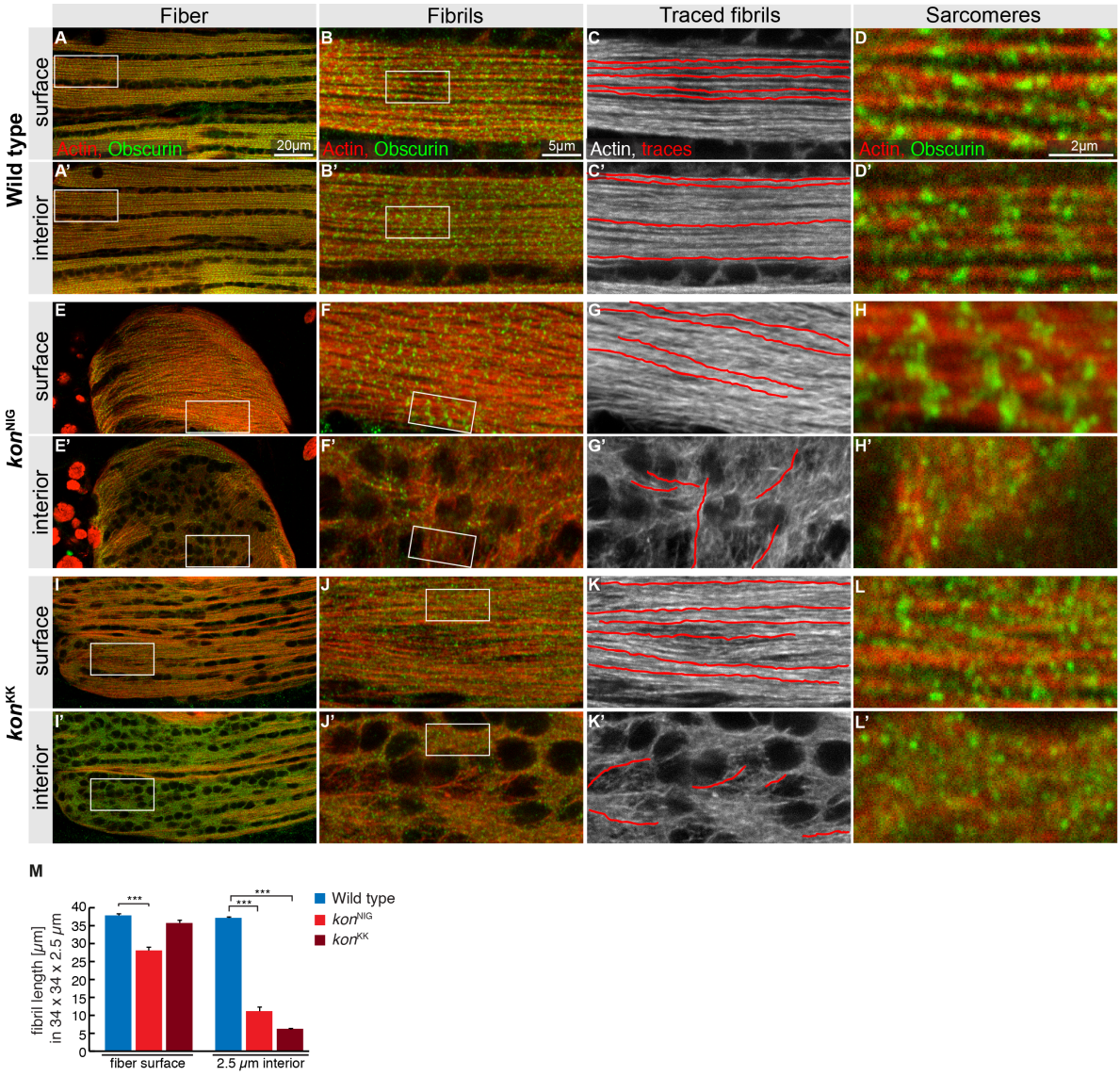

Figure 74 Myofibrillogenesis in *kon* knock-down fibers. Confocal images of dissected 30h APF *Mef2*-Gal4 (w^-, A-D'), kon^{NIG} (E-H') or kon^{KK} (I-L') pupae and myofibril length quantifications (M). A-D| w^-, surface; fibrils span the image area, Obscurin is displayed in a periodic pattern. A'D'| w^-, interior; fibrils span the image area, Obscurin is displayed in a periodic pattern. E-H| kon^{NIG}, surface; fibrils span large parts of the image area, Obscurin is displayed in a periodic pattern. E'-H'| kon^{NIG}, interior; actin forms short actin filaments instead of long actin fibrils, Obscurin is disorganised. I-L| kon^{KK}, surface; fibrils span large parts of the image area, Obscurin is partially displayed in a periodic pattern. I'-L'| kon^{KK}, interior; actin forms short actin filaments instead of long actin fibrils, Obscurin is disorganised. M| Quantification of fibril length. Error bars represent SEM, $p<0.001$ (two tailed unpaired T-test), box in fibers shows magnified area for fibrils, box in fibrils shows magnified area for sarcomeres.

As the incapability to form fibrils throughout the interior of the myofiber is not only detected in round kon^{NIG} myofibers, but also in elongated kon^{KK} fibers this effect is not caused by the rounded shape per se but by the loss of *kon* and the resulting defective attachment initiation. Interestingly, 30h APF kon^{KK} myotubes are significantly longer when compared to the wild type control (Figure 75), demonstrating a strong defect in

compaction of *kon*^{KK} myotubes. As tension increases with myotube compaction (section 3.2.8.1) it is tempting to speculate that a less compacted myotube could experience less tension.

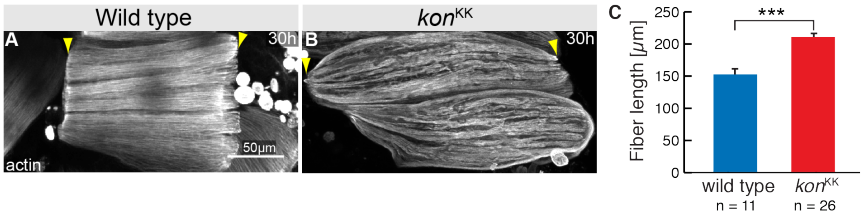

Figure 75 Quantification of *kon*^{KK} myofiber length at 30h APF. Confocal images of dissected 30h APF pupae of *Mef2*-Gal4 crossed to w^- (A) or *kon*^{KK} (B) and myofiber length quantifications (C). A| w^-, compacted myofiber, myofiber tips are straight. B| *kon*^{KK}, less compacted myofiber, myofiber tips are roundish. C| Myofiber length quantification, *kon*^{KK} myofibers are significantly longer than w^- control myofiber. Error bars represent SEM, $p<0.001$ (two tailed unpaired T-test, images and quantification from A. Kaya-Çopur).

Less compacted *kon*^{KK} myofibers form only few tendon connections (section 3.2.3), further supporting the hypothesis that tension in the system is lower since this less connected myotube-tendon system is less likely to withstand the same tension as a fully connected system. Interestingly, most connections to tendons are found at the myofiber surface, where fibrils are formed and β-PS integrin localises. To depict this correlation between tendon attachment, β-PS integrin localisation and myofibrillogenesis, 30h APF *Mef2*-Gal4>GFP-Gma, *kon*^{KK} myotubes were dissected and stained with Shot and β-PS integrin (Figure 76). Confocal imaging of an interior z-plane shows fibrils only at the left and right extreme of the myofiber representing the fiber surface (Figure 76A, B). Importantly, myofibrils coincide with tendon contact and β-PS integrin localisation (Figure 76C, D) further indicating a connection between attachment and myofibrillogenesis. Orthogonal sectioning of a confocal z-stack of the same myotube shows in the YZ-view fibrils and β-PS integrin restriction to the myotube surface (Figure 76F-I). Moreover, the XZ-view displays fibrils at the myofiber surface, contacting tendon elongations and β-PS integrin localisation to these contact sites (Figure 76J-M). Formation of fibrils seems to occur mainly at places that are attached to tendon cells as shown by β-PS integrin staining, indicating possible anchoring of myofibrils by tendon cells and β-PS integrin.

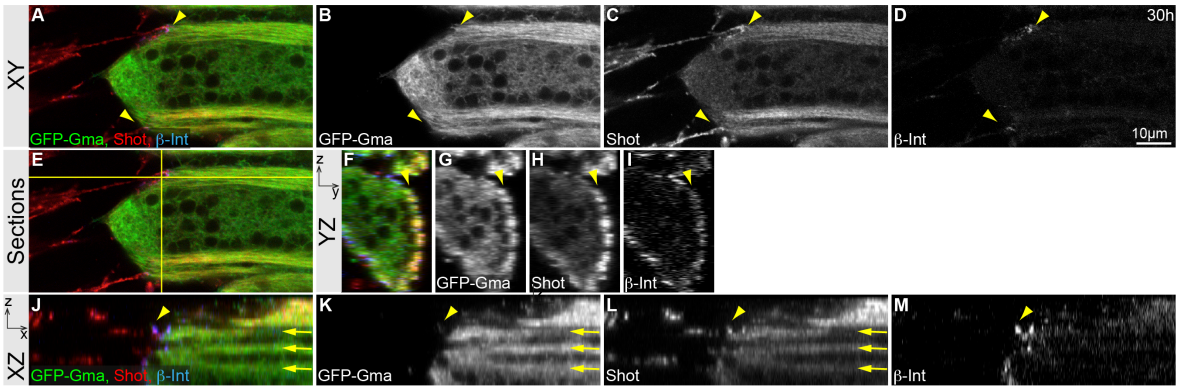

Figure 76 Myofibrillogenesis at attachment sites in of *kon*^{KK} myofibers. Single plane of a confocal stack of dissected 30h APF pupae of *Mef2-Gal4>GFP-Gma, kon*^{KK} pupae (A-D) and orthogonal cross-sections (E-M). A-D| Single z-plane at myofiber interior; rounded myofiber tip, surface is in contact with tendons and displays fibrils, β-PS integrin localises to myofiber-tendon contact sites. E| Single z-plane image; area for orthogonal sectioning is indicated. F-I| YZ-view, fibrils, Shot and β-PS integrin are restricted to the myofiber surface. J-M| XZ-view; surface is covered with fibrils, tendons connect to fibrils, β-PS integrin localises to tendon-contact sites. Arrowheads point to tendon contact sites or myofiber surface, arrows indicate fibrils in J and K, lines in E indicate areas for orthogonal sectioning.

3.2.8.2.2 Myofibrillogenesis after tension release by optical tendon-severing along myotubes

The previous section showed that preventing tension formation by impairment of attachment initiation results in severe myofibrillogenesis defects indicating that tension or attachment initiation are essential for myofibrillogenesis. To distinguish between the effects of defective attachment initiation and defective tension build-up an alternative strategy was pursued. *sr*-Gal4, *Mef2*-Gal4>UAS-CD8-GFP myotubes were allowed to initiate attachment. After attachment initiation, during compaction, tendons were severed to release tension and pupae were further aged until 30h APF. Surprisingly, even cuts of several tendon extensions were repaired efficiently (Figure 77A-C). Therefore, it is necessary to cut all tendon elongations from at least the 2 adjacent DLMs to prevent tissue repair and allow permanent separation of tendons. Permanent severing of tendons caused rounding of the corresponding/associated myotube demonstrating successful tension release (Figure 77D-K).

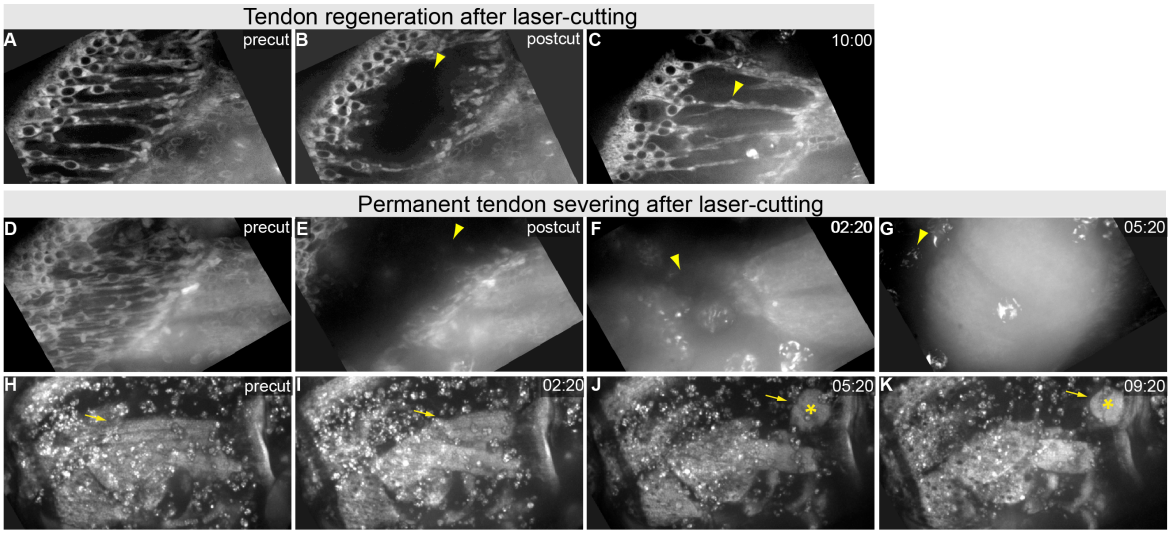

Figure 77 Tension release via laser-cutting of tendon elongations. Spinning disc confocal images of *sr*-Gal4, *Mef2*-Gal4>UAS-GFP-Gma pupae at 22h APF before and after laser-cutting and postcut frames at indicated time points. A| DLMs and tendons; precut. B| DLMs and tendons; after laser-cutting; most tendons along the first DLM are severed. C| DLM and tendons, 10h after laser-cutting; new tendon elongations connect DLM. D| DLMs and tendons, precut. E| DLMs and tendons, after laser-cutting; most tendons along the first and second as well as tendons of the third DLM are severed. F| DLMs 2:20h postcut; no new tendon elongations visible, myotube displays round tips. G| DLMs 5:20 postcut; myotube is round. H| Overview image of D, precut; DLMs are compacting. I| Overview image of F, 2:20h postcut; DLMs are shortening. J| Overview image of G; precut myotube is round, unsevered posterior end of round myotube is still connected to tendons. K| Overview image 09:20h postcut; round DLM moved further to the posterior tendon cells. Arrowheads point to tendon elongations or the place where they should be. Arrows point to the cut DLM, asterisk mark the round myotube. A-C are single slides, D-K show maximum projections.

To analyse myofibrillogenesis after tension release, tendon extensions of 22h APF *sr*-Gal4, *Mef2*-Gal4>UAS-GFP-Gma pupae were severed using a pulsed UV-laser. Pupae were aged to 30h APF, dissected, stained with anti-GFP and Obscurin and imaged with a confocal microscope. Myofibrillogenesis was analysed analogously to myofibrillogenesis in kon^{IR} (section 3.2.8.2.1). The corresponding DLM of the unsevered, second DLM sextet in the other half of the pupal thorax served as control to exclude any effects of the laser-cutting on pupal development. Control DLMs show elongated fibers and are filled with parallel bundles of actin, stretching horizontally through the fiber (Figure 78A-D'). Myofibrils on the surface are not distinguishable from fibrils in the interior of the myofiber. Moreover, fibrils display a fairly regular Obscurin pattern (Figure 78B-D'). In round myotubes attached to the severed tendons however fibrils are formed exclusively on the myotube surface while the interior displays only short actin filaments. Consequently, Obscurin is not organised in a periodic pattern (Figure 78E-H'). To quantify fibril length at the surface, fibrils were traced in a 34 x 34 x 2.5µm area at the myofiber surface and directly below this area for the interior measurements (Figure 78C, C', G, G', I). Fibrils

span the complete area in the unsevered control both on the surface and in the interior. Myofibrils on the surface of round myofibers are significantly shorter than control myofibrils. Moreover, short actin filaments in the interior of round myotubes are more than 3 fold shorter than in the control (Figure 78I). Taken together, these data show, that myofibrillogenesis is strongly defective after tension release via laser-cutting of tendon elongations, further demonstrating that tension is essential for simultaneous myofibrillogenesis.

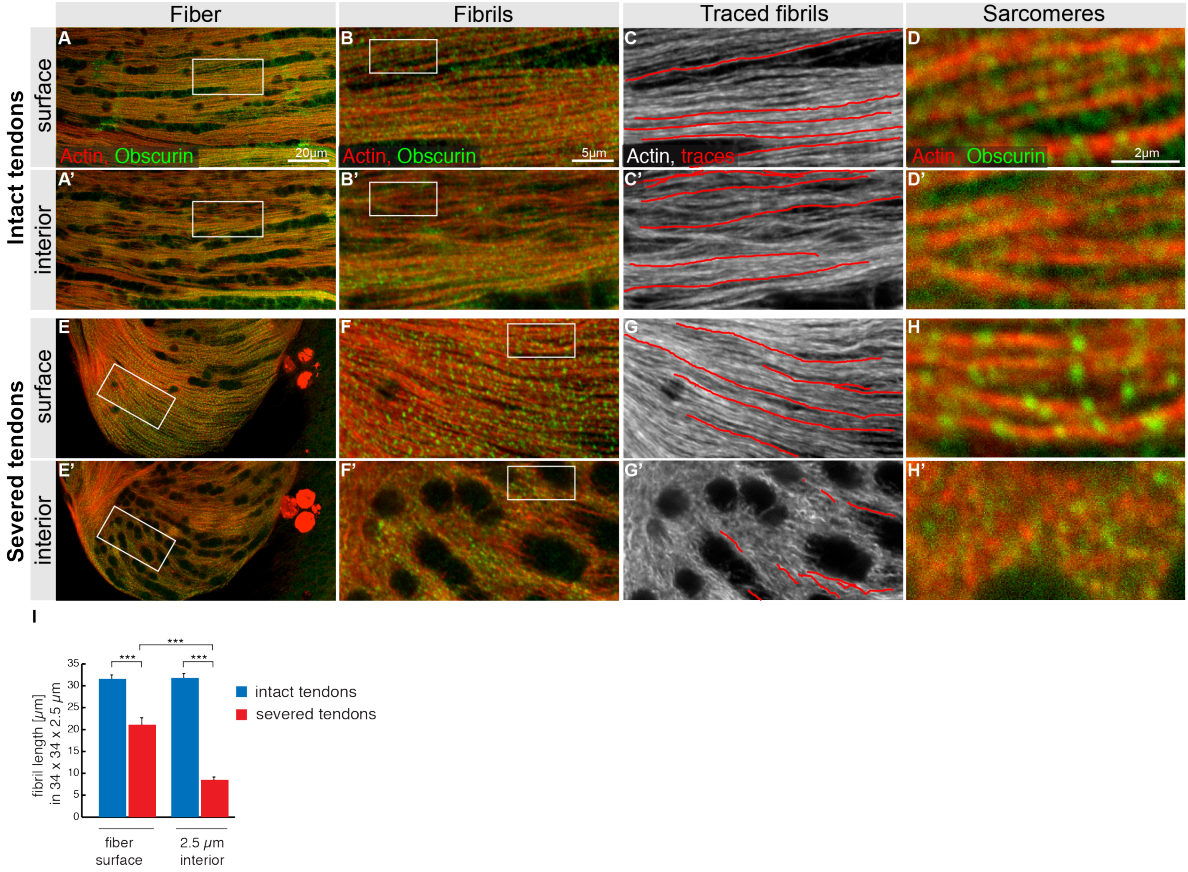

Figure 78 Myofibrillogenesis after tension release via laser-cutting of tendon elongations. Confocal images of dissected 30h APF *sr*-Gal4, *Mef2*-Gal4>UAS-GFP-Gma pupae (A-H') and fibril length quantifications (I). A-D| Control DLMs with unsevered tendons, surface; fibrils span the image area, Obscurin is displayed in a periodic pattern. A'D'| Control DLMs with unsevered tendons, interior; fibrils span the image area, Obscurin is displayed in a periodic pattern. E-H| DLM with severed tendons, surface; fibrils span large parts of the image area, Obscurin is displayed in a periodic pattern. E'-H'| DLM with severed tendons, interior; actin forms short actin filaments instead of long actin fibrils, Obscurin is disorganised. I| Quantification of fibril length. Error bars represent SEM, $p<0.001$ (two tailed unpaired T-test), box in Fibers shows magnified area for fibrils, box in fibrils shows magnified area for sarcomeres.

The analysis of myofibrillogenesis in both, attachment deficient *kon*^{IR} pupae as well as wild type pupae after tendon-severing demonstrates that tension increase after attachment initiation is essential for proper myofibril and sarcomere formation in DLMs (Figure 79).

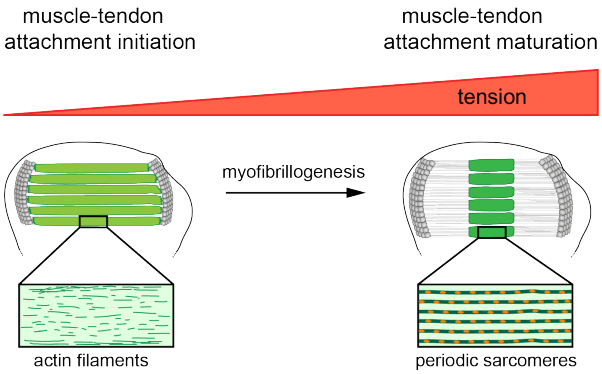

Figure 79 Attachment initiation and tension increase are essential for proper myofibrillogenesis. Tension increases after attachment initiation causing actin filaments (green lines) to organise together with Mhc, Obscurin (orange dots) and other sarcomeric components into a periodic pattern visible throughout the highly compacted myofibers and at later stages.

4 Discussion

Correct development of the skeletal muscle system enables body movements and is an essential prerequisite for viability of most animals. Therefore, it is important to understand the processes that regulate muscle development. Since the basic myogenic processes are largely conserved between *Drosophila* and mammals, the genetically easily accessible *Drosophila* system was used here to study myogenesis (Richardson et al., 2008; Schweitzer et al., 2010). This work identified novel players involved in the main myogenic steps; myoblast specification, migration and fusion, myotube-tendon attachment and myofibrillogenesis and sarcomerogenesis.

Moreover, the two poorly understood processes, attachment formation as well as myofibrillogenesis and sarcomerogenesis were studied in detail. Development of live imaging during attachment initiation allowed to analyse the dynamics of myotube-tendon contact formation. Additionally, in-depth morphological and molecular studies of wild type myotubes during attachment initiation and maturation combined with the functional characterisation of the candidate gene *kon* resulted in novel insights into attachment formation. Moreover, this study presents the first evidence of tension build-up during attachment in vivo and demonstrates that this tension increase is essential for myofibrillogenesis and sarcomerogenesis.

4.1 Identification of novel regulators for adult myogenesis

To identify novel regulators for adult myogenesis, candidate genes were selected from a genome-wide muscle specific RNAi screen. In this pioneering RNAi screen, Schnorrer and colleagues identified 2785 genes with a potential role during *Drosophila* myogenesis. The gene-sets with a potential role for embryonic myogenesis as well as for flight muscle myogenesis had been additionally analysed for morphological defects upon muscle-specific knock-down (Schnorrer et al., 2010). However, the gene set indicating a role in adult myogenesis had not been analysed so far. Thus, late pupal and pharate lethal genes that had been found in the pioneering screen and are predicted transmembrane proteins or transcription factors were analysed for their function in adult myogenesis in this work.

The five morphological classes defined in the screen are (1) “fiber presence”, (2) “fiber shape”, (3) “fiber position”, (4) “fibrillar organisation” and (5) “sarcomeric organisation”. Each of these classes is further divided into different subclasses providing a more detailed description of the morphological defect. Overall analysis of the phenotypic classes is

provided for adult leg muscles, abdominal dorsal, ventral and lateral muscles as well as DLMs. For simplicity, a comprehensive analysis including all subclasses focuses on strong phenotypes in DLMs and abdominal dorsal muscles. Abdominal dorsal muscles serve as example for muscles formed de novo, while DLMs are formed by regeneration of larval templates. Both represent the muscle types that show the highest number of phenotypes in the adult myogenesis screen. Moreover, only these two muscle types are suited for both immunohistochemical analysis and in vivo live imaging allowing for detailed analysis of the identified candidate genes.

4.1.1 Reliability of the adult myogenesis screen

Systematic analysis of muscle-specific knock-down phenotypes identified morphological defects for 142 genes, representing 50% of the screened genes. This result is in accordance with the numbers of defects observed in the morphological analysis of embryonic myogenesis candidates (44% phenotypes) and candidates involved in flight ability (60% phenotypes) (Schnorrer et al., 2010).

The remaining 50% of genes show wild type morphology but had been classified as late pupal or pharate lethal. These gens could display other defects that were not scored in the adult myogenesis screen. For example neuronal innervation, organelle morphology and detailed sarcomeric morphology cannot be detected with the molecular marker used in this screen, and would therefore not be identified.

The pioneering screen that was used to select genes analysed in this study showed a false discovery rate of 5% (Schnorrer et al., 2010). As the *Mef2*-Gal4-line driving RNAi expression, the RNAi-lines and the temperature used were identical to the pioneering screen, a similar false discovery rate can be expected. Morphological screening of the larval lethal and the flightless classes from this screen resulted in a similar number of phenotypes observed compared to the adult myogenesis screen, further suggesting that the screening results are as reliable as the ones from the published screen (Schnorrer et al., 2010).

Nevertheless, additional RNAi-lines for a set of candidate genes were analysed and the phenotypes for 68% of these genes could be confirmed in at least one class (section 3.1.5). Some of these additional RNAi-lines were made using the same hairpin construct and can therefore only exclude positional effects but not off-targeting. Focusing on the RNAi-lines tested with a different hairpin construct shows that even with the strict analysis-criterion of muscle morphology more than 50% of the genes can be confirmed. This number is

significantly lower than the 95% confirmed genes that would be expected from the publication. However, the pioneering screen used survival and flight-ability as phenotypic criterion for verification, while the adult myogenesis screen used the more stringed criterion of muscle morphology. If a knock-down is less efficient it can still lead to lethality without showing the same morphological defect compared to a stronger knock-down.

Moreover, not only VDRC but also TRiP and NIG RNAi-lines were used for verification of the adult myogenesis screen. Importantly, additional overexpression of Dicer2 is recommended for some of these lines to enhance knock-down efficiency. As Dicer2 was not used in the adult myogenesis screen, it is possible that the knock-down using these lines was not working efficiently enough.

Even with the stringed criteria of myofiber morphology for verification of knock-down specificity, a major part of the analysed gene set could be confirmed indicating that many of the identified genes do indeed have a function during myogenesis. For detailed analysis of candidate genes identified in this screen, however, the first step should be additional verification of the knock-down phenotype, ideally using a mutant. With the recent advances in Talen and CRISPR methods the generation of conditional knock out alleles of any given gene has been greatly simplified (Peng et al., 2014; Zhang et al., 2014). Therefore, selected candidates could be additionally verified using new genomic approaches to design mutants that could also serve as a tool for further analyses of those genes.

4.1.2 Candidate genes for myoblast specification and migration – the “fiber presence” class

The class “fiber presence” is subdivided into “additional myofibers” and “missing myofibers”. Both have been shown to be associated with the number of AMPs. For example ablation of AMPs in early second instar larvae results in deletion of the corresponding muscle or reduction of myofibers (Broadie and Bate, 1991). An incorrect number of AMPs could result from (1) specification defects in the embryo, (2) migration defects in embryo, larva or pupa, (3) proliferation defects in the larva or (4) specification of adult founder myoblasts. Since DLMs do not form by fusion to founders, but to templates that then split, reduction in DLM fiber number can be caused by fusion defects and will be discussed in section 4.1.3. For abdominal dorsal myotubes, both missing and additional myotubes are observed in the screen. As missing myofibers could also result

from degradation, a subset of the abdominal dorsal specification candidates was developmentally analysed. For the "missing myofiber" class more than 70% of the analysed genes display the same phenotype at early stages; suggesting that early myogenic steps like myoblast specification, migration or proliferation are affected. Moreover, all of the genes displaying additional myofibers at 90h APF also showed excess myofibers during development. Thus, the dorsal abdominal "fiber presence" class harbours strong candidates for AMP specification and migration.

4.1.2.1 Specification and asymmetric cell division of progenitors

As AMPs and embryonic founders originate from common progenitors any defect in progenitor specification or asymmetric cell division of progenitors could lead to inaccurate numbers of AMPs (Bate et al., 1991). Indeed *numb* mutant embryos have twice the amount AMPs. In contrast, overexpressing *numb* in embryos reduces the number of AMPs. Consequently, the adults, which develop only in rare cases, lack adult muscles (Ruiz and Bate, 1997). However, gene knock-down, especially in the early specification processes, is not efficient in the embryo. For example muscle-specific knock-down of *Notch* results only in pupal lethality although it is known to mediate the selection of progenitor cells in the embryo (Carmena et al., 2002; Gildor et al., 2012). This allows for identification of genes that, similar to *Notch*, are reused during adult myogenesis.

Therefore, adult fiber presence phenotypes most likely represent defects that arise after embryonic stages.

4.1.2.2 Patterning and migration of AMPs

AMPs, once born, stay quiescent and migrate to imaginal discs or abdominal histoblast nests. Already in the embryo, however, AMPs are pre-patterned, for example a subset of six AMPs displays *vestigial* expression in the embryo. These *vestigial* (+) AMPs migrate to and associate with the wing disc, where they proliferate and develop into indirect flight muscles (Sudarsan et al., 2001). The patterning of AMPs is essential for indirect flight muscle-fate and *vestigial* mutation results in loss of indirect flight muscle fate accompanied by loss of myofibers (Schönbauer et al., 2011; Sudarsan et al., 2001). Importantly, intrinsic patterning of AMPs is highly dependent on extrinsic cues like epidermal Wingless (Wg) signalling. Wg signalling from the disc, for instance, has been shown to sustain the maintenance of *vestigial* expression in disc-associated AMPs (Sudarsan et al., 2001). If extrinsic signals are missing or changed the AMP fate can be reprogrammed, as has been shown using transplantation experiments of wing discs into the

abdomen (Lawrence and Brower, 1982; Roy and Vijayraghavan, 1997). Therefore, extrinsic signalling from epithelia or neurons can induce expression of specific transcription factors determining AMP fate. Interestingly, 33% (7 genes) of candidate specification genes identified in the adult myogenesis screen are potentially involved in transcriptional regulation (Transcription factors, histone modifiers, helicases) indicating a function in patterning of AMPs. These genes might initiate a cell type specific program, possibly as downstream targets of external signalling.

Moreover, the transplantation experiments indicate that AMPs that migrate to ectopic places adopt a different muscle fate resulting in additional myotubes at these ectopic locations (Lawrence and Brower, 1982; Roy and Vijayraghavan, 1997). Therefore, genes involved in migration could lead to the aberrant myofiber presence and thus be represented in the "fiber presence" class of the adult myogenesis screen. Indeed 32% (6 genes) of the genes that score as strong in the class "dorsal abdominal fiber presence" represent potential metalloproteinase and adhesion proteins. Both protein groups have been shown to be essential modulators of cell migration (Bellayr et al., 2013; Chen and Li, 2009; Laird et al., 2008; Ridley, 2011). Interestingly, metalloproteinases can also modulate the sensing of external cues by processing ECM molecules or transmembrane receptors, thus this class of proteins is particularly interesting for the integration of external cues.

4.1.2.3 Proliferation of AMPs and specification of adult founder cells

AMPs proliferate during larval life until they reach their final number (Currie and Bate, 1991). Thus, processes interfering with proliferation of AMPs could also lead to changes in AMP number.

Founder cells that seed adult muscles can be selected from the AMP pool by FGF signalling as has been shown for dorsal abdominal muscles. If FGF signalling is up-regulated, more founder cells and consequently more myotubes form and vice versa, demonstrating a direct correlation between founder and myofiber number (Dutta et al., 2005). Therefore, genes involved in founder specification, possibly by modulating FGF signalling pathways, can lead to changes in myofiber presence. Hence, it would be interesting to analyse if the number of adult founder cells in early pupae is changed in muscle-specific knock-down of the "dorsal abdominal fiber presence" genes identified in the adult myogenesis screen. If genes of this set are found to influence founder number it would be exciting to investigate if they show an interplay with the Heartless/FGF pathway. Interesting candidate genes for founder specification are the 33% of genes classified as

"dorsal abdominal fiber presence" that are possibly involved in transcriptional regulation (transcription factors, histone modifiers, helicases) (Table 3). In addition to a possible role in patterning, they could also be involved in founder selection.

4.1.3 Candidates for myoblast fusion – the "DLM fiber presence" class

During DLM development three larval templates adopt the role of founder cells (Dutta et al., 2004). Upon fusion of AMPs to these templates they split into 6 myotubes, demonstrating the role of fusion and splitting in determining myofiber number (Fernandes et al., 1991). In the absence of larval templates DLMs can form de novo resulting in excessive myofibers. As an excess of DLM fibers was not observed in the adult myogenesis screen, genes classified as "DLM fiber presence" should result from myofiber splitting defects or degradation.

Early analysis of a gene-subset from the "DLM myofiber presence" class indicates that 45% of the genes are not involved in fusion. Of these genes 40% do not show a knock-down defect at 18h APF; indicating that myotubes are degraded later, due to failure of later processes like myotube attachment. The remaining 60% of genes displays a shape defect at 18h APF indicating defects in myotube migration or adhesion, demonstrating that the defects leading to fiber presence phenotypes can be diverse. However, a total of 55% of the developmentally analysed genes from the "DLM fiber presence" class do show a myotube splitting defect. These splitting defects can arise from (1) reduced number of AMPs (2) defects in the fusion process or (3) defects in the splitting process itself.

Two genes that are showing a splitting defect in the adult myogenesis screen are *Notch* and *Delta*. It has been shown that *Notch* mutant DLMs do not undergo splitting (Anant et al., 1998). Moreover, *Delta* and *Notch* knock-down phenotypes in DLMs have been published during the course of this study (Gildor et al., 2012). Gildor and colleagues also observed a splitting defect for *Delta* knock-down. They propose a possible role for Notch in repressing *sns* expression. Moreover, they showed that *Notch* and *Delta* knock-down lead to strong decrease of nuclei number in DLMs. Their data suggest that Notch and its ligand Delta are essential to regulate the expression of fusion genes and are consequently required for fusion and splitting. The identification of Notch and Delta in the adult myogenesis screen shows that genes that are essential for fusion can be identified within the "DLM fiber presence" class. Moreover, 57% of the genes in the "DLM myofiber presence" class are also identified in the fusion list based on thin myotube morphology in section 3.1.3.1 (appendix, Table 16). This is consistent with the 55% genes from the "DLM fiber

presence" class found to be essential for splitting. These observations propose a role in myoblast fusion for more than half of the genes in the "DLM fiber presence" class.

4.1.4 Candidates for myoblast fusion – the "thin myofiber" subclass

If fusion is blocked, myotubes can form but remain very thin. For example, expression of dominant negative Rac1 prevents fusion, possibly by preventing actin foci formation. If Rac1 is expressed in adult muscles, abdominal muscles and indirect flight muscles are very thin (Dutta et al., 2004). Therefore, genes in the "thin myotubes" subclass are potential candidates for essential fusion genes (section 3.1.3.1).

Interestingly, 26% (11 genes) of the potential fusion genes are shown or predicted to encode for Metalloproteinases, transmembrane receptors or transporters. These proteins might play a role in myoblast migration, recognition or adherence of fusion competent myoblasts to adult founders or templates. Importantly, 10% of the genes identified as potential fusion genes are known to be involved in myogenic processes. Additionally, 12% of the potential fusion candidates are known to be involved in embryonic fusion suggesting an additional role for these proteins in myoblast fusion in adult *Drosophila* myogenesis.

As each fusion event adds one nucleus to the growing myofiber, the number of fusion events can easily be quantified by counting the nuclei number per myofiber, as shown for the example of *sns* knock-down (Figure 22). Therefore, a simple secondary screen using genetically labelled muscles and nuclei allows to validate the potential fusion genes.

Three interesting examples of potential fusion candidate genes are *VAP-33B, CG4552* and *nejire* (*nej*). *VAP-33B* encodes a predicted vesicle associated membrane protein. As vesicles are thought to transport the fusion machinery and to engulf and remove excess membranes, *VAP-33B* could be important for those steps (Doberstein et al., 1997). CG4552 has a predicted Rab GTPase activator activity and could thus be involved in Rab inactivation. Vertebrate Rab35 and *Drosophila* Rab11 have been shown to be involved in myoblast fusion, providing a possible platform for CG4552 function in fusion (Bhuin and Roy, 2009; Charrasse et al., 2013). Nej displays a histone acetylase function (Das et al., 2009). Moreover, it has been shown that the mammalian ortholog of Nejire, CBP-p300, is essential for muscle development though regulation of gene activity. CBP-p300 can activate muscle transcription and consequently myotube formation in concert with other transcription factors like Mef2 (McKinsey et al., 2001). In the adult myogenesis screen *nej* was identified as potential fusion gene using three different RNAi-lines. Two of these RNAi-lines harboured different hairpin constructs indicating high knock-down specificity.

In *nej* knock-down pupae, DLMs show a splitting defect and abdominal myotubes are very thin indicating a general fusion defect. Additionally, all muscles display a considerable number of unfused myoblasts, in some cases these unfused myoblasts also develop into additional thin myotubes, strongly indicating a myoblast specification defect. It is exciting to speculate that Nej might negatively regulate adult founder cell specific gene expression. In this scenario reduction of *nej* expression would result in excessive numbers of adult founder cells and decreased amounts of adult fusion competent myoblasts. This hypothesis could be tested by analysing the levels of founder cell markers, like Duf, in *nej* knock-down myoblasts.
In conclusion, the adult myogenesis screen successfully identified known fusion genes and interesting novel candidates for fusion related processes.

4.1.5 Candidates for myotube guidance – the "fiber position" class

Defective myotube guidance can result in attachment to the wrong tendon cells and consequently in aberrant myotube positioning. For example, mutants of the essential targeting and migration terminating gene *dGit* frequently attach to ectopic places within the epidermis (Bahri et al., 2009).
The adult myogenesis screen identified 15 genes that are possibly involved in myotube guidance. Ten of these genes display a position defect in abdominal dorsal muscles (appendix, Table 19). Remarkably, 70% of the abdominal dorsal guidance candidates display an additional "fiber presence" phenotype, indicating a specification defect. Two of these genes show additional myotubes; therefore, the myotube position defect reflects most likely a secondary defect, due to space limitations and occupancy of tendon cells. Also Dutta et al. observe position defects for excess abdominal myotubes (Dutta et al., 2005).
For the five genes additionally showing missing myotubes the defective myotube position might arise from a myoblast guidance or migration defect and consequently only a fraction might reach the place of myotube formation resulting in reduced myotube number. The fraction that reaches the place of myotube formation might not be able to recognise the correct tendon cells. Developmental analysis of four candidate genes revealed that the guidance phenotype is often already manifested before fusion. As observed by live imaging of *kon* knock-down myotubes, myoblast already misalign and then keep this incorrect orientation during fusion and myotube migration. These data indicate that for the genes showing a fiber position phenotype upon knock down, either myoblast polarity,

integration of external cues or myoblast migration and tendon recognition could be incorrect.

Interesting genes in the "dorsal abdominal fiber position" class are *Hormone receptor 78* (*Hr78*), which could possibly integrate signals from the surroundings and the two potential Metalloproteinases *Kul* and *CG3442* that might modulate receptor signalling and influence myoblast migration. As a proof of principle the embryonic guidance gene *kon* was also found in the adult myogenesis screen as guidance candidate for abdominal dorsal myotubes.

4.1.6 Candidates for myotube-tendon attachment – the "short myofiber" subclass

The round myofiber phenotype is a hallmark of muscle attachment defects. Since unattached myotubes cannot withstand the force of myotube contraction and round up. Consequently, null mutation or muscle-specific knock-down of integrin complex components display round muscles in *Drosophila* embryos and larvae (Newman and Wright, 1981; Schnorrer et al., 2010). The round phenotype has been successfully used to identify genes involved in myotube attachment like the Kindlin homologs *Fermitin1* and *Fermitin2* (Bai et al., 2008).

The adult myogenesis screen identified 46 potential attachment genes, 24 of which were classified as strong in DLMs and abdominal dorsal muscles (appendix, Table 15). Two interesting potential attachment genes are *Protein phosphatase 52F* (*Ptp52F*) and *CG34353*. *Ptp52F* encodes a receptor protein phosphatase essential for axon guidance. Interestingly, PTP52F has 5 extracellular Fibronectin III domains, indicating a function as cell-cell recognition receptor (Schindelholz et al., 2001). With its intracellular protein phosphatase domain PTP52F could transmit cell-cell recognition signals. An other protein with a Fibronectin III domain found in the screen is CG34353. Additionally, SMART predicts 3 immunoglobulin domains, indicating that CG34353 could act as transmembrane receptor (Schultz et al., 1998).

Of the 24 strong abdominal dorsal muscle and DLM attachment candidate genes 29% have been implied in embryonic myogenesis. One of those genes is *kon* that was selected for detailed analysis that identified an essential role of Kon in attachment initiation as will be discussed in section 4.2.3. The identification of Kon demonstrates that the screening method used for this study can indeed identify essential attachment genes.

4.1.7 Candidates for myotube differentiation and cytoskeleton rearrangement – the sarcomeric and fibrillar organisation classes

Sarcomeres and myofibrils are formed by the ordered arrangement of actin and myosin filaments and their association with additional sarcomeric proteins (Lange et al., 2006). Therefore, phenotypes in sarcomeric and fibrillar organisation should reflect defects in cytoskeletal arrangement and association with the structural components. In addition, this class could also reflect myoblast specification and myotube differentiation defects since sarcomerogenesis is the last step in myotube maturation. For example *salm* knock-down leads to a switch from fibrillar to tubular morphology (Schönbauer et al., 2011).

The adult myogenesis screen identified 64 genes with a sarcomeric knock-down phenotype. However, the screen settings did not include markers for sarcomeric structures, like M–line and Z-disc, and the highest magnification was taken using the 40x objective. Therefore, the resolution was not ideal to detect sarcomeric defects reliably. Moreover, sarcomeric defects can often be secondary since sarcomerogenesis is the last step during myogenesis. Thus, it is useful to restrict this set of potential sarcomerogenesis genes to genes that show a strong sarcomere phenotype but no strong fiber presence, shape or position phenotypes upon knock-down. This restricted set harbours 13 genes including five potential transcription factors (appendix, Table 18) that could possibly initiate or maintain muscle type specific gene expression.

4.1.8 The Activin branch of TGF-β signalling is essential for myogenesis

The adult myogenesis screen identified the three TGF-β pathway components *put*, *babo* and *Smox* as essential factors for correct fiber shape and number. Importantly, all three genes result in extremely similar knock-down phenotypes and all of them have been confirmed with a different hairpin construct, demonstrating the reliability of the knock-down phenotype. This indicates that TGF-β signalling plays a major role in myogenesis.

It is well established, that TGF-β signalling inhibits muscle growth in vertebrates (Sartori et al., 2014). Additionally, TGF-β signalling regulates protein homeostasis in maturating *Drosophila* muscles (Bai et al., 2013). However, these processes occur only in adults and not during myogenesis. Thus, the phenotypes observed in the adult myogenesis screen should be independent of these observations. The missing and thin myofibers in *put*, *babo* and *Smox* knock-down pupae indicate specification or proliferation defects. Hence, TGF-β signalling could play a major role in myoblast specification or proliferation. As

specification and proliferation depend on extracellular signals it is possible that the TGF-β pathway integrates extracellular stimuli in myoblasts or myotubes.

Interestingly, Put, Babo and Smox are the main components of the Activin triggered branch of TGF-β signalling. Therefore, a possible hypothesis for TGF-β function in myotubes is activation of Put and Babo by their extracellular ligands Activin or Myoglianin and subsequent phosphorylation of the downstream effector Smox that then can activate transcription in concert with other cofactors. If one of these components is missing, extracellular stimuli could not be translated into a transcriptional response. This would impair proper myoblast specification and lead to missing myotubes or fusion defects resulting in thin myotubes. Interestingly, TGF-β signalling triggered by Activin A has recently been implicated in myoblast differentiation using human skeletal muscle cells and in proliferation of satellite cells (Tabebordbar et al., 2013; Trendelenburg et al., 2012). In conclusion, the adult myogenesis screen suggests a novel role for TGF-β signalling during myoblast specification or proliferation.

4.1.9 Kon-tiki is essential for myotube guidance of dorsal abdominal myotubes

The orphan transmembrane receptor Kon is one of the guidance candidates identified in the adult myogenesis screen. It shows a strong guidance defect in abdominal dorsal, lateral and ventral muscles as well as leg muscles. Importantly, this phenotype is verified using three different hairpin constructs. Live imaging of *kon* knock-down myotubes demonstrated that myoblast misalign and then stay in this incorrect orientation during fusion and myotube growth. Moreover, these myotubes often seem to share an attachment site or to attach to each other. Interestingly, Kon deficient myotubes produce very long protrusions that often overshoot the future attachment site. These data indicate that Kon is essential for the recognition of tendon cells. The possible role in tendon recognition is supported by antibody staining of Kon demonstrating Kon localisation to myotube tips during myogenesis. Notably, Kon localises to the opposing poles indicating that it is essential for correct integration of external positional cues. Hence, processes that could possibly be affected by *kon* knock-down are myoblast and myotube polarity, myotube migration or tendon recognition. A recent publication also reports mislocalisation of abdominal dorsal myotubes after muscle-specific *kon* knock-down, reproducing the phenotype observed here (Pérez-Moreno et al., 2014). Additionally, Kon has been shown to guide a specific subset

of embryonic myotubes (VL muscles) in concert with the intracellular adapter Grip (Estrada et al., 2007; Schnorrer et al., 2007). The data presented in these studies also indicate a role for Kon in tendon recognition. It seems that the guidance or tendon-recognition function of Kon is reused for myogenesis of abdominal and leg muscles.

4.2 Novel insights into attachment formation and myofibrillogenesis

The candidate gene Kon identified in the adult myogenesis screen was selected for detailed analysis focusing on its role in DLM-tendon attachment formation. As DLMs are multi fiber muscles they are very similar to vertebrate muscles making them an ideal model for the analysis of different myogenic steps. Moreover, DLMs form highly structured myofibrils composed of precisely organised sarcomeres, allowing also to study myofibrillogenesis. Thus, the DLMs were not only used to study wild type myogenesis and the function of Kon during attachment formation, but also to analyse the formation of tension during attachment formation and its role for myofibrillogenesis.

4.2.1 Myotube migration is mediated by integrins

DLMs are formed by fusion of AMPs to three larval templates. The splitting myotubes then migrate towards the anterior and posterior tendon cells during myotube extension (Roy and Vijayraghavan, 1998). To investigate the role of integrins during myogenesis muscle-specific knock-down of different genes encoding integrin complex components was performed. Although the knock-down was incomplete, it results in a strong phenotype. *β-PS integrin* knock-down myotubes form extremely long protrusions but do not migrate to the anterior tendon cell and eventually round up, suggesting that integrin function is essential for myotube migration. Moreover, large accumulations of adult myoblasts are found at ectopic positions indicating aberrant myoblast migration. These data suggest that integrins are essential for myoblast and myotube migration during DLM development.

In *Drosophila* as well as in vertebrates, the role of integrins in migration of various cell types is well established. Integrins link the cytoskeleton to the ECM that can be used as template for cell migration. Moreover, integrins can also actively remodel the ECM and thereby change the path of migration (Huttenlocher and Horwitz, 2011). One example for an ECM protein mediating integrin-based cell migration is Laminin. Laminin has been show to be essential for neuronal path finding and migration of various cell-types (Tzu and Marinkovich, 2008). Moreover, *Drosophila* embryonic ventral oblique muscles do not

reach their epidermal attachment sites in Laminin mutants (Martin et al., 1999; Prokop et al., 1998). This PhD-thesis reveals that Laminin forms a network underneath tendon cells and is surrounding DLM myotubes. Also Perlecan, a heparan sulfate proteoglycan involved in axon guidance, is localised underneath tendons and around the myotube (Figure 45) (Cho et al., 2012). While it remains elusive, which cells secrete Perlecan, it has been shown, that Laminin can be secreted from muscles, tendons and to some degree from hemocytes (Volk, 1999). Both, Laminin and Perlecan are components of the basement membrane (Yurchenco, 2011). Therefore, it is tempting to speculate that myotubes and tendons might secrete their own basement membrane including Laminin and Perlecan and that this basement membrane serves as template to guide integrin-mediated myotube migration.

4.2.2 Initial myotube-tendon attachment includes Cadherin mediated cell-cell contacts

After migration of both myotube ends to their respective tendon cells, tendons are recognised, migration is stalled and myotube-tendon attachment is formed. Live imaging combined with immunohistochemical analysis revealed that filopodia of myotubes and tendons are in close dynamic contact and could recognise and adhere to each other directly (section 3.2.2). Interestingly, electron microscopic studies of embryos showed the presence of focal adherence junctions in early myotube-tendon attachments (Prokop et al., 1998; Tepass and Hartenstein, 1994). Adherence junctions are known from epidermal and vascular tissues. They are based on homophilic Cadherin interactions of two opposing cells and also include intracellular adapters linking Cadherin to the cytoskeleton. Formation of the adherence junction in concert with Cadherin signalling to the cytoskeleton promotes expansion of the cell-cell contact (Maître and Heisenberg, 2013; Takeichi, 2014). Interestingly, data presented in this thesis could show that E-Cadherin localises to myotube-tendon contact sites during attachment initiation (Figure 46). A functional role for these adherence junctions remains to be shown. This could for example be achieved by muscle specific knock-down of Cadherin. Taken together, these data indicate that during attachment initiation Cadherin based focal adherence junctions are present (Figure 80).

4.2.3 Attachment initiation is mediated by Kon

Muscle specific knock-down of *kon* leads to a strong defect in attachment initiation. This conclusion is supported by localisation of Kon to myotube tips and the missing contact

formation between Kon deficient myotubes and tendons. Reduced myotube-tendon contact formation is accompanied by reduced localisation of E-Cadherin and Shot at myotube-tendon contacts sites. Additionally, integrin recruitment to myotube-tendon contact sites is strongly impaired in *kon* knock-down pupae. Interestingly, Kon deficient myotubes are reaching and sometimes even overshooting the tendon cells, strongly indicating that tendon recognition is impaired in Kon deficient myotubes (section 3.2.3). In summary, these results suggest that Kon is mediating tendon recognition and subsequent initiation of myotube-tendon attachment. Kon's function in the DLMs is similar to the function described in the embryonic VL muscles as Kon's role in the VL muscles also seems to involve recognition of tendon cells (Estrada et al., 2007; Schnorrer et al., 2007). The use of Kon in another system indicates that the function of Kon as a cell recognition receptor is conserved.

Kon is a highly conserved protein (Schnorrer et al., 2007). The human ortholog of Kon, chondroitin sulfate proteoglycan 4 (CSPG4), is a stem cell marker that is also expressed in myogenic cells (Dye et al., 2013; Nishiyama et al., 2009). CSPG4 is used as marker for different cancers like sarcomas that originate from mesenchymal tissue and most prominently for melanomas, where it is also used as therapeutic target. (Dye et al., 2013; Ping Bie, 2014). Interestingly, CSPG4 is expressed in myoblasts, myotubes and the sarcolemma of skeletal muscles (Petrini et al., 2003). CSPG4 and its mouse ortholog NG2 are thought to act as co-receptors for receptor tyrosine kinases facilitating MAPK signalling and consequently migration and proliferation. Additionally, CSPG4 has been shown to interact with various ECM proteins like Fibronectin, different Collagens and Laminin, suggesting that CSPG4 can sense the surrounding and mediate signals to the cell. For example by activating FAK and integrins, which can impact cytoskeletal reorganisation or survival (Price et al., 2011). Many functions of the mammalian Kon homologs are thought to depend on the presence of the chondroitin sulfate chain (Dye et al., 2013). However, Kon does not contain the homologous sequences to the region that is usually linked with chondroitin sulfate chains and it has been shown that the major part of Kon proteins in *Drosophila* is not linked to chondroitin sulfate (Schnorrer et al., 2007). Therefore, it is not clear if Kon can similarly influence integrin activation or receptor tyrosine signalling in *Drosophila*. However, the intracellular binding of Kon to Grip is observed in *Drosophila* and mammals, where it is believed to facilitate receptor clustering and recruitment of signalling molecules (Estrada et al., 2007; Schnorrer et al., 2007; Stegmüller et al., 2003). Interestingly, Grip is localising Kon to the myotube tip and Grip

knock-down resembles a hypomorphic *kon* knock-down (section 3.2.6) showing that Kon localisation or Grip mediated signalling are essential for attachment initiation and suggesting that this process could be conserved.

4.2.4 Attachment maturation is mediated by integrins

Integrins and the adaptor protein Talin that links integrins to the cytoskeleton are strongly recruited to the myotube-tendon contact site after attachment initiation. Additionally, Tsp as well as pFAK accumulate strongly after attachment initiation (section 3.2.4.2). These data suggest that the initial myotube-tendon contacts mature into a stable, force resistant myotube-tendon attachment composed of integrin complexes.

Integrins have been shown to play a conserved role in muscle-tendon attachment (Schejter and Baylies, 2010). In *Drosophila* embryonic myotendinous junctions, β-PS/α-PS1 integrin complexes on the tendon cell bind ECM molecules like Laminin, while β-PS/α-PS2 integrin complexes on the myotubes bind the ECM component Tsp (Brown et al., 2000; Charvet et al., 2012). Tsp has been shown to be essential in early steps of myotube-tendon attachment in *Drosophila* and zebrafish (Chanana et al., 2007; Subramanian and Schilling, 2014; Subramanian et al., 2007). Recently, Slowdown (Slow), a Tsp interaction partner that is secreted from tendon cells, has been discovered. Slow mediates gradual accumulation of integrins and Tsp at myotube-tendon contacts. Interestingly, premature localisation of integrins or Tsp to *slow* mutant myotube tips results in aberrant formation of myotendinous junctions and muscle or tendon rupture. The same result was observed with overexpression of β-PS/α-PS2 in muscles (Gilsohn and Volk, 2010b). Also in the DLM system gradual accumulation of Tsp, integrin, Talin and pFAK was observed after attachment initiation (Figure 50). Accumulation of these integrin complex and signalling components could be achieved by removal of inhibiting signals like Slow or by increase of positive recruitment signals.

In *kon* deficient DLM myotubes, integrin complex components fail to localise to myotube tips, demonstrating that Kon or Kon mediated attachment initiation is essential for integrin complex recruitment. As mentioned in the last section, the Kon homolog CSPG4/NG2 has been shown to interact with integrins and to stimulate FAK phosphorylation. It is however not clear if this interaction can occur in *Drosophila* (Dye et al., 2013). A genetic interaction between Kon and α-PS1 integrin as well a its ligand Laminin has been discovered in *Drosophila* embryos, but it has not been analysed if this interaction is based

on a direct interaction between these molecules (Estrada et al., 2007; Wolfstetter and Holz, 2012).

Additionally, pathways or processes induced by attachment initiation itself could foster integrin recruitment. For example, tendon maturation is triggered by myotube-tendon contact and leads to Tsp secretion (Schweitzer et al., 2010). Moreover, tension increases after attachment initiation (Figure 73). This increasing tension could foster integrin accumulation at myotube tips. Using FRAP experiments on muscles of hyper-contraction mutants Pines et al. revealed that integrin turnover increases when tension on the myotendinous junction is reduced and vice versa (Pines et al., 2012). As reduced integrin turnover under higher force results in integrin accumulation at the myotendinous junction it can be inferred that the increasing tension during myotube-tendon attachment maturation could cause integrin accumulation by similar means.

4.2.5 Mechanotransduction and myofibrillogenesis

Different models describing myofibrillogenesis and sarcomerogenesis hypothesise that tension could influence myofibrillogenesis (De Deyne, 2001; Engler, 2004; Kagawa et al., 2006; Yoshinaga et al., 2010). Live imaging combined with laser-cutting of tendon extensions, presented in this thesis, demonstrates for the first time that tension is formed during myogenesis in vivo.

4.2.5.1 Integrins are mechano-sensors and link the ends of fibrils to myotube-tendon attachments

Integrin, Talin and pFAK that are strongly localised to the myotendinous junction have been shown to transmit mechanical stimuli into the cell. Integrins and Talin are essential components of focal adhesions, sensing ECM stiffness and cell tension, and initiate signalling cascades that lead to cytoskeletal rearrangement as well as transcriptional responses (Legate et al., 2009; Wehrle-Haller, 2012). Interestingly, the molecular composition of costameres and myotube-tendon attachments is very similar to focal adhesions. Thus, the regulation and function of focal adhesions, costameres and myotube-tendon attachments, might also be similar. Therefore, integrins could be the tension-sensing unit of the muscle. This hypothesis is supported by the observation that only those pre-costameres that experience tension will develop into costameres while the others disassemble (Sharp et al., 1997). Moreover, costameres are known to mediate force transmission of contracting myotubes (Peter et al., 2011). Therefore, it is very likely that

integrins at myotendinous junctions are transmitting the global force, generated during myotube compaction, to the myotube resulting in mechanical and biochemical responses.

4.2.5.2 Tension is essential for myofibrillogenesis

Morphological analysis of myotubes showed that a cortical actin wall is formed during attachment initiation while the interior of the fibers is devoid of long actin filaments. This actin cortex displays many thin actin filaments spanning large areas of the myotube and possibly connecting both myotube ends. Interestingly, these fibrils display irregular actin and Shot accumulations, indicating a stress fiber-like appearance. As stress fibers can generate force, this actin cortex could possibly possess contractile functions if myosin would be present at the actin cortex (Burridge and Wittchen, 2013). A cortical actin ring has also been detected in mouse myoblasts and myotubes ex vivo and is associated with non-muscle myosin in those cells (Wells et al., 1997). Hence, the formation of a cortical actin ring in developing myotubes seems to be a general feature. It is enticing to speculate about a possible role of this actin cortex for myotube compaction and force generation.

During attachment maturation at 30h APF the cytoskeletal arrangement of the myofibers is completely changed and they are filled with thick myofibrils harbouring periodically organised actin filaments. Also Mhc starts to show a periodic pattern on these myofibrils around 30h APF (Figure 69). Importantly, tension increase after attachment initiation is essential for the cytoskeletal rearrangements leading to myofibrillogenesis. This was demonstrated with three approaches. (1) Muscle specific *kon* knock-down preventing myotube-tendon attachment and thus tension formation, (2) muscle specific hypomorphic *kon* knock-down leading to patchy attachment, most likely resulting in reduced tension or an inhomogeneous force field, and (3) complete separation of myotube and tendon cells after attachment initiation, allowing for signalling induced by attachment initiation before tension is released. All approaches result in myotubes that are devoid of myofibrils and display only cortical actin fibrils at 30h APF. This cortical actin wall could possibly be linked by integrin to the basement membrane surrounding the myotube and thereby experience a local tension.

4.2.5.3 Tension increase and simultaneous appearance of a periodic Mhc pattern are compatible with the pre-myofibril and the two-state model

Myhre and Pilgrim combine the presence of a cortical actin wall with the premyofibril model and suggest that non-muscle myosin is incorporated into the actin wall, forming pre-myofibrils with mini-sarcomeres (Myhre and Pilgrim, 2012). Therefore, it is possible that

the cortical actin wall observed in DLM myotubes during attachment initiation represents developing pre-myofibrils. The pre-myofibril model envisions a gradual exchange of non-muscle myosin for muscle myosin. A periodic Mhc pattern is not yet visible in nascent myofibrils, which is explained by overlapping of unregularly organised Mhc filaments. Only maturing myofibrils that incorporate Z-disc and M-line proteins and completely exchanged non-muscle myosin with Mhc, show a striated Mhc pattern (Sanger et al., 2010). This theory would be compatible with the observation that a periodic Mhc pattern appears simultaneously in DLM myofibers around 30h APF. These Mhc containing myofibrils would then correspond to maturing sarcomeres that are still growing in size.

In the premyofibril model an increase in global tension could not only foster actin polymerisation at pre-costameres but could also be a trigger for the alignment of myosin and actin filaments resulting in the simultaneous appearance of the Mhc pattern. As in vivo and ex vivo studies do not observe Mhc during the early myofibrillogenesis, it would be useful to add an earlier marker to further analyse if sarcomeres are indeed formed simultaneously. For example, in vivo imaging of α-actinin could be very insightful since α-actinin is a component of I-Z-I bodies and among the first molecules detected in a periodic pattern in cell culture and developing chicken hearts (Littlefield and Fowler, 1998).

Based on the current data about the cortical actin wall that was observed in DLMs during 18h APF it is not clear if myosin is incorporated into the actin wall and how these structures develop over time until 30h APF when myofibrils fill the myotube. Thus, cortical actin filaments could also be unrelated to premyofibrils.

In addition to the exchange of non-muscle myosin by muscle myosin in pre-myofibrils, the simultaneous appearance of a periodic Mhc pattern could also represent a state when myofibrils align into register to form striated patterns, or when multiple independently formed complexes are aligned into a mature sarcomere as suggested by the two step-model (Rui et al., 2010). In the two-step model, tension could serve as trigger for the second step that aligns I-Z-I, myosin, titin and other preformed complexes with each other. Rui et al. suggest a local tension at pre-costameres as trigger for the interdigitation of thick and thin filaments. In order to form these filaments in the complete myotube and not only at the myotube surface, the preformed complexes should be linked to each other, which is not anticipated in the two-state model. However, global tension applied along the myotube could trigger interdigitation of preformed complexes not only on the myotube surface but simultaneously through the complete myofiber. Thus, it is possible that increasing tension during attachment maturation reaches a threshold around 30h APF that triggers

simultaneous assembly of sarcomeres. As the complete myotube is exposed to the same tension, this mechanical signal could provide a way to transmit information simultaneously over a long distance. Tension as mechanical stimulus is for example also used in synchronising dorsal closure at the leading edge of the *Drosophila* epidermis and to maintain a stable compartment boundary in wing imaginal discs (Landsberg et al., 2009; Solon et al., 2009).

4.2.6 A revised model of DLM development

The results of this thesis combined with published work can be summarised in the following model. Both myotube ends migrate in an integrin dependent fashion until they reach their proper tendon attachment sites. During this time Grip localises Kon to myotube tips. While the filopodia of myotubes and tendons intercalate intensively, Kon could bind an unknown ligand on the tendon cells, resulting in tendon recognition and attachment initiation. This initial attachment might be formed via E-cadherin based focal adherence junctions between myotubes and tendon cells forming on different filopodial contact-sites. The adherence junctions could then extend from these different points and join each other. Adhesion should trigger tendon differentiation and subsequent secretion of the integrin ECM ligand Tsp. Increasing tension generated by the myotube could further increase integrin recruitment to the myotube tips, fostering a remodelling of the focal adherence junctions into hemiadherence junctions that connect muscle integrins to Tsp (attachment maturation). Integrin-assisted remodelling of the actin-myosin cytoskeleton could trigger or increase myotube compaction, which in turn amplifies tension on the myotendinous system, promoting integrin localisation to myotube tips in a positive feedback loop. This process would continue until a tension threshold is reached and simultaneous myofibrillogenesis is triggered (Weitkunat et al., 2014) (Figure 80).

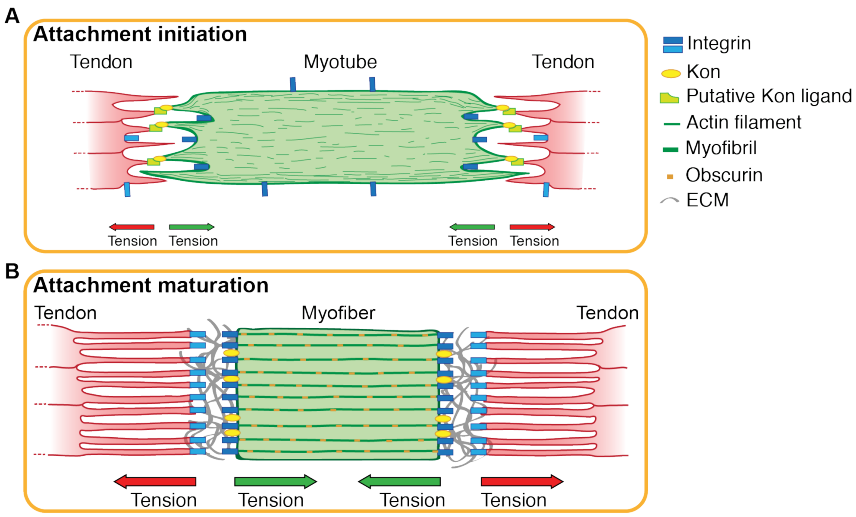

Figure 80 Model for attachment and myofibrillogenesis. A| Attachment initiation; Kon, mediates the initiation of a muscle-tendon attachment at myotube tips. Actin is forming thin filaments at the myotube cortex of these attached myotubes. B| Attachment maturation and myofibrillogenesis; following attachment initiation myotubes compact but are still connected to tendon cells, which are elongating at the same time. Concomitantly with myotube compaction, tension increases significantly, integrins and integrin associated molecules localise to myotube tips, Tsp accumulates at the myotendinous junction and actin organises into myofibrils.

5 Materials and Methods

5.1 *Drosophila melanogaster* maintenance and handling

Fly work was performed according to standard procedures. Flies were kept on standard fly food (Table 5) supplied by an in-house facility.

Table 5 Fly food ingredients.

Agar	117g
Maize flour	1kg
Soya flour	100g
Yeast	185g
Diamalt	400g
Sugar beet syrup	400g
Nipagin	25g
Ethanol (20%)	200mL
Phosphoric acid	100mL
Water	30L

Flies were kept at 25°C or 18°C and were transferred to new food every two or four weeks, respectively. Crosses using the binary GAL4/UAS expression system (Brand and Perrimon, 1993), were performed at 27°C to enhance Gal4 activity. Gal4-lines, GFP-fusion and GFP-reporter lines are listed in Table 6 and Table 7.

Table 6 Gal4-lines.

Construct	Cell type	Reference
1151-GAL4	Adult AMPs, early myotubes and internal leg tendons	(Anant et al., 1998)
Mef2-GAL4	Myoblasts and myotubes during all stages	(Ranganayakulu et al., 1996)
stripe-GAL4	Tendon cells	(Schnorrer et al., 2007)

Table 7 GFP-fusion and GFP-reporter lines.

Construct	Localisation	Reference
UAS-CD8-GFP	Membrane	(Lee and Luo, 1999)
UAS-GFP-Gma	Actin	(Bloor and Kiehart, 2001)
UAS-palm-Cherry	Membrane	(Förster and Luschnig, 2012)
mhc-TauGFP	Microtubules in body muscles	(Chen and Olson, 2001)
Mhc$^{wee\text{-}P26}$-GFP	Thick filament in body muscles	(Orfanos and Sparrow, 2013)

5.2 RNA interference (RNAi)

RNAi was used to knock-down the activity of individual genes; for recent review see (Perrimon et al., 2010). Large collections of UAS-RNAi-lines are available from different sources (Table 8) allowing for tissue specific hairpin expression using the GAL4/UAS system. For muscle specific knock-down *Mef2*-Gal4 (Ranganayakulu et al., 1996) was used unless otherwise stated. The strategy used for RNAi screening is elucidated in the reference section (3.1.2). The 400 RNAi-lines used for the adult myogenesis screen are listed in the appendix, Table 25. The RNAi-lines used for knock down of other genes were obtained from VDRC (Table 9).

Table 8 Source for RNAi-lines.

Source	Link
Vienna *Drosophila* RNAi Center (VDRC)	http://stockcenter.vdrc.at
National Institute of Genetics (NIG)	http://www.shigen.nig.ac.jp/fly/nigfly/
Transgenic RNAi Project at Harvard Medical School (TRiP)	http://www.flyrnai.org/TRiP-HOME.html

Table 9 List of RNAi-lines used for Grip, integrin and Talin knock-down.

Target gene	RNAi-line	Construct
Grip	39310	15768
inflated (if)	44885	1175
myospheroid (mys)	29619	15002
rhea	40399	12050

5.3 Dissection of *Drosophila* adult muscles

Dissections of dorsal abdominal muscles and DLMs are described in detail in (Weitkunat and Schnorrer, 2014). For staging white pre-pupae (0h APF) were isolated and aged until the desired stage. The duration of aging is indicated in hours APF and refers to aging at 27°C.

5.3.1 Dissection of DLMs

90h APF pupae were freed from their pupal case and fixed. Abdomen and legs were cut off and thoraxes were fixed for 7min at room temperature using relaxing solution (Table 10), preserving sarcomeres in their relaxed state. To expose DLMs fixed thoraxes were cut sagittally using a sharp microtome blade (PFM C35, No. 207500003) followed by three washing steps (10 min) using Phosphate buffered saline with 0.3% Triton X-100 (PBS-T).
As DLMs are significantly smaller at 18h and 30h AFP these stages were dissected differently. The pupa was glued onto double sticky tape and carefully freed from the pupal case. Next, the pupa was pinned onto a silicon filled petri dish and covered with cold PBS. The ventral thorax half was carefully removed using fine scissors (Fine Science Tools, No. 15000-02). Then, the two big trachea were removed using forceps. Fat was carefully removed with a PBS flow. Next, both thorax halves were separated from each other and from the abdomen. The then exposed DLMs remained on the thorax halves and were fixed for 15 min at room temperature using PBS-T with 4% PFA and washed three times in PBS-T.

Table 10 Relaxing solution. Relaxing solution was prepared fresh and kept on ice; ATP was thawed on ice.

Paraformaldehyde (PFA) (Vol.-8% in H_2O)	2.5mL
Sodium phosphate buffer 100mM; pH7.0	1.0mL
$MgCl_2$ (50mM)	800µL
Triton X-100 (1% in H_2O)	500µl
H_2O MilliQ	100µL
EGTA (0.5M; pH 8.0)	50µL
ATP (0.5M)	50µL

5.3.2 Dissection of abdominal dorsal muscles

Pupae were freed from their pupal case and dissected at the desired age.

Pupae were pinned onto a silicon filled petri dish and covered with cold PBS. Using fine scissors (Fine Science Tools, No. 15000-02) the ventral half of the abdomen was cut off. Next, the dorsal abdomen was pinned flat on the silicon and gut, trachea and fat were carefully removed using blunt forceps and by applying a gentle PBS flow, exposing the dorsal abdominal muscles. Next, PBS was removed and fixing solution was added. 90h APF pupae were fixed in relaxing solution (Table 10), 28h and 48h APF pupae were fixed in 4% PFA in PBS-T. Followed by 30 min incubation at room temperature and by three washing steps with PBS-T.

5.4 Immunohistochemistry and imaging

Fixed samples were blocked for 30min at room temperature using normal goat serum (1:30) in PBS-T. Primary antibody (Table 11) was diluted in PBS-T and samples were incubated over night at 4°C. Next, three washing steps in PBS-T were performed. Then, samples were incubated in secondary antibody (1:500 in PBS-T, Table 12) for 2h at room temperature and followed by three washing steps in PBS-T. Only 90h samples were incubated on a shaker since the movement can lead to loss of muscles for early dissections, when muscles are not attached to tendons yet. Stained samples were mounted in Vectashield for confocal microscopy. Images were acquired with a Zeiss LSM 780 or Leica SP5 and processed with Fiji (ImageJ) and Photoshop.

GFP-Booster (1:250, Chromotek) was used to enhance GFP signal and rhodamine phalloidin (1:500, Invitrogen) was used to label actin. Both were added to the secondary antibody mixture.

Table 11 List of primary antibodies.

Antibody	Organism	Dilution	Source
anti-Dlg1	Mouse	1:1000	DSHB (4F3)
anti-E-Cadherin	Rat	1:50	DSHB (DCAD2)
anti-Fas3	Mouse	1:50	DSHB (7G10)
anti-Futsch	Mouse	1:100	DSHB (22C10)
anti-Kon	Rabbit	1:1000	(Schnorrer et al., 2007)
anti-Laminin	Rabbit	1:2000	(Gutzeit et al., 1991)
anti-Obscurin	Rabbit	1:500	(Burkart et al., 2007)
anti-Perlecan	Rabbit	1:1000	(Friedrich et al., 2000)
anti-pFAK (Y397)	Mouse	1:500	Biosource
anti-Robo	Mouse	1:10	DSHB (13C9)
anti-Shot	Guinea pig	1:500	(Strumpf and Volk, 1998)
anti-Talin	Mouse	1:500	DSHB (1:1 mix of A22A and E16B)
anti-Tsp	Rat	1:500	(Subramanian et al., 2007)
anti-α-PS1	Mouse	1:500	DSHB (DK.1A4)
anti-α-PS2	Mouse	1:500	DSHB (CF.2C7)
anti-β-PS	Mouse	1:500	DSHB (CF.6G11)

Table 12 List of secondary antibodies.

Antibody	Host organism	Conjugate	Source
Anti-Guinea pig IgG	Goat	Cy3	Jackson ImmunoResearch
Anti-mouse IgG	Goat	Alexa 568	Molecular Probes
Anti-mouse IgG	Goat	Alexa 633	Molecular Probes
Anti-Rabbit IgG	Goat	Alexa 568	Molecular Probes
Anti-Rabbit IgG	Goat	Alexa 633	Molecular Probes
Anti-Rat IgG	Goat	Alexa 568	Molecular Probes
Anti-Rat IgG	Goat	Alexa 633	Molecular Probes

5.5 Live imaging of *Drosophila* adult myogenesis

Live imaging of *Drosophila* abdominal dorsal muscles and DLMs is described in detail in (Weitkunat and Schnorrer, 2014). Movies were processed using the Metamorph software or Fiji (ImageJ).

5.5.1 Live imaging of abdominal dorsal muscles

Myoblasts and developing myotubes were labelled with a GFP marker to enable live imaging. In this case *Mef2*-Gal4>UAS-CD8-GFP pupae were used. A small opening was cut into the pupal case covering one half of an abdominal dorsal segment. Next, the pupa was transferred into a custom-made imaging chamber that holds it in the correct position. The hole was covered with 70% glycerol and a cover slip was added. Movies were acquired using a spinning disc confocal (Zeiss, Visitron), equipped with a 40x objective (NA = 1.1, Zeiss) and a heated stage set on 27°C. Z-stacks were acquired every 15 min.

5.5.2 Two-photon live imaging of DLMs

Tissues of interest were labelled with a GFP marker to enable live imaging, the combination of driver and GFP-reporter lines for each movie are pointed out in the respective results section.

A small opening was cut into pupal case. The whole was positioned above the dorsal thorax covering almost the complete length and approximately half the width of the dorsal thorax. Next, the pupa was transferred into a custom-made imaging chamber that holds the pupa in the correct position. The hole was covered with 70% glycerol and a cover slip was added. Movies were acquired with a two-photon set up (LaVision) using a long distance 20x objective (NA = 1.0, Zeiss) and a heated stage set on 27°C. Z-stacks were acquired every 10-20 min.

5.5.3 Two-colour live imaging of DLMs and tendons

Myotubes were labelled with *mhc*-TauGFP and tendons with *sr*-Gal4 driving UAS-palm-Cherry. A small opening was cut into the pupal case covering one half of an abdominal dorsal segment. Next, the pupa was transferred into a custom-made imaging chamber that holds it in the correct position. The hole was covered with 70% glycerol and a cover slip was added. Movies were acquired with a spinning disc confocal (Zeiss, Visitron), equipped with a 40x objective (NA = 1.1, Zeiss) and a heated stage set on 27°C. Z-stacks were acquired every 5 min.

5.6 Tension measurements

Laser ablations were carried out using a previously described set-up (Grill et al., 2001). *Mef2-GAL4, stripe-GAL4* > UAS-CD8-GFP pupae were staged for 15h, 20h and 24h APF at 25°C corresponding to approximately 13h, 18h and 22h APF at 27°C, respectively. For better comparison with the analysis of morphological experiments that used RNAi and, therefore, were carried out at 27°C, the results part refers to these corresponding ages. Pupae were prepared as described for live imaging (section 5.5).

In principal laser cutting and recoil velocity measurements as a function of time-post-cut were carried out as described previously (Mayer et al., 2010). Using a pulsed UV laser a 2µm line was severed using 1.5 shots per µm and 20 pulses per shot. Within a 2µm z-range, 2 z-positions were targeted. The piezo was set on 1.8. When myotubes compact, DLMs gradually move deeper into the thorax. Thus, the UV light has to pass more tissue before it reaches the DLMs, therefore less should reach the DLMs. A Laser intensity of 1.5 was sufficient to cut tendons at 15h APF. However, the same intensity only caused bleaching of tendons at 20h or 24h APF. Thus the laser intensities were adjusted as follows: 1.5 at 15h APF, 2.5 at 20h APF and 3.5 at 24h APF. Frames were recorded every 150msec. The resultant particle image velocimetry (PIV) flow fields were determined and averaged over two regions (17µm x 26µm) that were 0.4µm away from the cut line. Velocity data as a function of time-post-cut were then fit using a least-square-fitting-algorithm (MATLAB) to an exponential function with constant offset to obtain the initial recoil velocity and the relaxation time constant. Initial recoil velocity was additionally measured using the first and second frame after cutting.

5.7 Tendon severing

Tendon severing was achieved using the setup as described in section 5.6. *Mef2*-GAL4*, stripe-GAL4* > UAS-CD8-GFP pupae were staged for 24h APF at 25°C corresponding to approximately 22h APF at 27°C. Pupae were prepared as described for live imaging (section 5.5). All visible anterior tendons of the left DLM sextet were severed by the UV laser. Pupae were kept in the imaging chamber, to keep the hole in the pupal case covered and transferred to a 25°C incubator allowing for further development. If pupae were kept until 95h APF they eclosed, demonstrating that pupal development was not impaired by the treatment. At 36h APF, which is morphologically similar to 30h APF at 27°C, pupae were dissected and stained as described in sections 5.3.1 and 5.4. The severed DLMs of the

left thorax halves and the intact tendons of the right control thorax halves were stained in the same well allowing for better comparison.

5.8 Myofibril length quantification

The Simple Neurite Tracer tool in Fiji was used to manually trace myofibrils of a confocal z-stack within an area of 34µm x 34µm x 2.5µm (Longair et al., 2011). Both, the myofibrils within the topmost 0 - 2.5µm (surface) and the myofibrils within the adjacent 2.5 - 5µm (interior) were traced in the same z-stack.

5.9 Myofiber length quantification

Myofibers were measured manually using the line tool in Fiji (Image J).

5.10 Measuring of intensity levels

Intensity levels of confocal images were measured using Fiji (ImageJ). Regions of interest with a similar size were selected using the ROI manager and mean intensity in these regions was measured using the measuring tool.

5.11 Statistical analysis

Two-tailed students t-tests were performed using Microsoft Excel. p-Values are presented in the figure legends.

6 Acknowledgements

First of all I want to thank Dr. Frank Schnorrer for opening the fascinating world of *Drosophila* research to me and for giving me the opportunity to work on this exciting research project. I am deeply grateful to him, for his generous support during the past years. Of special value to me was that he encouraged and enabled me to go to various scientific conferences, where I could present my work and get in contact with fellow researchers allowing me to broaden my scientific horizon. I am also especially thankful for his enthusiasm for the tension measurements that resulted in a very successful collaboration with Prof. Dr. Stephan Grill.

I am very grateful to Prof. Dr. Stephan Grill for receiving me so openly into his laboratory and for introducing a new and exciting research field to me. I thank him for sharing expertise, instruments and reagents that enabled me to establish tension measurement and manipulation of the *Drosophila* muscle tendon system. The time in his lab was a truly inspiring experience to me.

Furthermore, I would like to express my sincere gratitude to Prof. Dr. Ulrike Gaul for being my Doktormutter. I would like to thank her for support, advice and stimulating discussions during my TAC meetings. Additionally, I want to thank her for time and support in organising the defence.

I am grateful to Prof. Dr. Magdalena Götz for support, advice and stimulating discussions during my TAC meetings. I am very thankful that she agreed to be the second referee for my thesis.

I am grateful to Dr. Krzysztof Jagla for travelling all the way to Munich to attend my TAC meetings. I thank him for sharing his expertise in the field of *Drosophila* muscle development, for stimulating discussions and for his enthusiasm for my work.

I want to thank the members of my examination board; Prof. Dr. Ulrike Gaul, Prof. Dr. Magdalena Götz, Prof. Dr. Klaus Förstemann, PD Dr. Dietmar Martin, Prof. Dr. Roland Beckmann and Prof. Dr. Martin Biel, for their time and dedication to review my thesis.

I also thank Prof. Dr. Reinhard Fässler for hosting our group in his department and for generously sharing equipment. Additionally, I want to thank him for stimulating scientific discussions during department seminars.

Moreover, I am deeply grateful to the present and former members of the Schnorrer lab for constant support and encouragement as well as many exciting scientific discussions and valuable input into my project. Thank you for all the fun times in the fly room and during our lab-outings. I also want to thank our lunch and birthday cake group for nice chats during brakes.

I am very grateful to Aynur for our successful collaboration and her help during the Kon project. I am also thankful for many inspiring discussions, great moral support and excellent copy-editing.

Special thanks go also to Stefan Berchtold for great support, especially with screening of the second hairpins.

Additionally, I would like to thank the members of the Grill lab for stimulating discussion as well as for sharing lab space and valuable microscope time with me. I especially want to thank Sundar Naganathan and Stoyno Stoynov for support and introduction to the microscope. Furthermore, I would like to thank the fly community of the MPI CBG for sharing their fly room with me.

I also want to thank Maria Novatchkova for providing us with bioinformatical predictions of transmembrane proteins and transcription factors used for the selection of the adult myogenesis screen set.

I would like to thank Dr. Thomas Wollert for kindly providing a quiet place to write my thesis.

Many thanks go also to the IMPRS-LS coordination office for providing support and organising excellent workshops.

Additionally, I want to thank the fly community; in particular, Sanford Bernstein, Belinda Bullard, John Sparrow and Talila Volk for sharing flies and reagents.

Finally, I would like to thank my family and friends for their love, encouragement and constant support. In particular, I want to thank my husband for his understanding and patience and for giving me the freedom and the strength that were fundamental for this work.

7 Abbreviations

A-P	Anterior to posterior
AMP	Adult muscle progenitor
ARP2/3	Actin-related protein
Babo	Baboon
Cad86c	Cadherin 86c
Dlg1	Discs large 1
DLM	Dorsal longitudinal flight muscle
Duf	Dumbfounded
DVM	Dorsal ventral flight muscle
E(y)3	Enhancer of yellow 3
EGFR	Epidermal growth factor receptor
ECM	Extracellular matrix
F-actin	Fibrous actin
FAK	Focal adhesion kinase
Fas3	Fasciclin 3
FC	Founder cell
FCM	Fusion competent myoblast
G-actin	Globular actin
Grip	Glutamate receptor binding protein
Hbs	Hibris
IR	Inverted repeat
Kon	Kon-tiki
Kto	Kohtalo
Kul	Kuzbanian-like
L’sc	Lethal of scute
Lan	Laminin
LOM	Larval oblique muscle
Lrt	Leucine-rich tendon-specific protein
P-D	Proximal to distal
PIV	Particle image velocimetry
Put	Punt
Robo	Roundabout

ROI	Region of interest
Rst	Roughest
Salm	Spalt major
Smox	Smad on X
Sr	Stripe
Sns	Sticks and stones
Trn	Transportin
Tn-Tm	Troponin-Tropomyosin
Tsp	Thrombospondin
WASP	Wiskott-Aldrich syndrome protein
Wg	Wingless
Wip	WASP-interacting protein

8 Appendix

Table 13 List of genes selected for adult myogenesis screening. Table is continued on the next page.

Gene name	Annotation symbol	Gene name	Annotation symbol	Gene name	Annotation symbol	Gene name	Annotation symbol
Abd-B	CG11648	*CG4552*	CG4552	*CG9034*	CG9034	*CG17766*	CG17766
AdoR	CG9753	*CG4645*	CG4645	*CG9090*	CG9090	*CG17928*	CG17928
amos	CG10393	*CG4655*	CG4655	*CG9400*	CG9400	*CG18418*	CG18418
apt	CG5393	*CG4753*	CG4753	*CG9536*	CG9536	*CG18469*	CG18469
Atet	CG2969	*CG4763*	CG4763	*CG9571*	CG9571	*CG18870*	CG18870
ato	CG7508	*CG4854*	CG4854	*CG9657*	CG9657	*CG30340*	CG30340
babo	CG8224	*CG4908*	CG4908	*CG9664*	CG9664	*CG30373*	CG30373
beat-Ic	CG4838	*CG4936*	CG4936	*CG9723*	CG9723	*CG30377*	CG30377
betaInt-nu	CG1762	*CG5078*	CG5078	*CG9747*	CG9747	*CG30389*	CG30389
bin	CG18647	*CG5096*	CG5096	*CG9895*	CG9895	*CG31120*	CG31120
bun	CG5461	*CG5326*	CG5326	*CG10219*	CG10219	*CG31367*	CG31367
Ca-P60A	CG3725	*CG5621*	CG5621	*CG10320*	CG10320	*CG31431*	CG31431
Cap	CG9802	*CG5899*	CG5899	*CG10354*	CG10354	*CG31530*	CG31530
Catsup	CG10449	*CG5969*	CG5969	*CG10413*	CG10413	*CG31648*	CG31648
CCKLR-17D	CG6857	*CG5999*	CG5999	*CG10908*	CG10908	*CG31717*	CG31717
Ccp84Ag	CG2342	*CG6017*	CG6017	*CG10979*	CG10979	*CG31738*	CG31738
Cdk9	CG5179	*CG6231*	CG6231	*CG11137*	CG11137	*CG32069*	CG32069
Chd1	CG3733	*CG6364*	CG6364	*CG11665*	CG11665	*CG32193*	CG32193
Cht7	CG1869	*CG6470*	CG6470	*CG11781*	CG11781	*CG32206*	CG32206
clumsy	CG8681	*CG6475*	CG6475	*CG11880*	CG11880	*CG32343*	CG32343
cnc	CG17894	*CG6495*	CG6495	*CG12124*	CG12124	*CG32521*	CG32521
Cnx99A	CG11958	*CG6600*	CG6600	*CG12400*	CG12400	*CG32532*	CG32532
crc	CG8669	*CG6666*	CG6666	*CG12404*	CG12404	*CG33144*	CG33144
crp	CG7664	*CG6737*	CG6737	*CG12499*	CG12499	*CG33169*	CG33169
CSN3	CG18332	*CG6785*	CG6785	*CG13011*	CG13011	*CG33523*	CG33523
ct	CG11387	*CG7011*	CG7011	*CG13029*	CG13029	*CG34127*	CG34127
Ctr1A	CG3977	*CG7026*	CG7026	*CG13047*	CG13047	*CG34139*	CG34139
cue	CG12086	*CG7056*	CG7056	*CG13101*	CG13101	*CG34353*	CG34353
CG1161	CG1161	*CG7203*	CG7203	*CG13130*	CG13130	*CG34420*	CG34420
CG1291	CG1291	*CG7372*	CG7372	*CG13217*	CG13217	*CycG*	CG11525
CG1531	CG1531	*CG7638*	CG7638	*CG13223*	CG13223	*cype*	CG14028
CG1599	CG1599	*CG7818*	CG7818	*CG13287*	CG13287	*D*	CG5893
CG1603	CG1603	*CG7987*	CG7987	*CG13511*	CG13511	*Ddr*	CG33531
CG1965	CG1965	*CG8271*	CG8271	*CG13674*	CG13674	*Dl*	CG3619
CG2943	CG2943	*CG8306*	CG8306	*CG14020*	CG14020	*dm*	CG10798
CG2990	CG2990	*CG8320*	CG8320	*CG14635*	CG14635	*dnt*	CG17559
CG3192	CG3192	*CG8444*	CG8444	*CG15168*	CG15168	*Doa*	CG33553
CG3409	CG3409	*CG8531*	CG8531	*CG15237*	CG15237	*dom*	CG9696
CG3509	CG3509	*CG8584*	CG8584	*CG15321*	CG15321	*Dref*	CG5838
CG3625	CG3625	*CG8743*	CG8743	*CG15357*	CG15357	*dup*	CG8171
CG3634	CG3634	*CG8860*	CG8860	*CG15506*	CG15506	*e(y)3*	CG12238
CG3803	CG3803	*CG8885*	CG8885	*CG15740*	CG15740	*ebi*	CG4063
CG4078	CG4078	*CG8974*	CG8974	*CG16903*	CG16903	*Eip93F*	CG18389
CG4288	CG4288	*CG9000*	CG9000	*CG17462*	CG17462	*enok*	CG11290

Gene name	Annotation symbol	Gene name	Annotation symbol	Gene name	Annotation symbol
Ent2	CG31911	*not*	CG4166	*Taf4*	CG5444
esg	CG3758	*Or33b*	CG16961	*Taf6*	CG32211
Ets97D	CG6338	*Osi16*	CG31561	*Task6*	CG9637
fra	CG8581	*Osi21*	CG14925	*TFAM*	CG4217
ftz-f1	CG4059	*ox*	CG8764	*tin*	CG7895
fz	CG17697	*perd*	CG10275	*Top2*	CG10223
fz2	CG9739	*ph-p*	CG18412	*Trf2*	CG18009
glu	CG11397	*pHCl*	CG33989	*Trn*	CG7398
Gnf1	CG1119	*PNUTS*	CG33526	*Trn-SR*	CG2848
H15	CG6604	*por*	CG6205	*Tsp29Fb*	CG9496
Hr4	CG16902	*Poxm*	CG9610	*ttm50*	CG2713
Hr78	CG7199	*primo-1*	CG33748	*Ugt36Ba*	CG13270
Hsf	CG5748	*Ptp52F*	CG18243	*Use1*	CG14181
Ir	CG6747	*put*	CG7904	*Vap-33-1*	CG5014
kek1	CG12283	*R*	CG1956	*Vha100-2*	CG18617
kek6	CG1804	*Rbf*	CG7413	*VhaM9.7-2*	CG7625
kis	CG3696	*rdgA*	CG34344	*VhaPPA1-1*	CG7007
kto	CG8491	*Rga*	CG2161	*W*	CG5123
Kul	CG1964	*Rpb10*	CG13628	*wun2*	CG8805
l(1)G0232	CG32697	*Rpd3*	CG7471	*Z4*	CG7752
l(1)G0289	CG2221	*RpII15*	CG3284		
l(2)44DEa	CG8732	*RpL28*	CG12740		
l(2)k01209	CG4798	*Rx*	CG10052		
lbe	CG6545	*Scm*	CG9495		
Lcch3	CG17336	*Scr*	CG1030		
lmd	CG4677	*Sec61gamma*	CG14214		
lolal	CG5738	*sens-2*	CG31632		
LRR47	CG6098	*sesB*	CG16944		
mAcR-60C	CG4356	*Sirt6*	CG6284		
Mad	CG12399	*slmo*	CG9131		
Marf	CG3869	*Smox*	CG2262		
mbf1	CG4143	*sns*	CG33141		
mbo	CG6819	*Sox100B*	CG15552		
MED17	CG7957	*Sox14*	CG3090		
MED7	CG31390	*Spase18-21*	CG2358		
mmd	CG9163	*sr*	CG7847		
Mnt	CG13316	*Stat92E*	CG4257		
msl-1	CG10385	*Su(var)2-10*	CG8068		
Msp300	CG42768	*Surf1*	CG9943		
mthl1	CG4521	*synaptogyrin*	CG10808		
N	CG3936	*Syx1A*	CG31136		
na	CG1517	*Syx5*	CG4214		
Nep1	CG5905	*Syx7*	CG5081		
nerfin-1	CG13906	*Taf1*	CG17603		

Table 14 Genes classified as “fiber shape”, “short myofibers” for any muscle type

Gene	Phenotype strength	Gene	Phenotype strength
AdoR	Strong	*glu*	Strong
amos	Weak	*H15*	Strong
ato	Strong	*kon*	Strong
CG1965	Weak	*Kul*	Strong
CG6470	Weak	*lbe*	Strong
CG7372	Strong	*Mnt*	Weak
CG8974	Strong	*Msp300*	Strong
CG9747	Strong	*N*	Strong
CG10413	Strong	*nej*	Strong
CG10979	Strong	*not*	Weak
CG13029	Strong	*ph-p*	Weak
CG13287	Strong	*PNUTS*	Strong
CG14020	Strong	*por*	Strong
CG31431	Strong	*Ptp52F*	Strong
CG31530	Strong	*R*	Weak
CG31738	Strong	*rdgA*	Strong
CG32069	Strong	*sing*	Strong
CG33169	Strong	*slmo*	Strong
CG34353	Strong	*Syx5*	Strong
Der-1	Strong	*Top2*	Strong
dnt	Strong	*Tsp29Fb*	Strong
Doa	Strong	*W*	Weak
Dref	Strong	*Z4*	Weak

Table 15 Genes classified as strong in "fiber shape", "short myofiber" for abdominal dorsal muscles and DLM.

Gene	Muscle type	Process or characteristic (predicted)
lbe	Abdominal dorsal muscle	Myogenesis
Msp300	Abdominal dorsal muscle	Myogenesis
Ptp52F	Abdominal dorsal muscle	Axon guidance
CG9747	Abdominal dorsal muscle	FA desaturase domain
CG34353	Abdominal dorsal muscle	Immunoglobulin domains
Doa	Abdominal dorsal muscle	Kinase
rdgA	Abdominal dorsal muscle	Kinase
PNUTS	Abdominal dorsal muscle	Phagocytosis
por	Abdominal dorsal muscle	Protein processing, Wnt signalling
ato	Abdominal dorsal muscle	Transcription factor
CG7372	Abdominal dorsal muscle	Transcription factor
CG31530	Abdominal dorsal muscle	Transporter domain
CG33169	Abdominal dorsal muscle, DLM	Transmembrane domain
dnt	DLM	Myogenesis
kon	DLM	Myogenesis
nej	DLM	Myogenesis
sing	DLM	Myogenesis
slmo	DLM	Myogenesis
Der-1	DLM	Protein degradation
AdoR	DLM	Receptor
CG10979	DLM	Transcription factor
CG13287	DLM	Transcription factor
CG13029	DLM	Transferase
CG8974	DLM	

Table 16 Genes classified as strong in "fiber presence" for DLMs. Fusion phenotype in other muscles is based on the classification as "thin myofibers" represented in **Table 1**

Gene	Fusion phenotype in other muscles	Process or characteristic (predicted)
Dl	yes	Fusion
N	yes	Fusion
lmd	yes	Fusion
sing	yes	Fusion
dnt	no	Myogenesis
H15	yes	Myogenesis
kon	yes	Myogenesis
nej	yes	Myogenesis
AdoR	yes	Receptor
Cdk9	no	Cell cycle
CG16903	no	Cell cycle
dup	yes	Replication
MED7	yes	Mediator complex subunit
MED17	yes	Mediator complex subunit
kis	no	Helicase
Mnt	no	Transcription factor
CG6470	yes	Transcription factor
CG13287	yes	Transcription factor
Smox	no	Transcription factor
Atac3	no	Acetyltransferase
cnc	no	Microtubule polarisation
slmo	no	Mitochondrial process
CG3625	no	

Table 17 Potential myotube guidance proteins. Genes classified as "fiber position" in any muscle type.

Gene	Phenotype strength	Process or characteristic (predicted)
kon	Stong	Myogenesis
nej	Stong	Myogenesis
dnt	Weak	Myogenesis
lmd	Weak	Myogenesis
Poxm	Weak	Myogenesis
Cad86C	Stong	Cadherin repeats
CG34420	Weak	Metalloproteinase
Kul	Weak	ADAM metalloproteiase
Atac3	Stong	Acetyltransferase
CG14020	Stong	N-acteylglucosamin ransferase
Hr78	Stong	Receptor
na	Weak	Channel
Cdk9	Weak	cell cycle
CG6470	Weak	Transcription factor
glu	Weak	Strucutral maintenance of chromosome

Table 18 Potential sarcomerogenesis genes. List of genes that show a strong phenotype in "sarcomeric organisation" but not in "fiber presence", "fiber shape" or "fiber position".

Gene	Process or characteristic (predicted)
CG15506	Transcription factor
CG1603	Transcription factor
CG4854	Transcription factor
esg	Transcription factor
Taf4	Transcription factor
CG12404	Golgi protein vesicular transport
CG5078	Transporter
CG6475	Glucuronosyltransferase
Nlg4	Neuroligin, Cell adhesion
ox	Mitochondrial respiratory chain
ph-p	Chaperone binding
pHCl	pH sensitive Chloride channel
Spase18-21	Peptidase, signal peptide processing

Table 19 Potential abdominal dorsal myotube guidance proteins. Genes classified as "fiber position" in abdominal dorsal muscle type.

Gene	Phenotype strength	Process or characteristic (predicted)
kon	Stong	Myogenesis
nej	Stong	Myogenesis
lmd	Weak	Myogenesis
Cad86C	Stong	Cadherin repeats
Hr78	Stong	Receptor
CG34420	Weak	Metalloproteinase
Kul	Weak	ADAM metalloproteiase
CG14020	Stong	N-acteylglucosamin ransferase
CG6470	Weak	Transcription factor
glu	Weak	Strucutral maintenance of chromosome

Table 20 Early phenotypes. Includes a complete list of genes screened for early phenotypes. As Thorax presence only includes the subclass "missing" no subclass is specified in the table. In column abd. dorsal presence "-" stands for the subclass missing fibers and "+" stands for the subclass additional fibers.

Gene name	DLM presence		DLM shape		abd. dorsal presence		abd. dorsal shape		abd. dorsal position	
	90h	early	90h	early	90h	early	90h	early	90h	early
nej	strong	strong								
CG6470	strong	strong			strong "+"	strong "+"	strong		weak	
Dl	strong	strong								
Mnt	strong	strong			strong "+"	strong "+"				weak
CG16903	strong	weak		weak						
sing	strong	strong	strong							
CG3625	strong			strong						
cnc	strong			strong	strong "-"	strong "-"				
kon	strong		strong		weak "-"	weak "-"			strong	strong
lmd	strong			strong	weak "-"				weak	
Smox	strong									
CG14020	weak	strong			strong "-"	strong "-"			strong	strong
Sirt6	weak	weak		strong	strong "+"	strong "+"				strong
CG13029			strong	strong	strong "+"	strong "+"		strong		
Cad86C					strong "+"	strong "+"			strong	weak
Etl1					strong "+"	strong "+"				
ebi					strong "-"	strong "-"				
Kul					strong "-"	strong "-"	strong	weak	weak	strong
mmd					strong "+"	strong "+"		weak		
Nep1					strong "-"	strong "-"				
Rpd3					strong "+"	strong "+"				
amos					strong "-"		weak			
CG34420					strong "-"		weak		weak	
CG8974			strong							
dnt			strong							
ato							strong			
CG34353							strong			
CG7372							strong			
CG9747							strong			
Doa							strong			
lbe							strong			
PNUTS							strong			
por							strong			
Ptp52F							strong			
rdgA							strong			

Table 21 Genes that are confirmed with a least one different construct (part1). Genes that display a strong phenotype in one class and a strong or weak phenotype in the same class for at least one out of the 5 main classes are counted as confirmed.

Gene name	Transformant	Construct	Fiber presence	Fiber shape	Fiber position	Fibrillar org.	Sarcomeric org.
(potential) Involved in myogenesis							
kon	36246	14368	strong	strong	strong		strong
	1159	TR00148A.1	weak	weak			strong
	37283	2633	strong	weak			
	102751	10275R-1	strong	strong	weak		
	106680	102101	strong	strong	strong		strong
lmd	28377	12792	strong	strong	weak		
	103821	107849	strong	weak			
nej	46534	8975	strong	strong	weak		strong
	46535	8975		strong		strong	
	102885	113191	strong	strong	strong		strong
slmo	109335	107326	strong	strong			strong
	44362	14130		strong			strong
Delta/Notch							
Delta	27187	14459	strong	strong			strong
	2867	TR02121P.1	strong	weak			weak
	37287	2642	strong				strong
N	1112	144	strong	strong			
	27228	14477					
	100002	102890	strong				
TGF-beta pathway							
babo	106092	108186	strong	weak			
	853	51	strong				
put	37279	2545	strong	strong			strong
	849	49	weak	weak			strong
Smox	14609	6452	strong	strong			
	2320	TR01197P.1	strong	strong			
	22621	2262R-1	strong	strong			
	105687	111163					
(potential) Histone modifiers							
Atac3	15741	4326	strong	weak	strong		
	1631	TR01665A.1					
	104385	108127	strong				
Rpd3	30600	4513	strong				
	607	SH00953.N	weak	weak			
	46929	17233			weak		

Table 22 Genes that are confirmed with a least one different construct (part 2). Genes that display a strong phenotype in one class and a strong or weak phenotype in the same class for at least one out of the 5 main classes are counted as confirmed.

Gene name	Transformant	Construct	Fiber presence	Fiber shape	Fiber position	Fibrillar org.	Sarcomeric org.
(potential) Transcription factors							
ato	48675	16434		strong			
	2924	1379	weak	weak	weak		
	48674	16434					
Mnt	10970	4469	strong	weak			
	101991	108462		strong		strong	
CG13287	36601	14859	strong	strong			strong
	36602	14859	strong	weak			weak
	109806	108096	weak				
CG32532	37046	15354	weak	strong		strong	
	106534	112057		weak			
CG7372	35214	12218		strong			strong
	73721	7372R-1		strong			
	108023	103821	weak	weak			
other genes							
cnc	37674	4437	strong				
	108127	101639	weak				
Hr4	37067	1464		weak		strong	
	37066	1464		weak		strong	
	102096	110718				strong	
PNUTS	35579	12783	strong	strong			
	35580	12783	strong	weak			strong
	106862	109923					strong
	316573	31657R-3					weak
rdgA	24574	7789		strong			strong
	JF03371	TR02681P.1					strong
	24573	7789		strong			strong
	102909	113317					
Trn	6543	33	strong	weak	weak	strong	
	6544	33		strong		strong	strong
	105181	108990		strong			
CG34353	47349	6319		strong			strong
	102326	111343					
	106528	111926					
	107519	111573		weak			weak
CG34420	8346	2430	strong	weak	weak		
	59171	5917R-1					
	59173	5917R-3	weak	weak			

Table 23 Genes that are confirmed with a least one different transformant. Genes that display a strong phenotype in one class and a strong or weak phenotype in the same class for at least one out of the 5 main classes are counted as confirmed.

Gene name	Transformant	Construct	Fiber presence	Fiber shape	Fiber position	Fibrillar org.	Sarcomeric org.
(potential) Involved in myogenesis							
sing	12202 12203	3396 3396	strong strong	strong strong			
H15	28415 28416 106875	12818 12818 110915	strong strong	strong strong		strong	strong strong
Other genes							
AdoR	1385 1386	380 380	strong weak	strong strong		strong weak	strong weak
CycG	19688 19689	1483 1483	strong strong				
CR13130	1457 1576 1577	397 397 397	strong strong strong				weak
Der-1	44211 44210	818 818		strong weak			
Dref	22209 22210	11784 11784		strong strong			
ox	35828 35829	13728 13728		 weak			strong strong
RpL28	18090 18091	7589 7589		strong strong		strong	strong strong
Syx5	3859 3857	1743 1743		strong strong			strong
Vap-33B	37237 37238 44377 110519	2326 2326 2326 109603		strong strong strong		 strong	
Uncharacterised genes							
CG10979	16144 16145	7154 7154		strong strong			strong strong
CG13047	42310 43463	14886 14886		strong strong			 strong
CG33169	30642 30643	4627 4627		strong strong			strong
CG8974	7188 5572	3381 3381		strong strong			strong weak

Table 24 Genes that could not be confirmed. Genes that display a strong phenotype in one class and a strong or weak phenotype in the same class for at least one out of the 5 main classes are counted as confirmed.

Gene name	Transformant	Construct	Fiber presence	Fiber shape	Fiber position	Fibrillar org.	Sarcomeric org.
amos	11796 100511	1521 104651	strong	weak		weak	
CG1161	44965 102003	3907 108998		strong		strong	strong
CG15506	1357 1356	366 366					strong
CG1603	19640 19641	9160 9160					strong
CG31738	29905 997	14390 107		strong			
CG3625	40855 106124	780 102383	strong			strong	strong
CG4753	1730 109865	457 111235	strong	weak			
CG6470	27633 108699	11933 105975	strong	strong	weak		strong
Doa	19066 20120 102520 310493	8588 8588 111879 31049R-3	weak	strong			strong
e(y)3	38637 105946	7544 112108	strong	strong			
ebi	40862 108208	1329 101485	strong			strong	
kto	23142 23143	13207 13207		strong			
Kul	28346 19643	12729 1964R-3	strong	strong	weak		
lbe	12662 102377	4157 109261	weak	strong			strong
mmd	1025 103449	119 113278	strong				
Nep1	27538 7108	11797 3251	strong		weak		
por	9150 100780 100780	3424 108587 108587		strong			strong
Ptp52F	3116 39175	2599 14408		strong			
Sirt6	22483 1009	11877 SH00809.Nb	strong	weak			
VhaPPA1-1	33343 47188	2991 16478				strong	

Table 25 List of RNAi-lines and respective construct IDs as well as target genes. Continued on next pages.

Target gene	RNAi line	Construct	Target gene	RNAi line	Construct	Target gene	RNAi line	Construct
CG10052	44716	4076	*CG12283*	43521	28	*CG15321*	46535	8975
CG10219	26776	12583	*CG12399*	12635	4121	*CG15321*	102885	113191
CG10223	30625	4570	*CG12400*	37462	3652	*CG15357*	26970	13340
CG10275	36246	14368	*CG12400*	37463	3652	*CG15506*	1356	366
CG10275	37283	2633	*CG12404*	1463	404	*CG15506*	1357	366
CG10275	106680	102101	*CG12499*	24550	7745	*CG15552*	45961	4588
CG10275	10275R-1	10275R-1	*CG12740*	18090	7589	*CG15740*	5548	3320
CG10275	JF 01159	TR00148A.1	*CG12740*	18091	7589	*CG1599*	13317	4531
CG1030	3033	1527	*CG1291*	32116	7863	*CG1603*	19640	9160
CG1030	3034	1527	*CG13011*	12202	3396	*CG1603*	19641	9160
CG1030	46499	17052	*CG13011*	12203	3396	*CG16902*	37066	1464
CG10320	8837	3811	*CG13029*	8503	3600	*CG16902*	37067	1464
CG10354	27254	6954	*CG13047*	42310	14886	*CG16902*	102096	110718
CG10385	9239	1242	*CG13047*	43463	14886	*CG16903*	37570	4164
CG10393	11796	1521	*CG13101*	3428	395	*CG16944*	48581	16160
CG10393	100511	104651	*CG13130*	1457	397	*CG16961*	7583	591
CG10413	3883	1761	*CG13130*	1576	397	*CG17336*	42546	3384
CG10449	7183	1635	*CG13130*	1577	397	*CG17462*	19801	4093
CG10798	2948	1419	*CG13217*	9965	1925	*CG17559*	27056	14372
CG10808	8784	3785	*CG13223*	1683	423	*CG17603*	41099	4594
CG10908	44210	818	*CG13270*	3864	1746	*CG1762*	42234	14392
CG10908	44211	818	*CG13287*	36601	14859	*CG17697*	43077	4614
CG10979	16144	7154	*CG13287*	36602	14859	*CG17766*	14531	6377
CG10979	16145	7154	*CG13287*	109806	108096	*CG17894*	37674	4437
CG11137	8463	2789	*CG13316*	10970	4469	*CG17894*	108127	101639
CG11137	8464	2789	*CG13316*	101991	108462	*CG17928*	3861	1745
CG11137	48241	17109	*CG13511*	8840	3814	*CG18009*	10443	4168
CG1119	10943	4455	*CG13628*	29253	14573	*CG1804*	39507	2515
CG11290	37526	4037	*CG13674*	23265	13321	*CG1804*	39510	2515
CG11387	4138	1237	*CG13906*	12584	4082	*CG18243*	3116	2599
CG11397	10937	4454	*CG14020*	44221	911	*CG18243*	39175	14408
CG11525	19688	1483	*CG14028*	13404	908	*CG18332*	12821	4778
CG11525	19689	1483	*CG14181*	42548	2382	*CG18389*	45856	4449
CG1161	44965	3907	*CG14214*	11989	4660	*CG18412*	10679	4480
CG1161	102003	108998	*CG14635*	102890	113204	*CG18418*	9008	2311
CG11648	12024	4680	*CG14925*	13595	1086	*CG18469*	4940	2049
CG11665	7314	1807	*CG15168*	12248	3659	*CG18617*	30297	3647
CG11781	49583	17318	*CG15168*	48614	16328	*CG18617*	30298	3647
CG11880	22869	12636	*CG15168*	48615	16328	*CG18647*	9409	1225
CG11958	42397	15382	*CG1517*	3306	1172	*CG1869*	42878	2270
CG12086	1043	133	*CG1517*	3307	1172	*CG18870*	3471	2129
CG12124	42978	7494	*CG15237*	47254	16803	*CG18870*	3472	2129
CG12238	38637	7544	*CG1531*	22901	12698	*CG1956*	33437	9686
CG12238	105946	112108	*CG15321*	46534	8975	*CG1964*	28346	12729

Target gene	RNAi line	Construct
CG1964	1964R-3	1964R-3
CG1965	43943	4423
CG2161	20826	9741
CG2221	27247	14489
CG2221	46376	2502
CG2221	107283	102740
CG2262	14609	6452
CG2262	105687	111163
CG2262	2262R-1	2262R-1
CG2262	JF02320	TR01197P.1
CG2342	5765	2837
CG2358	9055	3910
CG2713	5586	1161
CG2848	33569	9833
CG2848	33571	9833
CG2943	8477	2851
CG2969	42750	883
CG2990	30507	4254
CG30340	7387	1902
CG30373	4014	1868
CG30377	7358	1855
CG30389	19002	3559
CG3090	10856	4416
CG31120	3402	742
CG31136	33112	564
CG31367	37626	4323
CG31390	11504	4593
CG31431	1128	93
CG31530	49748	17659
CG31561	5761	2829
CG31632	21386	10311
CG31648	44226	914
CG31717	7662	1057
CG31717	7663	1057
CG31738	997	107
CG31738	29905	14390
CG31911	7618	953
CG3192	30413	3998
CG32069	9202	3868
CG32193	5342	2708
CG32206	14339	6181
CG32211	34452	10817
CG32343	15741	4326
CG32343	104385	108127
CG32343	JF01631	TR01665A.1
CG32521	43699	9327
CG32521	43700	9327
CG32532	37046	15354
CG32532	106534	112057
CG32697	21276	10130
CG3284	11219	4234
CG33141	877	65
CG33144	17081	7573
CG33169	30642	4627
CG33169	30643	4627
CG33523	37237	2326
CG33523	37238	2326
CG33523	44377	2326
CG33523	110519	109603
CG33526	35579	12783
CG33526	35580	12783
CG33526	106862	109923
CG33526	31657R-3	31657R-3
CG33531	29720	15146
CG33553	19066	8588
CG33553	20120	8588
CG33553	102520	111879
CG33553	31049R-3	31049R-3
CG33748	23079	12511
CG33989	11020	2478
CG3409	37139	1829
CG34127	18121	5568
CG34139	102676	112106
CG34344	24573	7789
CG34344	24574	7789
CG34344	102909	113317
CG34344	JF03371	TR02681P.1
CG34353	47349	6319
CG34353	102326	111343
CG34353	106528	111926
CG34353	107519	111573
CG34420	8346	2430
CG34420	5917R-1	5917R-1
CG34420	5917R-3	5917R-3
CG3509	48704	16380
CG3619	27187	14459
CG3619	37287	2642
CG3619	JF02867	TR02121P.1
CG3625	40855	780
CG3625	106124	102383
CG3634	16720	2761
CG3696	46685	16331
CG3725	4474	436
CG3733	26277	11058
CG3758	9793	1437
CG3803	3596	2191
CG3869	40478	11094
CG3936	1112	144
CG3936	27228	14477
CG3936	100002	102890
CG3977	46757	16726
CG4059	2959	1450
CG4063	40862	1329
CG4063	108208	101485
CG4078	37607	4251
CG4143	12751	4736
CG4143	12752	4736
CG4166	45775	11236
CG4214	3857	1743
CG4214	3859	1743
CG4217	37819	5041
CG4257	43866	4492
CG42768	109023	113643
CG4288	8620	3675
CG4356	33124	630
CG4521	33135	727
CG4552	40537	11348
CG4645	10164	3336
CG4655	26586	11388
CG4677	28377	12792
CG4677	103821	107849
CG4753	1730	457
CG4753	109865	111235
CG4763	3587	2187
CG4798	26628	11430
CG4838	36268	14389
CG4854	41929	12796
CG4908	44845	1055
CG4936	6252	1576
CG4936	6253	1576
CG5014	30404	3990
CG5078	8085	2752
CG5081	5413	2767

Target gene	RNAi line	Construct
CG5096	4765	2525
CG5123	8269	1673
CG5179	30449	4078
CG5326	47681	17148
CG5393	4289	1367
CG5444	12600	4090
CG5461	19679	1392
CG5621	47549	3092
CG5621	47550	3092
CG5738	9571	4694
CG5738	9572	4694
CG5738	9573	4694
CG5748	37699	4464
CG5838	22209	11784
CG5838	22210	11784
CG5893	2940	1412
CG5899	15679	4183
CG5905	7108	3251
CG5905	27538	11797
CG5969	47116	16253
CG5999	33339	2961
CG6017	8487	3594
CG6098	108096	101367
CG6205	9150	3424
CG6205	100780	108587
CG6205	100780	108587
CG6231	42656	3067
CG6284	22483	11877
CG6284	HMS01009	SH00809.Nb
CG6338	12633	4119
CG6364	11693	229
CG6470	27633	11933
CG6470	108699	105975
CG6475	40932	3101
CG6495	42794	1076
CG6545	12662	4157
CG6545	102377	109261
CG6600	5054	2328
CG6604	28415	12818
CG6604	28416	12818
CG6604	106875	110915
CG6666	6031	2912
CG6737	42791	1075
CG6737	42792	1075
CG6747	28430	12824
CG6747	28431	12824
CG6785	22700	12825
CG6819	47691	12047
CG6857	7233	730
CG7007	33343	2991
CG7007	47188	16478
CG7011	46860	17164
CG7026	48830	17023
CG7056	15721	4293
CG7199	37072	1465
CG7203	2746	979
CG7203	2748	979
CG7372	35214	12218
CG7372	108023	103821
CG7372	7372R-1	7372R-1
CG7398	6543	33
CG7398	6544	33
CG7398	105181	108990
CG7413	10696	4484
CG7471	30600	4513
CG7471	46929	17233
CG7471	HMS00607	SH00953.N
CG7508	2924	1379
CG7508	48674	16434
CG7508	48675	16434
CG7625	30384	3898
CG7638	8235	3587
CG7664	26885	13194
CG7664	26886	13194
CG7752	25541	9955
CG7818	48560	16300
CG7847	9921	1540
CG7895	32510	4155
CG7904	849	49
CG7904	37279	2545
CG7957	44027	4153
CG7987	22649	12343
CG8068	30709	5048
CG8171	23131	13203
CG8224	853	51
CG8224	106092	108186
CG8271	4609	1940
CG8306	23136	13204
CG8320	8797	3793
CG8320	8798	3793
CG8444	5830	2871
CG8491	23142	13207
CG8491	23143	13207
CG8531	24122	13954
CG8581	6557	68
CG8584	107849	103752
CG8669	2934	1407
CG8669	2935	1407
CG8681	1478	413
CG8681	1479	413
CG8732	3222	1638
CG8743	45989	555
CG8764	35828	13728
CG8764	35829	13728
CG8805	4176	1900
CG8860	8768	3779
CG8885	7861	898
CG8974	5572	3381
CG8974	7188	3381
CG9000	47523	2046
CG9000	47524	2046
CG9034	30420	4003
CG9090	44297	2105
CG9131	44362	14130
CG9131	109335	107326
CG9163	1025	119
CG9163	103449	113278
CG9400	43296	6426
CG9495	3796	1526
CG9496	2824	1018
CG9536	7905	949
CG9571	10477	4301
CG9610	48123	16705
CG9637	9073	3931
CG9657	43922	3270
CG9664	42467	388
CG9696	7787	1420
CG9723	37412	3395
CG9739	44390	2719
CG9747	1392	383
CG9753	1385	380
CG9753	1386	380
CG9802	39207	14684
CG9895	41035	4303
CG9943	5079	2341

9 References

Abmayr, S.M., and Pavlath, G.K. (2012). Myoblast fusion: lessons from flies and mice. Development *139*, 641–656.

Agarkova, I., and Perriard, J.-C. (2005). The M-band: an elastic web that crosslinks thick filaments in the center of the sarcomere. Trends Cell Biol *15*, 477–485.

Alves-Silva, J., Hahn, I., Huber, O., Mende, M., Reissaus, A., and Prokop, A. (2008). Prominent actin fiber arrays in Drosophila tendon cells represent architectural elements different from stress fibers. Mol Biol Cell *19*, 4287–4297.

Anant, S., Roy, S., and Vijayraghavan, K. (1998). Twist and Notch negatively regulate adult muscle differentiation in Drosophila. Development *125*, 1361–1369.

Applegate, D., and Pardee, J.D. (1992). Actin-facilitated assembly of smooth muscle myosin induces formation of actomyosin fibrils. J. Cell Biol. *117*, 1223–1230.

Atreya, K.B., and Fernandes, J.J. (2008). Founder cells regulate fiber number but not fiber formation during adult myogenesis in Drosophila. Dev Biol *321*, 123–140.

Bahri, S.M., Choy, J.M., Manser, E., Lim, L., and Yang, X. (2009). The Drosophila homologue of Arf-GAP GIT1, dGIT, is required for proper muscle morphogenesis and guidance during embryogenesis. Dev Biol *325*, 15–23.

Bai, H., Kang, P., Hernandez, A.M., and Tatar, M. (2013). Activin Signaling Targeted by Insulin/dFOXO Regulates Aging and Muscle Proteostasis in Drosophila. PLoS Genet *9*, e1003941.

Bai, J., Binari, R., Ni, J.-Q., Vijayakanthan, M., Li, H.-S., and Perrimon, N. (2008). RNA interference screening in Drosophila primary cells for genes involved in muscle assembly and maintenance. Development *135*, 1439–1449.

Bate, M. (1990). The embryonic development of larval muscles in Drosophila. Development *110*, 791–804.

Bate, M., Rushton, E., and Currie, D.A. (1991). Cells with persistent twist expression are the embryonic precursors of adult muscles in Drosophila. Development *113*, 79–89.

Batters, C., Veigel, C., Homsher, E., and Sellers, J.R. (2014). To understand muscle you must take it apart. Front Physiol *5*, 90.

Baylies, M.K., and Bate, M. (1996). twist: a myogenic switch in Drosophila. Science *272*, 1481–1484.

Baylies, M.K., Bate, M., and Ruiz-Gómez, M. (1998). Myogenesis: a view from Drosophila. Cell *93*, 921–927.

Beall, C.J., Sepanski, M.A., and Fyrberg, E.A. (1989). Genetic dissection of Drosophila myofibril formation: effects of actin and myosin heavy chain null alleles. Genes Dev *3*, 131–140.

Bellayr, I., Holden, K., Mu, X., Pan, H., and Li, Y. (2013). Matrix metalloproteinase inhibition negatively affects muscle stem cell behavior. Int J Clin Exp Pathol *6*, 124–141.

Bhuin, T., and Roy, J.K. (2009). Rab11 is required for myoblast fusion in Drosophila. Cell Tissue Res *336*, 489–499.

Bloor, J.W., and Kiehart, D.P. (2001). zipper Nonmuscle myosin-II functions downstream of PS2 integrin in Drosophila myogenesis and is necessary for myofibril formation. Dev Biol *239*, 215–228.

Bour, B.A., Chakravarti, M., West, J.M., and Abmayr, S.M. (2000). Drosophila SNS, a member of the immunoglobulin superfamily that is essential for myoblast fusion. Genes Dev *14*, 1498–1511.

Bour, B.A., O'brien, M.A., Lockwood, W.L., Goldstein, E.S., Bodmer, R., Taghert, P.H., Abmayr, S.M., and Nguyen, H.T. (1995). Drosophila MEF2, a transcription factor that is essential for myogenesis. Genes Dev *9*, 730–741.

Brand, A.H., and Perrimon, N. (1993). Targeted gene expression as a means of altering cell fates and generating dominant phenotypes. Development *118*, 401–415.

Broadie, K.S., and Bate, M. (1991). The development of adult muscles in Drosophila: ablation of identified muscle precursor cells. Development *113*, 103–118.

Brown, N.H., Gregory, S.L., and Martin-Bermudo, M.D. (2000). Integrins as mediators of morphogenesis in Drosophila. Dev Biol *223*, 1–16.

Brown, N.H., Gregory, S.L., Rickoll, W.L., Fessler, L.I., Prout, M., White, R.A.H., and Fristrom, J.W. (2002). Talin is essential for integrin function in Drosophila. Developmental Cell *3*, 569–579.

Brummel, T., Abdollah, S., Haerry, T.E., Shimell, M.J., Merriam, J., Raftery, L., Wrana, J.L., and O'Connor, M.B. (1999). The Drosophila Activin receptor Baboon signals through dSmad2 and controls cell proliferation but not patterning during larval development. Genes Dev *13*, 98–111.

Bryson-Richardson, R.J., and Currie, P.D. (2008). The genetics of vertebrate myogenesis. Nat Rev Genet *9*, 632–646.

Buff, E., Carmena, A., Gisselbrecht, S., Jiménez, F., and Michelson, A.M. (1998). Signalling by the Drosophila epidermal growth factor receptor is required for the specification and diversification of embryonic muscle progenitors. Development *125*, 2075–2086.

Bullard, B., and Pastore, A. (2011). Regulating the contraction of insect flight muscle. J Muscle Res Cell Motil *32*, 303–313.

Bullard, B., Burkart, C., Labeit, S., and Leonard, K. (2006). The function of elastic proteins in the oscillatory contraction of insect flight muscle. J Muscle Res Cell Motil *26*, 479–485.

Burkart, C., Qiu, F., Brendel, S., Benes, V., Hååg, P., Labeit, S., Leonard, K., and Bullard, B. (2007). Modular Proteins from the Drosophila sallimus (sls) Gene and their Expression in Muscles with Different Extensibility. J Mol Biol *367*, 953–969.

Burridge, K., and Wittchen, E.S. (2013). The tension mounts: stress fibers as force-generating mechanotransducers. J Cell Biol *200*, 9–19.

Callahan, C.A., Bonkovsky, J.L., Scully, A.L., and Thomas, J.B. (1996). derailed is required for muscle attachment site selection in Drosophila. Development *122*, 2761–2767.

Campbell, K.B., and Chandra, M. (2006). Functions of stretch activation in heart muscle. J. Gen. Physiol. *127*, 89–94.

Carmena, A., Buff, E., Halfon, M.S., Gisselbrecht, S., Jiménez, F., Baylies, M.K., and Michelson, A.M. (2002). Reciprocal regulatory interactions between the Notch and Ras signaling pathways in the Drosophila embryonic mesoderm. Dev Biol *244*, 226–242.

Chanana, B., Graf, R., Koledachkina, T., Pflanz, R., and Vorbrüggen, G. (2007). αPS2 integrin-mediated muscle attachment in Drosophila requires the ECM protein Thrombospondin. Mechanisms of Development *124*, 463–475.

Charrasse, S., Comunale, F., De Rossi, S., Echard, A., and Gauthier-Rouvière, C. (2013). Rab35 regulates cadherin-mediated adherens junction formation and myoblast fusion. Mol Biol Cell *24*, 234–245.

Charvet, B., Ruggiero, F., and Le Guellec, D. (2012). The development of the myotendinous junction. A review. Muscles Ligaments Tendons J *2*, 53–63.

Chen, E.H., and Olson, E.N. (2001). Antisocial, an intracellular adaptor protein, is required for myoblast fusion in Drosophila. Developmental Cell *1*, 705–715.

Chen, X., and Li, Y. (2009). Role of matrix metalloproteinases in skeletal muscle: migration, differentiation, regeneration and fibrosis. Cell Adh Migr *3*, 337–341.

Chesarone, M.A., DuPage, A.G., and Goode, B.L. (2010). Unleashing formins to remodel the actin and microtubule cytoskeletons. Nature Publishing Group *11*, 62–74.

Cho, J.Y., Chak, K., Andreone, B.J., Wooley, J.R., and Kolodkin, A.L. (2012). The extracellular matrix proteoglycan perlecan facilitates transmembrane semaphorin-mediated repulsive guidance. Genes Dev *26*, 2222–2235.

Craig, R., and Woodhead, J.L. (2006). Structure and function of myosin filaments. Current Opinion in Structural Biology *16*, 204–212.

Currie, D.A., and Bate, M. (1991). The development of adult abdominal muscles in Drosophila: myoblasts express twist and are associated with nerves. Development *113*, 91–102.

Daczewska, M., Picchio, L., Jagla, T., Figeac, N., and Jagla, K. (2010). Muscle development and regeneration in normal and pathological conditions: learning from Drosophila. Curr. Pharm. Des. *16*, 929–941.

Das, C., Lucia, M.S., Hansen, K.C., and Tyler, J.K. (2009). CBP/p300-mediated acetylation of histone H3 on lysine 56. Nature *459*, 113–117.

Das, P., Inoue, H., Baker, J.C., Beppu, H., Kawabata, M., Harland, R.M., Miyazono, K., and Padgett, R.W. (1999). Drosophila dSmad2 and Atr-I transmit activin/TGFbeta signals. Genes Cells *4*, 123–134.

Davies, K.E., and Nowak, K.J. (2006). Molecular mechanisms of muscular dystrophies: old and new players. Nature Publishing Group *7*, 762–773.

De Deyne, P.G. (2000). Formation of sarcomeres in developing myotubes: role of mechanical stretch and contractile activation. American Journal of Physiology Cell Physiology *279*, C1801–C1811.

De Deyne, P.G. (2001). Application of passive stretch and its implications for muscle fibers. Phys Ther *81*, 819–827.

de Joussineau, C., Bataillé, L., Jagla, T., and Jagla, K. (2012). Diversification of muscle types in Drosophila: upstream and downstream of identity genes. Curr. Top. Dev. Biol. *98*, 277–301.

Delon, I., and Brown, N.H. (2007). Integrins and the actin cytoskeleton. Curr Opin Cell Biol *19*, 43–50.

DeMali, K.A., Barlow, C.A., and Burridge, K. (2002). Recruitment of the Arp2/3 complex to vinculin: coupling membrane protrusion to matrix adhesion. J. Cell Biol. *159*, 881–891.

Dietzl, G., Chen, D., Schnorrer, F., Su, K.-C., Barinova, Y., Fellner, M., Gasser, B., Kinsey, K., Oppel, S., Scheiblauer, S., et al. (2007). A genome-wide transgenic RNAi library for conditional gene inactivation in Drosophila. Nature *448*, 151–156.

Doberstein, S.K., Fetter, R.D., Mehta, A.Y., and Goodman, C.S. (1997). Genetic analysis of myoblast fusion: blown fuse is required for progression beyond the prefusion complex. J. Cell Biol. *136*, 1249–1261.

Du, A., Sanger, J.M., Linask, K.K., and Sanger, J.W. (2003). Myofibrillogenesis in the first cardiomyocytes formed from isolated quail precardiac mesoderm. Dev Biol *257*, 382–394.

Duan, H., Skeath, J.B., and Nguyen, H.T. (2001). Drosophila Lame duck, a novel member of the Gli superfamily, acts as a key regulator of myogenesis by controlling fusion-competent myoblast development. Development *128*, 4489–4500.

Dutta, D., Anant, S., Ruiz-Gomez, M., Bate, M., and Vijayraghavan, K. (2004). Founder myoblasts and fibre number during adult myogenesis in Drosophila. Development *131*, 3761–3772.

Dutta, D., Shaw, S., Maqbool, T., Pandya, H., and Vijayraghavan, K. (2005). Drosophila Heartless acts with Heartbroken/Dof in muscle founder differentiation. PLoS Biol *3*, e337.

Dworak, H.A., Charles, M.A., Pellerano, L.B., and Sink, H. (2001). Characterization of Drosophila hibris, a gene related to human nephrin. Development *128*, 4265–4276.

Dye, D.E., Medic, S., Ziman, M., and Coombe, D.R. (2013). Melanoma biomolecules: independently identified but functionally intertwined. Front Oncol *3*, 252.

Ehler, E., Rothen, B.M., Hämmerle, S.P., Komiyama, M., and Perriard, J.C. (1999). Myofibrillogenesis in the developing chicken heart: assembly of Z-disk, M-line and the thick filaments. J Cell Sci *112 (Pt 10)*, 1529–1539.

Ehler, E., and Gautel, M. (2008). The sarcomere and sarcomerogenesis. Adv. Exp. Med. Biol. *642*, 1–14.

Engler, A.J. (2004). Myotubes differentiate optimally on substrates with tissue-like stiffness: pathological implications for soft or stiff microenvironments. J Cell Biol *166*, 877–887.

Estrada, B., Gisselbrecht, S.S., and Michelson, A.M. (2007). The transmembrane protein Perdido interacts with Grip and integrins to mediate myotube projection and attachment in the Drosophila embryo. Development *134*, 4469–4478.

Fernandes, J.J., and Keshishian, H. (1996). Patterning the dorsal longitudinal flight muscles (DLM) of Drosophila: insights from the ablation of larval scaffolds. Development *122*, 3755–3763.

Fernandes, J.J., Celniker, S.E., and Vijayraghavan, K. (1996). Development of the indirect flight muscle attachment sites in Drosophila: role of the PS integrins and the stripe gene. Dev Biol *176*, 166–184.

Fernandes, J., Bate, M., and Vijayraghavan, K. (1991). Development of the indirect flight muscles of Drosophila. Development *113*, 67–77.

Figeac, N., Jagla, T., Aradhya, R., Da Ponte, J.P., and Jagla, K. (2010). Specification and behavior of AMPs, muscle-committed transient Drosophila stem cells. Fly *5*.

Förster, D., and Luschnig, S. (2012). Src42A-dependent polarized cell shape changes mediate epithelial tube elongation in Drosophila. Nature Cell Biology *14*, 526–534.

Friedrich, B.M., Fischer-Friedrich, E., Gov, N.S., and Safran, S.A. (2012). Sarcomeric pattern formation by actin cluster coalescence. PLoS Comput. Biol. *8*, e1002544.

Friedrich, M.V., Schneider, M., Timpl, R., and Baumgartner, S. (2000). Perlecan domain V of Drosophila melanogaster. Sequence, recombinant analysis and tissue expression. Eur J Biochem *267*, 3149–3159.

Frommer, G., Vorbrüggen, G., Pasca, G., Jäckle, H., and Volk, T. (1996). Epidermal egr-like zinc finger protein of Drosophila participates in myotube guidance. Embo J *15*, 1642–1649.

Geeves, M.A., and Holmes, K.C. (1999). Structural mechanism of muscle contraction. Annu Rev Biochem *68*, 687–728.

Gildor, B., Schejter, E.D., and Shilo, B.-Z. (2012). Bidirectional Notch activation represses fusion competence in swarming adult Drosophila myoblasts. Development *139*, 4040–4050.

Gilsohn, E., and Volk, T. (2010a). Fine tuning cellular recognition: The function of the leucine rich repeat (LRR) trans-membrane protein, LRT, in muscle targeting to tendon cells. Cell Adh Migr *4*, 368–371.

Gilsohn, E., and Volk, T. (2010b). Slowdown promotes muscle integrity by modulating integrin-mediated adhesion at the myotendinous junction. Development *137*, 785–794.

Gregorio, C.C., and Antin, P.B. (2000). To the heart of myofibril assembly. Trends Cell Biol *10*, 355–362.

Greig, S., and Akam, M. (1993). Homeotic genes autonomously specify one aspect of pattern in the Drosophila mesoderm. Nature *362*, 630–632.

Grice, S.J., Sleigh, J.N., Liu, J.-L., and Sattelle, D.B. (2011). Invertebrate models of spinal muscular atrophy: Insights into mechanisms and potential therapeutics. Bioessays n/a–n/a.

Grill, S.W., Gönczy, P., Stelzer, E.H., and Hyman, A.A. (2001). Polarity controls forces governing asymmetric spindle positioning in the Caenorhabditis elegans embryo. Nature *409*, 630–633.

Gutzeit, H.O., Eberhardt, W., and Gratwohl, E. (1991). Laminin and basement membrane-associated microfilaments in wild-type and mutant Drosophila ovarian follicles. J Cell Sci *100 (Pt 4)*, 781–788.

Hartenstein, V. (1993). Atlas of Drosophila development. Cold Spring Harbor Laboratory Press.

Holtzer, H., Hijikata, T., Lin, Z.X., Zhang, Z.Q., Holtzer, S., Protasi, F., Franzini-Armstrong, C., and Sweeney, H.L. (1997). Independent assembly of 1.6 microns long bipolar MHC filaments and I-Z-I bodies. Cell Struct. Funct. *22*, 83–93.

Huttenlocher, A., and Horwitz, A.R. (2011). Integrins in cell migration. Cold Spring Harb Perspect Biol *3*, a005074.

Huxley, H.E. (2004). Fifty years of muscle and the sliding filament hypothesis. Eur J Biochem *271*, 1403–1415.

Iwamoto, H., and Yagi, N. (2013). The Molecular Trigger for High-Speed Wing Beats in a Bee. Science *341*, 1243–1246.

Kagawa, M., Sato, N., and Obinata, T. (2006). Effects of BTS (N-benzyl-p-toluene sulphonamide), an inhibitor for myosin-actin interaction, on myofibrillogenesis in skeletal muscle cells in culture. Zool. Sci. *23*, 969–975.

Kramer, S.G., Kidd, T., Simpson, J.H., and Goodman, C.S. (2001). Switching repulsion to attraction: changing responses to slit during transition in mesoderm migration. Science *292*, 737–740.

LaBeau-DiMenna, E.M., Clark, K.A., Bauman, K.D., Parker, D.S., Cripps, R.M., and Geisbrecht, E.R. (2012). Thin, a Trim32 ortholog, is essential for myofibril stability and is required for the integrity of the costamere in Drosophila. Proc Natl Acad Sci USA *109*, 17983–17988.

Lahaye, L.L., Wouda, R.R., de Jong, A.W.M., Fradkin, L.G., and Noordermeer, J.N. (2012). WNT5 Interacts with the Ryk Receptors Doughnut and Derailed to Mediate Muscle Attachment Site Selection in Drosophila melanogaster. PLoS ONE *7*, e32297.

Laird, D.J., Andrian, von, U.H., and Wagers, A.J. (2008). Stem cell trafficking in tissue development, growth, and disease. Cell *132*, 612–630.

Landsberg, K.P., Farhadifar, R., Ranft, J., Umetsu, D., Widmann, T.J., Bittig, T., Said, A., Jülicher, F., and Dahmann, C. (2009). Increased cell bond tension governs cell sorting at the Drosophila anteroposterior compartment boundary. Curr Biol *19*, 1950–1955.

Lange, S., Ehler, E., and Gautel, M. (2006). From A to Z and back? Multicompartment proteins in the sarcomere. Trends Cell Biol *16*, 11–18.

Lawrence, P.A., and Brower, D.L. (1982). Myoblasts From Drosophila Wing Disks Can Contribute to Developing Muscles Throughout the Fly. Nature *295*, 55–57.

Le Clainche, C., and Carlier, M.-F. (2008). Regulation of actin assembly associated with protrusion and adhesion in cell migration. Physiol. Rev. *88*, 489–513.

Lee, T., and Luo, L. (1999). Mosaic analysis with a repressible cell marker for studies of gene function in neuronal morphogenesis. Neuron *22*, 451–461.

Legate, K.R., Wickström, S.A., and Fässler, R. (2009). Genetic and cell biological analysis of integrin outside-in signaling. Genes Dev *23*, 397–418.

Leptin, M. (1991). twist and snail as positive and negative regulators during Drosophila mesoderm development. Genes Dev *5*, 1568–1576.

Lilly, B., Zhao, B., Ranganayakulu, G., Paterson, B.M., Schulz, R.A., and Olson, E.N. (1995). Requirement of MADS domain transcription factor D-MEF2 for muscle formation in Drosophila. Science *267*, 688–693.

Littlefield, R., and Fowler, V.M. (1998). Defining actin filament length in striated muscle: rulers and caps or dynamic stability? Annu. Rev. Cell Dev. Biol. *14*, 487–525.

Longair, M.H., Baker, D.A., and Armstrong, J.D. (2011). Simple Neurite Tracer: open source software for reconstruction, visualization and analysis of neuronal processes. Bioinformatics *27*, 2453–2454.

Luther, P.K. (2009). The vertebrate muscle Z-disc: sarcomere anchor for structure and signalling. J Muscle Res Cell Motil *30*, 171–185.

Maître, J.-L., and Heisenberg, C.-P. (2013). Three Functions of Cadherins in Cell Adhesion Review. Current Biology *23*, R626–R633.

Maqbool, T., Soler, C., Jagla, T., Daczewska, M., Lodha, N., Palliyil, S., Vijayraghavan, K., and Jagla, K. (2006). Shaping leg muscles in Drosophila: role of ladybird, a conserved regulator of appendicular myogenesis. PLoS ONE *1*, e122.

Martin, D., Zusman, S., Li, X.T., Williams, E.L., Khare, N., DaRocha, S., Chiquet-Ehrismann, R., and Baumgartner, S. (1999). wing blister, a new Drosophila laminin alpha chain required for cell adhesion and migration during embryonic and imaginal development. J. Cell Biol. *145*, 191–201.

Mayer, M., Depken, M., Bois, J.S., Jülicher, F., and Grill, S.W. (2010). Anisotropies in cortical tension reveal the physical basis of polarizing cortical flows. Nature *467*, 617–621.

McKinsey, T.A., Zhang, C.L., and Olson, E.N. (2001). Control of muscle development by dueling HATs and HDACs. Curr Opin Genet Dev *11*, 497–504.

Michelson, A.M., Gisselbrecht, S., Zhou, Y., Baek, K.H., and Buff, E.M. (1998). Dual functions of the heartless fibroblast growth factor receptor in development of the Drosophila embryonic mesoderm. Dev Genet *22*, 212–229.

Miller, A. (1950). The internal anatomy and histology of the imago of Drosophila melanogaster. (New York: Wiley).

Moerman, D. (2006). Sarcomere assembly in C. elegans muscle. WormBook.

Mosqueira, M., Willmann, G., Ruohola-Baker, H., and Khurana, T.S. (2010). Chronic hypoxia impairs muscle function in the Drosophila model of Duchenne's muscular dystrophy (DMD). PLoS ONE *5*, e13450.

Mukherjee, P., Gildor, B., Shilo, B.-Z., Vijayraghavan, K., and Schejter, E.D. (2011). The actin nucleator WASp is required for myoblast fusion during adult Drosophila myogenesis. Development *138*, 2347–2357.

Myhre, J.L., and Pilgrim, D.B. (2012). At the Start of the Sarcomere: A Previously Unrecognized Role for Myosin Chaperones and Associated Proteins during Early Myofibrillogenesis. Biochemistry Research International *2012*, 1–16.

Nalbandian, A., Donkervoort, S., Dec, E., Badadani, M., Katheria, V., Rana, P., Nguyen, C., Mukherjee, J., Caiozzo, V., Martin, B., et al. (2011). The multiple faces of valosin-containing protein-associated diseases: inclusion body myopathy with Paget's disease of bone, frontotemporal dementia, and amyotrophic lateral sclerosis. J. Mol. Neurosci. *45*, 522–531.

Newman, S.M., and Wright, T.R. (1981). A histological and ultrastructural analysis of developmental defects produced by the mutation, lethal(1)myospheroid, in Drosophila melanogaster. Dev Biol *86*, 393–402.

Nguyen, H.T., and Xu, X. (1998). Drosophila mef2 expression during mesoderm development is controlled by a complex array of cis-acting regulatory modules. Dev Biol *204*, 550–566.

Nishiyama, A., Komitova, M., Suzuki, R., and Zhu, X. (2009). Polydendrocytes (NG2 cells): multifunctional cells with lineage plasticity. Nat Rev Neurosci *10*, 9–22.

Nongthomba, U., Pasalodos-Sanchez, S., Clark, S., Clayton, J.D., and Sparrow, J.C. (2001). Expression and function of the Drosophila ACT88F actin isoform is not restricted to the indirect flight muscles. J Muscle Res Cell Motil *22*, 111–119.

O'Donnell, P.T., and Bernstein, S.I. (1988). Molecular and ultrastructural defects in a Drosophila myosin heavy chain mutant: differential effects on muscle function produced by similar thick filament abnormalities. J. Cell Biol. *107*, 2601–2612.

Ohtsuki, I., and Morimoto, S. (2008). Troponin: Regulatory function and disorders. Biochemical and Biophysical Research Communications *369*, 62–73.

Ono, S. (2010). Dynamic regulation of sarcomeric actin filaments in striated muscle. Cytoskeleton (Hoboken) *67*, 677–692.

Orfanos, Z., and Sparrow, J.C. (2013). Myosin isoform switching during assembly of the Drosophila flight muscle thick filament lattice. J Cell Sci *126*, 139–148.

Ostendorp, T., Diez, J., Heizmann, C.W., and Fritz, G. (2011). The crystal structures of human S100B in the zinc-and calcium-loaded state at three pH values reveal zinc ligand swapping. Biochimica Et Biophysica Acta (BBA) - Molecular Cell Research *1813*, 1083–1091.

Otey, C.A., and Carpen, O. (2004). Alpha-actinin revisited: a fresh look at an old player. Cell Motil. Cytoskeleton *58*, 104–111.

Peng, Y., Clark, K.J., Campbell, J.M., Panetta, M.R., Guo, Y., and Ekker, S.C. (2014). Making designer mutants in model organisms. Development *141*, 4042–4054.

Perrimon, N., Ni, J.-Q., and Perkins, L. (2010). In vivo RNAi: today and tomorrow. Cold Spring Harb Perspect Biol *2*, a003640.

Peter, A.K., Cheng, H., Ross, R.S., Knowlton, K.U., and Chen, J. (2011). The costamere bridges sarcomeres to the sarcolemma in striated muscle. Progress in Pediatric Cardiology *31*, 83–88.

Petrini, S., Tessa, A., Carrozzo, R., Verardo, M., Pierini, R., Rizza, T., and Bertini, E. (2003). Human melanoma/NG2 chondroitin sulfate proteoglycan is expressed in the sarcolemma of postnatal human skeletal myofibers. Abnormal expression in merosin-negative and Duchenne muscular dystrophies. Mol Cell Neurosci *23*, 219–231.

Pérez-Moreno, J.J., Bischoff, M., Martin-Bermudo, M.D., and Estrada, B. (2014). The conserved transmembrane proteoglycan Perdido/Kon-tiki is essential for myofibrillogenesis and sarcomeric structure in Drosophila. J Cell Sci *127*, 3162–3173.

Pines, M., Das, R., Ellis, S.J., Morin, A., Czerniecki, S., Yuan, L., Klose, M., Coombs, D., and Tanentzapf, G. (2012). Mechanical force regulates integrin turnover in Drosophila in vivo. Nature Cell Biology *14*, 935–943.

Ping Bie, H.Z. (2014). NG2/CSPG4 Proteoglycan as a Novel Prognostic Indicator and Therapeutic Target in Malignant Cancer. J Stem Cell Res Ther *04*.

Pollard, T.D. (2007). Regulation of Actin Filament Assembly by Arp2/3 Complex and Formins. Annu. Rev. Biophys. Biomol. Struct. *36*, 451–477.

Price, M.A., Colvin Wanshura, L.E., Yang, J., Carlson, J., Xiang, B., Li, G., Ferrone, S., Dudek, A.Z., Turley, E.A., and McCarthy, J.B. (2011). CSPG4, a potential therapeutic target, facilitates malignant progression of melanoma. Pigment Cell Melanoma Res *24*, 1148–1157.

Prokop, A., Martín-Bermudo, M.D., Bate, M., and Brown, N.H. (1998). Absence of PS integrins or laminin A affects extracellular adhesion, but not intracellular assembly, of hemiadherens and neuromuscular junctions in Drosophila embryos. Dev Biol *196*, 58–76.

Ramachandran, I., Terry, M., and Ferrari, M.B. (2003). Skeletal muscle myosin cross-bridge cycling is necessary for myofibrillogenesis. Cell Motil. Cytoskeleton *55*, 61–72.

Ranganayakulu, G., Schulz, R.A., and Olson, E.N. (1996). Wingless signaling induces nautilus expression in the ventral mesoderm of the Drosophila embryo. Dev Biol *176*, 143–148.

Richardson, B.E., Nowak, S.J., and Baylies, M.K. (2008). Myoblast fusion in fly and vertebrates: new genes, new processes and new perspectives. Traffic *9*, 1050–1059.

Ridley, A.J. (2011). Life at the leading edge. Cell *145*, 1012–1022.

Rochlin, K., Yu, S., Roy, S., and Baylies, M.K. (2010). Myoblast fusion: when it takes more to make one. Dev Biol *341*, 66–83.

Roy, S., and Vijayraghavan, K. (1997). Homeotic genes and the regulation of myoblast migration, fusion, and fibre-specific gene expression during adult myogenesis in Drosophila. Development *124*, 3333–3341.

Roy, S., and Vijayraghavan, K. (1998). Patterning muscles using organizers: larval muscle templates and adult myoblasts actively interact to pattern the dorsal longitudinal flight muscles of Drosophila. J Cell Biol *141*, 1135–1145.

Roy, S., and Vijayraghavan, K. (1999). Muscle pattern diversification in Drosophila: the story of imaginal myogenesis. Bioessays *21*, 486–498.

Roy, S., Shashidhara, L.S., and Vijayraghavan, K. (1997). Muscles in the Drosophila second thoracic segment are patterned independently of autonomous homeotic gene function. Current Biology *7*, 222–227.

Rudy, D.E., Yatskievych, T.A., Antin, P.B., and Gregorio, C.C. (2001). Assembly of thick, thin, and titin filaments in chick precardiac explants. Dev Dyn *221*, 61–71.

Rui, Y., Bai, J., and Perrimon, N. (2010). Sarcomere formation occurs by the assembly of multiple latent protein complexes. PLoS Genet *6*, e1001208.

Ruiz, M.G., and Bate, M. (1997). Segregation of myogenic lineages in Drosophila requires numb. *124*, 4857–4866.

Ruiz-Gómez, M. (1998). Muscle patterning and specification in Drosophila. Int. J. Dev. Biol. *42*, 283–290.

Ruiz-Gómez, M., Coutts, N., Price, A., Taylor, M.V., and Bate, M. (2000). Drosophila dumbfounded: a myoblast attractant essential for fusion. Cell *102*, 189–198.

Sanger, J.W., Kang, S., Siebrands, C.C., Freeman, N., Du, A., Wang, J., Stout, A.L., and Sanger, J.M. (2005). How to build a myofibril. J Muscle Res Cell Motil *26*, 343–354.

Sanger, J.W., Wang, J., Fan, Y., White, J., and Sanger, J.M. (2010). Assembly and Dynamics of Myofibrils. Journal of Biomedicine and Biotechnology *2010*, 1–9.

Sartori, R., Gregorevic, P., and Sandri, M. (2014). TGF-beta and BMP signaling in skeletal muscle: potential significance for muscle-related disease. Trends Endocrinol Metab *25*, 464–471.

Schejter, E.D., and Baylies, M.K. (2010). Born to run: creating the muscle fiber. Curr Opin Cell Biol *22*, 566–574.

Schindelholz, B., Knirr, M., Warrior, R., and Zinn, K. (2001). Regulation of CNS and motor axon guidance in Drosophila by the receptor tyrosine phosphatase DPTP52F. Development *128*, 4371–4382.

Schnorrer, F., and Dickson, B.J. (2004). Muscle building; mechanisms of myotube guidance and attachment site selection. Developmental Cell *7*, 9–20.

Schnorrer, F., Kalchhauser, I., and Dickson, B.J. (2007). The transmembrane protein Kon-tiki couples to Dgrip to mediate myotube targeting in Drosophila. Developmental Cell *12*, 751–766.

Schnorrer, F., Schönbauer, C., Langer, C.C.H., Dietzl, G., Novatchkova, M., Schernhuber, K., Fellner, M., Azaryan, A., Radolf, M., Stark, A., et al. (2010). Systematic genetic analysis of muscle morphogenesis and function in Drosophila. Nature *464*, 287–291.

Schönbauer, C., Distler, J., Jährling, N., Radolf, M., Dodt, H.-U., Frasch, M., and Schnorrer, F. (2011). Spalt mediates an evolutionarily conserved switch to fibrillar muscle fate in insects. Nature *479*, 406–409.

Schultheiss, T., Lin, Z.X., Lu, M.H., Murray, J., Fischman, D.A., Weber, K., Masaki, T., Imamura, M., and Holtzer, H. (1990). Differential distribution of subsets of myofibrillar proteins in cardiac nonstriated and striated myofibrils. J. Cell Biol. *110*, 1159–1172.

Schultz, J., Milpetz, F., Bork, P., and Ponting, C.P. (1998). SMART, a simple modular architecture research tool: identification of signaling domains. Proc Natl Acad Sci USA *95*, 5857–5864.

Schweitzer, R., Zelzer, E., and Volk, T. (2010). Connecting muscles to tendons: tendons and musculoskeletal development in flies and vertebrates. Development *137*, 2807–2817.

Sens, K.L., Zhang, S., Jin, P., Duan, R., Zhang, G., Luo, F., Parachini, L., and Chen, E.H. (2010). An invasive podosome-like structure promotes fusion pore formation during myoblast fusion. J Cell Biol *191*, 1013–1027.

Serrels, B., Serrels, A., Brunton, V.G., Holt, M., McLean, G.W., Gray, C.H., Jones, G.E., and Frame, M.C. (2007). Focal adhesion kinase controls actin assembly via a FERM-mediated interaction with the Arp2/3 complex. Nature Cell Biology *9*, 1046–1056.

Sharp, W.W., Simpson, D.G., Borg, T.K., Samarel, A.M., and Terracio, L. (1997). Mechanical forces regulate focal adhesion and costamere assembly in cardiac myocytes. Am J Physiol *273*, H546–H556.

Skwarek-Maruszewska, A., Hotulainen, P., Mattila, P.K., and Lappalainen, P. (2009). Contractility-dependent actin dynamics in cardiomyocyte sarcomeres. J Cell Sci *122*, 2119–2126.

Soeno, Y., Shimada, Y., and Obinata, T. (1999). BDM (2,3-butanedione monoxime), an inhibitor of myosin-actin interaction, suppresses myofibrillogenesis in skeletal muscle cells in culture. Cell Tissue Res *295*, 307–316.

Solon, J., Kaya-Copur, A., Colombelli, J., and Brunner, D. (2009). Pulsed Forces Timed by a Ratchet-like Mechanism Drive Directed Tissue Movement during Dorsal Closure. Cell.

Sparrow, J.C., and Schöck, F. (2009). The initial steps of myofibril assembly: integrins pave the way. Nat Rev Mol Cell Biol *10*, 293–298.

Spudich, J.A. (2001). The myosin swinging cross-bridge model. Nat Rev Mol Cell Biol *2*, 387–392.

Stegmüller, J., Werner, H., Nave, K.-A., and Trotter, J. (2003). The proteoglycan NG2 is complexed with alpha-amino-3-hydroxy-5-methyl-4-isoxazolepropionic acid (AMPA) receptors by the PDZ glutamate receptor interaction protein (GRIP) in glial progenitor cells. Implications for glial-neuronal signaling. J Biol Chem *278*, 3590–3598.

Strumpf, D., and Volk, T. (1998). Kakapo, a novel cytoskeletal-associated protein is essential for the restricted localization of the neuregulin-like factor, vein, at the muscle-tendon junction site. J Cell Biol *143*, 1259–1270.

Strünkelnberg, M., Bonengel, B., Moda, L.M., Hertenstein, A., de Couet, H.G., Ramos, R.G., and Fischbach, K.F. (2001). rst and its paralogue kirre act redundantly during embryonic muscle development in Drosophila. Development *128*, 4229–4239.

Subramanian, A., and Schilling, T.F. (2014). Thrombospondin-4 controls matrix assembly during development and repair of myotendinous junctions. eLife.

Subramanian, A., Prokop, A., Yamamoto, M., Sugimura, K., Uemura, T., Betschinger, J., Knoblich, J.A., and Volk, T. (2003). Shortstop recruits EB1/APC1 and promotes microtubule assembly at the muscle-tendon junction. Curr Biol *13*, 1086–1095.

Subramanian, A., Wayburn, B., Bunch, T., and Volk, T. (2007). Thrombospondin-mediated adhesion is essential for the formation of the myotendinous junction in Drosophila. Development *134*, 1269–1278.

Sudarsan, V., Anant, S., Guptan, P., Vijayraghavan, K., and Skaer, H. (2001). Myoblast diversification and ectodermal signaling in Drosophila. Developmental Cell *1*, 829–839.

Swan, L.E., Schmidt, M., Schwarz, T., Ponimaskin, E., Prange, U., Boeckers, T., Thomas, U., and Sigrist, S.J. (2006). Complex interaction of Drosophila GRIP PDZ domains and Echinoid during muscle morphogenesis. Embo J *25*, 3640–3651.

Swan, L.E., Wichmann, C., Prange, U., Schmid, A., Schmidt, M., Schwarz, T., Ponimaskin, E., Madeo, F., Vorbrüggen, G., and Sigrist, S.J. (2004). A glutamate receptor-interacting protein homolog organizes muscle guidance in Drosophila. Genes Dev *18*, 223–237.

Tabebordbar, M., Wang, E.T., and Wagers, A.J. (2013). Skeletal Muscle Degenerative Diseases and Strategies for Therapeutic Muscle Repair. Annu. Rev. Pathol. Mech. Dis. *8*, 441–475.

Takeichi, M. (2014). Dynamic contacts: rearranging adherens junctions to drive epithelial remodelling. Nature Publishing Group *15*, 397–410.

Taylor, M.V. (1995). Muscle development. Making Drosophila muscle. Current Biology *5*, 740–742.

Tepass, U., and Hartenstein, V. (1994). The development of cellular junctions in the Drosophila embryo. Dev Biol *161*, 563–596.

Thompson, R.C., Buvoli, M., Buvoli, A., and Leinwand, L.A. (2012). Myosin filament assembly requires a cluster of four positive residues located in the rod domain. FEBS Lett *586*, 3008–3012.

Tixier, V., Bataillé, L., and Jagla, K. (2010). Diversification of muscle types: recent insights from Drosophila. Experimental Cell Research *316*, 3019–3027.

Tokuyasu, K.T. (1987). Immunocytochemical studies of cardiac myofibrillogenesis in early chick embryos. II. Generation of alpha-actinin dots within titin spots at the time of the first myofibril formation. J Cell Biol *105*, 2795–2801.

Trendelenburg, A.U., Meyer, A., Jacobi, C., Feige, J.N., and Glass, D.J. (2012). TAK-1/p38/nNFκB signaling inhibits myoblast differentiation by increasing levels of Activin A. Skelet Muscle *2*, 3.

Tskhovrebova, L., and Trinick, J. (2003). Titin: properties and family relationships. Nature Publishing Group *4*, 679–689.

Tzu, J., and Marinkovich, M.P. (2008). Bridging structure with function: structural, regulatory, and developmental role of laminins. Int. J. Biochem. Cell Biol. *40*, 199–214.

Uchino, R., Nonaka, Y.-K., Horigome, T., Sugiyama, S., and Furukawa, K. (2013). Loss of Drosophila A-type lamin C initially causes tendon abnormality including disintegration of cytoskeleton and nuclear lamina in muscular defects. Dev Biol *373*, 216–227.

Vicente-Manzanares, M., Choi, C.K., and Horwitz, A.R. (2009a). Integrins in cell migration--the actin connection. J Cell Sci *122*, 199–206.

Vicente-Manzanares, M., Ma, X., Adelstein, R.S., and Horwitz, A.R. (2009b). Non-muscle myosin II takes centre stage in cell adhesion and migration. 1–13.

Vigoreaux, J.O. (2001). Genetics of the Drosophila flight muscle myofibril: a window into the biology of complex systems. Bioessays *23*, 1047–1063.

Volk, T. (1999). Singling out Drosophila tendon cells: a dialogue between two distinct cell types. Trends Genet *15*, 448–453.

Vorbrüggen, G., and Jäckle, H. (1997). Epidermal muscle attachment site-specific target gene expression and interference with myotube guidance in response to ectopic stripe expression in the developing Drosophila epidermis. Proc Natl Acad Sci USA *94*, 8606–8611.

Wayburn, B., and Volk, T. (2009). LRT, a tendon-specific leucine-rich repeat protein, promotes muscle-tendon targeting through its interaction with Robo. Development *136*, 3607–3615.

Wehrle-Haller, B. (2012). Structure and function of focal adhesions. Curr Opin Cell Biol *24*, 116–124.

Weitkunat, M., and Schnorrer, F. (2014). A guide to study Drosophila muscle biology. Methods *68*, 2–14.

Weitkunat, M., Kaya-Çopur, A., Grill, S.W., and Schnorrer, F. (2014). Tension and force-resistant attachment are essential for myofibrillogenesis in Drosophila flight muscle. Curr Biol *24*, 705–716.

Wells, C., Coles, D., Entwistle, A., and Peckham, M. (1997). Myogenic cells express multiple myosin isoforms. J Muscle Res Cell Motil *18*, 501–515.

Wiesner, S., Legate, K.R., and Fässler, R. (2005). Integrin-actin interactions. Cell. Mol. Life Sci. *62*, 1081–1099.

Wolfstetter, G., and Holz, A. (2012). The role of LamininB2 (LanB2) during mesoderm differentiation in Drosophila. Cell. Mol. Life Sci. *69*, 267–282.

Woods, D.F., and Bryant, P.J. (1991). The Disks-Large Tumor Suppressor Gene of Drosophila Encodes a Guanylate Kinase Homolog Localized at Septate Junctions. Cell *66*, 451–464.

Woods, D.F., Wu, J.W., and Bryant, P.J. (1997). Localization of proteins to the apico-lateral junctions of Drosophila epithelia. Dev Genet *20*, 111–118.

Wright, K.J., Marr, M.T., and Tjian, R. (2006). TAF4 nucleates a core subcomplex of TFIID and mediates activated transcription from a TATA-less promoter. Proc Natl Acad Sci USA *103*, 12347–12352.

Yarnitzky, T., Min, L., and Volk, T. (1997). The Drosophila neuregulin homolog Vein mediates inductive interactions between myotubes and their epidermal attachment cells. Genes Dev *11*, 2691–2700.

Yoshinaga, N., Joanny, J.F., Prost, J., and Marcq, P. (2010). Polarity Patterns of Stress Fibers. Phys. Rev. Lett. *105*.

Yurchenco, P.D. (2011). Basement membranes: cell scaffoldings and signaling platforms. Cold Spring Harb Perspect Biol *3*.

Zhang, X., Koolhaas, W.H., and Schnorrer, F. (2014). A Versatile Two-Step CRISPR- and RMCE-Based Strategy for Efficient Genome Engineering in Drosophila. G3 (Bethesda).